Nuclear architecture and structural dynamics

- molecular basis of chromatin remodeling induced by human ISWI machines -

Dissertation zur Erlangung des Doktorgrades
der Naturwissenschaften (Dr. rer. nat.)
der naturwissenschaftlichen Fakultät III - Biologie und vorklinische Medizin -
der Universität Regensburg

vorgelegt von
Josef H. Exler
aus Ibbenbüren

Mai 2010

Promotionsgesuch eingereicht am: 19.05.2010
Die Arbeit wurde angeleitet von: Prof. Dr. Gernot Längst

Prüfungsausschuss:	Vorsitzender:	Prof. Dr. Armin Kurtz
	Erstgutachter:	Prof. Dr. Gernot Längst
	Zweitgutachter:	Prof. Dr. Reinhard Sterner
	Weiterer Prüfer:	Prof. Dr. Ralf Wagner

Contents

List of Figures

List of Tables

List of Abbreviations

E. coli	Escherichia coli
g	relative centrifugal force
$^{\circ}C$	degree Celsius
aa	amino acid
AAA+	ATPases Associated with various cellular Activities
Amp	Ampicillin
APS	Ammonium Persulfate
ARPs	Actin-Related Proteins
ASF1	Alternative Splicing Factor 1
ATP	Adenosine-5'-triphosphate
BAF	Brahma-Associated Factor
bp	base pair
BPTF	Bromodomain PHD Finger Transcription Factor
BRG1	Brahma-Related Gene 1
BRM	Brahma
BSA	Bovine Serum Albumine
C-terminal	carboxy terminal
CAF1	Chromatin Assembly Factor 1
CERC2	Cat Eye Syndrome Chromosome Region, Candidate 2
CERF	CERC2 Remodeling Factor
CHD	Chromo-ATPase/Helicase-DNA-binding protein
CHRAC	Chromatin Accessibility Complex
CNS	Central Nervous System
CpG	Cytosine-phosphatidyl-guanosine
CT	Chromosome Territories
CT-IC	Chromosome Territory Interchromatin Compartment
Da	Dalton
DMSO	Dimethylsulfoxide
DNA	Deoxyribonucleic Acid
DNMT	DNA-Cytosine-5-Methyltransferase

dNTP ..... 2'-deoxynucleotide triphosphate
EDTA ..... Ethyleneiaminotetraacetate
EGTA ..... Ethylene Glycol Tetraacetic Acid
ENCODE ..... Encyclopedia of DNA Elements
ESCs ..... Embryonic Stem Cells
FACT ..... Facilitates Chromatin Transcription
FCS ..... Fetal Calf Serum
FISH ..... Fluorescence in situ hybridization
FRET ..... Fluorescence Energy Transfer
g ..... gram
h ..... hour
H3Kxme3 ..... tri-methylation at lysine x of histone H3
H4Kxac ..... acetylation at lysine x of histone H4
HDAC ..... Histone Acetyltransferase
HIRA ..... Histone Regulatory Protein A
HMT ..... Histone Methyltransferase
HP1 ..... Heterochromatin binding Protein 1
IMC ..... Inner Cell Mass
IPTG ..... Isopropylthiogalactoside
ISWI ..... Imitating Switch
$K_{1/2}$ ..... half maximal binding constant, apparent K_M
kb ..... kilobases
kDa ..... Kilodalton
l ..... litre
LB ..... Luria-Bertani
LCR ..... Ligase Chain Reaction
M ..... molar
MAR ..... Matrix Attachment Regions
MBP ..... Methyl-CpG-binding Proteins
min ..... minute
MOI ..... Multiplicity of Infection
MOR ..... Moria
MW ..... Molecular Weight
n ..... Hill coefficient
N-terminal ..... amino terminal
NAP1 ..... Nucleosome Assembly Protein 1

NOR	Nucleolar Organizer Region
NoRC	Nucleolar Remodeling Complex
NPS1	Nucleosome Positioning Sequence 1
nt	nucleotide
NuRD	Nucleosome Remodeling and Deacetylase
NURF	Nucleosome Remodeling Factor
PAA	Polyacrylamide
PBS	Phosphate Buffered Saline
PCR	Polymerase Chain Reaction
PHD	Plant Homeodomain
PTMs	Post-translational Modifications
rcf	relative centrifugal force
rDNA	ribosomal DNA
RNA	Ribonucleic Acid
RNAPI	RNA Polymerase I
RNAPII	RNA Polymerase II
rpm	rounds per minute
RSF	Remodeling and Spacing Factor
s	second
SAM	S-adenosyl-L-methionine
SANT	SWI3, ADA2, N-CoR and TFIIIB
SAR	Scaffold Attachment Regions
SDS	Sodium Dodecyl Sulfate
SDS-PAGE	Sodium Dodecyl Sulfate Polyacrylamide Gel Electrophoresis
SLIDE	SANT-Like Domain
SNF2H	Snf2 homolog protein
SWI/SNF	Switching defective/Sucrose Non-Fermenting
TAM	Tip5/ARBP/MBD
Taq	Thermus aquaticus
TBE	Tris Borate EDTA
TE	Tris EDTA
TEMED	N,N,N',N'-tetramethylethylenediamine
TIP5	TTF-I interacting protein 5
Tris	tris(hydroxymethyl)aminomethane
TTF1	Transcription Termination Factor 1
U	unit

1 Summary

One striking observation made when revealing the genetic code of humans was the relative small number of protein encoding genes that were found. The increased complexity of this biological system was not reflected by an increased number of genes. Nevertheless for higher vertebrates an expansion in genome sizes was observed [Yoo and Crabtree, 2009]. Only a small fraction of the genetic code is translated into proteins (approximately 2 %), although over 90 % of the genome is transcribed. Therefore, not the number of coding sequences grew, but the complexity of the machinery helping to interpret and functionally use the information increased during evolution [International Human Genome Sequencing Consortium, 2004; Carninci et al., 2008].

A complex interaction network generates a specific spatial and temporal pattern of cellular activities. This allows formation of complex organisms based on a limited number of genes. The highly dynamic chromatin structure is a prerequisite for the flexible interpretation of the genetic information. One important class of enzymes directly changes the structure of chromatin by assembling and repositioning nucleosomes. These chromatin remodeling complexes nicely reflect the complexity of the DNA organization and interpretation machinery. Assembly of chromatin remodeling complexes from several ATP-dependent DNA translocases in combination with numerous regulatory subunits generates a large combinatorial diversity [Rippe et al., 2007; Ho and Crabtree, 2010].

Especially during development of the nervous system, activity of diverse remodeling complexes is crucial [Yoo and Crabtree, 2009]. ATPases of the ISWI class are often found in complexes playing an important role during neural development. The genome of the fruit fly *Drosophila melanogaster* encodes only one ISWI ATPase. In mammalians like human and mouse it is more complex, they have two different ISWI class remodeler named SNF2H and SNF2L. Although having a highly similar protein structure, both enzymes show a distinct spatial and temporal expression pattern [Lazzaro and Picketts, 2001]. Nevertheless, the detailed differences and molecular basis of this specialization remained unclear.

The data presented in this thesis reveal that human ISWI remodeler are highly cooperative nucleosome binder. It is shown that cooperative binding of these chromatin modifiers is predominately seen for nucleosomal substrates. DNA is bound much less cooperative,

but with a high affinity. In addition, both enzymes form higher molecular weight complexes, mainly di- and tetramers, also in absence of DNA or nucleosomal substrates.
They both differ qualitatively and quantitatively in the way they bind to nucleosomes. For mono-nucleosomal substrates, SNF2H shows a more cooperative binding than SNF2L does, while affinity to nucleosomes is higher for SNF2L. These differences were also observed for dynamic binding in presence of ATP. Under competitive conditions, SNF2H preferentially binds nucleosomes with longer linker DNA, while substrate binding of SNF2L is not affected by linker length.
In contrast to substrate binding, ATP-hydrolysis activity of SNF2L is dependent of nucleosomal linker DNA length and increases with longer linkers, whereas hydrolysis activity of SNF2H is already maximal stimulated by nucleosome core particles. As also published by other groups SNF2H is unable to translocate such linker less nucleosomes [He et al., 2008]. Strikingly, SNF2L pushes the histone octamere over the end of the nucleosomal DNA. In summary, activity of both paralogs is regulated with respect to the substrate structure, but on contrary levels.
In order to analyze chromatin structure and dynamical changes *in vivo*, induced e. g. by chromatin remodeling machines, an effective method to differentially characterize accessible, active chromatin regions and inactive heterochromatin is crucial. As shown in this thesis, limiting amounts of micrococcal nuclease allow a specific characterization of accessible euchromatin regions. The isolated chromatin fragments displayed a specific nuclear distribution within distinct decondensed regions as determined by fluorescence *in situ* hybridization. Comparative microarray hybridization to an ENCODE chip revealed a correlation of these open chromatin fractions with active and therefore euchromatic marks, like histone H3K4 methylation, RNA polymerase II association and transcriptional activity.
Furthermore, differences in methylation of mono-, di- and tri-nucleosomal DNA also revealed a specific global pattern of 5-methyl-cytosine modifications within human chromatin. DNA methylation *in vivo* is mainly restricted to nucleosomal linker regions. Therefore, the established method can be used for further characterisation of active chromatin domains in a relative high resolution. As a next step, the dynamical changes of chromatin structure can be analysed. Direct manipulation by knock-down or overexpression of distinct remodeling enzymes, e. g. SNF2H and SNF2L, within HeLa cells will address the question how chromatin structure and status of these initially charaterized regions changes. Furthermore the question whether DNA methyltransferases gain access to their substrate by structural dynamics, or if their activity is limited to linker DNA regions in general, can be dissected by this approach in a more detailed way.

2 Introduction

2.1 Chromatin structure

2.1.1 Chromatin

During his microscopic studies at the end of the 19th century Walter Flemming discovered a stainable substance filling the nucleus of an eukaryotic cell. Deduced from the Greek word *"chroma"*, meaning coloured, he introduced the term "chromatin".
With respect to differences in the density of the chromatin, it is divided into euchromatin and heterochromatin. Decondensed euchromatin is mainly found in the center of a nucleus, whereas heterochromatin is located at the periphery. Today it is known that one major component of chromatin is the genomic DNA. In addition with proteins, like histones, and non-conding (nc) RNA as essential structural and functional component, eukaryotic genomes are organized into specialized nucleoprotein complexes [Pederson and Bhorjee, 1979; Rodríguez-Campos and Azorín, 2007; Mondal et al., 2010]. Heterochromatin is further divided into constitutive heterochromatin, rich in repetitive DNA sequences from telomeres and centromeres, encoding only few genes, and in facultative heterochromatin, formed by potentially active regions that can adopt the structural and functional characteristics of heterochromatin.

The observed differences in the density reveal the two contradictory demands the genetic information has to meet within the nucleus. First, the DNA of a human cell with a length of 1.7 meters has to fit into a cellular compartment with an average diameter of only 10 µm. These spatial constraints underline the need for a 10,000 fold compaction of the genetic information. Second, this highly compacted DNA has to be rapidly accessible to allow the readout of stored information. All important cellular processes like replication, repair and recombination are dependent on access to DNA [Felsenfeld, 1978]. Therefore chromatin has a highly dynamic architecture allowing structural changes in response to external and internal signals.

2.1.2 The nucleosome

Several distinct levels of compaction are essential to generate a chromatin structure that allows high condensation while being accessible at the same time. The basic structural unit of chromatin is the nucleosome, which compacts DNA about sevenfold [McGhee and Felsenfeld, 1980; Kornberg, 1974; Ho and Crabtree, 2010]. The nucleosome core particle is formed by a stretch of 147 bp DNA wrapped in 1.7 left handed superhelical turns around a core of eight basic histone proteins. This nucleoprotein complex is stabilized by 14 direct histone-DNA-interactions. The histone core is composed of a $(H3/H4)_2$ tetramer and two histone (H2A/H2B) dimers [Luger et al., 1997; Richmond and Davey, 2003].
Beside these canonical nucleosomal particles, also smaller non-octameric ones are known. These non-canonical nucleosomes somehow reflect the assembly and disassembly pathway of nucleosome reconstitution. During assembly, the $(H3/H4)_2$ tetramer binds first to DNA followed by recruitment of (H2A/H2B) dimers [Luger, 2003]. If DNA is wrapped around a core formed by a $(H3/H4)_2$ tetramer associated with only one (H2A/H2B) dimer, the complex is called "hexasome" (figure 2.1). These particles are found *in vitro* [de la Escalera et al., 1988] and *in vivo*, but the biological functions are not fully understood. Whether a hexasome is formed by eviction of a (H2A/H2B) dimer from an octamer, or by *de novo* assembly is still unclear, but hexasome formation seems to coincide with RNA polymerase II activity [Zlatanova et al., 2009].
Also the relevance of a tetrasome remains obscure, representing an alternative non-canonical nucleosome [Alilat et al., 1999]. As a consequence of the smaller histone core, consisting only of a $(H3/H4)_2$ tetramer, less than one superhelical turn of DNA is wrapped around it.
In all cases, the basic N-terminal histone domains extend from the nucleosomal surface and are accessible for modifying enzymes (section 2.1.3) or chromatin remodeling machines (section 2.3.1).

2.1.3 Histone proteins

All four core histones H4, H3, H2A and H2B are 11 - 16 kD small basic proteins that are highly conserved throughout different species (figure 2.2). The central "histone fold domains", consisting of three α-helices connected by two loop regions, are most conserved. In contrast to this, the N-terminal domains are much more variable and unstructured, also extremely basic due to several lysine and arginine residues. These positive charged "tails" facilitate interactions with the negative charged DNA and these amino acids can be post-translationally modified (section 2.2.2) [Khorasanizadeh, 2004].

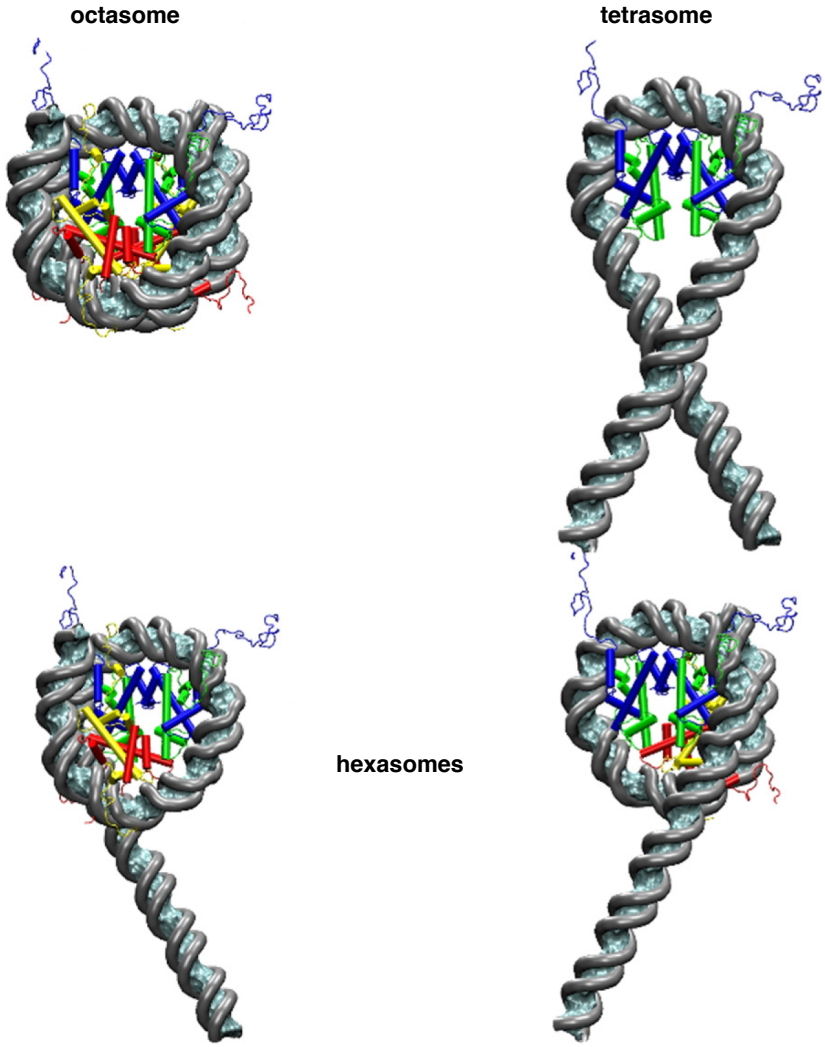

Figure 2.1: **Models of different nucleosomes**
147 bp B-form DNA is modelled in 1.7 left handed superhelical turns around an octamer of H2A (yellow), H2B (red), H3 (blue) and H4 (green), called octasome. The tetrasome contains four histones $(H3/H4)_2$ and DNA is wrapped in less than one superhelical turn. Formation of a hexasome from an octamer releases 48 bp, but still more than one superhelical turn of DNA stays bound. The two different structures represent both possible hexasome forms: $(H2A/H2B)(H3/H4)_2$ or $(H3/H4)_2(H2B/H2A)$ (according to [Zlatanova et al., 2009]).

During evolution, further specialized variants of histones developed and adopted specific functions. Differences in their stability, DNA wrapping, domains that regulate access to DNA, and post-translational modifications are known today (see also section 2.2.2). In contrast to their canonical counterparts, transcription of most histone variant genes

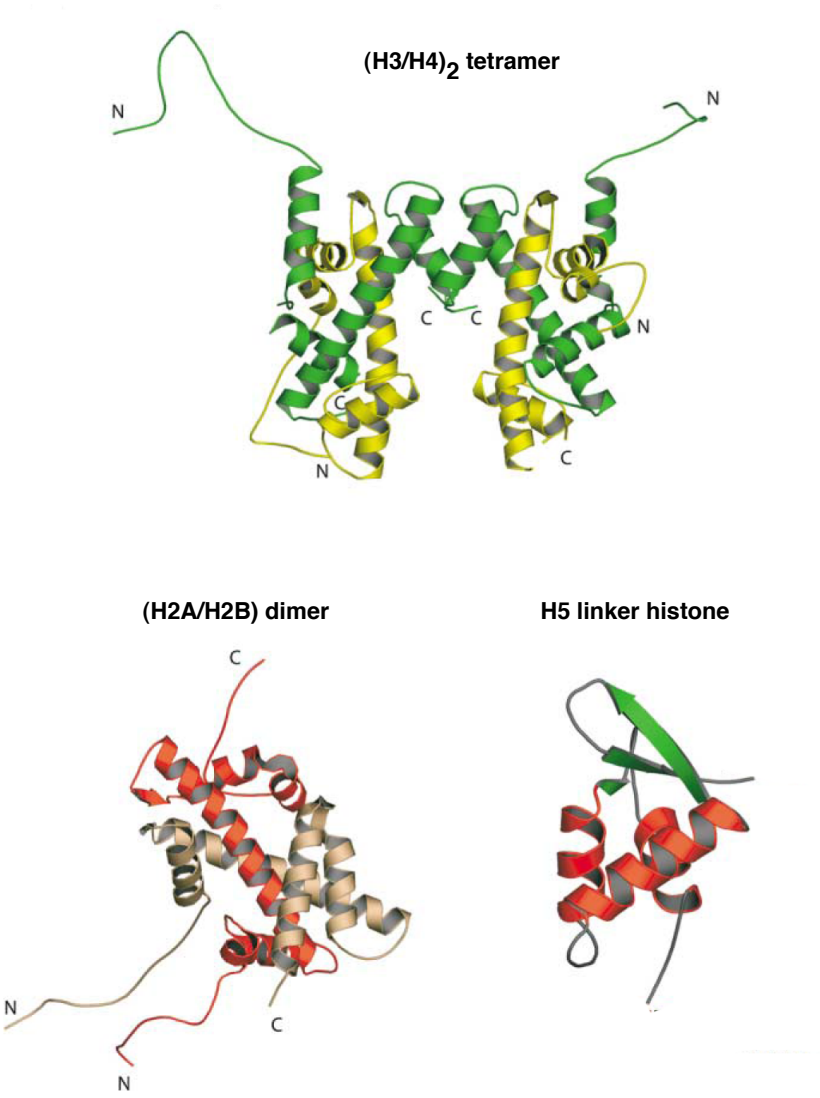

Figure 2.2: **Struture of core and linker histones**
H3 (green) and H4 (yellow) form a tetramer by interacting with central domains consisting of three α-helices. N-terminal domains are unstructured and protruding from the central core. H2A (red) and H2B (pink) form a dimer. The linker histone H5 has a conserved wing helix fold (according to [Khorasanizadeh, 2004]).

is independent of S-phase [Wu and Bonner, 1981; Talbert and Henikoff, 2010]. Histone H3 variants exist in different forms. One, named CENP-A (**Cen**tromere **P**rotein **A**) or CenH3, is maintaining the specific structure and functionality of centromeres [Black et al., 2007; Panchenko and Black, 2009].

Another variant of H3, H3.3, is detected at promoter regions of active genes, whereas transcribed regions show a reduced occupancy [Mito et al., 2005]. An alternative H2A histone called H2A.Z displays only 60 % sequence identity with H2A [Wu and Bonner, 1981] and is globally enriched in regions close to promoter sequences. Furthermore, it is proposed to positively influence transcriptional activity [Guillemette and Gaudreau, 2006], although it is additionally found in facultative heterochromatin [Greaves et al., 2006]. MacroH2A is another, larger form of H2A, with a C-terminus of unknown function. It is co-localizing with transcriptionally repressed X chromosome and pericentromeric heterochromatin [Chakravarthy et al., 2005].

The non-nucleosomal histones H1 and H5 interact with the linker DNA between two nucleosome core particles and in contrast to the core histones are not well conserved between species. Their structure is based on three different domains: a globular, non-polar central domain, essential for interactions with DNA and two unstructured highly basic N- and C-terminal domains. These are target sites for different post-translational modifications. Linker histones are known to influence spacing of nucleosomes and they facilitate interactions between adjacent nucleosomes *in vivo*. Therefore they play an important role in higher-order compaction of chromatin.

2.1.4 Higher-order chromatin structures

Partial digestion of chromatin revealed that *in vivo* octameric nucleosome core particles form regularly spaced arrays. This observation was also confirmed by electron microscopic studies, displaying "beads on a string" like structures [Olins and Olins, 2003]. The nucleosome core particles are connected by stretches of linker DNA. The size of these DNA stretches is dependent on species, cell type and developmental stage [van Holde, 1989]. Under physiological conditions, the nucleosome core particles are associated with linker histones H1/H5. These linker histones bind to a stretch of 20 bp DNA at the nucleosomal entry/exit site, where the non-nucleosomal linker DNA protrudes from the octamer surface [Wolffe, 1997; Wolffe and Kurumizaka, 1998]. This first level of compaction is also called "11 nm fiber".
Interaction of adjacent nucleosomes facilitated by linker histones induces formation of the so-called "30 nm fiber" . The detailed structure of this second level of chromatin folding, and also all higher levels, are still unknown. Despite the lack of high resolution structures, there is evidence supporting two proposed models for the 30 nm fiber [Tremethick, 2007]. In the solenoid model, consecutive nucleosomes are next to each other within a fiber, following the same helical path folding into a one-start helix [Robinson and Rhodes, 2006].

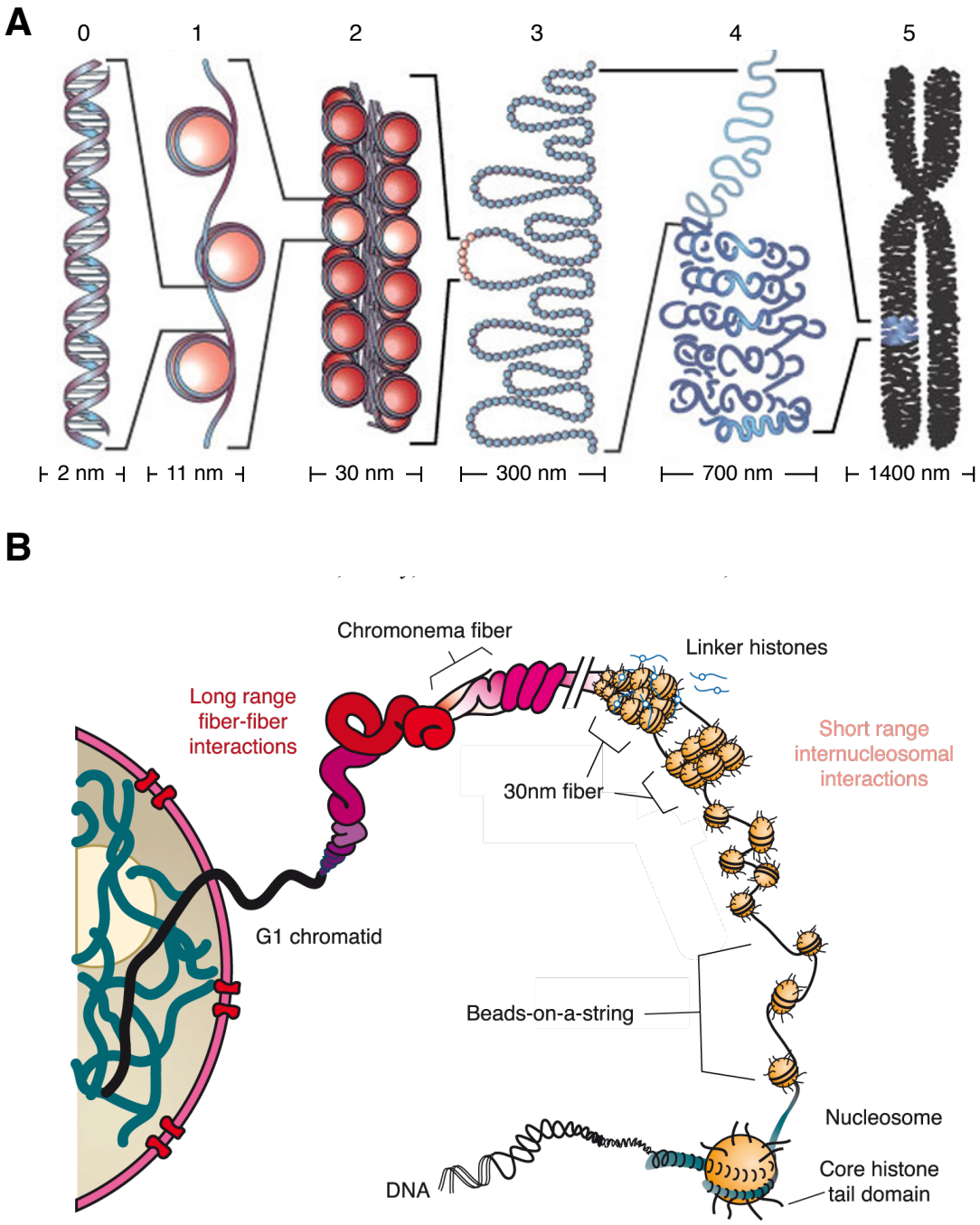

Figure 2.3: **Different levels of DNA compaction in chromatin**
(A) Folding of DNA to static metaphase chromosomes. First level of DNA compaction is reached by wrapping of DNA (0) around the histone octamer, forming the nucleosomes (1). These strings of nucleosomes are further condensed forming the second level with the 30-nm fibers through histone tail-mediated nucleosome-nucleosome interactions (2). Further levels of compaction (3-5) still remain unclear, but at the end a microscopically visible metaphase chromosome is formed (5) (modified from [Felsenfeld and Groudine, 2003]).
(B) Model of chromatin compaction in a nucleus of a G1 active cell. First and second level folding as described in A, tail-mediated association of individual fibers produces tertiary structures, like chromonema fibers. In contrast A during G1 chromatin is not condensed to the highest level, the metaphase chromosome (taken from [Horn and Peterson, 2002])

The second model, called zigzag helix, proposes a two-start helix, in which the 10 nm fiber folds into a zigzag structure. Consecutive nucleosomes are next to each other in different helical stacks, connected by straight linker DNA [Khorasanizadeh, 2004; Schalch et al., 2005].
Analyses of DNA accessibility within *in vitro* assembled chromatin fibers revealed an interesting effect. The access of restriction enyzmes to nucleosomal DNA decreased up to 8 fold when a higher-order chromatin fiber was formed. Strikingly, the accessibility to the linker DNA decreased as much as 50 fold compared to free DNA [Poirier et al., 2008]. These results indicate that in higher-order chromatin nucleosomes are not only the first level of compaction, but furthermore maintain dynamic accesses to the genomic information. The next folding steps on the way to an optically visible metaphase chromosome remain elusive. As displayed in figure 2.3 A, two further levels of condensation are proposed (3 and 4) until the 10,000 fold compacted metaphase chromosome is formed. Formation of these very condensed separable chromatin units takes only place during mitosis, after the nucleus has disintegrated. The model depicted in 2.3 B shows an example of the chromatin condensation within the nucleus of a cell in G1-phase. Even if little is known about the detailed structure of the higher hierarchy levels, more and more evidence is found, indicating that non-coding RNA plays an important role in establishing these structures [Pederson and Bhorjee, 1979; Mondal et al., 2010].
It is thought that the three-dimensional organization within the nucleus is maintained by tethering large chromatin domains to a karyoskeleton. These structures are called nuclear-matrix or scaffold and the specific DNA elements binding to it are termed **M**atrix **A**ttachment **R**egions (MAR) or **S**caffold **At**tachment **R**egions (SAR) accordingly [Hancock, 2000; Cremer et al., 2004].

2.1.5 Nuclear compartments

A first model addressing the question how chromosomes, visible during mitosis, are organized during interphase was proposed by Carl Rabel in 1885. He proposed a local distribution of single chromosomes in defined territories even during interphase [Rabel, 1885]. A few years later the term "chromosome territories" was introduced by Theodor Boveri [Boveri, 1909].
These territories do not only reflect the proximity of adjacent regions of an individual chromosome, but also display a specific non-random radial distribution within a nucleus. Gene-poor, inactive chromsomal segments are located in the nuclear periphery and gene-rich, active regions are more centrally positioned [Zink et al., 1998; Tanabe et al., 2002]. This correlation of structure and function is also observed for chromosome territories.

For example the human chromosome 19, with the highest gene density, is found in the interior of nuclei, whereas the gene poor chromosome 18 is located at the nuclear periphery [Croft et al., 1999; Cremer et al., 2001, 2003].

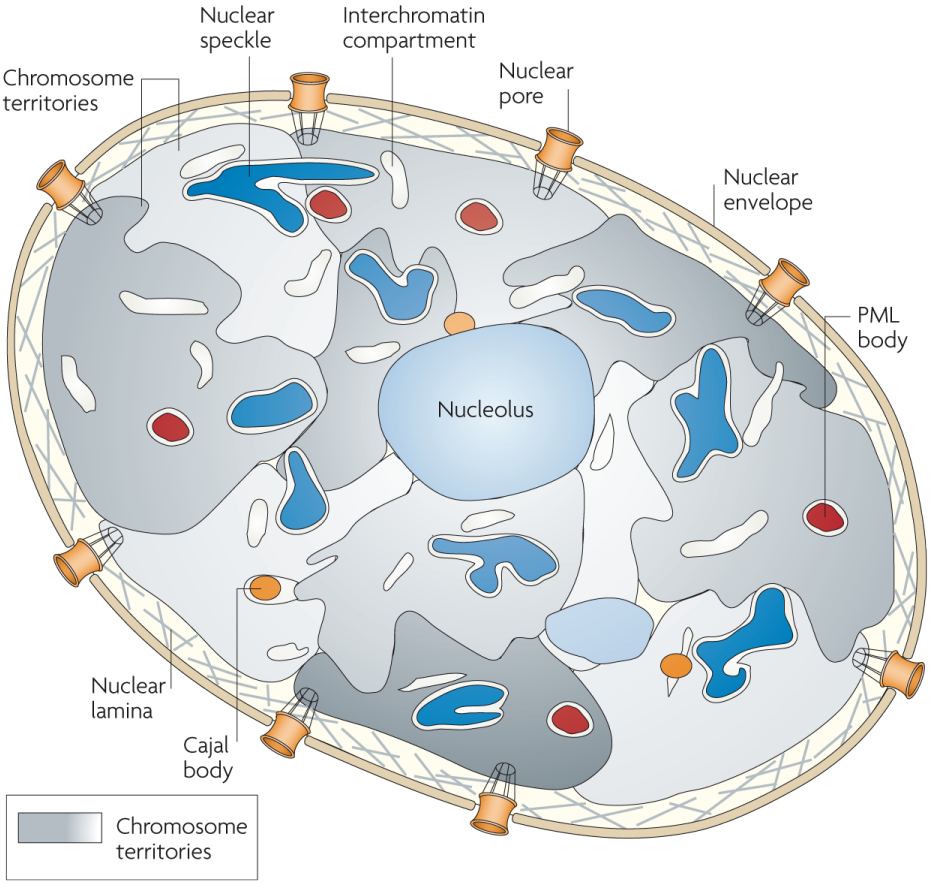

Figure 2.4: **Chromosome territories within a human nucleus**
The nuclear envelope and lamina define the border of the nucleus, while pores allow gated transport through this barrier. Chromosomes are localized within the nucleus at defined chromosome territories (CTs), and also higher-order chromosome territory interchromatin-compartments (CT-IC) are depicted (white). Nuclear organizer regions (NORs) form the nucleolus. Several distinct substructures can be found in larger ICs: Nuclear speckles (dark blue), Cajal bodies (orange) and PML bodies (red) (taken from [Lanctôt et al., 2007]).

But the nuclear architecture is even more complex since there exist many subcompartments in the nucleus (figure 2.4). Between these higher-order chromatin compartments, also chromatin-free domains are present. Lined by chromatin-domains, ribonucleoprotein networks are located within these areas.

One of these RNA-rich compartments are the Cajal bodies, involved in processing of nuclear RNA and assembly of spliceosomal components [Stanek and Neugebauer, 2006]. Another defined structure are the PML bodies, specified by an enrichment of the **P**ro-**m**yeolotic **L**eukemia (PML) RING-finger protein. Several functions in DNA repair, tumor suppression, viral pathogenicity and transciptional regulation are implicated [Brand et al., 2010], but the precise functions of PML bodies in these processes is still unknown. However their formation seems to be mediated by telomeric DNA [Brouwer et al., 2009]. Nuclear speckles are irregular structures with high concentrations of splicing factors and small ribonucleoprotein particles [Lanctôt et al., 2007].
The nucleolus is formed by clustering of **N**ucleolar **O**rganizer **R**egions (NORs) of the acrocentric chromosomes. The function of this compartment is well known. RNA polymerase I dependent transcriptional activity of *rRNA* genes and maturation of ribosomal RNA takes place within the nucleolus. As a consequence of the high transcriptional activity, the DNA is in a very open conformation. Therefore, the nucleolus appears as a region of low DNA density under the microscope.

2.2 Chromatin dynamics

2.2.1 Chromatin movement

Recent advances in high resolution single cell microscopy further indicate that higher-order structure of chromatin has a major impact on gene expression and regulation [Cremer et al., 2004; Lanctôt et al., 2007]. Generally, transcriptionally active euchromatin is supposed to adopt open conformations. Therefore, gene-rich domains are enriched in open chromatin fibers, whereas more condensed heterochromatin is inactive [Gilbert et al., 2004].
Long term changes in the activity of gene expression coincide with remodeling of higher-order chromatin structure. With respect to changes of the gene activity chromatin domains move closer to open, internal regions or to compacted areas in the nuclear periphery (figure 2.5) [Cremer et al., 2001]. Using the *E. coli* lacO/lacI repressor system in human cells, it could be shown that recruitment to the nuclear lamina leads to down regulation of adjacent chromatin domains. The down regulation of gene expression in the nuclear periphery was dependent on the activity of histone deacetylases [Finlan et al., 2008]. Obviously, remodeling of chromatin is one cause for alterations in transcriptional activity, rather than being a consequence of this effect. From this point of view, the process of cell differentiation implicates not only a cell specific expression pattern, but also generation of a nuclear architecture reflecting this specific activity profile [Cremer et al., 2001].

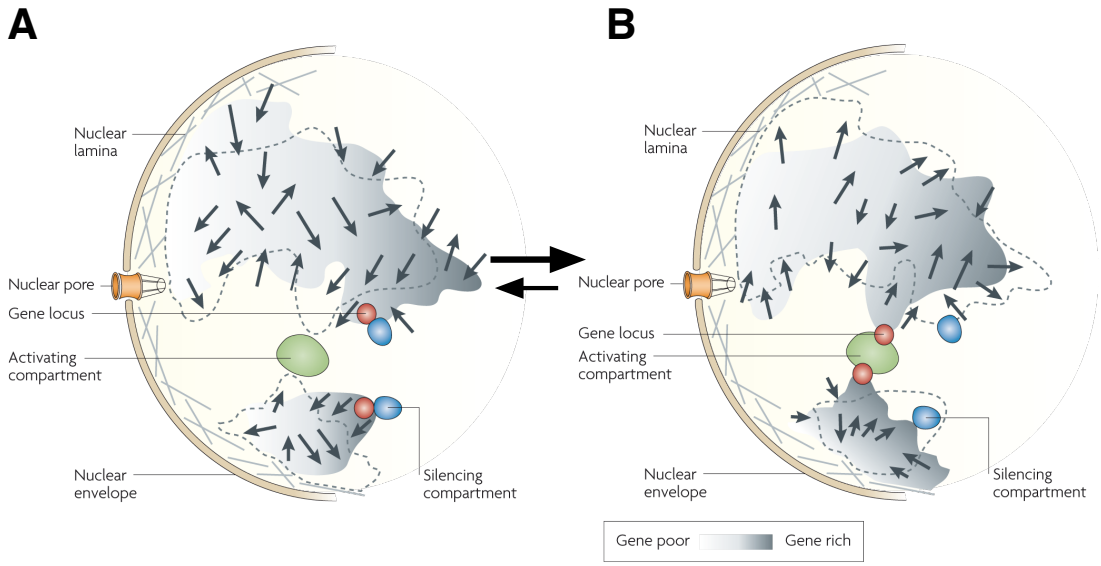

Figure 2.5: **Chromatin movement within a nucleus**
(A) Two gene loci (red) of different chromosome territories (grey) are interacting with a pre-existing silencing compartment (blue). Movement of the chromosome territories is indicated by arrows, structural changes before and after remodeling are superimposed by dotted lines.
(B) Repositioning of these loci from the silencing compartment to an activating one (green) induces gene activity (from [Lanctôt et al., 2007]).

2.2.2 Histone modifications

Another important level at which activity of genomic elements is regulated are post-translational modifications of histones. These modifications affect chromatin directly at the nucleosomal level. As already mentioned in section 2.1.3, unstructured N-terminal histone domains are the primary target site for such covalent modifications. These structural alterations are highly dynamic and well regulated by specific enzymes. The vast variety of modifications and the combinatorial complexity, which generates modification patterns, led to the proposal of a "histone code" hypothesis [Strahl and Allis, 2000; Fischle et al., 2003]. The defined histone patterns affect chromatin structures and direct interacting proteins, therefore specifically regulate the activity of chromatin regions.

2.2.2.1 Histone methylation

Methylation of arginine and lysine residues are the best described post-translational modifications of histone proteins. For histone H3 mono-, di- and tri-methylation at residue K4, K9, K27 and K36 is known, and at lysine K20 for histone H4.

Additionally, also lysine 79 within the globular domain can be modified [Vakoc et al., 2006; Vaquero et al., 2003]. Modification of H3K4 is involved in the activation of gene transcription and marks active genes [Santos-Rosa et al., 2002; Vaquero et al., 2003; Bannister et al., 2005; Bernstein et al., 2005]. Genome wide studies revealed an increase of H3K4 di- and tri-methylation at open, DNaseI sensitive sites [Consortium et al., 2007].

In contrast, methylation of lysine 9 of histone 3 (H3K9) is associated with heterochromatin formation and transcriptional repression. As expected for heterochromatin H3K9 tri-methylation is underrepresented in early replicating genome segments. Late replicating ones show a higher occupancy of histones with this mark [Consortium et al., 2007] and are found in pericentromeric regions, together with mono-methylated H3K27 [Peters et al., 2003; Martens et al., 2005]. At these sites, no enrichment of the mono- and di-methylated forms of H3K9 (H3K9me2 and H3K9me1) or H3K27me2 and H3K27me3 is detected, underlining the specific functions of differentially methylated histones [Peters et al., 2003; Vakoc et al., 2006]. In contrast to these findings, H3K9me3 is also found at some active genes [Margueron and Reinberg, 2010; Campos and Reinberg, 2009]. For H3K27, it is known that methylation strongly facilitates binding of the polycomb (PC) protein, mediated by the methylation sensitive chromo domains. This binding leads to silencing of the developmentally important homeotic (Hox) genes [Cao et al., 2002].

The transfer of a methyl group from **S**-**A**denosyl-L-**M**ethinone (SAM) to the ϵ-amino group of theses lysine residues is catalyzed by **H**istone **M**ethyl **T**ransferases (HMT). The corresponding modification of arginine residues is catalyzed by **P**rotein **A**rginine **M**ethyl**t**ransferases (PRMT) [Vaquero et al., 2003]. The homolog to *Drosophila* Suvar3-9 (**Su**ppressor of position effect **var**iegation) was the first human HMT [Rea et al., 2000], with a SET domain as active core [Zhang and Reinberg, 2001]. Suvar3-9 catalyzes the methylation of histon H3 at lysine 9 and therefore plays an important role in heterochromatin formation. H3K9 methylation if followed by binding of **H**eterochromatin **P**rotein **1** (HP1). Binding of HP1 to the methylated H3 is also mediated by chromodomains and represents a characteristic mark of inactive heterochromatin [Lachner et al., 2001].

Until discovery of the first enzyme catalyzing the removal of methyl groups from histones, these marks were thought to be an irreversible modification, due to the kinetic stability of the nitrogen-methyl bond. This picture changed when the first demethylase LSD1 was found, catalyzing demethylation of lysine 4 in histone H3 [Shi et al., 2004]. Therefore, also histone methylation is a highly dynamic epigenetic modification.

2.2.2.2 Histone acetylation

Another well studied post-translational modification is the acetylation of histones. **H**istone **A**cetyl **T**ranferases (HAT) catalyze the transfer of an acetyl group from acetyl-coenzyme-A to the ϵ amino group of a histone lysine residue. This modification is observed at the N-terminal domains of all four core histones [Vaquero et al., 2003]. H3 is acetylated at lysine K9, K14, K18, and K23, histone H4 at residue K5, K8, K12, and K16, histone H2B at K5, K12, K15, and K20 and histone H2A only at K5 and K9 [Roth et al., 2001; Sterner and Berger, 2000].
One consequence of the acetylation at these residues is the neutralization of the positive charge of the amino groups. This decreases the affinity of histone tails to DNA and the ability to interact with other histones (see section 2.1.4) [Hong et al., 1993; Workman and Kingston, 1998; Vaquero et al., 2003]. In general, histone H3 and H4 acetylation is related to active gene transcription. Therefore, genome wide studies revealed a correlation of H3K4me2 and H3K4me2 methylated histone H3 and acetylation of H3 and H4 [Consortium et al., 2007].
The acetyl groups can be removed by one of the 18 human HDAC enzymes. The consequence of deacetylation of histone tails is an increased intranucleosomal binding of these domains, because of the repolarization of the amino groups of the lysine residues [Luger and Richmond, 1998; Robinson et al., 2008]. Furthermore, loss of these marks results in a decreased binding of transcription factors, like TAFII mediated by bromodomains [Jacobson et al., 2000; Dovey et al., 2010]. All together, hypoacetylation by HDACs results in transcriptional repression [Vaquero et al., 2003].

2.2.2.3 Other histone modifications

Phosphorylation is an important post-translational modification regulating the activity of diverse cellular proteins. The four core histones and linker histone H1 are phosphorylated *in vivo* [Vaquero et al., 2003]. Modification of histone H1 and H3 by phosphorylation has been shown to play a role in condensation and segregation of chromosomes [Guo et al., 1995; Vaquero et al., 2003]. Phosphorylation of serine 10 in H3 (H3S10) obviously inhibits methylation of H3 at lysine 9, thus these two histone marks are mutually exclusive [Rea et al., 2000].
Another serine residue phosphorylated in eukaryotes is H3S28. Phosphorylation of H3P10 increases during cell cycle at the beginning of the G2 phase. First, pericentromeric heterochromatin is affected and then the signal spreads until metaphase to the rest of each chromosome [Hendzel et al., 1997]. Modification of H3 is catalyzed by several kinases [Vaquero et al., 2003].

Covalent conjugation of the 76 amino acid large ubiquitin protein to histones has two different functions [Conaway et al., 2002]. Poly-ubiquitination is a general cellular signal for protein degradation by the 26 S proteasome [Pickart, 2001]. In contrast to this mono-ubiquitination of histones acts in transcriptional regulation. Like acetylation, also ubiquitination of H2A and H2B can affect the chromatin structure by destabilizing the interactions with $(H3H4)_2$ tetramers [Li et al., 1993].
It was also reported that H3K4 methylation by Set1p is linked to mono-ubiquitination of H3K123 in yeast [Sun and Allis, 2002]. Ubiquitination of histones H2A and H2B are most abundant, but H3 and H1 are also conjugated to ubiquitin [Belz et al., 2002]. Mono-ubiquitination of H1 acts as an activating signal in combination with the transcriptional coactivator TAFII250 [Pham and Sauer, 2000]. Additionally, also a role in gene silencing is proposed [Huang et al., 1997].

Further support for a "histone code" is given by ADP-ribosylation of histones. NAD^+ as co-substrate links this modification to the activity of HDAC class III (see section 2.2.2.2) [Vaquero et al., 2003]. Because NAD^+ is also an important metabolic intermediate, these modifications can connect the transcriptional activity of a cell to the cellular energy state. Transfer of ADP-ribose to glutamic acid residues within stretches of polyglutamate or to single arginine residues is predominantly observed for histone H1 and H2B, but in general all histones can be ADP-ribosylated [Jacobson and Jacobson, 1999]. For histone H4, a strong correlation of ADP-ribosylation and hyperacetylation is observed [Golderer and Gröbner, 1991].

Lysine residues of histones are also substrates for carboxylases. Biotinylated forms of all histones can be found within a nucleus. Histone H4K8- and K12-biotinylation appears to be involved in the formation of heterochromatin structures and in gene silencing [Hassan and Zempleni, 2006; Vaquero et al., 2003].

Finally, also sumoylation, propionylation, and butyrylation of histones is observed [Smith and Denu, 2009]. In summary, post-translational modifications of histones allow the establishment of very defined signal patterns, however the detailed functions of all known modifications remain elusive.

2.2.3 DNA methylation

One of the most important epigenetic modifications is directly affecting the DNA. In the human genome DNA methylation occurs at the C-5 position of a cytosine base when being part of a CpG di-nucleotide [Hermann et al., 2004]. Positioned in the major groove of the DNA, this modification is very accessible for interacting proteins, while not interfering with the encoding Watson/Crick base-pairing. Hence 5-methyl-cytosine is very stable and plays an important and specific role in regulation of genetic activity. It is also referred as the 5th base of the genetic code.
DNA methylation generally leads to gene silencing, therefore playing an important role in gene regulation. Furthermore, it is crucial for maintaining the genome stability by inactivating transposable repetitive DNA elements [Yoder et al., 1997b].
In total only 1 % of all bases are 5-methyl-cytosine, but 70 - 80 % of all CpG di-nucleotides are methylated [Ehrlich et al., 1982; Jeltsch, 2002]. CpG di-nucleotides are unevenly distributed through out the genome. Regions enriched in CpG nucleotides are called **C**p**G** **I**slands (CGIs) [Jones and Liang, 2009]. Interestingly theses sequence motifs are over-represented in promoter and exonic regions of approximately 40 % of all mammalian genes [Kim et al., 2009]. Other parts of these genomes contain only a few CpG di-nucleotides, and these are largely methylated [Larsen et al., 1992; Kim et al., 2009].

2.2.4 Chromatin assembly

The process of assembling DNA into chromatin by deposition of positively charged histone proteins onto the negatively charged DNA is catalyzed and controlled by assembly factors. By this mechanisms the access of DNA dependent factors is tightly controlled and directly affects the activity of packed DNA sequences. The large pool of specialized histone variants (see section 2.1.3) in combination with the numerous post-translational modifications (see section 2.2.2), of which some are modified before deposition (e. g. H4K5 and K12 acetylation [Sobel et al., 1995]), make highly dynamic changes of chromatin structure and therefore also functionality possible.
Especially after replication histone deposition plays a crucial role for inheriting the epigenetic marks [Margueron and Reinberg, 2010]. The specific and well controlled process of chromatin assembly is catalyzed by specific protein factors. One class of these proteins facilitating nucleosome formation are histone chaperones. Factors like the **A**lternative **S**plicing **F**actor **1** (ASF1) interact with dimers of H3/H4 [English et al., 2006; Natsume et al., 2007] and load these nucleosome building blocks onto both strands of newly replicated DNA [Campos and Reinberg, 2009]. It is suggested that H3/H4 is deposited as tetramer, therefore two molecules ASF1 interacting with H3/H4 dimers are supposed to

transfer the histones to **C**hromatin **A**ssembly **F**actor **1** (CAF1), in turn assembling a tetramer onto the DNA [Ransom et al., 2010]. The tetramer assembly is followed by recruitment of two H2A/H2B dimers binding to each side of $(H3/H4)_2$ [Eitoku et al., 2008]. Other histone chaperones, e. g. **N**ucleosome **A**ssembly **P**rotein **1** (NAP1), and histone chaperone-like factors like for example FACT (**Fa**cilitates **C**hromatin **T**ranscription) or nucleoplasmin bind preferentially to H2A/H2B dimers. This suggests a role as supplier of histone H2A/H2B dimers to each histone $(H3/H4)_2$ tetramer during formation of a new nucleosomes [Eitoku et al., 2008]. NAP1 is not only described as assembly factor for core nucleosomes, but also for linker histone H1, modulating binding of H1 to the chromatin fiber [Kepert et al., 2005].
An important replication independent assembly activity is the exchange of canonical histones and variants. The SWR1 complex is known to specifically remove canonical H2A/H2B dimers and to replace them by H2A.Z/H2B dimers, thereby integrating H2A.Z into chromatin [Clapier and Cairns, 2009]. This is predominantly observed at promoters, where H2A.Z nucleosomes typically flank the nucleosome free regions. Histone variant H3.3 is deposited by the **Hi**stone **R**egulatory Protein **A** (HIRA) complex [Tagami et al., 2004].
Finally, the activity of nucleosome spacing factors is required to generate regularly spaced arrays of newly assembled nucleosomes, which is characteristic for the native conformation of chromatin [Haushalter and Kadonaga, 2003]. The **A**TP-utilizing **C**hromatin Assembly **F**actor (ACF), a protein complex containing the ATP-dependent nucleosome remodeling enzyme ISWI (**I**mitating **Swi**tch), is known to assemble chromatin *in vitro*. In the presence of the histone chaperone NAP1, it establishes regularly spaced nucleosomal arrays, including linker histone H1 [Haushalter and Kadonaga, 2003; Lusser et al., 2005]. A comparable activity is also shown by the CHD1 (**C**hromo-ATPase/**H**elicase-**D**NA-binding protein **1**), apart from H1 assembly into chromatin [Lusser et al., 2005].

2.2.5 ATP-dependent chromatin remodeling

Repositioning of nucleosomes changes of chromatin structure during replication, when newly synthesized DNA gets assembled into regularly spaced arrays. This activity is also needed independent from this process in order to alter the chromatin structure locally. The translocation of histone octameres relative to the bound DNA is catalyzed by so called "chromatin remodeling factors" in an ATP-dependent reaction.
Factors like ACF are known to rearrange nucleosomes to form regularly spaced arrays.

However, repositioning of nucleosomes in a DNA specific manner is much more complex. For example, ACF is capable of translocating nucleosomes at promoter sequences to defined positions, dependent on the underlying DNA sequence [Rippe et al., 2007].

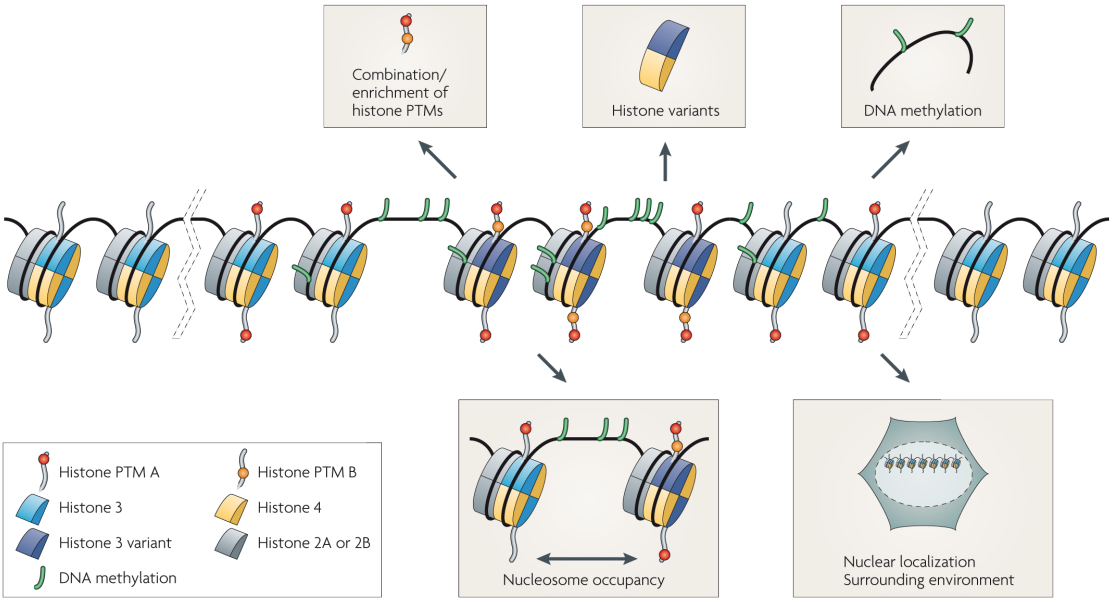

Figure 2.6: **Different levels of chromatin changes**
Chromatin is modified at different levels. Changes like post-translational modifications (PTMs) of histones, methylation of DNA, exchange of canonical histones, nucleosome occupancy and global nuclear arrangement of chromatin contribute to the characteristic of certain chromatin domains, influencing also the activity of these genomic regions (from [Margueron and Reinberg, 2010]).

The combination of all the different modifications depicted in figure 2.6 generates a specific landscape with patterns characteristic for individual chromatin domains. Since all modifications are dynamically regulated, this complex network allows a highly specific control of the nuclear activity of a human cell. But neither the detailed mechanisms of each regulatory level are known, nor the complex interactions connecting all processes within a nucleus are fully understood.

2.3 Chromatin remodeling

Chromatin remodeling resembles the basic level of structural dynamics. Global changes conducting transition processes during development and differentiation are based on molecular changes on the nucleosomal level. Remodeling enzymes regulate not only the access to DNA itself by changing the chromatin structure, but also interact in a coordinated manner with all different classes of chromatin modifying enyzmes, like HMTs, HDACs and DNMTs.

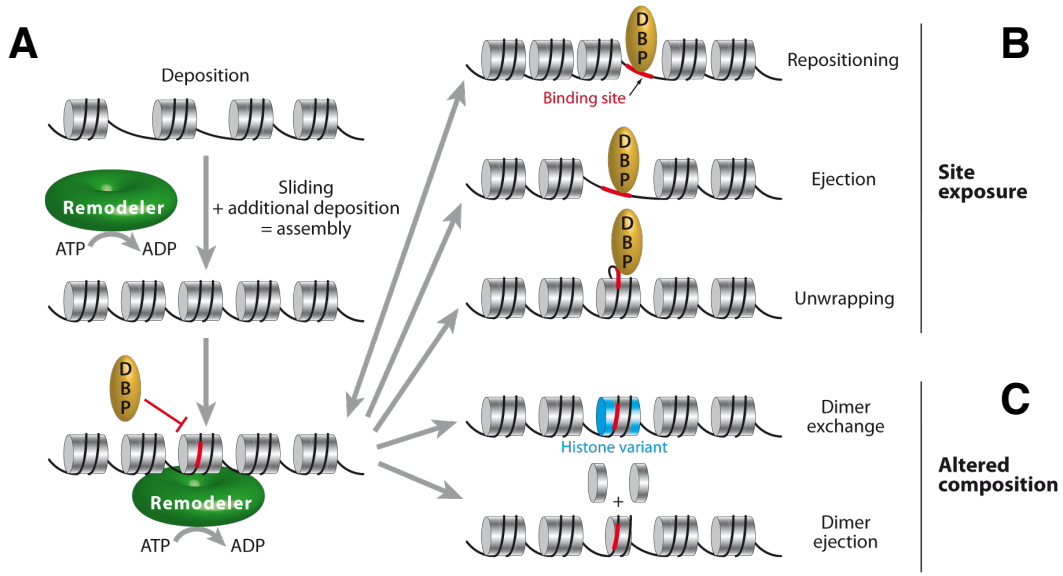

Figure 2.7: **Different activities of chromatin remodeling enzymes**
(A) Remodeling ATPases (green) can facilitate chromatin assembly and regularly space assembled nucleosomes.
(B) Repositioning or ejection of a nucleosome generates access to DNA (red) for a DNA-binding protein (yellow). The same accounts for local unwrapping of nucleosomal DNA.
(C) Remodeling enzymes also catalyze changes in the chromatin composition by exchange of histone dimers (e. g. H2A/H2B dimers) with an alternative dimer containing a histone variant (blue), or by ejection of dimers (from [Clapier and Cairns, 2009]).

2.3.1 Remodeling machines

The diversity of cellular processes accounts for a highly complex machinery to regulate chromatin structure specifically. This complexity is generated by a combination of active motor proteins and regulatory subunits, forming a large number of remodeling complexes.

The human genome encodes for 32 genes of non-redundant remodeling enzymes. Combinatorial assembly of several hundred different chromatin remodeling complexes expands the diversity of specifically controlled gene expression patterns [Rippe et al., 2007; Ho and Crabtree, 2010]. All ATP-dependent DNA translocases show two recA-like helicase domains in their active center, characteristically for helicase-like **S**uper**f**amily **2** (SF2). Conformational changes between these two domains, induced by hydrolysis of a bound ATP molecule, are the driving force of the translocation reaction, hence converting the chemical energy into mechanical force [Ye et al., 2004].

Based on the sequence similarity to the Snf2 protein from *Saccaromyces cerevisiae* members of this helicase-like superfamily are grouped into the Snf2 family (see figure 2.8). The gene coding for the yeast Snf2 protein was first described as ***S**ucrose **n**on-**f**ermenting gene **2** (sfn2)*, hence strains with a mutated allelw of this gene are unable to metabolize glucose [Neigeborn and Carlson, 1984]. Later, it was shown that Snf2 is a DNA stimulated ATPase relevant for transciptional activation [Laurent et al., 1993]. Today, 24 distinct subfamilies of the Snf2 family are identified [Flaus et al., 2006]. Although the Snf2 family is a large group of ATP-dependent enzymes, ubiquitously found in eukaryotes, not all members of this family are DNA tranlocases. For example Rad54 and Rad51 promote strand pairing, while Mot1 displaces the TATA-binding protein from DNA [Flaus et al., 2006]. Nevertheless, a large pool of Snf2 family members displays chromatin remodeling activity and participates in many DNA-mediated processes like transcriptional regulation, DNA repair, homologous recombination and chromatin assembly [Lusser and Kadonaga, 2003; Clapier and Cairns, 2009].

Apart from this classification based on multisequence alignments the remodeling enzymes are also grouped according to the domains flanking the catalytic helicase domains. Based on this more functional comparison four major classes of chromatin remodeling enzymes are distinguished: SWI/SNF, CHD, INO80 and the ISWI family [Clapier and Cairns, 2009] (see figure 2.9). According to the subfamily classification introduced by Flaus et al. shown in figure 2.8, the INO80 class is formed by subfamily members of the Swr1-like group, whereas SWI/SNF, CHD and ISWI class belong to the Snf2-like group.

2.3.1.1 SWI/SNF remodeler

The first member of the SWI/SNF (**Swi**tching defective/**S**ucrose **N**on-**F**ermenting) family remodeler was purified from *Saccharomyces cerevisiae* and composed of 8 to 14 subunits [Clapier and Cairns, 2009]. The characteristic bromodomain recognizes acetylated lysine residues. For yeast RSC4 it was shown, that the protein interacts not only with H3K14ac *in vitro* but also activates gene transcription *in vivo* [Kasten et al., 2004].

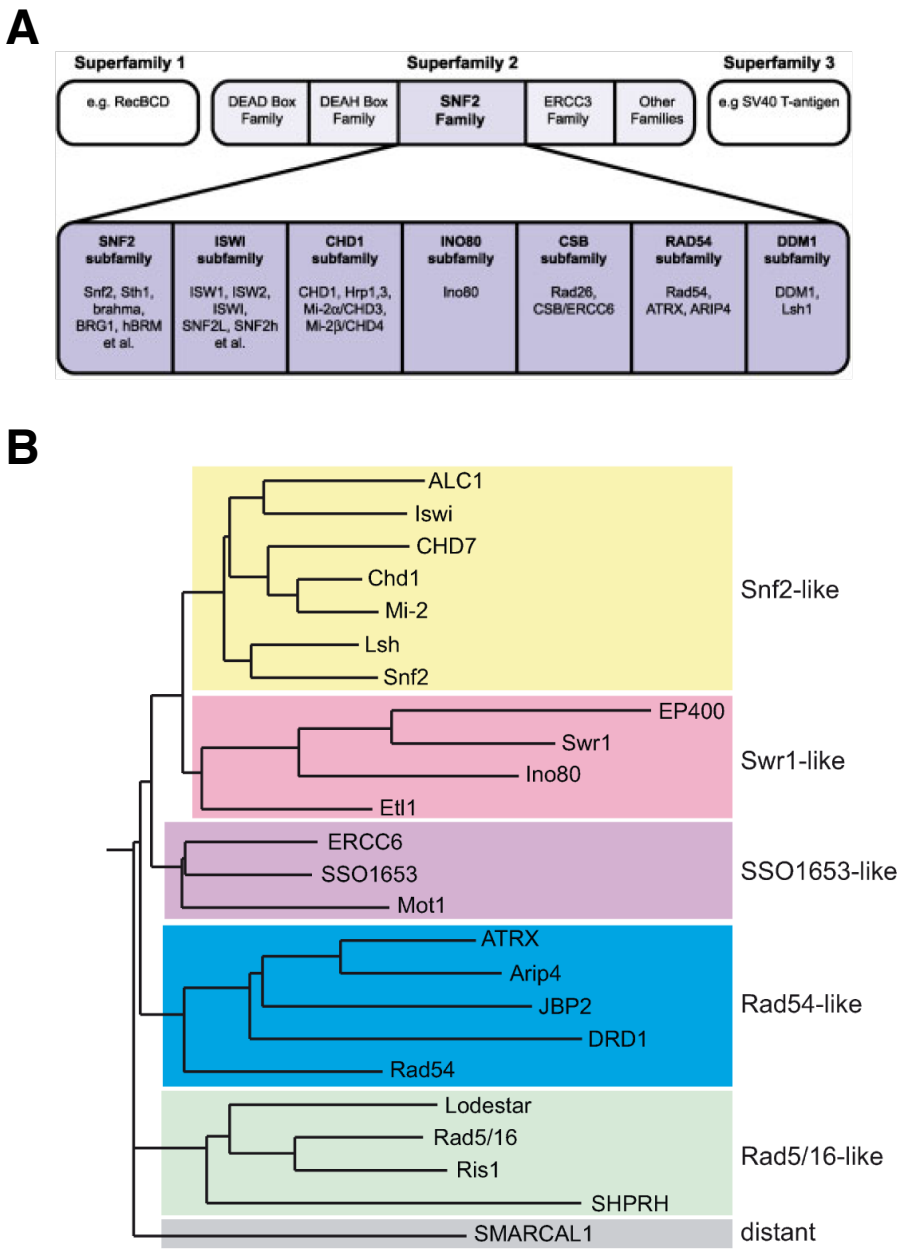

Figure 2.8: **Snf2 family of ATPases**

(A) Following the hierarchical classification, the SNF2 family is part of the helicase-like superfamily **2** (SF2). A similarity of the helicase-like regions to yeast Snf2p is characteristic for the Snf2 family. The Snf2 family is composed of a larger group of ATP-dependent enzymes, further grouped into subfamilies. A subset of these Snf2 subfamilies shows a chromatin remodeling activity [Lusser and Kadonaga, 2003].

(B) Relative distance of subfamily members shown as rooted tree, calculated using HMM profiles for full-length alignments of the helicase regions. Grouping of subfamilies is depicted by different colours (from [Flaus et al., 2006]).

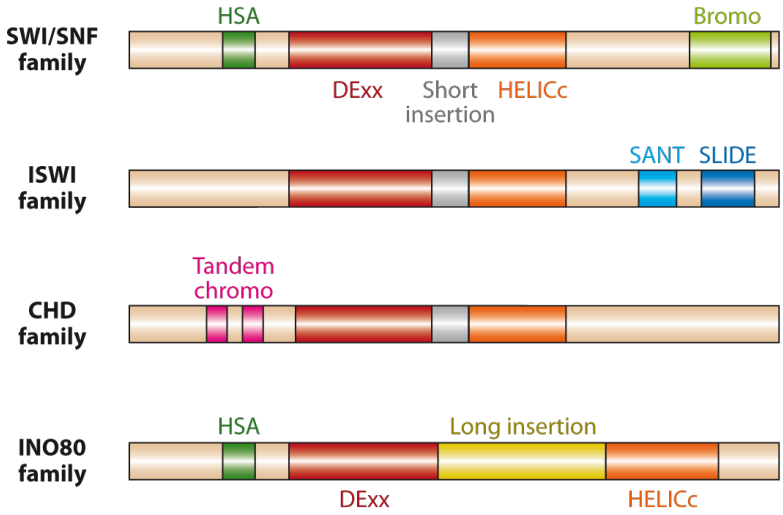

Figure 2.9: **Domain structure of remodeling ATPases**
The catalytic core of all remodeling ATPases is formed by two recA-like helicase domains: DExx (red) and HELICc (orange). The INO80 group has a characteristic long insertion (yellow) splitting both domains, whereas in all other families both helicase motifs are in relative proximity with a short insertion (grey). The bromodomain (light green) is characteristic for the SWI/SNF family, like the SANT-SLIDE module (blue) for ISWI family and the tandem chromodomains (magenta) for the CHD family. A HSA (helicase-SANT) domain (dark green) is present in members of SWI/SNF and the INO80 family (from [Clapier and Cairns, 2009]).

Mammalian genomes encode two homologous ATPases of the SWI/SNF complex. BRM (**Br**ah**m**a) and BRG1 (**B**rahma-**R**elated **G**ene **1**) are present in distinct complexes, e. g. in association with BAF155 or BAF170 (**B**rahma-**A**ssociated **F**actor).
These BAF complexes play an important role during development and undergo progressive changes in subunit composition during these processes [Ho and Crabtree, 2010]. Recent studies reported, that BAF complexes are essential for maintaining pluripotency and self-renewal in mouse **E**mbryonic **S**tem **C**ells (ESCs) [Yan et al., 2008; Gao et al., 2008; Ho et al., 2009]. The stem cell specific complex, called esBAF, contains BRG1 as an ATPase instead of BRM and BAF155 rather than BAF170 [Yan et al., 2008], regulating the transcriptional network of the ESCs [Ho and Crabtree, 2010]. Deletion of BAF155 is lethal to the embryo prior implantation [Klochendler-Yeivin et al., 2000; Kim et al., 2001]. Furthermore RNAi-mediated depletion prevents silencing of *Nanog* and suppressed compaction of chromatin and heterochromatin formation during differentiation. This underlines the crucial role of esBAF for facilitating the exit from self-renewal state and subsequent differentiation into cells of distinct lineages [Ho and Crabtree, 2010].

2.3.1.2 CHD remodeler

The CHD (**C**hromodomain, **H**elicase, **D**NA binding) remodeler are characterized by their two chromodomains and were first described in *Xenopus laevis*. These domains mediate binding to methylated lysine, but also interact with DNA and RNA [Brehm et al., 2004]. The tandem chromodomains of hCHD1 were shown to bind to H3K4me2 or me3, therefore recruiting the remodeler to active chromatin [Flanagan et al., 2005; Sims et al., 2005]. On polytene chromosomes from salivary glands of *Drosophila melanogaster* larvae dCHD1 localizes to regions associated with high transcriptional activity [Stokes et al., 1996]. CHD1 ATPase from *Drosophila* is active as monomeric protein, although it can associate with further regulatory subunits [Lusser et al., 2005]. *In vitro* dCHD1 shows a chromatin spacing and assembly activity, but does not incorporate the linker histone H1 into nucleosomal arrays. Furthermore, it generates a shorter nucleosome repeat length compared to other remodeling factors [Lusser et al., 2005].
In mouse embryonic stem cells CHD1 is essential to keep chromatin in an hyperdynamic euchromatic state, therefore maintaining pluripotency [Gaspar-Maia et al., 2009]. In contrast to this activating complex, others including the vertebrate Mi2 (CHD3/CHD4) machines act as repressors. For example the NuRD (**Nu**cleosome **R**emodeling and **D**eacetylase) complex is associated with repressive functions. The **M**ethyl-CpG-**B**inding **Do**main (MBD) within this complex links DNA methylation to the activity of the associated histone deacetylases (HDAC1/2) [Flaus et al., 2006].

2.3.1.3 INO80 remodeler

Remodeling ATPases of the INO80 group are characterized by the relatively large insertion between both helicase domains (see figure 2.9). The yINO80 enzyme was the archetype ATPase of this group found in yeast, functionally related to the inositol biosynthesis [Ebbert et al., 1999]. Up to 15 subunits form the yINO80 complex. Interestingly also two proteins related to the bacterial RuvB DNA helicase, actin and three **A**ctin-**R**elated **P**roteins (ARP4, 5 and 8) are present in this complexes [Bao and Shen, 2007]. Mammalian ATPases of the AAA+ type (**A**TPases **A**ssociated with various cellular **A**ctivities) Tip49a and Tip49b, like RVB1 and RVB2 from yeast, show a limited homology to bacterial RuvB, the Holliday Junction DNA Helicase [Bao and Shen, 2007]. Since the purified INO80 complex is active as an ATP-dependent helicase, INO80 and possibly also SWR1 may represent eukaryotic homologous of RuvB. The helicase activity in combination with the nucleosome remodeling capacity suggests that the INO80 complex participates in multiple DNA repair pathways by regulating the accessibility of DNA repair proteins to double strand breaks [Shen et al., 2000; Bao and Shen, 2007].

Another important remodeler of the INO80 class is the SWR1 ATPase. The homonymous SWR1 complex consists of 13 further subunits, including actin, ARP4, RVB1 and RVB2, that are also present in the yINO80 complex. In the human system SRCAP (**S**nf2-**R**elated **C**REB-binding Protein **A**ctivator **P**rotein) is the homolog to ySWR1. An active complex with hSRCAP as motor protein catalyzes the exchange of H2A/H2B dimers with the variant H2A.Z/H2B, thereby integrating this alternative form into chromatin [Flaus et al., 2006; Bao and Shen, 2007].

2.3.1.4 ISWI remodeler

The first discovered member of the ISWI class remodeler was the **I**mitation **Swi**tch (ISWI) factor from *Drosophila melanogaster* [Elfring et al., 1994]. They all have two catalytic DExx and HELICc domains that are highly conserved between most remodeling enzymes. Further are three characteristic binding domains found at the C-terminal end of the proteins. The SANT (**S**WI3, **A**DA2, **N**-CoR and **T**FIIIB) domain belongs to the cMyb domains and is negatively charged, therefore promoting binding to positively charged histone tails. This interaction significantly enhances activity of the enzyme [Boyer et al., 2002; Grüne et al., 2003; Boyer et al., 2004]. Close to this nucleosome binding module, separated by a small spacer, is also a DNA binding motif, the positively charged SLIDE domain (**S**ANT-**Li**ke **D**omain).
Binding to DNA is essential for the catalytic activity, whereas deletion mutants lacking the SANT domain remain basal ATPase and remodeling activity [Grüne et al., 2003]. The third domain is the HAND domain, directly linked to the SANT domain. Crosslinking experiments with yeast ISW2 revealed, that the HAND domain binds DNA near the entry site of the DNA at the nucleosomal surface, whereas the SLIDE domain binds DNA 20 bp distant from the nucleosome surface [Dang and Bartholomew, 2007]. Furthermore, it was proposed that the HAND domain might play a role in oligomerization of these motor proteins [Racki and Narlikar, 2008]. In contrast to most other remodeling enzymes, members of the ISWI class lack motifs binding to modified histone tails, like bromo- or chromodomains [Corona and Tamkun, 2004].
The ISWI ATPase itself shows nucleosome spacing activity *in vitro*, facilitating assembly and regular distribution of nucleosome arrays. Furthermore, its nucleosome mobilizing activity assists DNA binding factors to gain access to target sequences within chromatin [Längst et al., 1999; Di Croce et al., 1999; Hamiche et al., 1999; Whitehouse et al., 2003]. *In vivo* studies demonstrated that dISWI is predominantly found at heterochromatic sites of polytene chromosomes. ISWI plays an important role in condensation and heterochromatin formation of the X chromosome of male fruit flies [Deuring et al., 2000].

ACF Association of ISWI motors with distinct regulatory subunits, containing specialized binding motifs, increases specificity of the chromatin remodeling activity. The PHD domain (**P**lant **H**ome**d**omain) of ACF1 recognizes globular domains of histones, allowing a more specific targeting of the ACF (**A**TP-utilizing **C**hromatin Assembly and Remodeling **F**actor) complex. This multimeric complex is formed by a tetramer of two ISWI and two ACF1 proteins [Strohner et al., 2005; Racki et al., 2009]. Dimerization of two ACF1 molecules is supposed to be mediated by the HAND domains [Racki and Narlikar, 2008]. Association to dACF1 significantly increases remodeling and ATPase activity of dISWI [Ito et al., 1999; Eberharter et al., 2001].
But the non-catalytic ACF1 subunit has further functional impact than just stimulating the activity of the motor protein. The formation of the ACF complex changes the way sequence/structure information is interpreted and also the directionality of movement of mononucleosomes [Eberharter et al., 2001; He et al., 2006a; Rippe et al., 2007; He et al., 2008]. Human and *Drosophila* ACF has also the capability to generate regularly spaced nucleosomal arrays. hACF establishes these defined structures by generating a dynamic distribution of nucleosome positions. Kinetic discrimination of different flanking DNA lengths leads to accumulation of arrays with distinct spacing [Racki and Narlikar, 2008]. The mammalian ACF complex, formed by ACF1 and SNF2H, the homolog to ISWI, is enriched in replicating pericentric heterochromatin, suggesting that this complex is required for efficient replication through condensed heterochromatin [Collins et al., 2002].

CHRAC The **Chr**omatin-**A**ccessibility **C**omplex (CHRAC) is an ISWI complex closely related to ACF. The first CHRAC complex was described in *Drosophila* with a catalytically active core formed by ISWI associated with ACF1. Additionally two histone-fold proteins CHRAC14 and CHRAC16, CHRAC15 and CHRAC17 accordingly in humans, bind to these remodeling factors [Varga-Weisz et al., 1997; Eberharter et al., 2001; Poot et al., 2000].
Yeast Dpb4, an ortholog to human CHRAC17 and *Drosophila* CHRAC14, is supposed to anchor itself to a region of extranucleosomal DNA, therefore facilitating binding of ACF1 [Dang et al., 2007]. Other groups studying the influence of these *Drosophila* histone-fold proteins reported a dynamic interaction enhancing the nucleosome movement [Hartlepp et al., 2005].
However, CHRAC is a highly abundant nucleosome remodeling complex, able to catalyze histone octamer sliding on DNA and its characteristic histone-fold proteins are highly evolutionarily conserved [Li et al., 2006].

RSF Another structurally well studied human ISWI-containing remodeling complex is RSF (**Re**modeling and **S**pacing **F**actor). This heterodimer harbors besides the hSNF2H ATPase a regulatory RSF1 (p325) protein. As shown for the other ISWI based complexes RSF also mediates nucleosome deposition and generates regularly spaced nucleosome arrays [LeRoy et al., 1998; Loyola et al., 2003].
Drosopila RSF is involved in replacement of H2A by its variant H2A.Z (called H2Av in *Drosophila*) and heterochromatin formation. Deletion of the RSF1 subunit reduces the level of H2A.Z. It is proposed that formation of heterochromatin propagates by assembly of nucleosomal arrays. Subsequent H3K9 methylation and HP1 binding, leads to further chromatin compaction [Hanai et al., 2008].

NoRC The diversity of functional different remodeling complexes generated by combination of one ATPase with distinct regulatory factors is nicely displayed by the **N**ucle**o**lar **R**emodeling **C**omplex (NoRC). As a consequence of the association with TIP5 (**T**TF1 **I**nteracting **P**rotein 5), SNF2H becomes specifically targeted to *rRNA* genes in mammals [Strohner et al., 2001; Santoro et al., 2002; Strohner et al., 2004; Németh et al., 2004].
Binding to a region upstream of the *rRNA* gene promoter is mediated by TTF1 and induces local remodeling of chromatin. This leads to a repressive environment around the transcription start site suppressing **RNA P**olymerase **I** (RNAPI) dependent transcription of ribosomal *RNA* genes.
Additionally, also a 150 - 250 nucleotide intergenic transcript of non-coding RNA plays a functional role in targeting of NoRC. As part of the active remodeling complex, the binding of this "**p**romoter **RNA**" (pRNA) to the *rRNA* promoter was shown to be a prerequisite for heterochromatin formation and nucleolar localization of NoRC [Mayer et al., 2006, 2008].
High resolution mapping of the nucleosome positions at this promoter revealed that NoRC induces translocation of a promoter-bound nucleosome. This moves from position - 157 to - 2 relative to transciption start site further downstream into the transcribed region to position - 132 to + 22, therefore down regulating RNAPI activity [Li et al., 2006; Felle et al., 2010].
Upon interaction with other chromatin modifying enzymes, *in vivo*, additional epigenetic modifications become covalently linked to the chromatin, establishing a pattern of repressive marks at these sites. Recruitment of DNA methyltransferases DNMT1 and DNMT3a results in methylation of *rRNA* genes and the histone deacetylases HDAC1 and HDAC4 remove activating marks, altogether efficiently inactivating these genes [Santoro et al., 2002; Strohner et al., 2004; Santoro and Grummt, 2005].

NURF In *Drosophila*, the **Nu**cleosome **R**emodeling **F**actor (NURF) was shown to alter the nucleosome positioning at the hsp70 promoter by using ISWI as motor protein and NURF301/NURF55 as regulatory factors [Tsukiyama and Wu, 1995; Martínez-Balbás et al., 1998; Xiao et al., 2001]. Human NURF is an example for the increased complexity within mammalian systems. Mammalian genomes encode two highly related ISWI homologs, as already mentioned SNF2H, and in addtion also SNF2L. hNURF was the first complex described using SNF2L as motor protein instead of SNF2H. BPTF (**B**romodomain **P**HD Finger **T**ranscription **F**actor) and RbAp46/48 (**R**etino**b**lastoma **P**rotein) are the human orthologs to NURF301 and NURF55 [Barak et al., 2003].
Interestingly, although using the same motor protein as ACF and CHRAC, NURF does not assemble regularly spaced chromatin rather than randomizing the spacing, which could assist RNAPII activation [Clapier and Cairns, 2009]. *In vivo* NURF-dependent remodeling is directly coupled to H3K4me3, mediated by the PHD domain of the hBPTF/ dNURF301 subunit, therefore maintaining expression of *Hox* genes during development [Wysocka et al., 2006]. Furthermore, inactivation of dISWI or dNURF301 displays the importance of NURF for maintenance of higher-order chromatin structure. In male fruit flies, mutation of both proteins causes decondensation of the X chromosome and moderate decondensation of mitotic polytene chromosomes [Badenhorst et al., 2002; Clapier and Cairns, 2009].

CERF The transcription factor CERC2 (**C**at **E**ye Syndrome Chromosome **R**egion, **C**andidate **2**), involved in neurulation, forms the CERF complex (**CE**RC2 **R**emodeling **F**actor) together with SNF2L. CERF represents the second chromatin remodeling complex with SNF2L as motor protein [Banting et al., 2005]. Like other regulatory subunits of remodeling complexes, also CERC2 contains AT hooks and a highly conserved bromodomain [Chen et al., 2010].
ATP hydrolyzing activity of CERF is stimulated by nucleosomes and displays *in vitro* activity in nucleosome remodeling assays. Together with the predominantly neural expression of CERC2 in mouse embryos, it is suggested that this chromatin remodeling complex plays a critical role in neurulation [Banting et al., 2005].

2.3.2 Diversity of human ISWI remodeler

In contrast to *Drosophila*, human and mouse genomes encode two different remodeler homologs to dISWI called SNF2H (**S**urcorse **N**on-**F**ermenting **2** **H**omolog) and SNF2L. *In vivo* studies with mouse embryos showed a specific spatial and temporal expression pattern for SNF2H and SNF2L. Both genes are expressed during development of the

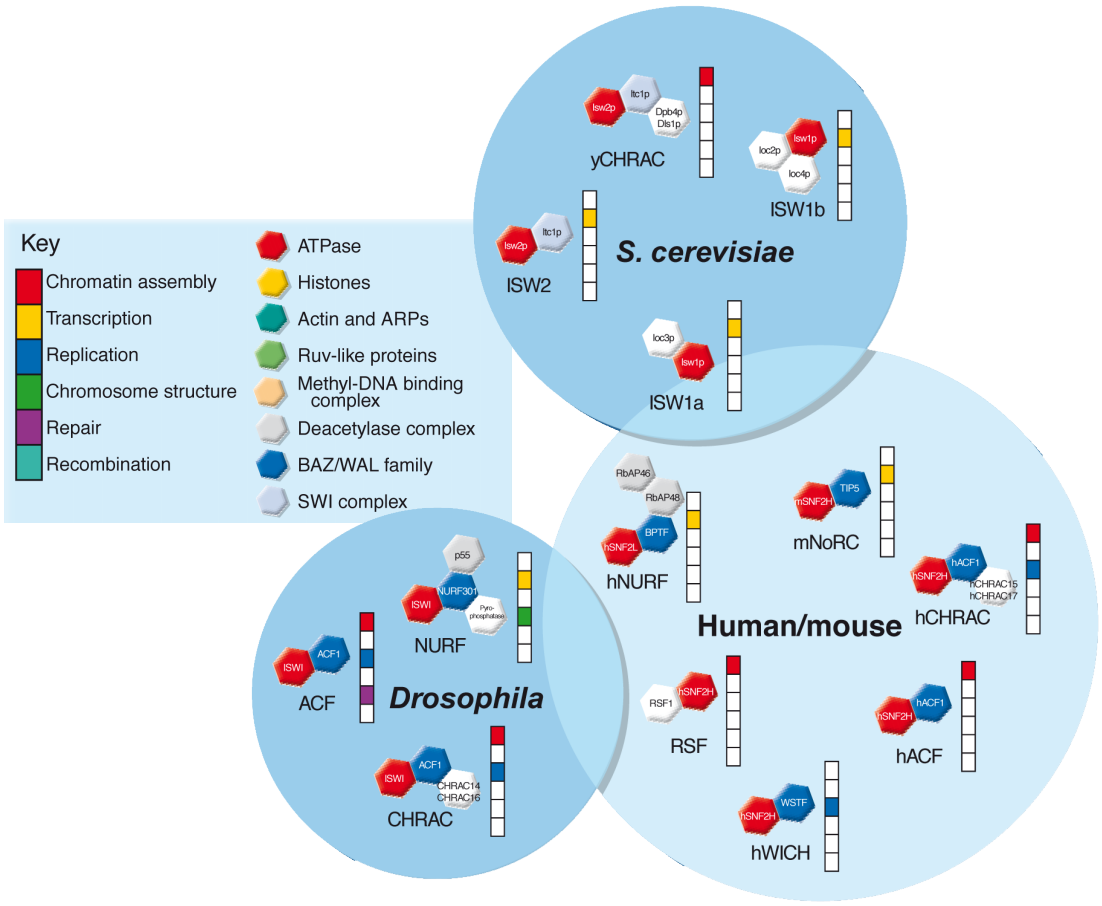

Figure 2.10: **Diverse complexes formed with ISWI ATPases**
The scheme illustrates the large number of different remodeling complexes that use an ISWI ATPase as motor protein. Here a comparison of different model organisms is shown, yeast, *Drosophila*, human and mouse (from [Eberharter and Becker, 2004]).

nervous system, but mSNF2H is only transiently expressed to high levels in proliferating cells during embryogenesis. In contrast to this, the expression of mSNF2L is increased when neuronal cells become post mitotic [Lazzaro and Picketts, 2001]. Further support for the idea of a special role of SNF2L in the neuronal development is given by the fact that this ISWI ortholog is predominantly found in remodeling complexes known for neurone specific activity.
Human and murine ACF, CHRAC, RSF and NoRC are dependent on the activity of SNF2H, whereas SNF2L is found in NURF and CERC complexes. This formation of specialised NURF complexes is not observed in *Drosophila* with only one ISWI remodeler.

In mouse, it was shown that mNURF regulates the expression of the *engrailed* gene, coding for a homeodomain protein crucial for neuronal development in the mid-hindbrain [Barak et al., 2003]. SNF2L is expressed only in the brain and gonadal tissue. In contrast to this, human SNF2L is expressed ubiquitously, like SNF2H. Interestingly, in human tissue specific remodeling activity is regulated by isoform variation. Therefore, in non-neuronal tissues a catalytically inactive SNF2L splice variant, called SNF2L+13, carrying an additional in-frame exon within the ATPase domain is predominantly expressed. By this mechanism, the activity of SNF2L is mainly restricted to neuronal and gonadal tissue, like in mouse [Barak et al., 2004].
Further interesting functional differences were observed by knock-down experiments in diverse human cancer cell lines. The knock-down of hSNF2H did not inhibit growth, but some highly malignant human cancer cell lines, e. g. cervix carinoma cells of the HeLa line, showed a decreased growth rate and went into apoptosis after depletion of hSNF2L. Over-expression of hSNF2h in these SNF2L knock-down cells did not rescue the cells from induced apoptosis. It is suggested that SNFL is a crucial factor for survival, growth, and renewal of these cancer cells [Ye et al., 2009].
Furthermore these results support a functional difference of both homologs also for human cells. Despite all these hints pointing to a specialized function of these orthologous, the molecular basis of these observed differences remains poorly understood.

2.3.3 Developmental role of chromatin remodeling complexes

Chromatin remodeling complexes are important factors influencing nuclear programming, differentiation and pluripotency of stem cells [Ho and Crabtree, 2010; Ho et al., 2009]. Only little is known about the detailed functions of chromatin remodeler within this complex cellular network, but as depicted in figure 2.11 some key player of certain developmental steps are already identified. For example CHD1 is crucial for pluripotency of ESCs by opening chromatin stucture [Gaspar-Maia et al., 2009]. SNF2H containing complexes are essential during early development, since mice lacking SNF2H die after embryonic implantation [Stopka and Skoultchi, 2003]. For SNF2L, a role in neuronal development is known [Banting et al., 2005]. The esBAF complex is in general required for pluripotency and self-renewal [Fazzio et al., 2008]. However, after depletion of BRG1 in murine ESCs a more complex pattern of up- and down-regulated genes is observed. Certain genes important for pluripotency like *Oct4* and *Nanog* become de-repressed, while other genes are down-regulated [Ho et al., 2009; Ho and Crabtree, 2010]. These results indicate the essential function of esBAF during development, although detailed functions of the expression patterns regulated by this complex remain unclear.

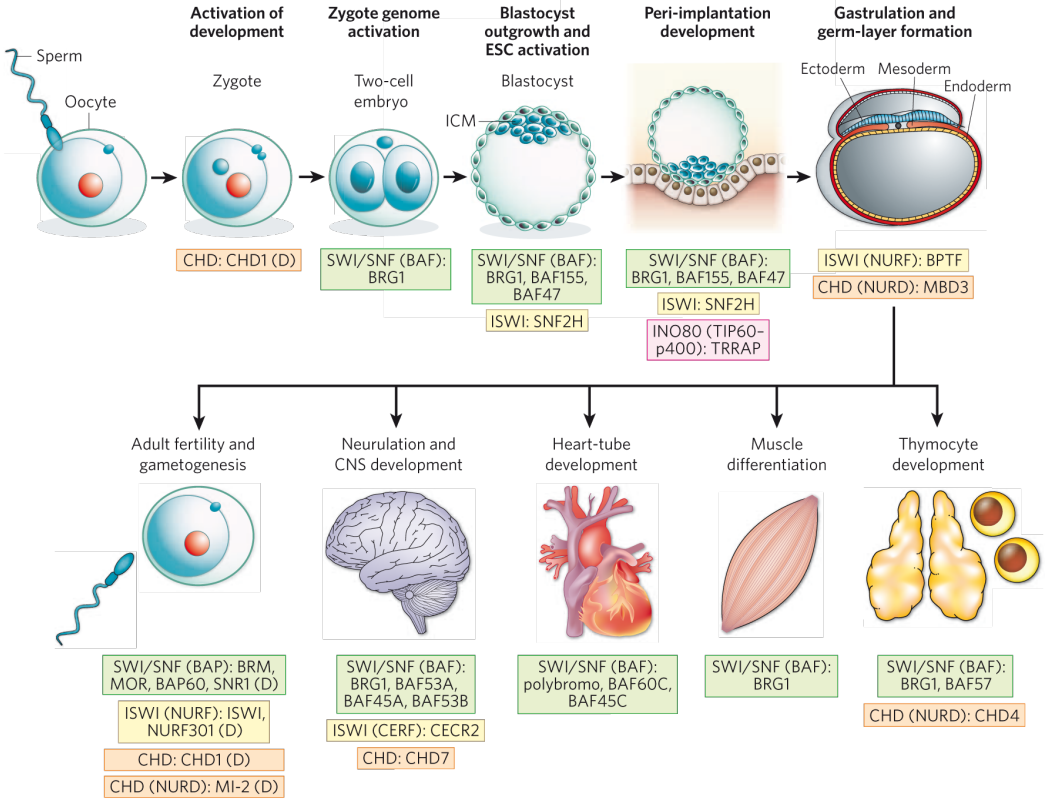

Figure 2.11: **Role of chromatin remodeling ATPases during development** Each remodeler class is highlighted by different colours: SWI/SNF (green), ISWI (yellow), CHD (orange) and INO80 (pink). The family name and the name of known proteins playing an important role are mentioned at the corresponding developmental step. In general, development of the mouse model is shown, in cases where only the function of a *Drosophila melanogaster* protein is known, it is commented by a (D). CNS: central nervous system, IMC: inner cell mass, MOR: moria (from [Ho and Crabtree, 2010]).

2.3.4 Mechanism of nucleosome remodeling

For a better understanding how distinct remodeling complexes generate these specific readouts from the same genomic information, the detailed steps of the translocation reaction have to be considered. After several years of intensive work and discussions the so called "loop recapture" model seems to display a common mechanism explaining the translocase activity of remodeling ATPase in general [Strohner et al., 2005; Cairns, 2007].

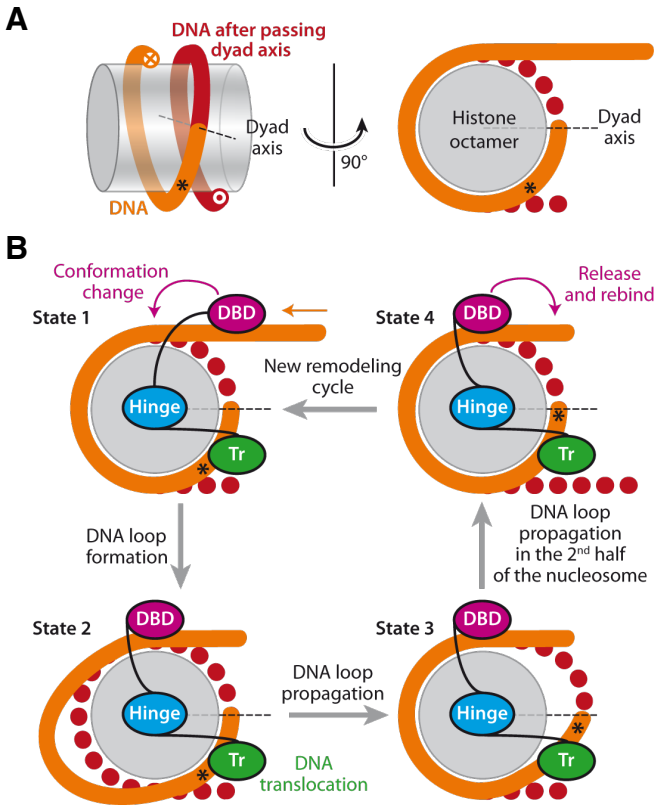

Figure 2.12: **DNA movement around the histone octamer during remodeling reaction**
(A) DNA (red/orange) is wrapped in two helical turns around the disc shaped histone octamer core (grey). The asterisk (*) marks a reference point to illustrate movement of the DNA.
(B) According to the "loop recapture" model, the translocation reaction is initiated (State 1) by binding of the **D**NA-**B**inding **D**omain (DBD: pink) and the catalytic **tr**anslocase domain (Tr: green) to the nucleosomal DNA. (State 2) A conformational change induced by the translocase domain leads to local disruption of DNA-histone-contacts and formation of a DNA loop. (State 3) The remodeling enzyme stays fixed to the substrate, therefore the loop propagates into the nucleosome. (State 4) After the loop has resolved and the conformation of the remodeler is reset, the system can initiate a new remodeling cycle (from [Clapier and Cairns, 2009]).

A prerequisite for physical movement of the histone octamer is the stable binding of the molecular machine to at least two different topological sites of the substrate. For the ISWI remodeler, it was already mentioned in section 2.3.1.4 that the SLIDE domain resembles a specialized DNA binding domain, contacting DNA close to the entry/exit site of the nucleosome. Cross-linking studies also revealed binding of the catalytic translocase domain [Kagalwala, 2004; Zofall et al., 2006].

The conformational change induced by the catalytic helicase domains changes the relative distance of both nucleosome binding domains (see also figure 2.12). This coordinated movement of the DNA binding domain and the translocase domain disrupts local histone-DNA contacts and forms a small DNA loop. The energy costs of such local disruption of DNA-histone contacts are much smaller than for a complete dissociation of DNA from the histone octamere surface, which would make the reaction very unlikely from an energetic point of view. Keeping the DNA bound at the site of initiation, the DNA loop has to propagate around the histone octamer surface in a one dimensional diffusion. This stepwise disruption and reformation of histone DNA contacts is driven by the mechanical stress introduced by the initial conformational changes and does not cost further energy. When the loop meets the distal nucleosomal boundary it resolves when detaching from the histone octamer surface. As a consequence of this, DNA has moved around the histone octamer surface. From this point a new round of loop initiation and propagation could start [Strohner et al., 2005; Cairns, 2007; Clapier and Cairns, 2009].

The directionality of this movement and the number of single translocation reactions, determining the total remodeling distance, can be modified by regulatory subunits. For example, SNF2H was shown to change its remodeling activity when associated with regulatory factors like ACF1. In comparison, the solely motor protein of this complex shows other substrate preferences regarding linker length and reactivity [He et al., 2006a; Yang et al., 2006; He et al., 2008; Racki et al., 2009]. One factor influencing the outcome of the remodeling reaction is the additional binding motif present in the regulatory subunits (e. g. bromodomain). Furthermore ACF obviously functions as a dimer of ATPases [Strohner et al., 2005; Racki et al., 2009]. Therefore the relative arrangement of the motor proteins within the complexes could influence the directionality of the transloction reaction.

After a successful remodeling reaction, different endpoints are possible. For ACF and CHD1 it was shown that these machines dissociate from the nucleosome after remodeling due to a reduced affinity (10 fold higher K_D) to the end-products of the translocation reaction, according to the so called "release" model. The enzymes are released and can again adopt an active conformation to start a new remodeling reaction.

Theoretically, an inverse mechanism is also possible, called "arrest" model, where the remodeling reaction is driven to end-product formation by an increased affinity to the remodeled nucleosome. In this case the remodeling complex stays bound to the nucleosome, resembling kind of a structural component of chromatin [Rippe et al., 2007]. Although there is evidence of some remodeler like NoRC following this mechanism, a conclusive experimental support is missing yet.

2.4 Methods for genome wide and single cell analyses

Recent advances in high resolution microscopy and genome wide sequencing technologies have a fundamental impact on the way the molecular assembly of DNA based biological structures can be dissected. These methods and technologies comprise automated high throughput DNA sequencing as well as sophisticated single cell imaging.

2.4.1 Next generation sequencing technologies

After great achievements that were made with the automated Sanger sequencing method, like the finished-grade human genome sequence and the first diploid genome sequence of a single person, a new generation of sequencing technologies emerged [Lander et al., 2001; Venter et al., 2001; International Human Genome Sequencing Consortium, 2004; Levy et al., 2007; Metzker, 2010]. All these so called "next generation sequencing" methods have in common that they allow a fast and cost effective determination of DNA sequence information even from large genomes. The commercially most successful methods, like the Solexa sequencing from Illumina and 454 sequencing from Roche, are based on clonal amplification of template DNA. Solid phase amplification for Solexa generates local clusters of clonal template molecules. The incorporation of specifically fluorescent labelled nucleotides during template dependent activity of DNA polymerase is followed optically. To allow a realtime analysis of single polymerase steps at these clusters, cyclic reversible 3'-terminated nucleotides are used. High resolution optics and the dense packaging of small clonal clusters allow several million independent sequencing reactions in parallel on a single chip. The incomplete chemical removal of 3'-terminator blocks from the incorporated nucleotides limits the sequencing depth to less than 100 bp.
Pyrosequencing like 454 is based on a chemoluminescent reaction following every nucleotide incorporation catalyzed by the polymerase. Here specificity of the reaction is controlled by diffusion of only single nucleotides into the reaction flow chambers. Therefore instead of terminator nucleotides, unmodified deoxy-nucleotides are used, allowing longer continuos sequencing reads with a few hundred base pairs. The less compact assembly of reaction chambers compared to clonal DNA clusters for Solexa sequencing limits the number of reads performed in parallel. Both methods deliver millions of base pair reads within a single sequencing reaction. Differences in the sequencing depth and number of independent reads obtained make both methods complimentary for specific applications. For *de novo* sequencing of complex genomes, the longer reads from 454 sequencer offer a better characterization of repetitive DNA elements, whereas comparative re-sequencing of genomes is more efficiently done with Solexa.

2.4.2 The ENCODE project

The fast growing number of sequenced genomes allows design and production of highly specific DNA microarrays covering these genomes. Although next sequencing technologies allow direct determination of sequence information, for certain applications microarrays are still competitive. One advantage is that in general for hybridization arrays, no clonal amplification of the template DNA is necessary. Therefore experimental errors induced by amplification bias of AT-rich or GC-rich target sequences are excluded [Metzker, 2010]. Of course microarray based approaches will address biological questions only within a pre-defined frame.
The ENCODE DNA hybridization chip is a good example how sequence information and additional functional genome studies can be performed with hybridization arrays. The finished-grade publication of the human genome sequence raised the question how genomic elements are temporally and spatially organized and how the functional readout, the gene expression, is controlled by this [Lander et al., 2001; Venter et al., 2001; Consortium et al., 2007].
To answer this, the **Enc**yclopedia **o**f **D**NA **E**lements (ENCODE) Project was founded. The aim was to identify and catalogue a set of functional DNA elements for further biological analyses. 35 international groups provided relevant sequence information covering roughly 1 % of the 3 billion base pairs of the human genome. These 30 Mb of cover 44 genomic regions, with 15 Mb chosen from 14 biologically well characterized regions and the other 15 Mb coming from 30 regions selected by a stratified random-sampling method [Consortium et al., 2007].
By defining this catalog of DNA elements, now a platform is established enabling a more focused work elucidating the functional meaning of genome information. For these annotated regions covering a broad set of functional genomic data is present and additional experimental data are still added. Therefore numerous transcripts, transcription start sites and transcriptional activity, chromatin accessibility and histone modification pattern, DNaseI hypersensitve sites and a lot more genomic features are already described for these ENCODE regions [Consortium et al., 2007]. Today, DNA microarrays with probes complementary to this 1 % of the human genome are commercially available at relative low costs.

2.4.3 Single cell microscopy

The high throughput sequencing of entire genomes using next generation sequencing technologies and the functional annotation and comparison have a dramatic impact on the way chromatin architecture can be analyzed. But these high throughput technologies share one general downside: They are all based on experiments performed with populations of cells. The heterogeneity of these populations is one general factor influencing the directness and impact of obtained experimental results. Furthermore higher organisms are diploid and most genes are expressed from only one of the two allels [Lanctôt et al., 2007]. Therefore, an intermediate global activity can be based on a repressed and a highly active copy of the same gene.
Single cell analyses resemble an elegant way to prove the general validity of results and models derived from high throughput data. Recent advances in high resolution microscopy enable imaging of single nuclei at resolutions beyond the classical Abbe limit [Lanctôt et al., 2007]. Multi-colour DNA and RNA fluorescent *in situ* hybridization and labelling of proteins allows a four-dimensional analysis of chromatin structure *in vivo* also addressing the question of cell-to-cell variability [Lanctôt et al., 2007; Strickfaden et al., 2010].

3 Objectives

3.1 Structural and functional analysis of human chromatin

Human epithelia carcinoma cells from the HeLa line are a well studied model system to analyze the functional and structural nature of human chromatin. Several approaches have been used to elucidate the organization of eukaryotic chromatin at the basic level. Enzymatic hydrolysis of DNA by micrococcal nuclease (MNase) and subsequent isolation of DNA fragments was done in several studies.
Saturating amounts of MNase were used and chromatin was digested down to nucleosomal core particles protecting 147 bp of DNA [Segal et al., 2006; Miele et al., 2008; Valouev et al., 2008]. Here all information encoded within the linker DNA as well as unstable nucleosomal particles were lost.
By using limited amounts of MNase to differentially digest chromatin to fragments larger than mono-nucleosomes, chromatin accessibility will be analyzed in a relative high resolution. This accessibility should display not only the nuclear architecture, but also reflect the activity of the genome region. Once a method for identification of active chromatin domains is established, this could be used to further study structural changes. The partial digestion will provide additional information from the linker DNA and will allow detection of less stable nucleosomes.

3.2 Comparative analysis of human ISWI homologs

SNF2H and SNF2L are two highly similar chromatin remodeling ATPases homologous to ISWI from *Drosophila*. Despite their highly similar protein structure, knock-down experiments in human cancer cell lines and a distinct spatial and temporal expression pattern of both homologs in mouse revealed that they are not redundant isoforms [Lazzaro and Picketts, 2001; Ye et al., 2009]. Nevertheless the detailed differences and molecular basis of this specialization remained unclear. Therefore an accurate functional comparison of both human ISWI remodeler in defined *in vitro* systems should gain insight into the molecular basis of the differences observed *in vivo*. The binding to nucleosomes, remodeling activity and also the ATPase activity will be dissected in these studies.

4 Materials and Methods

4.1 Materials

Unless otherwise stated, all common chemicals and materials were purchased from GE Healthcare (Freiburg), Merck (Darmstadt), Invitrogen (Karlsruhe), Fermentas (St. Leon-Rot), New England Biolab (Frankfurt am Main), Promega (Mannheim), Roche (Mannheim), Roth (Karlsruhe), Serva (Heidelberg), Bio-Rad (Munich), Stratagene/Agilent (Waldbronn) and Sigma-Aldrich (Munich). Radioactively labelled nucleotides were ordered at Hartmann Analytic (Brunswig).

4.1.1 Laboratory chemicals and biochemicals

Table 4.1: **Overview about used standard chemicals and biochemicals**

Material	**Supplier**
Acrylamide (Rotiphorese Gel™30)	Roth, Karlsruhe
Agarose (ME, LE GP and low melting)	Biozym, Hessisch Oldenburg
Ammonium acetate	Merck, Darmstadt
Ampicillin	Roth, Karlruhe
Aprotinin	Sigma-Aldrich-Aldrich, Munich
ATP	Sigma-Aldrich, Taufkirchen
α -^{32}P-ATP (300Ci/mmol)	Hartmann Analytic, Brunswig
γ-^{32}P-ATP(300Ci/mmol)	Hartmann Analytic, Brunswig
Bacto Agar	BD, France
Bacto Peptone	BD, France
Bacto Trypton	BD, France
Blue Gal	Invitrogen, Karlsruhe
Boric acid	Merck, Darmstadt
Bovine serum albumin (BSA), 98% pure	Sigma-Aldrich, Munich

Material	Supplier
BSA, purified	NEB, Frankfurt am Main
Bromphenolblue	Serva, Heidelberg
β-Mercaptoethanol	Sigma-Aldrich, Munich
Chloramphenicol	Roth, Karlsruhe
Coomassie G250	Serva, Heidelberg
DEAE Sepharose	GE Healthcare, Munich
DNA Ladder GeneRuler 1 kb Plus	Fermentas, St. Leon-Rot
DNA Ladder 2-Log	NEB, Frankfurt am Main
Dimethylsulfoxid (DMSO)	Merck, Darmstadt
Dithiothreitol (DTT)	Merck, Darmstadt
EDTA	Sigma-Aldrich, Munich
EGTA	Sigma-Aldrich, Munich
Ethidium bromide	Sigma-Aldrich, Munich
Glycerin	Merck, Darmstadt
Glycogen	Roche, Mannheim
HEPES	Roth, Karlsruhe
Hydrochloric acid	Merck, Darmstadt
IPTG	Roth, Karlsruhe
Orange G	Sigma-Aldrich, Munich
Phenylmethylsulfonylfluorid (PMSF)	Roth, Karlsruhe
Potassium chloride	Merck, Darmstadt
M2-agarose (Flag-beads)	Sigma-Aldrich, Munich
Magnesium chloride	Merck, Darmstadt
Nickel-NTA-agarose (Ni^{2+}-beads)	Qiagen, Hilden
TEMED	Serva, Heidelberg
PEG 8000	Roth, Karlsruhe
Sodium chloride	VWR, Munich
Sodium dodecyl sulfate (SDS)	Roth, Karlsruhe
Sodium hydroxide	Merck, Darmstadt
SYBR Safe	Invitrogen, Karlsruhe
Tris(hydroxymethyl)-aminomethan (TRIS)	USB, Cleveland, Ohio
TWEEN	Serva, Heidelberg

4.1.2 Membranes, culture dishes, reaction tubes and columns

Table 4.2: **Dialysis membranes, reaction tubes, dishes and columns**

Material	**Supplier**
BioMaxMS Foto Film	Kodak Film, Stuttgart
Columns, 1 ml, small filter 35 µm pore	MoBiTec, Göttingen
Columns, Sephadex G-50	GE Healthcare, Munich
Dialysis membranes, 6 - 8 kD MWCO	Spectra Por, Breda, Netherlands
Green Membrane Caps MWCO 3.5 kD	Bio-Rad, Munich
Micro tube, siliconized 1.5 ml	Bio-Rad, Munich
MICROCON centrifugal filter devices YM-30	Millipore, Billerica, USA
Millex GV Durapore PVDF sterile filters, 0.22 µm	Millipore, Billerica, USA
MonoQ 5/50 GL column	Amersham Bioscience, Freiburg
Reaction tube, 1.5 ml	Sarstedt, Nümbrecht
Reaction tube, 2 ml	Sarstedt, Nümbrecht
Reaction tube, 15 ml	Sarstedt, Nümbrecht
Reaction tube, 50 ml	Sarstedt, Nümbrecht
Reaction tube, siliconized 1.5 ml	Bio-Rad, Munich
Superose 6 PC 3.2/30 column	GE Healthcare, Freiburg
Syringe, 20 ml	Sarstedt, Nümbrecht
Tissue Culture Dish, 6-well	Sarstedt, Nümbrecht
Tissue Culture Dish, 10 x 2 cm	Sarstedt, Nümbrecht
Tissue Culture Dish, 15 x 2 cm	Sarstedt, Nümbrecht

4.1.3 Standard solutions

Stock solutions and buffers were made according to standard protocols [Sambrook and Russell, 2000; LabFAQS, 2010]. Protease Inhibitors (Leupeptin 0.5 µg/ml, Pepstatin 1 µg/ml, Aprotinin 1 µg/ml and PMSF 0.5 mM) were freshly added. Common solutions are listed below. Special buffers are described in the individual method sections.

Table 4.3: **Standard buffers and solutions**

Buffer	**Composition**
EX-X buffers	20 mM Tris-HCl pH 7.6
	1.5 mM $MgCl_2$
	0.5 mM EGTA
	10 % glycerol
	X mM KCl
	pH adjusted to 7.6 with HCl
Phosphate Buffered Saline (PBS)	140 mM NaCl
	2.7 mM KCl
	8.1 mM Na_2HPO_4
	1.5 mM KH_2PO_4
	pH adjusted to 7.4 with HCl
TBE-buffer	90 mM Tris
	90 mM Boric acid
	2 mM EDTA
Southern blot denaturation solution	0.5 M NaOH
	1.5 M NaCl
Southern blot ammonium acetate solution	1 M NH_4Ac
0.25 M HCl	20.7 ml 37 % HCl = 12.08 M, add 1000 ml H_2O dest
TE buffer	10 mM Tris-HCl pH 7.6
	1 mM EDTA
DNA sample buffer (10x)	50 % glycerol
	50 mM Tris-HCl pH 7.6
	10 mM EDTA
	0.05 % (w/v) bromophenol blue, xylene cyanol and Orange G
Orange G loading dye (10x)	50 % gycerin
	10 mM EDTA
	0.05 % (w/v) Orange G
SDS-protein sample buffer (5x)	300 mM Tris-HCl pH 6.8
	10 % (w/v) SDS

Buffer	**Composition**
	50 % glycerol
	5 % β-Mercaptoethanol
	0.2 % (w/v) bromphenol blue
SDS-PAGE stacking buffer (4x)	0.5 M Tris-HCl
	0.4 % SDS,
	pH 6.8 with HCl
SDS-PAGE separating buffer (4x)	1.5M Tris-HCl
	0.4 % SDS,
	adjust to pH 8.8 with HCl
SDS-PAGE running buffer	192 mM glycine
	25 mM Tris
	0.1 % (w/v) SDS
Coomassie staining solution	45 % water
	45 % methanol
	10 % acetate acid
	0.1 % (w/v) coomassie blue R250
Coomassie destain solution	45 % water
	45 % methanol
	10 % acetate acid
Silver staining fixing solution	50 % methanol
	12 % acetate acid
	0.05 % formaldehyde 37 %
Silver staining wash solution	50 % ethanol p.A.
Silver staining preincubation solution	20 % (w/v) $Na_2S_2O_3$
Silver staining stain solution	0.2 % (w/v) $AgNO_3$
	0.075 % formaldehyde 37 %
Silver staining developing solution	6 % (w/v) Na_2CO_3
	0.05 % formaldehyde 37 %
	0.5 % (w/v) $Na_2S_2O_3$
Silver staining stop solution	1 % acetate acid
High salt buffer for chromatin assembly	10 mM Tris/HCl pH 7.6
	2 M NaCl

Buffer	Composition
	1 mM EDTA
	0.05 % NP40
	1 mM β-mercaptoethanol
Low salt buffer for chromatin assembly	10 mM Tris/HCl pH 7.6
	50 mM NaCl
	1 mM EDTA
	0.05 % NP40
	1 mM β-mercaptoethanol

4.1.4 Enzymes

Table 4.4: **List of recombinant enzymes**

Enyzme	Supplier
Antartic Phosphatase	New England Biolabs, Frankfurt am Main
Apyrase	New England Biolabs, Frankfurt am Main
iProof DNA polymerase	Bio-Rad, München
Klenow enzyme	New England Biolabs, Frankfurt am Main
Micrococcus Nuclease (MNase)	Roche, Mannheim
Proteinase K	Sigma-Aldrich, München
PfuUltra II Fusion DNA Polymerase	Agilent, Waldbronn
Restriction endonucleases	New England Biolabs, Frankfurt am Main
RNase A	Roche, Mannheim
Shrimp alkaline phosphatase	New England Biolabs, Frankfurt am Main
T4 polynucleotide kinase (PNK)	New England Biolabs, Frankfurt am Main
T4 DNA ligase	New England Biolabs, Frankfurt am Main
Taq DNA polymerase	Genaxxon Bioscience, Ulm

4.1.5 Kits

Table 4.5: **Kits for standard applications**

Material	Supplier
Bac-to-bac Baculovirus Expression System	Invitrogen
Gateway LR Clonase II mix	Invitrogen
Gateway BP Clonase II MIX	Invitrogen
Imprint Methylated DNA Quantification Kit	Simga-Aldrich
Plasmid purification Kit	Qiagen
Plasmid isolation Kit	Qiagen, Invitrogen
Prime-a-Gene Labeling System	Promega
Prime-it Fluor Fluorescence Labeling Kit	Stratagene
QIAquick PCR purification Kit	Qiagen

4.1.6 Oligonucleotides

All oligonucleotides were purchased from Eurofins MWG Operon and diluted to final solutions of 100 µM with ddH_2O. R and F oligos for ligation of 6-NPS1-47 FRET constructs were synthesised by IBA BioTAGnology (Göttingen).

Table 4.6: **List of synthesized oligonucleotides**

name	sequence		T_M	amplicon
AP7	GATCCAGAATCCTGGTGCTGAG	for	61.0	NPS1
AP8	CTAGCTGTATATATCTGACACATGCCT	rev	59.0	NPS1
AP3	CATGGTATGACTTCCAGGTATGG	for	60.6	22-NPS1-22
AP13	GGCCTTAAGAGAAATTTCTCGAG	rev	58.9	22-NPS1-22
AP5	ATGTTTGGGCCACCTCCCC	for	63.9	40-NPS1-40
AP14	TAACGGCCTTAAGAGAAATTTCT	rev	57.3	40-NPS1-40
AP1	ATCTTTTGAGGTCCGGTTCTTT	for	56.0	77-NPS1-77
AP15	GTACAGAGAGGGAGAGTCACAAAAC	rev	65.0	77-NPS1-77
hsp70_for	AATTCGGATCCCACGATAAGC	for	60.8	hsp70
hsp70_rev	CAGATCTGAATTGACGTTCCG	rev	58.0	hsp70

name	sequence		T_M	amplicon
232/16_for	GTAAGACCCGGGAAAGCTATGGGCGC	for	53.3	rDNA232/16
232/16_rev	TTAAGACCCGGGAGGACAGCGTGTC AGTAC	rev	51.5	rDNA232/16
190/90_for	AGCTAGCCCGGGTATCAGTTCTCCG GGTT	for	50.8	rDNA190/90
190/90_rev	TAATGGCCCGGGAATAGGCTGGACA AGC	rev	51.3	rDNA190/90
6-NPS1-47_for	GGCCGCCCTGGAGAATC	for	60.6	6-NPS1-47
6-NPS1-47_rev	GCGTATAGGGTCCATCACATAACC	rev	61.8	6-NPS1-47
SNF2H_for	ATTGGATCCTCGTCCGCGGCCGA	for	60.1	BamHI-hSNF2H
SNF2H_rev	ACTGCGGCCGCTCATAGTTTCAGCTTC TTTTTTCTTCC	rev	61.8	hSNF2H-NotI
SNF2L_for	TATGGATCCGAGCAGGACACTGCCGCA	for	60.7	BamHI-hSNF2L
SNF2L_rev	GCTTCTAGATTAGGAAAATGCTGAAAAT TTTACCA	rev	61.5	hSNF2L-XbaI
SNF2L_w_for	AGACAAGGATGCCAGAGCT	for	60.6	sequencing
SNF2L_w_rev	TCTCTAAAGTAG GCATCCACTGC	rev	60.0	sequencing
SNF2H_w_for	TGTTTGATAGGAGATAAAGAACAA AGAG	for	60.0	sequencing
SNF2H_w_rev	AAGCTGTTCTTCTTTTTGTGCCTG	rev	62.3	sequencing
SNF2H_w_rev2	TGAACACAGACTTCTCTTTAATAAGCATT	rev	61.5	sequencing
Cen probe	TTGAGGCCCTTCGTTGGAAACGGGAATATC		60.1	centromeric probe
Alu probe	GGCCGGGCGCGGTGGCTCACGCCTGTAAT CCCAGCACTTTGGGAGG		65.9	alu repeat probe
Telo probe	TTAGGGTTAGGGTTAGGGTTAGGGTTAGG GTTAGGGTTAGGG		64.8	telomerc probe
5'ETS probe	CGGAGGCCCAACCTCTCCGACGACAGGT CGCCAGAGGACAGCGTGTCAGC		66.8	rDNA 5-ETS leader probe
sb3	GATCCTTCGGAGCGCGACCAGTACTCCGGGCGACA			duplex
sb4	GATCTGTCGCCCGGAGTACTGGTCGCGCTCCGAAG			duplex

name	**sequence**	**T_M**	**amplicon**
R1	GGGATTCTCCAGGGCGGCC		6-NPS1-47 FRET rev
R2	CGGTGCTAGAGCTTGCTACGACCA ATTGAGCGGCCTCGGCACC		6-NPS1-47 FRET rev
R3	TTGGCGGTTAAAACGCGGGGGACAGCGC GTACGTGCGTTTAAG		6-NPS1-47 FRET rev
R4	GCACAGGATGTATATATCTGACACGTGC CTGGAGACTAGGGAGTAATCCCC		6-NPS1-47 FRET rev
R5-Bio	GCGTATAGGGTCCATCACATAACCCGAGTC GCTGTTCAATACAT		6-NPS1-47 FRET rev
F1-64atto647N	GGCCGCCCTGGAGAATCCCGGTGC CGAGGCCGCTCAATTG		6-NPS1-47 FRET for
F2	GTCGTAGCAAGCTCTAGCACCGCTTAAAC GCACGTACGCGCTG		6-NPS1-47 FRET for
F3+14atto532	TCCCCCGCGTTTTAACCGCCAAG GGGATTACTCCCTAGTCTCCAG		6-NPS1-47 FRET for
F4	GCACGTGTCAGATATATACATCCTGTGCATGTATTG AACAGCGACTCGGGTTA		6-NPS1-47 FRET for
F5	TGTGATGGACCCTATACGC		6-NPS1-47 FRET for

4.1.7 Plasmids

List of plasmids used for the experiments shown. A complete list of all plasmids generated during this study is available on the Längst account on lablife (www.lablife.org).

Table 4.7: **Plasmids containing nucleosome positioning sequences (NPS)**

Plasmid	**Insert**	**RE**
pUC18 12x 601	12 repeats of 200 bp long 601 NPS in pUC18 plasmid (kindly provided by J. Widom)	NotI/AvaI
pUC19 1x hsp70	*Drosophila melanogaster hsp70* gene promoter from base pair - 348 to + 11 in pUC19 plasmid	EcoRI
pUC19 7x hsp70	7 repeats of *Drosophila melanogaster hsp70* gene promoter in pUC19 plasmid	EcoRI

Plasmid	Insert	RE
pUC19 1x -232/+16 rDNA	7 copies of murine rDNA promoter from base pair - 232 to + 16 in pUC19 plasmid	AvaI
pUC19 7x -232/+16 rDNA	7 copies of murine rDNA promoter from base pair - 232 to + 16 in pUC19 plasmid	AvaI
pUC19 1x -190/+90 rDNA	murine rDNA promoter from base pair - 190 to + 90 in pUC19 plasmid	AvaI
pUC19 10x -190/+90 rDNA	10 copies of murine rDNA promoter from base pair - 190 to + 90 in pUC19 plasmid	AvaI
pPCRScript-slo1-gla75 insert	dimeric nucleosome positioning sequence NPS1 with rDNA and hsp70 DNA flankings	BglII

Table 4.8: **Gateway plasmids encoding SNF2H and SNF2L genes**

Plasmid	Gene of interest	RE
pENTR3C hSNF2H	entry vector with human *SNF2H* (SMARCA5) gene without start codon	BamHI/NotI
pENTR3C hSNF2L	entry vector with human *SNF2L* (SMARCA1) gene gene without start codon	BamHI/XbaI
pDEST10 hSNF2H	destination vector with *hSNF2H* gene, with N-terminal hexa-His-tag, for recombination into baculo virus shuttle bacmid	
pDEST10 hSNF2L	destination vector with *hSNF2L* gene, with N-terminal hexa-His-tag, for recombination into baculo virus shuttle bacmid	

4.1.8 Baculoviruses

Table 4.9: **Overview about used baculoviruses**

GOI	Virus
hSNF2H (N-His_6)	pDEST10 hSNF2H was recombined into baculo bacmid DNA and recombinant virus was generated
hSNF2L (N-His_6)	pDEST10 hSNF2L was recombined into baculo bacmid DNA and recombinant virus was generated

GOI	Virus
hSNF2H (C-Flag)	C-terminal Flag-tagged hSNF2H gene recombined into baculo bacmid (virus generated by R. Stroner)

4.1.9 Bacteria

Table 4.10: **Bacterial strains used for plasmid propagation**

Strain	Resistance	Application
DB3.1	streptomycin	for propagation of *ccdB* gene containing pENTR plasmids
DH5α	none	general DNA plasmid propagation
DH10BAC	tetracycline, kanamycin	*E. coli* strain that carries the baculoviral shuttle vector bMON14272 with a lowcopy number mini-F replicon with a kanamycin resitance marker and Tn7 transposon attachment sites within the LacZa peptide. The helper plasmid pMON7124 encodes for the transposase and confers resistance to tetracycline.
XL1 Blue	tetracycline	F'episome, general DNA plasmid propagation, blue/white screening

4.1.10 Histones

Core histone octamers were purified from chicken erythrocytes (see supplementary information in the appendix) and provided in the laboratory by Regina Gröbner-Ferreira.

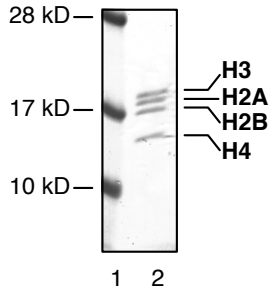

Figure 4.1: **Histone octamers purified from chicken erythrocytes**
1 µg of octamers was loaded onto a 17 % SDS PAGE and subsequently stained with coomassie blue. Bands of the four core histones H2A, H2B, H3 and H4 are depicted in lane 2.

4.1.11 Eukaryotic cell culture

Table 4.11: **Eukaryotic cell lines**

Name	Origin
HeLa	human adenocarcinoma cell line (epithelial cells)
lymphocytes	isolated from blood of human female
IMR90	femal human diploid fibroblast-like lung cells
3T3	mouse embryonic fibroblast cells
Sf21	insect cell line (*Spodoptera frugiperda*)

Table 4.12: **Media, serum and antibiotics used for cell culture**

Name	Composition	Supplier
Dulbecco's Modified Eagle Medium	+ 100 mg/L glucose + GlutaMAX + pyruvate	D-MEM Gibco, Invitrogen
Penicillin-Streptomycin	5 U/ml penicillin + 5 µg/ml streptomycin	Gibco, Invitrogen
Sf-900 II SFM	serum-free + L-Glutamine	Gibco, Invitrogen
Fetal Bovine Serum		FBS, Gibco, Invitrogen
Trypsin/EDTA	Trypsin 0.25 % in 1 mM EDTA	Gibco, Invitrogen

4.1.12 Software tools

Table 4.13: **List of used software tools**

Name	Distributor
Babelomics 4 tool	http://babelomics.bioinfo.cipf.es/functional.html
GEO repository	http://www.ncbi.nlm.nih.gov/geo/
GraFit V6.0	Erithacus Software
LabLife	LabLife Software (www.lablife.org)
Multigauge V3.1	FujiFilm
Netprimer	Premiersoft (www.premierbiosoft.com)
OligoPerfect Designer	Invitrogen (http://tools.invitrogen.com)

Name	**Distributor**
UCSC Genome Browser	(http://genome.ucsc.edu/ENCODE)
VectorNTI V10	Invitrogen

4.2 Methods

4.2.1 Working with DNA

Preparation and transformation of chemically-competent bacteria with DNA, amplification of plasmid DNA in *E. coli* bacteria, purification, concentration determination, restriction enzyme digestion, ligation of DNA fragments, analysis of DNA on agarose and polyacrylamide gels, and amplification of the DNA by the polymerase chain reaction (PCR) was performed according to the standard protocols [Sambrook and Russell, 2000]. Bacteria were cultured in LB-Lennox medium [Bertani, 1951] and selective antibiotics were added corresponding to the plasmid encoded resistance. Plasmid DNA was isolated with plasmid purification kits (Invitrogen/Qiagen). Isolation of DNA fragments from agarose gels was performed using the Qiagen Gel Extraction kit.

4.2.1.1 Determination of DNA quality and quantity

The DNA concentration of single and double stranded DNA was determined by absorption measurement at 260 nm using a NanoDrop ND1000 spectrophotometer (Peqlab). Protein impurities could be determined by absorption measurement at 280 nm and the ratio $A_{260/280}$. DNA impurities were determined by electrophoretically separation of DNA fragments using 0.8 - 2.0 % (w/v) agarose gels in 1x TBE supplemented with 0.01 % SybrSafe.

4.2.1.2 Polyacrylamide and agarose gel electrophoresis

Agarose gel electrophoresis was generally performed with gels containing 0.8 - 2 % agarose in 1x TBE buffer, supplemented with 0.01 % SYBR Safe (Invitrogen), in 1x TBE running buffer at a constant voltage of 100 V. DNA separation by polyacrylamide gel electrophoresis (PAGE) was done in 0.4x TBE at $4°C$ and 100 V. In order to remove unpolymerized acrylamide the gel was prerun for 20 - 30 min at 60 - 80 V. For visualization the gel was stained in 0.4x TBE containing ethidium bromide (0.5 mg/ml) for 15 min and washed twice with destilled water for 10 min each.

4.2.1.3 Restriction digest

Restriction enzymes were used at reaction conditions according to the manufacturer's recommendations concerning buffer, addition of BSA and temperature (see www.neb.com). For the analytical digest 0.1 - 1 µg DNA was incubated with 5 units of the respective restriction endonuclease in a total volume of 20 µl. The preparative restriction digest was

done with 15 µg DNA using 60 units restriction endonuclease in a total volume of 60 µl. The large scale digest, especially for nucleosome assembly, was done with 300 µg DNA using 150 units restriction endonuclease in a total volume of 150 µl. To check the completion of the digest, DNA was electrophoretically separated using 0.8 - 2.0 % TBE-agarose gels supplemented with SYBR Safe (Invitrogen).

4.2.1.4 Preparative DNA precipitation

DNA was precipitated (after PCR amplification, restriction digest, etc.) by addition of 0.5 volumes of 7.5 M ammonium acetate and 2 volumes of 100 % icecold EtOH. To increase precipitation in samples with low DNA concentration glycogen was also added (0.5 µg/µl). The general procedure was done as described [Sambrook and Russell, 2000].

4.2.1.5 Radioactive body labelling of DNA

For radioactive labelling of longer DNA sequences radioactive γ-^{32}P-dATP was added to a standard PCR reaction. 50 µl reaction volume contained 100 ng template DNA and of 500 nM of each primer, 100 µM of dCTP, dGTP and dTTP, 20 µM dATP and 16.7 nM γ-^{32}P-dATP. Random amplification using Prime-a-gene Labelling System (Promega) with Klenow Fragment and random primer was used according to manufacturer's protocol. In general non-incorporated nucleotides were separated from labelled DNA using spin columns prepacked with Sephadex G-50 (GE Healthcare). Labelling efficiency was measured by scintillation counter.

4.2.1.6 Radioactive end labelling of DNA

Short DNA sequences, especially oligonucleotide probes for southern blotting, were radioactively labelled with T4 polynucleotide kinase. A standard reaction in 1x T4-PNK buffer contained 0.66 pM oligonucleotide, 10 untis enzyme (NEB) and 90 µM α-^{32}P-dATP in 15 µl total volume. After 45 min incubation at 37°C reaction was stopped by adding 5 µl 0.2 M EDTA and 50 µl H_2O. Non-incorporated nucleotides were separated from labelled DNA using spin columns prepacked with Sephadex G-50 (GE Healthcare). Labelling efficiency was measured by scintillation counter.

4.2.1.7 Annealing of double stranded oligonucleotides

Similar quantities of complementary single strand oligonucleotides were mixed in annealing buffer, denatured in a thermoblock (95°C for 5 min) and slowly (1 - 2 hours) chilled to

room temperature (by switching the thermoblock off) to allow complete oligonucleotide annealing.

4.2.2 Protein biochemical methods

Proteins were purified and analyzed according to standard protocols [Sambrook and Russell, 2000]. Generally, proteins were stored at -80°C and kept on ice befor starting an experiment.

4.2.2.1 Determination of protein concentrations

Protein concentrations were determined using the colorimetric assay described by Bradford [Bradford, 1976]. Additionally the concentration of purified proteins was estimated according a titration curve of a standard protein (e. g. BSA) loaded onto a SDS-PAGE followed by Coomassie blue staining (see figure 4.2).

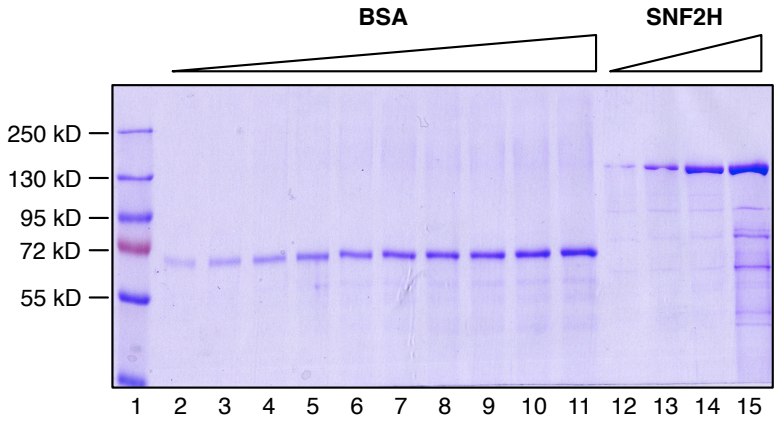

Figure 4.2: **Quantification of purified protein by comparison to a BSA standard curve**
Increasing amounts of BSA, ranging from 200 to 1100 µg were loaded onto a 7.5 % SDS PAGE (lane 2 - 11). Different amounts of purified protein, 1 to 4 µl (lane 12 - 15), were loaded in parallel and gel was stained with coomassie subsequently. Intensity of BSA bands was quantified, plotted as curve and comparison of the protein of interest specific bands allowed a quantification.

4.2.2.2 Denaturing SDS-polyacrylamide gel electrophoresis (SDS-PAGE)

Quantitiy and quality of recombinant proteins was initially analyzed by SDS-polyacrylamide gel electrophoresis (SDS-PAGE). Separating and stacking gels were prepared according to standard protocols using ready-to-use polyacrylamide solutions from Roth (Rotigel,

30 %, 49:1). For electrophoresis, protein samples were mixed with Laemmli SDS-PAGE sample buffer, heat-denatured for 5 min at 95°*C* and directly loaded onto the gel. Proteins were separated at 35 mA (4 mA/cm) until the dye front reached the bottom of the gel. The molecular weight of proteins was estimated by running pre-stained marker proteins (PAGE ruler, Fermentas) in parallel. Following electrophoresis, proteins were stained with either Coomassie Brilliant Blue or Silver.

4.2.2.3 Native polyacrylamide gel electrophoresis (Native Blue PAGE)

Based on the method described by Schägger and von Jagow proteins were analyzed under native conditions [Schägger and von Jagow, 1991]. Therefore protein-protein-interactions could be detected and size of the complexes was estimated by comparison to unstained marker proteins. According to manufacture's protocol for NativePAGE (Invitrogen) 1.5 µg BSA, SNF2H, SNF2L and 5 µl NativeMark unstained protein standard (Invitrogen) were loaded on a 4 - 16 % NativePAGE Novex Bis-Tris gel (Invitrogen). Separation of proteins was done at 4°*C* with 150 volts for 60 min, then voltage was increased to 250 V proteins for 90 min. Proteins were fixed in 40 % methanol, 10 % acetic acid and subsequently silver stained as described below. After documentation, the gels were dried onto a Whatman paper at 80°*C* for 2 h on a gel dryer (BioRad).

4.2.2.4 Coomassie blue staining of protein gels

Polyacrylamide gels were stained for approximately 15 min on a slowly rocking platform with Coomassie staining solution (0.1 % Coomassie Blue R in 10 % acetic acid, 45 % methanol). Gels were destained in 10 % acetic acid and 45 % methanol until protein band became clearly visible. After documentation, the gels were dried onto a Whatman paper at 80°*C* for 2 h on a gel dryer (BioRad).

4.2.2.5 Silverstaining of protein gels

The staining of protein gels with silver nitrate solution was carried out according to the protocol of Blum [Blum et al., 1987]. The gel was incubated for 6 min in fixing solution (50 % methanol, 12 % acetic acid and 0.05 % formaldehyde 37 %) and washed once in 50 % ethanol for 20 min. Before staining gel was preincubated for 1 min in preincubation solution (5 % $Na_2S_2O_3$), washed two times with water (ddH_2O, 20 sec) and subsequently staining solution was added for 20 min (0.2 % $AgNO_3$, 0.075 % formaldehyde 37 %). Afterwards the gel was washed with water (2 times, 20 sec each) and developed with the developing solution (6 % Na_2CO_3, 0.05 % formaldehyde 37 %, 0.5 % $Na_2S_2O_3$) until the

protein bands of interest were visible (typically, after 2 to 5 min). The staining reaction was stopped by incubating the gel in 1 % acetic acid stop solution (more than 5 min). The gel was documented and dried onto a Whatman paper at $80°C$ for 2 h on a gel dryer (BioRad).

4.2.3 GATEWAY cloning system

To express the human remodeling proteins an eukaryotic expression system was used. Insect cells derived from the *Spodoptera frugiperda* (Sf21) can be easily infected by a cell line specific virus, called baculovirus. Using a recombinant virus carrying a **G**ene-**o**f-**I**nterest (GOI) allows high level production of recombinant proteins in a eukaryotic cell system, including all kinds of post-translational modifications. Recombinant baculovirus were cloned with the GATEWAY cloning system from Invitrogen. With this system a GOI is first cloned into an entry vector. Form this vector the GOI can be transferred into different organism specific destination vector by recombination. Diverse protein-tags can be fused to the protein of interest by taking advantage of the numerous destination vectors. Also for other expression systems like *E. coli*, yeast or mammalian cells specific destination vectors are available and can be recombined with the same GOI containing entry plasmid. Thus the GATEWAY system allows not only efficient cloning of specific expression vectors, but also fast creation of large expression clone libraries.
The *ccdB* gene for negative selection is present in all GATEWAY vectors (destination and entry vectors) like the chloramphenicol resistance gene *(CmR)* for counterselection. After a BP or LR recombination reaction (refer to the Invitrogen manual for details), this cassette is replaced by the GOI to generate the entry clones and expression clones, respectively. The protein encoded by the *ccdB* gene interferes with *E. coli* DNA gyrase, thereby inhibiting growth of most *E. coli* strains (e. g. DH5α, TOP10, but not XL1 blue). Thus presence of the *ccdB* gene allows a strong negative selection of non recombined plasmids, reducing the number of false positive clones and fastening the process of clone selection. For propagation of *ccdB* gene containing vectors (pENTR3C, all donor and destination vectors) an *E. coli* strain carrying a mutation in the gyrase gene *(gyrA462)* that conferred resitance to the CcdB effects, like the DB3.1 strain, has to be used.

4.2.3.1 Creation of an entry clone

Gene sequence of human SNF2L (SMARCA1 pubmed accession number NM_139035.2) and SNF2H (SMARCA5 pubmed accession number NP_003592.2) were PCR amplified by PfuUltra II Fusion proof reading DNA polymerase from cDNA clones. Using mismatching primer the start codon was deleted and at the 5'-end a *BamHI* and at 3'-end

a *XbaI* restriction enzyme recognition site was introduced. According to manufactureńs protocol both genes were cloned into BamHI/XbaI linearized pENTR3C entry vector (Invitrogen). This vector contains a Shine Dalgarno and Kozak sequence.

4.2.3.2 Creation of a destination clone

To create an expression clone a LR-clonase reaction (LR Clonase II mix, Invitrogen) between a pENTR-GOI vector (attL sites, kanamycin resistance gene) and a pDEST10 vector (attR sites, ampicillin resitance gene, ccdB gene, chloramphenicol marker) was performed. An AcMNPV polyhedrin promoter allowed high expression levels of the GOI and the vector also encodes a N-terminal His_6-tag with a TEV protease cleavage site and a SV40 late polyadenylation signal flanked by transposition elements (Tn7). The reaction mixture was then transformed into DH5α or TOP10 competent cells and plated onto LB_{Amp} plates. Only the bacteria containing a pDEST-GOI plasmid were able to grow, since the *ccdB* gene was replaced. Remaining entry vectors do not confer ampicillin resistance.

4.2.3.3 Recombination into baculovirus bacmid DNA

The Bac-to-Bac system (Invitrogen) was used to obtain efficiently recombinant baculoviruses. The pDEST10 vectors contain the polyhedrin promoter, the GOI and a gentamycin resistance marker flanked by transposition elements (Tn7). The pDEST10-GOI plasmid was transformed into *E. coli* DH10bac chemically competent cells, which contained the bacmid DNA (tetracycline resistance marker) and a helper-plasmid (encoding a kanamycin resistance marker and a transposase). This transposase catalyzed the recombination of the Tn7 flanked region of the pDEST10 vector into to the bacmid DNA, which also contains Tn7 transposition elements. With the GOI also a gentamycin resistance marker got integrated into the viral genome. Triple antibiotic and blue-white selection resulted in the selection of the recombinant bacmid DNA (transposition of the GOI + gentamycin into the bacmid DNA destroying the *lacZ* gene).

4.2.3.4 Isolating recombinant bacmid DNA and tranformation in Sf21 cells

After transformation of the pDEST10-GOI construct into DH10Bac *E. coli* cells and after a successful transposition reaction, recombinant bacmid DNA was purified according the "bac-to-bac" manual (Invitrogen) from positive white transformants. Purified bacmid DNA was suitable for PCR analysis and transfection into Sf21 insect cells. The presence of the desired GOI in the high molecular weight bacmid DNA was verified by PCR (with

GOI and bacmid specifc primer, see section 4.1.6). The positive tested recombinant bacmid DNA was transfected into Sf21 cells (1x 10^6 cells in one well of a 6-well plate) with Cellfectin (Invitrogen) to produce a first viral stock. This virus stock was amplified and used for protein expression (see below).

4.2.4 Sf21 insect cell culture and baculovirus protein expression sytem

Baculoviruses are a group of large double-stranded DNA viruses infecting insects. They feature a narrow host range with each type of baculovirus being virulent only to a specific insect species, while not infecting other insects, plants or mammals. *Autographa californica* Nuclear Polyhedrosis Virus (AcNPV) is well-studied and together with *Spodoptera frugiperda* ovary cell culture (Sf21) a useful tool for recombinant protein expression. During the baculovirus life cycle, two different forms of virus are produced by the infected host cell: extracellular virus particles bud during the early stage of infection (release 24 hours post infection) and spread infection to other organs of the insect. During the late stage of infection, occluded virus particles form in the nucleus of the host cell. Occluded virus consists of many nucleocapsids enveloped by a matrix mainly formed polyhedrin, a structural protein expressed at very high levels. The polyhedrin matrix allows the virus to last in the environment after the death of the host. After ingestion of occluded virus, virions are released in the mid-gut of the next host and enter adjacent cells by endocytosis. In vitro, polyhedrin is not necessary for virus replication and can be deleted or replaced. As the polyhedrin promoter is the strongest promoter known at present, it allows high expression levels of heterologous proteins. In addition, the baculovirus genome and capsid structure tolerate insertions of sequence well, therefore large coding sequences can be introduced [Fitzgerald et al., 2006; Berger et al., 2004]). Baculovirus expression systems are very versatile tools for protein expression as they allow high-level expression of large proteins providing also signal peptide cleavage, intron splicing, nuclear transport, phosphorylation, glycosylation and acetylation, which often limits the use of bacterial expression systems.

4.2.4.1 Culturing of Sf21 cells

Sf21 cells were cultivated in Sf-900 II medium (Invitrogen) supplemented with 4 mM N-acetyl-L-alanyl-L-glutamine, 50 U/l penicillin, 50 µg/l streptomycin and 10 % fetal calf serum. Cells were grown as suspension cultures in spinner bottles at 75 rpm or in Erlenmeyer flasks at approximately 100 rpm (depending on diameter of the flask) or as monolayers at $27°C$. Cell density of spinner cultures was kept between 5x 10^5 and 2x 10^6 cells/ml.

4.2.4.2 Virus propagation by low MOI amplification

Amplification of baculovirus was undertaken to preserve the virus stock and to gain a higher titer of virus that was used for protein expression. MOI (multiplicity of infection) is defined as the number of baculoviruses/Sf21 cell. In order to avoid accumulation of defective virus particles, reducing heterologous protein expression, baculovirus amplification with a MOI of 0.1 is optimal. Low MOI infection was performed in spinner flasks with 50 - 100 ml culture volume and at a constant cell density of 10^6 cells/ml (always dilute back to this cell number). Once infected, Sf21 cells had to double once during the first 24 hours post-infection (e. g. 10 % of the cells were infected, whereas the other 90 % doubled). Under these conditions growth arrest was usually observed another 24 hours later. If the baculovirus titer was lower, it took some days (passages) until growth arrest was reached (after multiple rounds of virus amplification). Budded viruses were released starting from 24 hours after infection. In general viral supernatant was harvested 48 hours after the observed growth arrest.

4.2.4.3 Test expression of recombinant proteins in Sf21 cells

Once the baculovirus was amplified, the viral titer for large-scale protein expression had to be determined. In 2 ml medium 1x 10^6 cells were seeded per well of a 6-well plate. For the amount of virus added per well, a viral titer between 1 x 10^7 pfu/ml and 5x 10^8 pfu/ml was assumed. For expression a MOI of 3 was optimal. The estimated amount of virus (e. g. mock infection, 5, 15, 25, 50, 100, 150 µl of virus) was added and evenly distribute by shaking on a horizontal platform for 1 hour. The 6-well plate was sealed with parafilm and incubated for 48 - 72 hours at $27°C$ recording daily growth behavior and infection process, allowing a rough titer determination. Cells were harvested by scrapping off the plates and freezing pellets in liquid nitrogen. Recombinant protein expression and affinity tag purification was tested in a small scale purification.

4.2.4.4 Protein expression in Sf21 cells

After determination of the optimal amount of viral supernatant needed for sufficient protein expression a large scale expression was performed. Cells were grown in suspension in spinner flasks flasks (250 - 500ml) and infected at a cell density of 1x 10^6 cells/ml with the respective amount of recombinant baculovirus (as determined before with test infections). After 72 hours cells were harvested by centrifugation for 5 -10 min at 500 g, snap frozen in liquid nitrogen and stored at - $80°C$ until use.

4.2.5 Purification of recombinant proteins form Sf21 insect cells

4.2.5.1 Preparation of cell lysate

After optimizing protein expression a typical large-scale purification was done with 1 - 3x 10^8 insect cells (see section 4.2.4.4). Purification was performed in the cold room and samples were always kept on ice. Sf21 cell pellets were resuspended in 10 ml lysis buffer (EX 500) without NP40 and transferred into a 15 ml reaction tube. Protease inhibitors PMSF (0.5 mM), Leupeptin (0.5 µg/ml), Aprotinin (1 µg/ml), Pepstatin (1 µg/ml) were added to buffers prior to use. The cell suspension was snap frozen in liquid nitrogen and thawed in hand warm water. The freeze thaw procedure was repeated twice and the suspension subsequently further lysed by sonification with a Branson Sonifier 250D (small tip; 6x for 20 s at 50 % amplitude and 50 % duty cycle with a cooling period 20 s of in between). The lysate was cleared by centrifugation for 30 min, 20,000 g and 4°C. Supernatant was transferred to a 50 ml reaction tube and 10 ml of lysis buffer (EX 500) with 0.2 % NP40 were added and stored on ice.

4.2.5.2 Purification of His-tagged hSNF2H and hSNF2L

For affinity purification of hexa-histidin-tagged hSNF2H and hSNF2L by Ni-NTA agrose 300 µl of beads (Qiagen) were equilibrated in batch with EX500 (500 mM KCl, 20 mM Tris/HCl pH 7.6, 1.5 mM $MgCl_2$, 0.5 mM EGTA and 10 % glycerol), substituted with 0.1 % NP40 and 10 mM imidazole. Protease inhibitors PMSF (0.5 mM), Leupeptin (0.5 µg/ml), Aprotinin (1µg/ml), Pepstatin (1µg/ml) were added to buffers prior to use. 2x 150 µl equilibrated resin were incubated with 2x 10 ml of supernatant from 3x 10^8 lysed insect cells for 90 min at 4°C in a overhead shaker. The resin was washed five times with each 5 ml EX500 (containing 20 mM imidazole, protease inhibitors and 0.1 % NP40) and loaded into a 1 ml mini column. The flow through was collected and reloaded once. Bound proteins were eluted from the Ni-NTA-agarose by addition of 600 µl elution buffer (EX300 containing 0.1 % NP40, 250 mM imidazole and protein inhibitors) and incubation for 60 min at 4°C on overhead shaker. This elution step was repeated once. After last elution step beads were resuspended in 500 µl EX500 buffer and 100 µl 10x protein sample buffer was added. Individual fractions were collected and purification efficiency was analyzed by SDS-PAGE (Coomassie blue staining). Samples were aliquoted, snap frozen in liquid nitrogen and stored at - 80°C. Protein concentration was determined via bradford assay in comparison to a BSA standard curve.

4.2.5.3 Determination of DNA contamination of purified enzymes

Due to their function as in chromatin binding and remodeling co-purification of host cell DNA with the ectopically expressed SNF2H and SNF2L enzyme had to be excluded. To check for presence of DNA in the eluted protein samples 10 µg of remodeling enzyme were diluted in 10 µl of a 1 % SDS solution supplemented with 20 µg proteinase K. Reaction was incubated over night at $45°C$ and DNA was precipitated subsequently using ammonium acetate/ethanol. Pellet was resuspended in 50 µl 2x orange G loading dye and loaded on a 1 % agarose gel, stained with 1 µg/ml EtBr.

4.2.5.4 Nuclease activity of the purified enzyme fractions

Contamination of the eluted protein fractions with cellular nucleases would significantly disturb the functional experiments with nucleosomes and DNA. To exclude this kind of contamination a nuclease test with plasmid DNA and eluted remodeler was performed. 1 µg of remodeler and 1 µg of plasmid DNA were mixed in 10 µl EX buffer system (20 mM Tris/HCl pH 7.6, 1.5 mM $MgCl_2$, 0.5 mM EGTA and 10 % glycerol) and the concentration of monovalent anions (Cl^-) and cations (K^+/Na^+) was adjusted to 90 mM (standard conditions for most functional assays). The reaction was incubated for 2 h at $27°C$ and reaction was stopped by adding SDS to a final concentration of 1 % and 20 µg proteinase K. Deproteinization was performed over night at $45°C$ and DNA was precipitated subsequently using ammonium acetate/ethanol. Pellet was resuspended in 50 µl 2x orange G loading dye and loaded on a 1 % agarose gel, stained with 1 µg/ml EtBr.

4.2.6 *In vitro* reconstitution of chromatin

4.2.6.1 Preparation of DNA fragments for nucleosome assembly by restriction digest

Restriction digest of pUC plasmids containing several repeats of nucleosome positioning sequences flanked by restriction recognition sites allowed fast and specific production of DNA fragments for nucleosome assembly. 300 µg of plasmid DNA (pUC18 12x 601; pUC19 7x hsp70, pUC19 7x - 232/+ 16 rDNA and pUC19 10x - 190/ +90) was digested with 150 units restriction endonuclease in a total volume of 150 µl supplemented with 0.1 mg/ml BSA. Complete digestion was checked using 0.8 - 2.0 % TBE-agarose gels supplemented with SYBR Safe (Invitrogen).

4.2.6.2 Preparation of NPS DNA fragments by PCR

To generate nucleosomal DNA fragments of specific sizes a PCR was performed. As template the pPCRScript_slo1-gla75 insert was used, which contained two copys of the nucleosome positioning sequence NPS1 with rDNA and hsp70 DNA flankings (synthesized and cloned by Sloning). This NPS1 sequence is based on the 601 nucleosome positioning sequence [Lowary and Widom, 1998]. 128 of the 147 base pairs is identical to the 601 sequence, at the divergent positions in principle C was replaced by T to reduce the CpG contend (see appendix for full sequence). Prior to use as a PCR template the plasmid DNA was restriction digested with BglII in preparative scale to cut the dimeric NPS1 template down to two monomers. For production of NPS1 constructs with defined flanking DNA specific primer pairs were used. For the 0-NPS1-0 sequence without linker DNA the reverse primer (AP8) hybridized 5 bp upstream of 3'-border of the NPS1 sequence, hence amplifying a 142 bp DNA fragment instead of 147 bp. The contructs with DNA flanking NSP1 were 191 bp (22-NPS1-22), 200 bp (6-NPS1-47 and 33-NPS1-20), 227 bp (40-NPS1-40) and 301 bp (77-NPS1-77) in length. Preparative PCR reaction was performed in 2 ml scale with 2 µg template DNA, 0.2 mM dNTPs, 1 µM forward and reverse primer and 20 µl Taq DNA polymerase (Genaxxon) in 1x reaction buffer (Genaxxon). Reaction mix was split into 20x 100 µl into 200 µl PCR tubes and reaction was started as semi-hot start in a PCR cyler (PeqLab) using the following cycle steps.

Table 4.14: **PCR protocol for large scale amplification of NPS sequences**

Step	**Time**	**Temperature**	
initial denaturation	2 min	$94°C$	
denaturation	30 s	$94°C$	
annealing	30 s	$59°C$	35x
elongation	30 s	$72°C$	
final elongation	5 min	$72°C$	

Reaction were cooled down to $4°C$, 10 ng/µl glycogen was added and PCR products were precipitated with 7.5 M ammonium acetate and ethanol. Purity was checked on a 1.5 % agarose gel and conentration was determined using Nanodrop Photometer (PeqLab).

4.2.6.3 Assembly of chromatin by salt gradient dialysis

Nucleosomes were assembled from DNA and histones by the salt gradient dialysis technique according to Rhodes [Rhodes and Laskey, 1989]. The assembly reaction was performed in the lid of siliconized 1.5 ml tubes (Biozym). Dialysis membranes with a MWCO of 3.5 kD (Spectrapor) were pre-incubated for 5 min in high salt buffer (10 mM Tris/HCl pH 7.6, 2 M NaCl, 1 mM EDTA, 0.05 % NP40, 1 mM β-mercaptoethanol). This membrane was placed over the lid of a 1.5 ml tube with a big hole (O-ring). The membrane was fixed with a second tube, where the bottom was cut and the lid removed. The tubes were placed (in a styrofoam floater) into a 3 l beaker filled with 300 ml high salt buffer (containing a magnetic stirrer). Air bubbles below the membrane were removed with a bent pasteur pipette. Finally the assembly reaction were pipetted into the lid. 3 l of low salt buffer (10 mM Tris/HCl pH 7.6, 50 mM NaCl, 1 mM EDTA, 0.05 % NP40, 1 mM β-mercaptoethanol) were pumpend into this beaker with a flow rate of 300 ml per hour at room temperature. Hence salt concentration decreased slowly from 2 M to 227 mM allowing a specific assembly of the histone octamers onto the given DNA fragment.
For a test assembly reaction typically 5 µg of DNA were mixed with different amounts of histone octamers, varying from 3 to 6 µg, in a final volume of 50 µl high salt buffer, supplemented with 200 ng/µl BSA. If the DNA was generated by PCR reaction 250 ng pCMV14 DNA was also added as competitor, to avoid unspecific nucleosome assembly. After the optimal histon:DNA ratio had been determined, nucleosomes were assembled in large scale. In general 25 µg of DNA was mixed with an optimal amount of histones in 250 µl high salt buffer, supplemented with 200 ng/µl BSA. For PCR products 1 µg pCMV14 competitor plasmid DNA was added. The assembly mix was split into 5x 50 µl before loading into the dialysis chambers. In case of mono-nucleosomes quality of the assembly reactions was directly checked on native 6 % PAA gels in 0.4x TBE run for 60 - 70 min at 100 V. To control assembly of poly-nucleosomes on plasmid DNA (pUC18 12x 601 and pT11) a partial MNase digested had to be done (see below).

4.2.6.4 Chomatin analysis by micrococcal nuclease digestion

Micrococcal nuclease (MNase) cleaves DNA preferentially in the linker region between individual nucleosomes [von Hippel and Felsenfeld, 1964]. Partial MNase digestion generates a so-called nucleosomal ladder, thereby allowing qualitative analysis of the obtained grade of chromatin. Typically, 1.5 µg of chromatin was partially digested with MNase (MNase concentration had to be optimized for each assembly) for 30, 60 and 240 sec in the presence of 3 mM $CaCl_2$. The reaction was stopped by the addition of 0.2 volumes of stop solution (4 % SDS, 100 mM EDTA). Reactions were supplemented with proteinase K

(10 µg / reaction) and glycogen (10 µg) and deproteinized for at least 1 hour at 40°C. The DNA was purified by ethanol precipitation (0.5 vol 7.5M NH_4Ac and 2 volumes 100 % ethanol were added, incubated for 10 min on ice, centrifuged for 15 min at 13,000 rpm and washed once with 70 % ethanol), air dried, dissolved in 10 µl loading buffer and analysed on 1.3 % agarose gels supplemented with 0.01 % SYBR Safe.

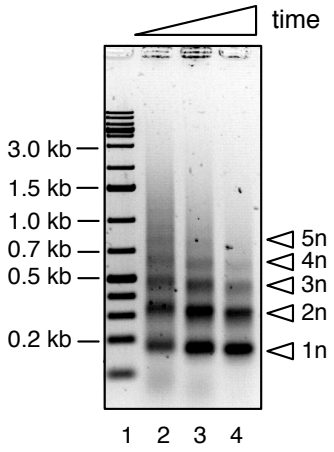

Figure 4.3: **Partial MNase digestion of *in vitro* assembled circular chromatin** Circular chromatin was assembled on plasmid DNA with chicken histiones by salt gradient analysis. 1.5 µg chromatin was digested with micrococcal nuclease and reaction was stopped after 20, 60 and 240 sec incubation (lanes 2 - 4). After digestion with proteinase K DNA was precipitated and analyzed on a 1.3 % agarose gel stained with 0.01 % SybrSafe.

4.2.7 Functional remodeling assays

4.2.7.1 Mono-nucleosome band shift assay

Binding of SNF2H and SNF2L to nucleosomes or DNA was analyzed by band shift experiments. In a standard experiment 150 nM of assembled nucleosomes were incubated with rising amounts of enzyme (50 - 1000 nM) in absence of ATP in a total Volume of 10 µl. To avoid unspecific binding reaction mixture was supplemented with 200 ng/µl BSA and siliconized 1.5 ml reaction tubes were used (Biozym). The reaction was performed in the EX buffer system (20 mM Tris/HCl pH 7.6, 1.5 mM $MgCl_2$, 0.5 mM EGTA and 10 % glycerol) and the concentration of monovalent anions (Cl^-) and cations (K^+/Na^+) was adjusted to 100 mM. For binding samples were incubated for 15 min at 30°C, then reactions were cooled on ice and 4 µl 10x Orange G loading dye was added. Polyacrylamid gels (4.5 or 6 %) in 0.4x TBE were pre-run for 20 - 30 min, samples loaded and gel run

for 60 - 90 min at 100 V. Optimal running time was controlled by using orange G as a marker. Subsequently DNA was stained with 0.5 mg/ml ethidium bromide in 0.4x TBE for 10 -15 min and destained 2x 10 min with dH_2O. Documentation was performed with the gel documentation system. Quantification of the signal intensities for the unbound nucleosomal fragments was done with Multi Gauge Software (FujiFilm). Direct comparison of signal of unbound nuclesomes to enzyme bound nucleosomes was not possible, because binding to the substrate lead a to formation of high molecular weight complexes that did not migrate into to gel. Therefore the signal intensity in the gel slot became saturated and did not correlate to DNA amount. Hence relative binding efficiency **B** was measured as ratio between the intensity of unbound nucleosomal signal $\mathbf{(I}_{nuc\ not\ bound}\mathbf{)}$ divided by intensity of input signal $\mathbf{(I}_{nuc\ input}\mathbf{)}$ in the first lane.

$$\mathrm{B} = \mathrm{I}_{nuc\ not\ bound} : \mathrm{I}_{nuc\ input}$$

Fitting of the binding curves derived from this well reproducible quantitative approach was done using GraFit V6.0 Software (Erithacus Software) and the following standard equitation for cooperative binding:

$$\mathrm{y} = \frac{cap * L^n}{K^n + L^n} + \mathrm{Back}$$

Where **cap** is the maximum binding capacity, **L** ligand concentration, **K** is the binding constant, **n** is the Hill coefficient and **Back** is the background.

4.2.7.2 Poly-nucleosome band shift assay

Binding of SNF2H and SNF2L to poly-nucleosomes was also analyzed by band shift experiments. In a standard experiment 3.3 nM of poly-nucleosomes assembled on linear 14 kB plasmid DNA were incubated with rising amounts of enzyme ranging from 50 to 1000 nM in a total volume of 10 µl. Binding was tested in absence and presence of 2 mM ATP. To avoid unspecific binding reaction mixture was supplemented with 200 ng/µl BSA and siliconized 1.5 ml reaction tubes were used. The reaction was performed in the EX buffer system (20 mM Tris/HCl pH 7.6, 1.5 mM $MgCl_2$, 0.5 mM EGTA ang 10 % glycerol) and the concentration of monovalent anions (Cl^-) and cations (K^+/Na^+) was adjusted to 100 mM. For binding samples were incubated for 15 min at $30°C$, then reactions were cooled on ice and 4 µl 10x Orange G loading dye was added. Unbound poly-nucleosomes were separated from formed complexes on a 1 % agarose gel in 0.4x TBE by electrophoresis for 2.5 h at 100 V. DNA was stained with 0.5 mg/ml ethidium bromide in 0.4x TBE for 10 - 15 min and destained 2x 10 min with dH_2O. Documentation and quanification was done according to the protocol described for mononucleosome band shift experiment (see section 4.2.7.1).

4.2.7.3 Nucleosome remodeling assay

The nucleosome remodeling assay allowed the visualization of single nucleosome movements, catalyzed by ATP dependent nucleosome remodeling factors [Längst et al., 1999]. All reactions were performed in siliconized tubes (Biozym). A typical reaction contained 100 nM mononucleosomes with defined translational positions and 2 mM ATP in a total volume of 10 µl in EX buffer system (20 mM Tris/HCl pH 7.6, 1.5 mM $MgCl_2$, 0.5 mM EGTA ang 10 % glycerol). The concentration of monovalent anions (Cl^-) and cations (K^+/Na^+) was adjusted to 90 mM. Nucleosomes were incubated with 50 - 200 nM of the enzymes indicated in the individual figures for 90 min at 27°C. The reaction was stopped by the addition of 1 µg competitor DNA (plasmid DNA) and further incubated for 5 min. Nucleosome positions were resolved by native gel electrophoresis in 4.5 % or 6 % polyacrylamide gels in 0.4x TBE. Gels were pre-run for 20 - 30 min and run for 60 - 90 min at 100 V. Optimal running time was controlled by using orange G as a marker. After separation of the nucleosomes positions by native gel electrophoresis, the nucleosomal DNA was visualized by staining with 0.5 mg/ml ethidium bromide in 0.4x TBE for 10 - 15 min and destaining 2x 10 min with dH_2O. Documentation was performed with the gel documentation system (Bio-Rad).

4.2.7.4 Chromatin spacing assay

Remodeling activity of SNF2H and SNF2L was also tested on poly-nucleosomal substrate. The circular pUC18 plasmid containing 12 repeats of 601 positioning sequence (pUC 18 12x 601) was assembled into chromatin using limited amounts of histones. Specifically the 601 nucleosome binding sequence was incorporated into nucleosomes, due to the increased affinity for histone octamers, compared to unstructured pUC18 sequence. Using these arrays of 601 sequences a nucleosome spacing of 200 bp (147 bp nucleosme positioning signal + 53 bp linker sequence) was generated. All reactions were performed in siliconized tubes (Biozym). For a standard spacing experiment 1 µg of pUC18 12x 601 chromatin was incubated with 550 nM remodeling enyzme. A typical reaction contained 1.5 mM ATP in a total volume of 16 µl in EX buffer system (20 mM Tris/HCl pH 7.6, 1.5 mM $MgCl_2$, 0.5 mM EGTA ang 10 % glycerol). The concentration of monovalent anions (Cl^-) and cations (K^+/Na^+) was adjusted to 80 mM. Nucleosomes were incubated with the enzymes indicated in the individual figures for 90 min at 27°C. The reaction was stopped by expanding the volume with EX80 to 60 µl and addition of MNase in presence of 3 mM $CaCl_2$. Typically 0.5 µg MNase were added and partial digested the linker DNA in a time course form 30, 80, 160 to 200 sec. The reaction was stopped by removing 15 µl from the reaction and adding 0.2 volumes of stop solution (4 % SDS, 100 mM EDTA).

Reactions were supplemented with proteinase K (10 µg / reaction) and glycogen (10 µg) and deproteinized for at least 1 hour at 40°*C*. The DNA was purified by ethanol precipitation (0.5 vol 7.5M NH_4Ac and 2 volumes 100 % ethanol), incubated for 10 min on ice, centrifuged for 15 min at 13000 rpm and washed once with 70 % ethanol, air dried, dissolved in 10 µl loading buffer and analyzed on 1.3 % agarose gels supplemented with 0.01 % SYBR Safe.

4.2.7.5 ATPase assay

ATPase assays were performed in the presence of γ-^{32}P-dATP (3000 Ci/mmol) with various substrates to analyze the specific activity. A typical reaction contained 240 nM of DNA or chromatin in 12.5 µl reaction volume with the following buffer conditions: 20 mM Tris pH 7.6, 75 mM monovalent anions (Cl^-) and cations (K^+/Na^+), 1.5 mM $MgCl_2$, 0.5 mM EGTA, 10 % glycerol, 200 ng/µl BSA, in the presence of 5 µM ATP together with 5 nM of γ-^{32}P-dATP. The reaction was kept on ice and incubated at 30°*C* after the addition of 120 nM remodeler. At different time points (typically after 0, 45 and 90 min) 2 µl of the reaction was added to 4 µl Tris/HCl pH 7.6 and 10 mM EDTA to stop ATPase reaction and stored on ice. The hydrolyzed phosphate was separated from unreacted ATP by gel electrophoresis. A 20 % PAA gel in 1x TBE was polymerized in a glas cassette and pre-run for 20 min at 80 V. 3 µl bromphenol blue loading dye was added to each reaction. Samples were separated at 10 mA until the bromphenol blue dye has run 2 cm into the gel (approximately 40 min). Gels were sealed in a plastic bag and exposed on BioMaxMS film (Kodak Film) for 30 - 45 min. ATP and hydrolyzed phosphate spots were quantified using the multigauge software. The percentage of hydrolyzed ATP ($\mathbf{R}_H$) was calculated according to the following equation:

$$\mathrm{R}_H = \frac{P_i + ATP}{P_i}$$

Where $\mathbf{P}_i$ was the signal intensity of hydrolyzed phosphate divided by sum of of left ATP signal and hydrolyzed phosphate signal $\mathbf{P}_i$ + **ATP**. Experiments were repeated twice and standard deviation were calculated.

4.2.7.6 MNase footprinting assay

A remodeling reaction with 150 nM 0-NPS1-0 mononucleosomes was done with 200 nM SNF2H and SNF2L according to the remodeling protocol described in section 4.2.7.3 in

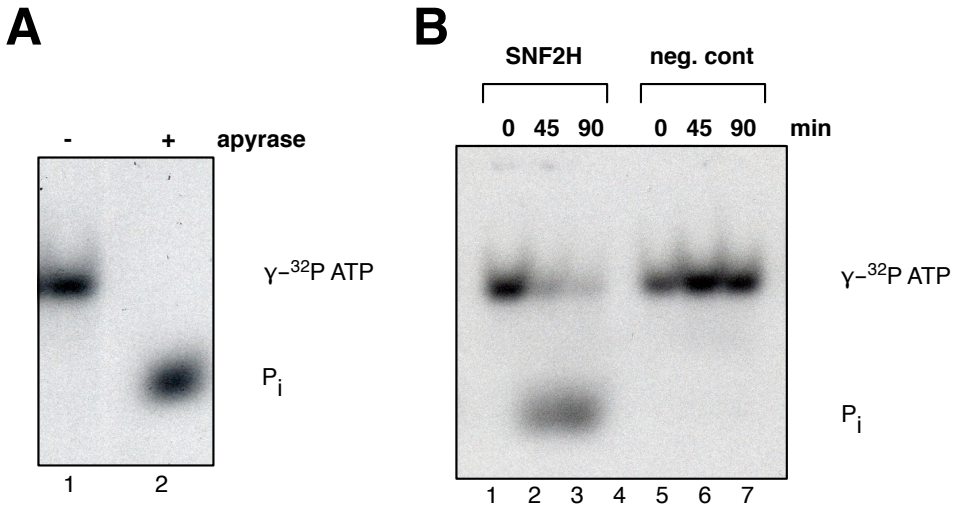

Figure 4.4: **Separation of ATP and phosphate on 20 % polyacrylamid gels** **(A)** 5 µM ATP mixed with 5 nM of γ-^{32}P-dATP in 50 µl 1x reaction buffer (NEB) were incubated with 10 units apyrase for 90 min at 30°C. 2µl of the reaction were loaded to a 20 % PAA gel in 1x TBE. **(B)** Example of ATPase test with 120 nM SNF2H in presence of 240 nM 77-NPS1-77 nucleosomes.

at total volume of 15 µl. The reaction was stopped by the addition of 1 µg (= 5 µM) 35 bp long double stranded competitor oligonucleotide (sb3 + sb4) and further incubated for 5 min. Accessible linker DNA was digested with 9 U MNase in total volume of 63 µl of EX80 supplemented with 3 mM $CaCl_2$. The reaction was stopped after 30 s, 60 s and 4 min by removing 15 µl from the sample and adding of 10 µl of stop solution (4 % SDS, 100 mM EDTA). Reactions were supplemented with proteinase K (10 µg / reaction) and glycogen (10 µg) and deproteinized for 45 min at 40°C. The DNA was purified by ethanol precipitation (0.5 vol 7.5 M NH_4Ac and 2 volumes 100 % ethanol were added, incubated for 10 min on ice, centrifuged for 15 min at 13,000 rpm and washed once with 70 % ethanol), air dried, dissolved in 10 µl ddH_2O. 1 µl of each samples was brought to a volume of 20 µl with ddH_2O and 1 µl of a 1:400 dilution of SYBR Green I in DMSO was added. The samples were loaded onto a capillary electrophoresis by electro-kinetically injection for 2 s at 33 V/cm in an uncoated 30 cm capillary with 5.5 % PVP in 1x TBE. DNA was separated for 9 min at 166 V/cm over 10 cm distance. For detection a 488 nm argon-ion Laser with a 488 nm notch filter and 560/20 nm bandpass filter was used. Relative laser signal intensities were plotted as a function of the retention time.

4.2.7.7 Analysis of remodeling kinetics by measurement of FRET burst

The dynamic binding studies based on FRET were done in collaboration with the group of Prof. Dr. Jens Michaelis at the Department of Chemistry and Biochemistry at the Ludwig-Maximilians-University Munich.

Synthesis of atto532 and atto647 double fluorescently labelled nucleosomal DNA by ligase chain reaction Design and synthesis of atto532 and atto647 fluorescently labelled NPS1 nucleosomal DNA was done by Barbara Treutlein from the group of Prof. Dr. Jens Michaelis. Labelled and unlabeled oligos for DNA syntheses were purchased via IBA BioTAGnology (Göttingen). The synthesis of 200 bp DNA from 10 oligonucleotides was based on the Ligase Chain Reaction (LCR) [Barany, 1991] using Taq DNA Ligase (New England Biolabs). A detailed description of the protocol established by Barbara Treutlein is presented in the supplementary information in the appendix.

FRET burst analysis FRET burst experiments and raw data analysis were done by Wolfgang Kügel from the group of Prof. Dr. Jens Michaelis. The method established by Wolfgang Kügel is described in all details in the appendix.

4.2.7.8 Localization of GFP- and RFP-tagged SNF2H and SNF2L in 3T3 nuclei

The nuclear localization of SNF2H and SNF2L was ananlyzed in collaboration with Fabian Erdel from the laboratory of Dr. Karsten Rippe at the Research Group Genome Organization & Function at the DKFZ and the BioQuant in Heidelberg. Murine NIH 3T3 cells were cultured in DMEM High Glucose/10% FCS. For live imaging of SNF2H and SNF2L, cells were seated in a LabTek-chamber and transiently transfected with autofluorescent constructs of SNF2H/SNF2L using Effectene (Qiagen). Confocal microscopy images were acquired with a Leica SP5 confocal microscope equipped with a 63x oil immersion objective. EGFP-tagged SNF2H was cloned as described [Collins et al., 2002] and accordingly a SNF2L EGFP construct was generated [Erdel et al., 2010].

4.2.8 Structural and functional analysis of human chromatin

4.2.8.1 Growing HeLa cells

Human adenocarcinoma cells of the HeLa line were cultured and propagated in D-MEM medium (+ 100mg/L Glucose + GlutaMAX + Pyruvate) supplemented with 10 % FCS and 50 U/l penicillin, 50 µg/l streptomycin (all from Invitrogen). Under optimal condition in a humidified chamber at $37°C$ with 5 % CO_2 cells numbers doubled ever 23 - 24 hours.

The culture supernatant was changed every 2 - 3 days depending of the confluency of the cells. The cells were split at an estimated confluency of 70 %. For splitting 3ml trypsin/EDTA solution was added to the of a confluent 15 cm dish (diameter) and the then incubated for 3 - 4min at 37°C. The reaction was stopped by adding culture medium at three time the volume as EDTA/Trypsin. After determination of cell density, an appropriate volume of cells was transferred to a new flask and filled with medium to the final volume.

4.2.8.2 Isolation of genomic DNA from HeLa cells

For preparation genomic HeLa DNA confluent 15 cm dishes (diameter) with approximately 2x 10^7 cells were once washed with PBS. Then 3 ml permeabilization buffer (15 mM Tris/HCl pH 7.6, 300 mM saccharose, 60 mM KCl, 15 mM NaCl, 3 mM $CaCl_2$, 0.5 mM EGTA, 0.2 % (v/v) NP40) was added and cells were incubated for 2 min at 37°C. Cellular RNA was digested by addition of 250 µg RNase A in 3 ml 50 mM Tris/HCl pH 8, 20mM EDTA and 1 % SDS. After 2 hours of digestion at 37°C 250 µg proteinase K was added to subsequently degrade all cellular proteins. This reaction was performed over night at 37°C. The next day the highly viscous DNA containing cell lysate was aspirated and vortex for 5 - 10 min to shear genomic DNA and increase solubility. Addition of 0.5 volumes of 7.5 M ammonium acetate and 2 volumes of 100 % icecold ethanol to the lysate precipitated DNA. This mixture was incubated for 10 min on ice and then centrifuged for 30 min at 4°C at 20,000 g. The DNA pellet was washed once with 70 % ethanol. Before dissolving DNA all ethanol had to be carefully removed and drying of the pellet had to be avoided, since this would highly reduce DNA solubility. Then the pellet was resuspended in 2 ml prewarmed ddH_2O and over night incubated at 45°C in thermo shaker to dissolve genomic DNA.

4.2.8.3 MNase digestion of HeLa chromatin

Chromatin of HeLa cells was analyzed by partial digestion of nucleosomal linker DNA. Confluent 15 cm dishes, in general 10 - 15 in total, with approximately 2x 10^7 cells were once washed with 5 ml PBS. Prior to use micrococcal nuclease (MNase) from *Staphylococcus aureus* was added to the permeabilization buffer (15 mM Tris/HCl pH 7.6, 300 mM saccharose, 60 mM KCl, 15 mM NaCl, 4 mM $CaCl_2$, 0.5 mM EGTA, 0.2 % (v/v) NP40 and fresh 0.5 mM 2-mercaptoethanol). Per dish 3 ml permeabilization buffer supplemented with, depending on the experiment, 100 - 2000 units MNase was added and cells were incubated for 3 min at 37°C. The nuclease reaction was stopped by addition of 3 ml stop

buffer (50 mM Tris/HCl pH 8, 20 mM EDTA and 1 % SDS) and RNA was digested by addition of 250 µg RNase A. After 2 hours of incubation at 37°*C* 250 µg proteinase K was added to subsequently degrade all cellular proteins. This reaction was performed over night at 37°*C*. The next day the viscous DNA containing cell lysate was aspirated and non-digested nucleosomal DNA was isolated as described below.

4.2.8.4 Preparative purification of nucleosomal DNA from HeLa cells

In general nucleosomal DNA was precipitated according to the ammonium acetate and ethanol protocol. To isolate DNA form HeLa lysate in a preparative scale this protocol had to be modified. One challenge when isolating DNA from 10x 15 cm dishes was the large volume increase of the precipitation mixture (60 ml lystate + 150 ml NH_4Ac/EtOH) and the limited capacity of centrifuges rotating with 20,000 *g*. After addition of 0.5 volumes of 7.5 M ammonium acetate and 2 volumes of 100 % icecold ethanol to the lysate the mixture was incubated for 10 min on ice. DNA precipitates were then separated by filtration instead of centrifugation. Precipitation suspension was loaded into 20 ml syringes with 0.22 µm Millex GV Durapore PVDF membrane filters (Millipore). The suspension was drawn through the filter by vacuum, and precipitates retained on the membrane. Filter were washed once with 3 ml icecold 70 % ethanol and after all alcohol was removed filters were dried on a thermo block at 60°*C*. To elute DNA filters were screwed to 5 ml syringes and the forcer was removed. Then filters were presoaked by addition of 500 µl warmed ddH_2O and after a few minutes further 500 µl water were added. Water was flushed through the filters and elutates were collected in 2 ml reaction tubes. This elution step was repeated once. DNA concentration of the eluate fraction was determined by absorption measurement at 260 nm using a NanoDrop ND1000 spectrophotometer (Peqlab). The total amount of DNA isolated from lysates of 2x 10^7 cells was approximately 200 µg DNA in elution one and 20 µg in the second elution. Estimating that a normal diploid human cell contains 7 pg of DNA in total [LabFAQS, 2010], and taking into account that HeLa cells have an abnormal karyotype with modal number of 82 (70 - 164), 13 pg of DNA can be found in one tumor cell. The lysate of a confluent 15 cm dish with 2x 10^7 cells contains approximately 260 µg of DNA. With 220 µg of purified DNA roughly a recovery rate of 85 % was reached with this method.

4.2.8.5 Isolation of nucleosomal DNAs of specific size after high MNase treatment

Incubation of permeabilized cells with MNase leads to fast degradation of free linker DNA within the chromatin. DNA sequences wrapped around the histone octamers are protected from endonucleolytic cleavage. Since the conditions used for MNase treatment were optimized to partially degrade chromatin, beside the 147 bp mono-nucleosomal fragment (1n) also di- (2n) and trinucleosomal (3n) DNA could be separated by agarose gel electrophoresis. For a preparative isolation of 1n, 2n and 3n nucleosomal DNAs separation was done using a 18 cm x 20 cm x 1.5 cm gel with 1.5 % agarose in 1x TBE pre-stained with 0.005 % SYBR Safe. Nuclesomal DNA was mixed with 10x DNA loading dye and 10 - 20 µg DNA were loaded per 3 cm lane. DNA fragments were separated for 3 - 4 h at 120 V. When 1n, 2n and 3n nucleosomal DNAs were clearly separated bands were excised with a sterile scalpel. From excised gel slides DNA was eluted using the Bio-Rad Electro-Eluter according to manufacturer's protocol for DNA elution. Green membrane caps with a molecular weight cut of 3500 dalton (Bio-Rad) and were pre-incubated in 1x DNA elution buffer (40 mM Tris, 20 mM acetic acid, 1 mM EDTA pH 8.0 and SDS 0.1 % w/v) for one hour at 60°C. Then the Electro-Eluter was assembled and each tube was filled with 1 - 1.5 gel slices. Elution was done at 10 mA per tube for 15 min in 1x DNA elution buffer. After elution DNA was removed from the dialysis membrane by inverting the polarity for 1 min. Approximately 400 - 600 µl eluate were recoverd from each membrane cap. Each cap was rinsed with 200 µl of fresh elution buffer and collected with the elution fraction. Glycogen, 0.5 µg/µl final concentration, was added to each sample and DNA was precipitated by ammonium acetate and ethanol as described. Purity of each nucleosomal DNA preparation was analyzed by agarose gel electrophoresis.

4.2.8.6 Isolation of nucleosomal DNAs of specific size after low MNase treatment

After digestion with reduced MNase amounts (e. g. 250 U per 15 cm dish) only a fraction of total HeLa chromatin was digested to mono- (1n), di- (2n) and tri-nucleosomes (3n). To purify sufficient amounts of 1n, 2n and 3n DNA fragments more cells had to be MNase treated and the DNA framents had to be enriched prior gel separation. When directly loading the precipitated nuclease extract on a preparative agarose gel, the 1n, 2n and 3n fragments resembled such a small fraction of total DNA, that elution and precipitation of these DNAs from excised bands failed. To enrich smaller DNA fragments a polyethylene glycol precipitation was done. The use of of polyethylenglycol 8000 (PEG 8000) at different concentrations allows the selective removal of smaller DNA fragments [Paithankar and Prasad, 1991]. DNA fragments larger than 600 bp precipitate when us-

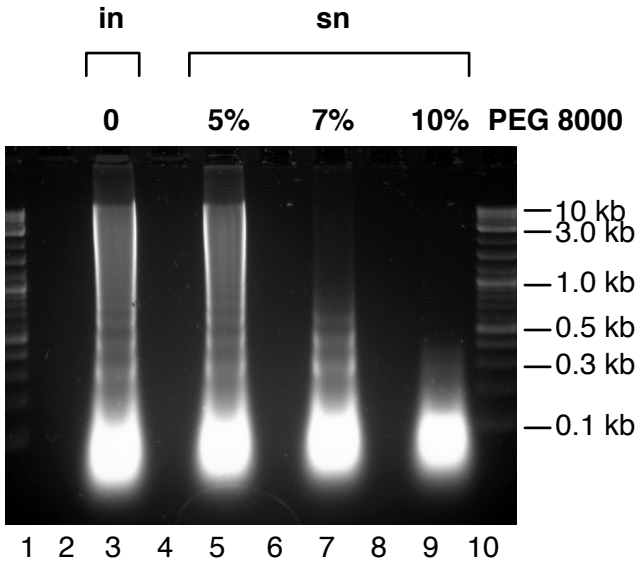

Figure 4.5: **Size selective precipitation of DNA fragments by PEG 8000** Chromatin of HeLa cells was partially digested with low dose of MNase. After purification of DNA (input, lane 3) samples were incubated with different concentrations of PEG 8000 ranging from 10 % to 5 %. DNA remaining in the supernatant (sn) was precipitated and also loaded on a 1.3 % agarose gel (lanes 5, 7 and 9). With higher PEG concentrations smaller DNA fragments were precipitated and only very small fragments remained in the supernatant.

ing PEG 8000 at 7 % and $MgCl_2$ at 10 mM final concentration. Low molecular weight DNA remained in the supernatant under these conditions. MNase treated DNA was mixed with 0.5 volume of PEG solution (21 % PEG8000, 30 mM $MgCl_2$), and incubate 10 - 30 min at room temperature. Samples were centrifuged ($22°C$, 13,000 g, 15 - 30min), and DNA within the supernatant was precipitated by ammonium acetate and ethanol as already described and washed with 70 % ethanol, airdried and dissolved in an appropriate volume of ddH_2O.

These pre-separated DNA samples were then mixed with 10x DNA loading dye also loaded on 18 cm x 15 cm x 1.5 cm gels with 2 % agarose in 1x TBE stained with 0.005 % SYBR Safe. DNA fragments were separated for 3 - 4 h at 120 V. When 1n, 2n and 3n nucleosomal DNA were clearly separated bands were excised with a sterile scalpel [Kissing, 1976]. Beside these fragments also a pool of smaller DNAs could be isolated under these conditions. Two populations of so called "sub-nucleosomal" DNA were isolated. Elution was done using Bio-Rad Electro-Eluter as already described above.

4.2.8.7 Southern blotting

Partially MNase digested chromatin from HeLa cells was purified and DNA fragments were electrophoretically separated on a 14 x 21 cm 1 % agarose gel in 1x TBE supplemented with 0.01 % SYBR Safe stain. Typically 5 µg DNA were mixed with loading dye and loaded per lane. As a size marker 5µl 1 kb GeneRuler (Fermentas) and as positive control 5 µg genomic DNA digested with specific restriction endonucleases (EcoRI, MspI, AluI) were run in parallel. After separation of the fragments for 5 h at 100 V the gel was documented using the FLA3000 (FujiFilm) and subsequently incubated for 12 min in 0.25 M HCl to partially hydrolyze DNA. This step was followed by denaturation of double stranded DNA in denaturation solution (0.5 M NaOH, 1.5 M NaCl) for 2x 15 min. The gel was incubated for 2x 15 min in 1 M ammonium acetate for neutralization. DNA was transferred to nitrocellulose membrane by semi dry blotting using a stack of 2x Whatman paper rinsed in NH_4Ac, 2 parafilm stripes paced at the edges for isloation (0.5 cm). The inverted gel was placed onto the Whatman paper and wet with NH_4Ac. Then the nitrocellulose membrane was rinsed in NH_4Ac and placed onto gel. 3x Whatman rinsed in NH_4Ac, 1 packet paper towels and a weigh were placed on top of this stack. After transfer over night DNA was cross linked by UV light (30 J/cm^2). Before radioactively labelled DNA probes were hybridized to the DNA fragments nitrocellulose membrane was pre-incubated for 60 - 90 min in 0.5 M sodium phosphate pH 7.2, 7 % SDS and 1 mM EDTA at 60°C in a rotating wheel. Repetitive DNA elements (Alu-repeats, telomeres, centromeres and rDNA) were detected using short oligonucleotides end-labelled with γ-^{32}P-dATP by PNK (see section 4.2.1.6). To generate probes from purified 3n nucleosomal (500 bp) DNA was bodylabelled with α-^{32}P-dATP by Klenow fragment and random primer (see section 4.2.1.5). All probes were added to pre-hybridization solution with a final activity of 10^6 - 10^7 cpm/ml and incubated over night at 60°C in a roating wheel. Not bound probe was washed of 2x 30 s with 40 mM sodium phosphate pH 7.2, 0.1 % SDS. Finally dried membrane was placed on a IP plate until significant radioactive signals were detectable with FLA3000 laser reader (FujiFilm).

4.2.8.8 Fluorescence *in situ* hybridization (FISH)

Hybridization of tri-nucleosomal DNA (3n) to metaphase spread chromosomes (2D) and to fixed nuclei (3D) were done by Dr. Attila Németh in the lab of Prof. Dr. Thomas Cremer at the Department Biology II, Ludwig-Maximilians University Munich. DNA probes were labelled with the Prime-it Fluour Fluorescence Labelling Kit from Stratagene according to manufacturer's protocol. 1 µg DNA was used and labelled with fuor-12-dUTP

or Cy3-dUTP by random prime labelling with Klenow fragment at 37°C over night.

2D FISH on metaphase chromosomes 2D FISH experiments were performed on HeLa and human female lymphocyte metaphase spreads according to standard protocols. Tri-nucleosomal DNA (3n) was labelled without amplification. For suppression of signals from repetitive DNA regions, 10µg Cot1 DNA was used.

3D FISH in HeLa nuclei 3D FISH experiments were performed as described [Cremer et al., 2008]. In localization experiments 3n nucleosomal DNAs were fluorescently labelled as decribed above and used on HeLa cervix carcinoma cells and IMR90 lung embryonic fibroblasts. Cells were fixed and 3D FISH experiments were performed. Confocal microscopy and image analysis was done after 3D FISH experiments as follows: series of optical sections through 3D-preserved nuclei were collected using a Leica TCS SP5 confocal system equipped with a Plan Apo 63-/1.4 NA oil immersion objective and a diode laser (excitation wave length 405 nm) for DAPI, a DPSS laser (561 nm) for Cy3 and a HeNe laser (633 nm) for Cy5. For each optical section, signals in different channels were collected sequentially. Stacks of 8-bit gray-scale images were obtained with z-step of 200 nm and pixel sizes 30 - 100 nm depending on experiment.

4.2.8.9 Relative methylation levels of 1n, 2n and 3n nucleosomal DNA

Methylation level 1n, 2n and 3n nucleosomal DNA was analyzed using an ELISA based assay. A methylation specific antibody allowed analysis of 50 to 100 µg nucleosomal DNA with the Imprint Methylated DNA Quantification Kit from Sigma-Aldrich according to manufacturer's protocol. The subsequent calorimetric reaction of the antibody bound enzyme was detected via absorbance at 450 nm on a plate reader. To avoid sample evaporation during incubation at 37°C, plates were sealed with a foil.

4.2.8.10 Hybridization of 3n nucleosomal DNA to ENCODE chip

Tri-nucleosomal DNA (3n) released from HeLa chromatin after partial digestion with 250 U (low MNase) and 1000 U MNase (high MNase) per 2x 10^7 cells was end labelled with fluorescent dyes and hybridized to an ENDODE (encyclopedia of DNA elements) DNA chip. For sample preparation 5 µg of 3n DNA were gel-purified, resolved in ddH_2O and puritiy was photometrically checked. A_{260}/A_{280} ratio was 1.8 for both samples and the

A_{260}/A_{230} ratios were 1.82 (low MNase) and 2.05 (high MNase), which both indicated a sufficient purity for chip hybridization. Further sample processing and chip hybridization was done by NimbleGen (Roche). DNA from low MNase conditions was labelled with Cy3 and high MNase samples were labelled with Cy5. After further quality controls, probes were hybridized to a 2007-10-25_HG18_ENCODE chip. On this isothermal hybridization chip 385,000 50 - 75mer probes were spotted with a median probe spacing of 60 bp. Since a standard ChIP-chip protocol was applied by NimbleGen high MNase samples were treated as background "control" whereas low MNases served as "sample" in the comparative analysis.

4.2.8.11 Bioinformatic analysis of comparative ENCODE chip

The bioinformatic analysis of the microarray data was done by our collaboration partner Javier Santoyo-Lopez, PhD, from the laboratory of Joaquin Dopazo, PhD at Bioinformatics & Genomics Department Prince Felipe Research Centre (CIPF), Valencia, Spain. The 3n low MNase Cy3 labelled peaks from the comparative ENCODE microarray hybridization were aligned to different functional data sets available from HeLa S3 cells. In principle correlation with active chromatin marks like histone modifications H3K4me3, H3K36me3, RNAPII association and repressive marks as H3K27me3 and DNA methylation was analysed. Furthermore also data from expression arrays detecting RNA transcripts from ENCODE regions were aligned to the peak pattern. The information about the microarrays and chromosomal coordinates was taken from the GEO repository (http://www.ncbi.nlm.nih.gov/geo/). A detailed list of the used data bases is shown below. The functional annotation was done by overlaying the coordinates from the described files with the ENCODE peak coordinates [Németh et al., 2010]. The analysis of HeLa expression was a standard presence absence call using the Babelomics4 tool [Medina et al., 2010].

Table 4.15: **Sources of functional ENCODE data from HeLa S3 cells**

Description	**Database**
DNaseSeq	wgEncodeDukeDNaseSeqPeaksHelas3V3.narrowPeak.gz
http://hgdownload.cse.ucsc.edu/goldenPath/hg18/encodeDCC/wgEncodeChromatinMap/	
RNAPII	wgEncodeUtaChIPseqPeaksHelas3Pol2.narrowPeak.gz
http://hgdownload.cse.ucsc.edu/goldenPath/hg18/encodeDCC/wgEncodeChromatinMap/	
H3K4me3	wgEncodeUwChIPSeqPeaksRep1Helas3H3k4me3.narrowPeakk.gz

Description	**Database**
http://hgdownload.cse.ucsc.edu/goldenPath/hg18/encodeDCC/wgEncodeChromatinMap/	
H3K27me3	wgEncodeUwChIPSeqPeaksRep1Helas3H3k27me3.narrowPeakk.gz
http://genome.ucsc.edu/cgi=bin/hgTrackUi?db=hg18&g=wgEncodeUwChIPSeq	
H3K36me3	wgEncodeUwChIPSeqPeaksRep1Helas3H3k36me3.narrowPeakk.gz
http://genome.ucsc.edu/cgi=bin/hgTrackUi?db=hg18&g=wgEncodeUwChIPSeq	
RNA	GSM472905
http://www.ncbi.nlm.nih.gov/geo/query/acc.cgi?acc=GSM472905	
RNA	GSM396650
http://www.ncbi.nlm.nih.gov/geo/query/acc.cgi?acc=GSM396650	

5 Results

5.1 Comparative analysis of human ISWI homologs SNF2H and SNF2L

Sequence alignments of both human ISWI remodeler revealed that 80 % of the amino acids of SNF2H are identical with SNF2L and even 87 % are conserved. The catalytic RecA-like ATP dependent DExx and HELICc domains, together with DNA and protein interacting HAND, SANT, SLIDE domains, are even higher conserved between both paralogs (95 %). In contrast, the termini are highly divergent. Only 20 % of the first 78 N-terminal and last 11 C-terminal amino acids are similar and predicted to form unstructured domains of an unknown function (see figure 5.1 A). Despite this high degree of conservation, there was evidence that SNF2H and SNF2L were not functionally redundant isoforms. In mouse it had been shown, that both proteins exhibit a distinct spatial and temporal expression pattern during development [Lazzaro and Picketts, 2001]. Depletion of SNF2L in human malignant cancer cell lines induced growth arrest and apoptosis, not observed after knock-down of SNF2H [Ye et al., 2009]. The molecular basis and the functional implications of this specialization was addressed in this study.

5.1.1 Purification of recombinant human ISWI homologs

Both human ISWI homologs were recombinantly expressed with a N-terminal hexa-histidin-tag in SF21 cells. Single step affinity purification using a Ni-NTA-matrix allowed quantitative purification of both proteins in high purity. As demonstrated by the analytical SDS-PAGE in figure 5.1 B and C, the first elution fractions showed a strong signal at a molecular weight of approximately 130 kD, which corresponded well to the estimated size of 127 kD for SNF2H and 126 kD of SNF2L. This elution fractions E1 were used for the presented experiments and typically, 300 - 450 µg recombinant protein was purified from 100 x10^6 cells.

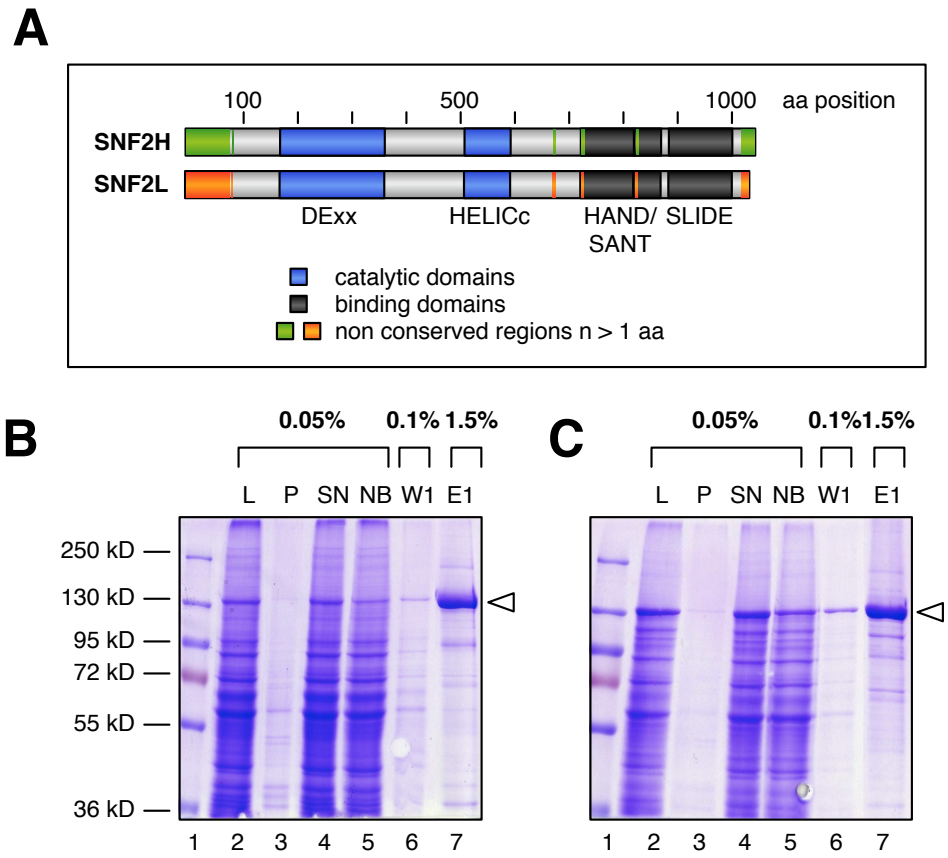

Figure 5.1: **Purification of recombinant human ISWI remodeler**
(A) SNF2H and SNF2L have a highly similar protein sequence. Catalytic helicase domains (blue) and interaction domains (black) are highly conserved between both homologs. In contrast N- and C-terminal blocks (aa position 1 - 76 and 1028 - 1052 of SFN2H and 1 - 79 and 1031 - 1042 of SNF2L) showed only 20 % conservation, in contrast to 95 % at the remaining amino acid positions.
(B) Purification of SNF2H. Hexa-His-tagged SNF2H was expressed in Sf21 insect cells and purified by His-tag affinity purification. Here, an analytical 7.5 % SDS PAGE is presented.
(C) Purification of SNF2L as described in (B). Number indicate the volume fraction of each sample loaded to the gel. Bands of the recombinant proteins highlighted by arrows. (L: lysate, P: pellet, SN: supernatant, NB: not bound to beads, W1: wash fraction, E1: elution fraction).

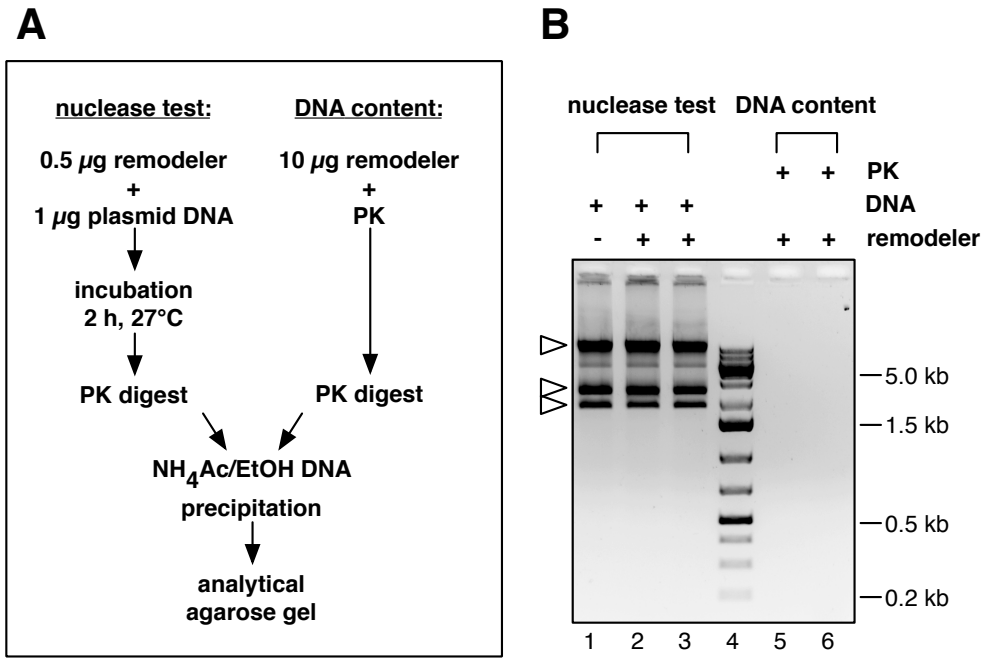

Figure 5.2: **Quality control of purified SNF2H and SNF2L fractions**
(A) Contamination of the recombinant proteins with cellular nucleases was excluded by a DNA degradation test. 1 µg plasmid DNA was incubated with 0.5 µg remodeler at standard remodeling conditions for 2 h. After protein digestion with proteinase K (PK) DNA was precipitated and checked on an agarose gel. To detect DNA, co-purified with the remodeling enzymes, 10 µg of each protein was digested with PK and remaining nucleic acids were precipitated in parallel to nuclease test samples.
(B) 1 % agarose gel loaded with the precipitated DNA from nuclease test (lanes 1 - 3) and dissolved DNA after quantitative PK digest (lanes 5 and 6). In lanes 2 and 5 SNF2H, lanes 3 and 6 SNF2L was tested. Different forms of super-coiled plasmid DNA are marked by arrows.

Before purified remodeling enzymes were tested in functional assays, the quality of the protein fractions was checked. Contamination of the enzymes with nucleases would lead to chromatin degradation, and co-purified DNA would interfere with quantitative binding measurements. As shown in figure 5.2 neither DNA degradation of the 3 kb plasmid was detected under standard remodeling conditions, nor DNA was precipitated after proteins had been digested. The different DNA bands reflect the three levels of super-coiling of the circular DNA. Since precipitation of all samples was done in parallel, precipitated plasmid DNA demonstrated the quantitative extraction of nucleic acids at this step.

5.1.2 Chromatin assembly

When analyzing the detailed mechanisms and functional differences of remodeling enzyme and chromatin substrate interactions *in vitro*, well characterized nucleosomal substrates are crucial.

To specifically position histone octamers on DNA fragments, a 147 bp long nucleosome positioning sequence, named NPS1, was used. This NPS1 sequence was based on the well-studied 601 DNA [Lowary and Widom, 1998] and 87 % of all bases were identical. At single positions, cytosine bases were replaced by thymine to remove CpG dinucleotides, in order to allow also DNA methylation studies with these substrates (not part of the work presented here). This exchange did not interfere with the sequence specific positioning of nucleosomes (see well defined bands figure 5.3 C), since the affinity of 601 sequence to histone octamers was in order of magnitudes higher, compared to any natural DNA positioning sequence [Lowary and Widom, 1998; Widom, 2001]. This strong nucleosome positioning signal was embedded into stretches of natural promoter sequences from the murine rDNA and *hsp 70* gene. A broad set of nucleosomes with a specific structure and symmetry was produced by amplifying the NPS1 sequence with primer pairs hybridizing to specific regions of the template sequence (figure 5.3). The promoter sequences served as linker DNA flanking the NPS1 nucleosome positioning sequence. With this DNA composed of the strong positioning sequences NPS1 flanked by natural promoter DNA well positioned nucleosomes were formed.

The *in vitro* assembly of chromatin by salt dialysis is based on the continuous decrease of the NaCl concentration from 2 M to 220 mM. DNA and chicken histone octamers were mixed in 2 M NaCl containing buffer. When the concentration of NaCl dropped below 1.5 to 1 M, affinity of the (H3/H4) tetramer for DNA significantly increased. At 1 to 0.6 M NaCl, the affinity of the (H2A/H2B) heterodimers increased, and they were also recruited to the nucleosome core particles, forming intact nucleosomes [van Holde, 1989]. As seen in figure 5.3 C, NPS1 containing DNA sequences amplified by preparative PCR formed well positioned nucleosomes after assembly, as analyzed on native polyacrylamid gels.

Another way to generate defined DNA fragments for chromatin assembly was restriction digestion of plasmid templates. Multiple copies of 200 bp nucleosomal DNA with the NPS1 sequence and 248 bp long rDNA promoter sequence or 359 bp *hsp 70* gene promoter sequence [Hamiche et al., 1999] formed arrays in pUC plasmids. 7 - 12 copies of these nucleosomal DNA sequences formed a repetitive module within a pUC18 or 19 plasmid backbone. These sequences were cleaved out of the pUC plasmids by specific restriction endonucleases.

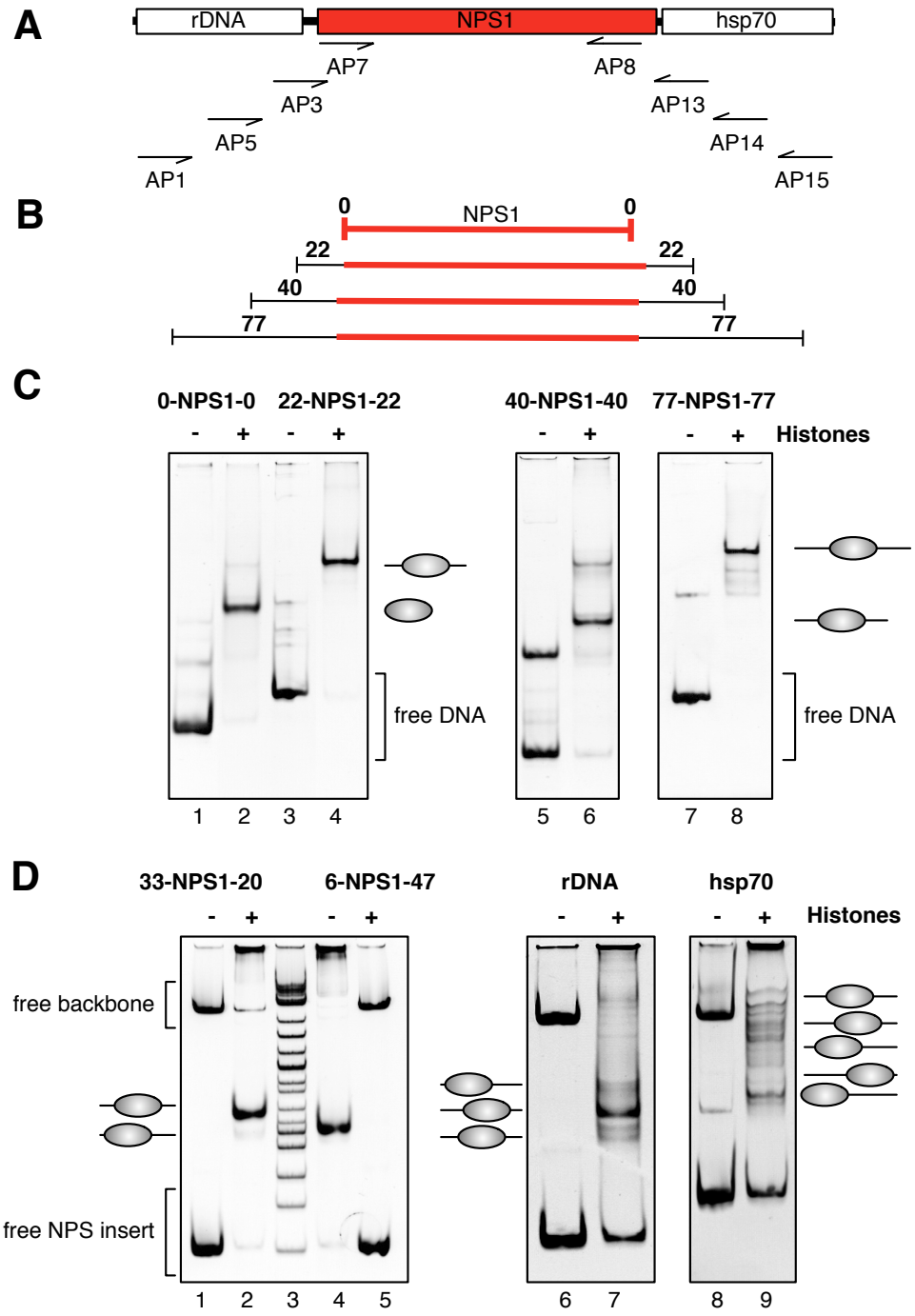

Figure 5.3: **Assembly mono-nucleosomes by salt gradient dialysis**
(A) Primer pairs for amplification of NPS1 containing nucleosomal DNA. 5'-end of AP8 hybridized 5 bp upstream of the 3'-end of NPS1, thus 0-NPS1-0 DNA fragment was 142 bp instead of 147 bp. **(B)** Indicated primer pairs allowed amplification of nucleosomal DNA with 0 bp, 22 bp 40 bp and 77 bp symmetric overhangs. **(C)** PCR amplified 0-NPS1-0, 22-NPS1-22, 40-NPS1-40, 77-NPS1-77 DNA was mixed with chicken histones (lanes 2, 4, 6, 8) and assembled into chromatin by salt gradient dialysis. **(D)** 200 bp 33-NPS1-20 and 6-NPS1-47 nucleosomal DNA, a 248 bp region of murine rDNA promoter (lanes 6, 7) and 359 bp *hsp70* promoter sequence (lanes 8, 9) were restriction digested from pUC plasmids. 2.8 kb pUC plasmid backbone (lanes 1, 4, 6, 8) served as competitor DNA during assembly and stacked into the wells. With the NPS1 DNA, nucleosomes assembled at a single position (lane 2, 5), in contrast to promoter sequences with nucleosomes at different distinct positions shown on a 4.5 % native PAA gel (lane 7, 9).

Nucleosome assembly of these positioning sequences led to formation of specific mono-nucleosomes. Packaging of the pUC plasmid backbone into chromatin formed unspecific higher molecular weight complexes, which remained inaccessible to native PAA gels (see wells of lanes 2, 4, 7 and 9 in figure 5.3 D). Mono-nucleosomal bands in 5.3 D lanes 2 and 4 were an example for the influence of the nucleosome symmetry on the migration behaviour within native gels. Both nucleosomes (33-NPS1-20 and 6-NPS1-47) were assembled on a 200 bp long NPS1 containing DNA fragment. The terminal positioned 6-NPS1-47 nucleosome migrated faster than the particle of the same size with a centrally positioned nucleosome (33-NPS1-20).
After assembly of nucleosomes onto the DNA sequences, covering the transcription start site of the rDNA locus (- 232/+ 16) and the *hsp 70* gene (- 348/+ 11), more than one single position on the DNA fragment was occupied by a histone octamer. As seen in figure 5.3 D lanes 7 and 9, distinct patterns of different positioned nucleosomes were detected on the native PAA gel. These positions reflect different thermodynamically favoured sites for histone binding. In contrast to the strong positioning sequence of the NPS1 constructs, the natural promoter sequences allow formation of nucleosomes at different translational positions.

Poly-nucleosomes were assembled on larger linearized or circular plasmid DNA. Using the optimized amount of histones large arrays of regularly spaced nucleosomes were assembled on the linearized 14 kb pT11 plasmid DNA. The correct assembly and nucleosome spacing was analyzed by partial MNase digestion of the nucleosomal DNA. Depending on the time point when the nuclease reaction was stopped, fragmentation down to different sizes was reached. This was subsequently analyzed by agarose gel separation of the remaining DNA in figure 5.4 A. The nucleosomes were evenly distributed and spacing of these arrays was approximately 170 bp. Chromatin with an increased nucleosomal spacing was generated by assembling limited amounts of histones to pUC18 plasmid DNA containing an array of 12x 200 bp of the 601 NPS sequence (see also 5.3 B lanes 2 and 4). Under limiting concentrations, histones preferentially assembled on the 601 NPS positioning sequences. As seen in figure 5.4 B mean spacing of the nucleosomes was 200 bp.

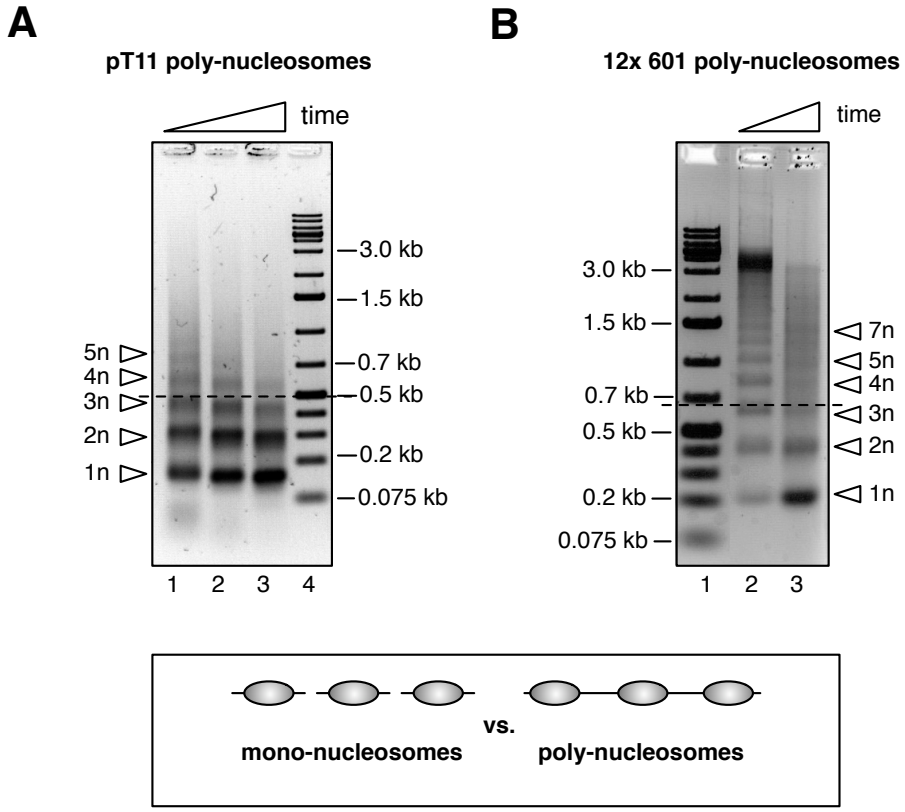

Figure 5.4: **Assembly of poly-nucleosomes by salt gradient dialysis**
(A) 11 kb long pT11 yeast plasmid DNA was linearized and assembled into chromatin by addition of chicken histone octamers and subsequent salt gradient dialysis. Formation of nucleosomal arrays was checked by partial MNase digestion. As shown in lanes 1 - 3, nuclease reaction was stopped after different time points, and DNA was loaded onto a 1.3 % agarose gel after deproteinization. Under these conditions, closed packed chromatin with nucleosomal spacing of approximately 170 bp was formed. The dotted line is a reference point for the length of trinuclosomes.
(B) To generate chromatin with an increased nucleosomal spacing, pUC18 plasmid containing an array of 12x 200 bp 601 NPS sequence was used. Under limiting histone concentrations during assembly, histones preferentially assembled on NPS1 positioning sequences. Thus poly-nucleosomes with a median spacing of 200 bp were generated, as analyzed by limited MNase digestion (lanes 2 and 3).
(C) Schematic representation of the differences between mono- and poly-nucleosomes (here trinucleosomes are shown).

5.1.3 Initial activity test of purified remodeling enzymes

Activity of the purified remodeling ATPases was analyzed in the presence of *in vitro* assembled chromatin. For this initial comparison, centrally positioned nucleosomes with symmetrical 77 bp long linker DNA (77-NPS1-77) were used as co-substrate. ATP-hydrolysis catalyzed by both enzymes was followed by detection of released radioactive phosphate. In a kinetic time course experiment the same amounts of SNF2H and SNF2L hydrolyzed comparable levels of ATP after 45 and 90 min of incubation (figure 5.5 A).
For the chromatin remodeling assay same amounts of SNF2H or SNF2L were incubated with 77-NPS1-77 nucleosomes in presence of ATP for 90 min. Relative nucleosome positions were analyzed subsequently on native polyacrylamid gels. Under these conditions movement away from the dyad axis of the DNA fragment increased mobility (Längst, G., *et al.*, 1999), whereas centrally positioned nucleosomes migrated slower. After incubation with both enzymes, efficient sliding of centered nucleosomes to end-positions was detected (figure 5.5 B). Both purified remodeling ATPases showed a comparable activity in these standard *in vitro* assays.

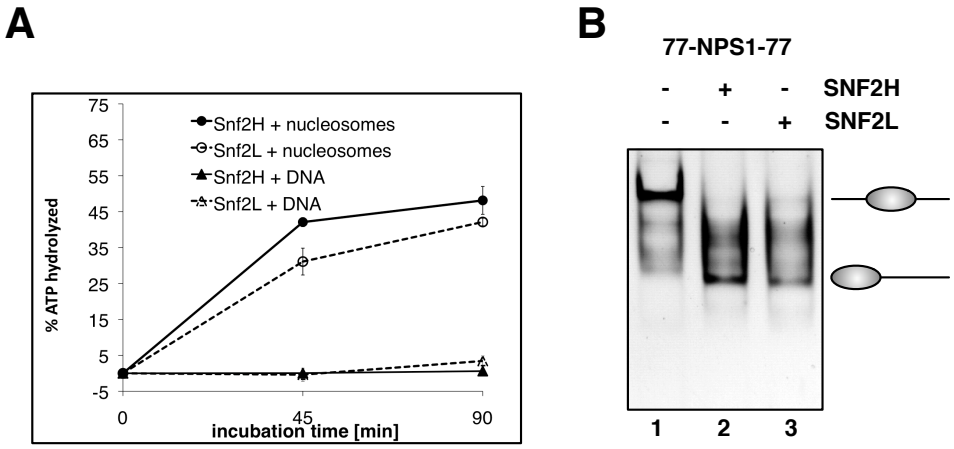

Figure 5.5: **ATP-hydrolysis and nucleosome sliding activity of purified enzymes**
(A) Quantification of hydrolyzed ATP (5 µM) in presence of 120 nM enzyme after 0, 45 and 90 min. 301 bp free DNA or assembled into chromatin was used as co-substrates (250 nM). Error bars represent standard deviation.
(B) Chromatin remodeling activity of both enzymes (100 nM) was tested using 301 bp long DNA assembled in chromatin (200 nM) and exposing 77 bp of extranucleosomal DNA in presence of ATP (2 mM). Different nucleosome positions were analyzed by EMSA on a native 4.5 % TBE-PAGE.

5.1.4 Mono-nucleosome binding

Interaction of ISWI remodeler to nucleosomes is dependent on the C-terminal substrate binding domains. The SLIDE domain allows efficient DNA binding, whereas the SANT domain binds to positively charged histone tails, enhancing the ATPase activity [Grüne et al., 2003].

Next, the binding of both ISWI homologs to different nucleosomal substrates was compared. Striking differences were observed when analyzing binding of SNF2H and SNF2L to central positioned 77-NPS1-77 nucleosomes with symmetric 77 bp long linker DNA. For both enzymes, formation of stable complexes with the nucleosomes was detected, as seen in the band shift experiments (figure 5.6). SNF2L showed a qualitatively different binding to these nucleosomes, defined intermediates formed distinct bands, suggesting a multimeric binding. Obviously, by single binding steps specific nucleosome-remodeler-complexes were formed (figure 5.6 B). In contrast to this, SNF2H did not form specific intermediates. Binding to the nucleosomes was detected, but interaction of the enzyme and the substrate resulted in formation of large complexes, inaccessible to the gel.

A quantitative analysis of the band shifts allowed a deeper insight into binding characteristics of both enzymes. Plotting the relative bound substrate as function of the enzyme concentration enabled the calculation of an apparent binding constant. Fitting the data revealed that formation of enzyme-substrate-complexes was not a linear function of the enzyme concentration. Both proteins interacted with the nucleosomes in a highly cooperative process. The calculated Hill coefficient (n) and apparent binding constant ($K_{1/2}$) for SNF2H was $n = 9.5 \pm 4.0$ and $K_{1/2}$ 527 ± 23 nM. In contrast to this, SNF2L showed a weaker cooperativity but a higher affinity as the calculated values for $n = 3.6 \pm 0.5$ and $K_{1/2} = 308 \pm 12$ nM indicated.

In the subsequent experiment, the structural determinants of cooperative binding were characterized. Instead of two equal 77 bp long DNA overhangs, 40 bp short linker were used (40-NPS1-40). SNF2L also formed distinct intermediate complexes, which was not the case for SNF2H (figure 5.7). Binding to nucleosomes with shorter DNA overhangs was still highly cooperative with Hill coefficients $n = 7.2 \pm 1.6$ for SNF2H and with $n = 2.4 \pm 0.3$ for SNF2L. The affinity to nucleosomes was weaker for SNF2H than for SNF2L ($K_{1/2}$ SNF2H $= 647 \pm 28$ nM vs. $K_{1/2}$ SNF2L $= 238 \pm 13$ nM).

Finally, nucleosomes with 22 bp short linker were tested (22-NPS1-22). Still distinct intermediate complexes formed by SNF2L were detectable (figure 5.7 D). Also binding to nucleosomes with short DNA overhangs was highly cooperative with $n = 7.1 \pm 1$ for SNF2H and with $n = 3.6 \pm 0.5$ for SNF2L. SNF2H bound these nucleosomes with a weaker affinity compared to SNF2L ($K_{1/2}$ SNF2H $= 638 \pm 16$ nM vs. $K_{1/2}$ SNF2L $= 471 \pm 21$ nM).

Whether cooperativity was facilitated by subsequent binding to both symmetric DNA linker was still unclear. To elucidate structural requirements of cooperative binding asymmetric nucleosomes (6-NPS1-47) were tested as substrate. As seen in figure 5.8 A and B, the binding to this substrate was still cooperative (SNF2H $n = 7.3 \pm 1.2$ and SNF2L $n = 2.4$ and ± 0.5). SNF2L showed also a higher affinity with a $K_{1/2} = 303 \pm 6$ nM compared to $K_{1/2} = 205 \pm 21$ nM. In presence of only one asymmetric DNA overhang SNF2L did not form smaller, detectable enzyme-nucleosome-complexes.

In foot printing experiments with *Drosophila* ISWI bound to nucleosomes, it had been shown that the enzyme binds to the nucleosomal entry/exit sites [Längst et al., 1999; Chin et al., 2004]. If interaction with core histones, mediated by the SANT domains, was a prerequisite for cooperative binding, or also free DNA was bound by the HAND/SLIDE domain in this way, was analyzed next.

Binding to radioactively labelled DNA displayed a significant decrease in cooperativity (SNF2H $n = 1.72 \pm 0.39$ and SNF2L $n = 1.72 \pm 0.29$) (figure 5.8 C). The higher sensitivity of the radioactive based assay, with labelled DNA in femto molar concentrations, allowed the determination of a dissociation constant K_d instead of apparent binding constants $K_{1/2}$. Under these conditions, the substrate concentration was 100 to 1000 fold smaller than the constant derived from the binding curve ($[S] \ll K_d$). Therefore the enzyme concentration at the point of half maximal binding corresponded to K_d. The dissociation constant of SNF2H with $K_d = 7.71 \pm 0.39$ nM was comparable to published values for K_d SNF2H = 1.5 nM [Aalfs et al., 2001]. For both, SNF2H and SNF2L, the interaction with the core histones has a major impact on the cooperativity of the binding process.

Binding of one SNF2L molecule to a nucleosomal entry/exit side, is a triggering signal for binding of next remodeler molecules. This coordinanted binding led to formation of defined complexes. In presence of only one DNA overhang, SNF2L was not able to bind to both strands of linker DNA at the entry/exit sites, suggesting a defined binding site relative to the nucleosome (see also figure 6.1 in the discussion). Binding of the first SNF2H complex recruited further enzyme molecules, but they did not form defined complexes, like it was the case for SNF2L. This symmetry dependent complex formation seemed not to influence cooperative substrate binding, because Hill coefficients of both enzymes did not significantly change when substrate symmetry was altered.

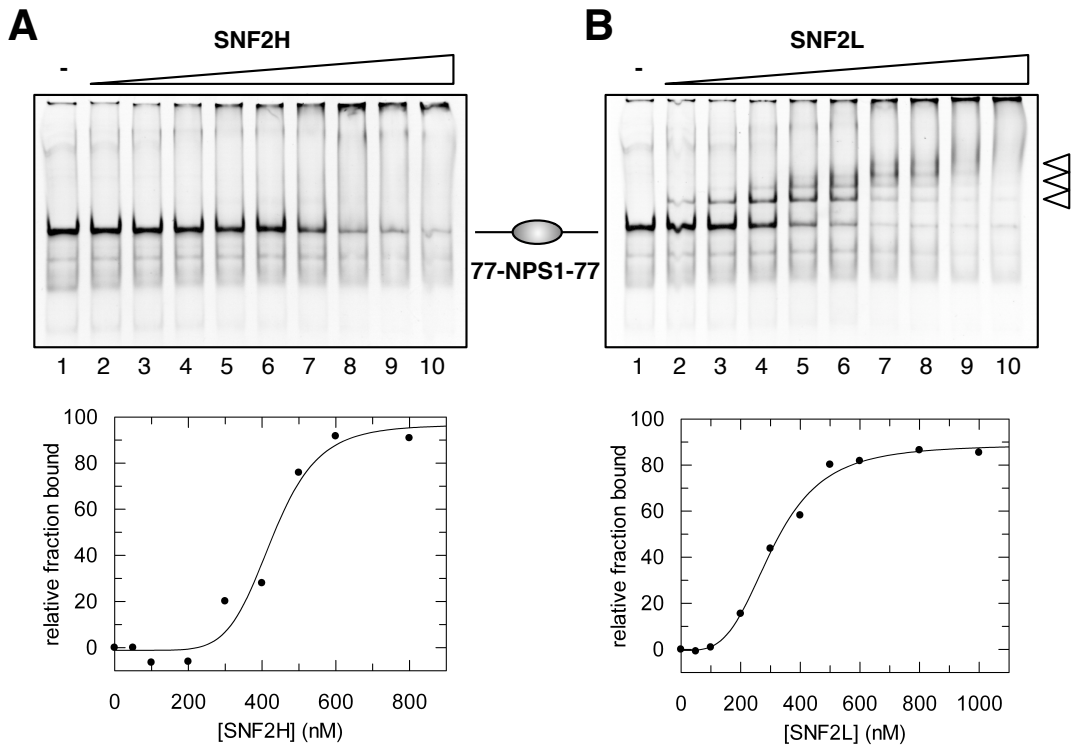

Figure 5.6: **Binding of SNF2H and SNF2L to 77-NPS1-77 mono-nucleosomes**
(A) 77-NPS1-77 mono-nucleosomes (150 nM) with 77 bp of free linker DNA were incubated with rising amounts of SNF2H (0, 50, 100, 200, 300, 400, 500, 600, 800 and 1000 nM, lanes 1 - 10) and enzyme-substrate-binding was analyzed in a band shift assay on 4.5 % native PAA gels. The curve in the lower panel shows the signal intensities of the substrate as a function of the remodeler concentration. Function was fitted using the general equation for cooperative binding (see method), and Hill coefficient for SNF2H was $n = 9.5 \pm 4.0$ with a half maximal binding $K_{1/2}$ at 527 ± 26 nM.
(B) Binding of SNF2L (0, 50, 100, 200, 300, 400, 500, 600, 800 and 1000 nM, lanes 1 - 10) to 77-NPS1-77 nucleosomes. Hill coefficient for SNF2L was $n = 3.6 \pm 0.5$ and $K_{1/2}$ 308 ± 12 nM for SNF2L. Intermediate complexes formed by remodeler and nucleosomes are highlighted by arrows.

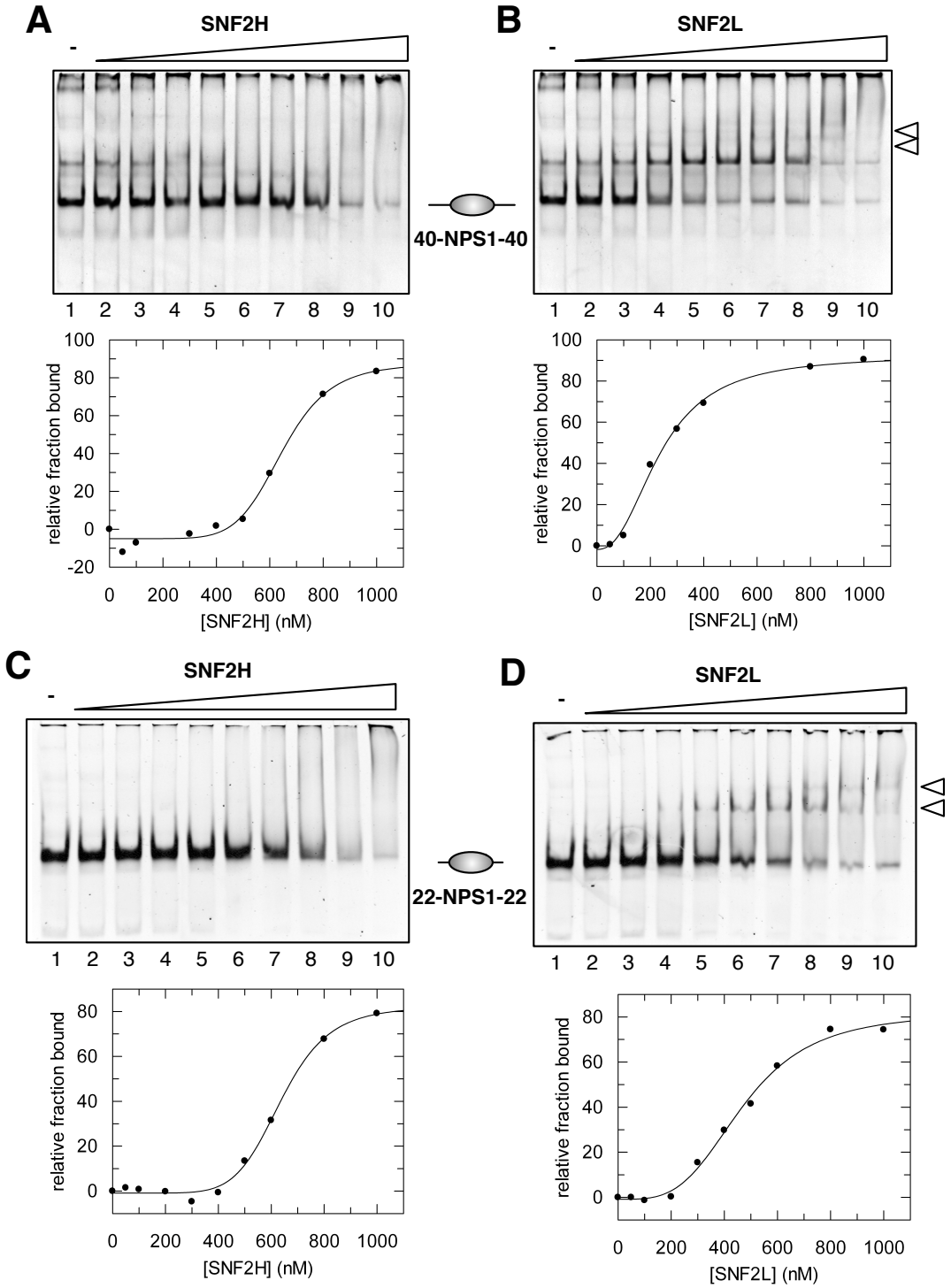

Figure 5.7: **Binding to 40-NPS1-40 or 22-NPS1-22 mono-nucleosomes**
(A) 150 nM 40-NPS1-40 mono-nucleosomes were incubated with 0, 50, 100, 200, 300, 400, 500, 600, 800 and 1000 nM of SNF2H (lanes 1 - 10). Formation of stable enzyme-substrate-complexes was analyzed on a 4.5 % native PAA gel. The curve shows the signal intensities of the substrate as a function of the remodeler concentration. Function was fitted (see method), and Hill coefficient for SNF2H $n = 7.2 \pm 1.6$ with a half maximal binding $K_{1/2}$ at 647 ± 28 nM was determined.
(B) Binding of SNF2L as described in (A), with $n = 2.4 \pm 0.3$ and $K_{1/2}$ 238 ± 13 nM.
(C) Binding of SNF2H to 22-NPS1-22 mono-nucleosomes as described in (A). $n = 7.1 \pm 1.0$ and $K_{1/2}$ at 638 ± 16 nM. **(D)** SNF2L and 22-NPS1-22 nucleosomes as described in (A). $n = 3.6 \pm 0.5$ and $K_{1/2}$ 471 ± 21 nM. Intermediate complexes are highlighted by arrows.

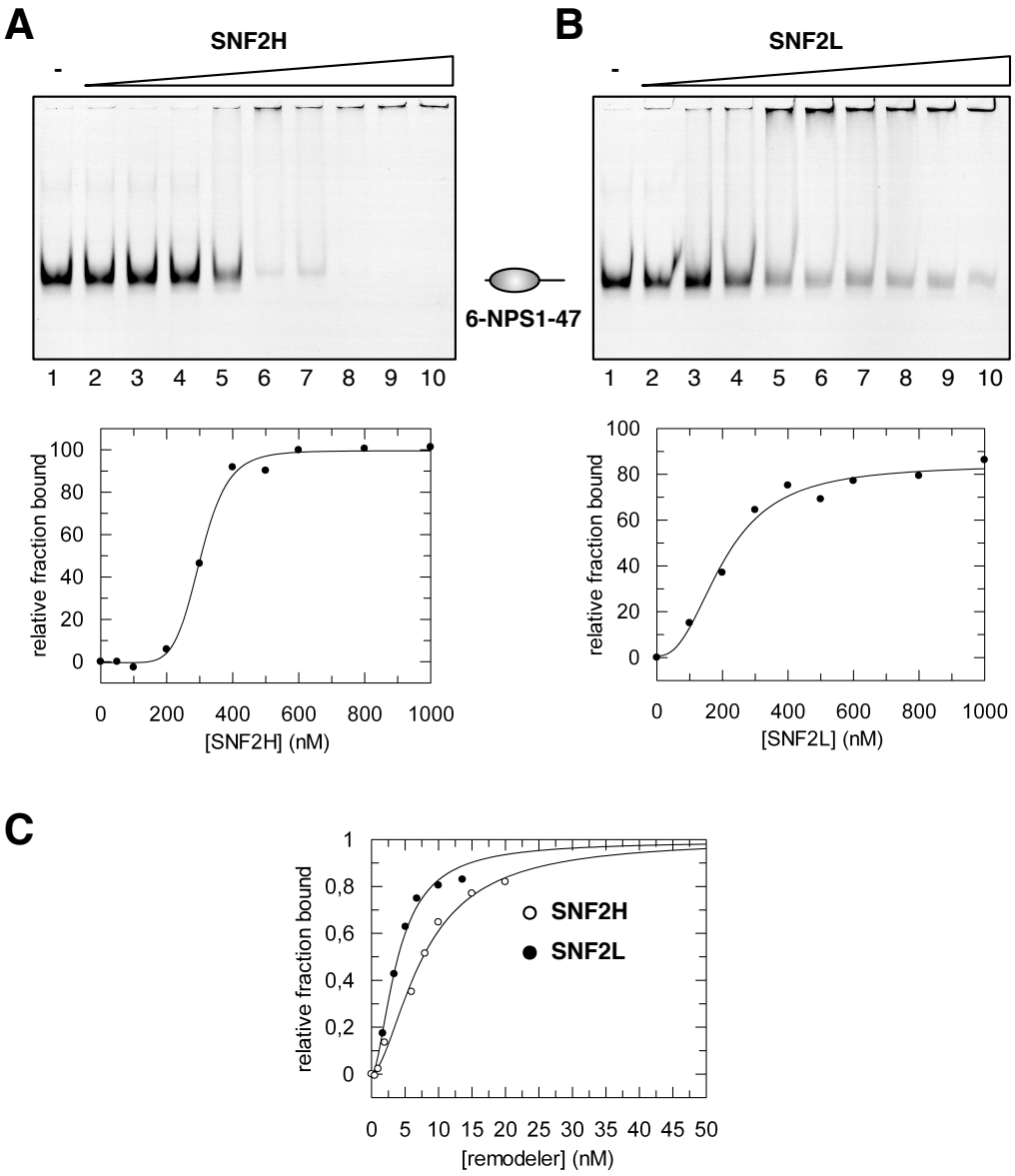

Figure 5.8: **Binding to asymmetric mono-nucleosomes and free DNA**
(A) 20 nM 6-NPS1-47 substrate, with an asymmetrically positioned nucleosome, was incubated with 0, 50, 100, 200, 300, 400, 500, 600, 800 and 1000 nM of SNF2H (lanes 1-10) and subsequently analyzed on 4.5 % native PAA gel. 5'-end of the 47 bp DNA overhang was labelled by Cy5 fluorescent dye. Fluorescent signals were plotted as a function of the remodeler concentration, fitted by general equation for cooperative binding. Hill coefficient for SNF2H $n = 7.3 \pm 1.2$ and a half maximal binding $K_{1/2} = 304 \pm 6$ nM was determined.
(B) Binding of SNF2L according to (A). Hill coefficient was $n = 2.4 \pm 0.6$ and $K_{1/2}$ 205 ± 21 nM.
(C) Binding of SNF2H (empty circles) and SNF2L (black circles) to free DNA. 77-NPS1-77 DNA was radioactively labelled and binding was quantified and normalized. Data were fitted and Hill coefficients were $n = 1.7 \pm 0.4$ for SNF2H and $n = 1.7 \pm 0.3$ for SNF2L. Dissociation constant of SNF2H were $K_d = 7.7 \pm 1.2$ nM and for SNF2L $K_d = 3.9 \pm 0.4$ nM.

5.1.5 Competitive nucleosome binding

To further explore the structural requirements enabling efficient binding to nucleosomes, competitive conditions were tested. Equimolar mixtures of nucleosomes with symmetric linker of varying length (77 bp to 0 bp) were incubated with increasing amounts of SNF2H and SNF2L.

Under such competitive conditions, SNF2H bound to nucleosomes with long extranucleosomal DNA (77 bp) with a higher affinity than to those with medium linker length (40 bp). Comparing lanes 5 and 6 (figure 5.9 A) shows that 40-NPS1-40 nucleosomes were bound only after almost the whole pool of 77-NPS1-77 was depleted. In contrast, SNF2L did not discriminate between 77 or 40 bp long DNA overhangs (figure 5.9 B). Both bands, corresponding to free 40-NPS1-40 and 77-NPS1-77, were shifted at comparable remodeler concentrations. Thus SNF2H bound longer flanking DNA with a higher affinity; in contrast to this, binding of SNF2L was independent of extranucleosomal DNA length.

To determine the role of the linker DNA in the direct interaction of the ISWI remodeler to a nucleosome core particle, next nucleosomes with short linker (22-NPS1-22) were compared to linker-less (0-NPS1-0) nucleosomes in competition with free DNA. The remodeling enzymes bound with the highest affinity to free DNA, followed by 22-NPS1-22 nucleosomes. In absence of any flanking DNA, only very weak binding to nucleosome core particles (0-NPS1-0) was detectable (compare figure 5.9 C middle bands in lane 4 with lanes 7 and 10), for SNF2H also reported by other groups [He et al., 2008]. Under these conditions, defined complexes of SNF2L and nucleosomes were formed (figure 5.9 C lanes 8 - 10). These results indicated that enzyme-DNA-interactions via the negatively charged SLIDE domain have a major impact on substrate binding. As already shown for yeast ISWI homolog ISW2 for stable binding a stretch of approximately 20 bp long extranucleosomal DNA is essential [Kagalwala, 2004].

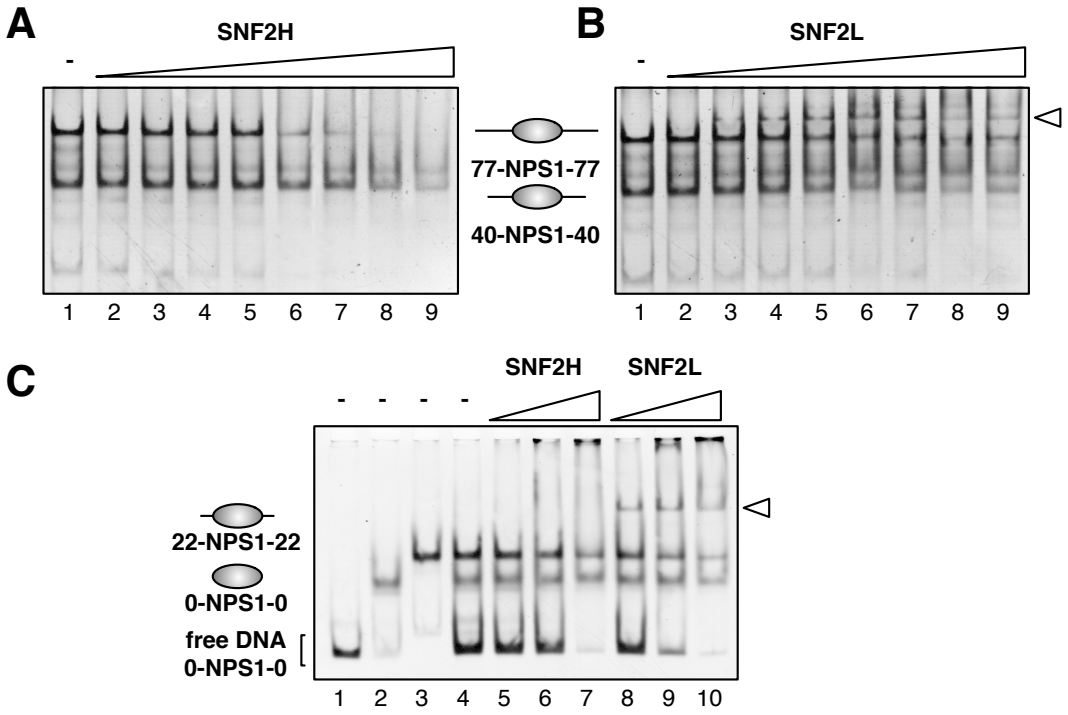

Figure 5.9: **Competitive binding of SNF2H and SNF2L to different substrates**
(A) Equal amounts (50 nM) of nucleosomes with 40 or 77 bp long linker DNA were incubated with rising amounts of SNF2H (50 nM steps from 50 to 400 nM, lanes 2 - 9). Nucleosomes with 77 bp DNA overhang were preferentially bound by SNF2H (compare lane 5 with 6).
(B) Binding of SNF2L (50 nM steps from 200 to 550 nM, lanes 2 - 9) respectively. SNF2L showed a higher affinity, comparing lane 6 (= 250 nM SNF2L) to SNF2H lane 6 panel (A) (= 400 nM SNF2H). Binding of SNF2L to 40-NPS1-40 and 77-NPS1-77 nucleosomes was comparable (lanes 5 and 6). Enzyme bound nucleosomes were marked by arrows.
(C) Nuclesomes with equal 22 bp short DNA overhangs (22-NPS1-22, lane 3), without extranucleosomal DNA (0-NPS1-0, lane 2), and free 0-NPS1-0 DNA (lane 1) were mixed (100 nM each) (lane 4). Free DNA was shifting significantly when enzyme concentrations were increased (100, 500 to 1000 nM), 22-NPS1-22 nucleosomes were bound with lower affinity (compare lane 4 with 6, 7 and 9, 10). Only weak binding to linker free nucleosomes (0-NPS1-0) was detecable.

5.1.6 Intrinsic oligomerization of human ISWI remodeler

The observed differences in Hill coefficients of n ≈ 7 for SNF2H and n ≈ 3.5 for SNF2L (see section 5.1.4) indicated, that upon nucleosome binding conformational changes allow additional binding of enzyme molecules. For SNF2H this impaired binding was more pronounced than in the case of its homolog SNF2L. To gain further insight into mutlimerization of the remodeling enzymes both proteins were analyzed under native conditions [Schägger and von Jagow, 1991]. Purified SNF2H and SNF2L separated into different high molecular weight complexes, but under the used conditions no monomeric form was detected. Both proteins formed oligomeric complexes. The stoichiometry of the complexes indicated a mixture of mainly di- and tetramers (figure 5.10), suggesting that both human ISWI homologs are intrinsically forming oligomers by direct protein-protein-interaction.

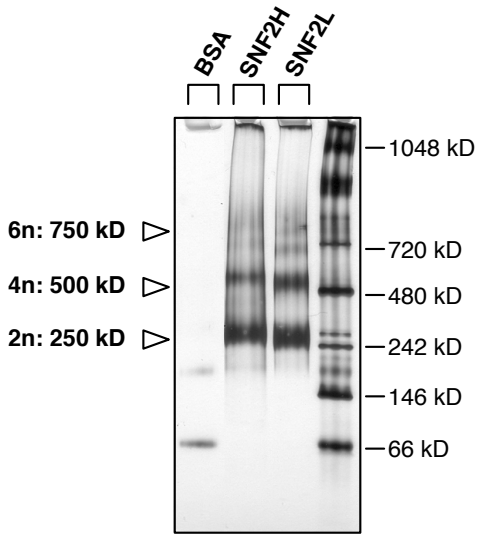

Figure 5.10: **Oligomerization of SNF2H and SNF2L**
Analyzing recombinant SNF2H and SNF2L on a native protein PAGE. 1.5 µg of both proteins, a BSA control and native protein marker were loaded on gradient gel under native conditions and subsequently silver stained. Sizes of the homo oligomers formed by 127 kDa SNF2H and 126 kDa SNF2L are indicated by arrows.

5.1.7 Mono-nucleosome remodeling

As SNF2H showed a higher affinity to long linker DNA compared to SNF2L, next it was tested whether DNA linker length influenced the outcome and the efficiencies of remodeling reactions. Figure 5.5 B already showed that both enzymes were able to translocate histone octamers from central positions to end positions, when long linker DNA was present (figure 5.11 A lanes 1 - 3). Decreasing the length of the extranucleosomal DNA from 77 bp down to 0 bp, sequentially reduced remodeling activity of SNF2H. Once the DNA became shorter than 40 bp (compare lanes 4 and 7), almost no remodeling activity was detected. The fact that SNF2H showed no remodeling activity on linker-free nucleosomes had also been reported by other groups [He et al., 2008]. Strikingly SNF2L remained active, even on substrates exhibiting no DNA overhang (figure 5.11 A lane 12). SNF2L dependent remodeling of the nucleosome core particles resulted in the appearance of a slower migrating nucleoprotein complex, forming a distinct band.
Remodeling experiments with natural DNA sequences revealed further differences in the positioning pattern. Mono-nucleosomes assembled on a 248 bp long DNA sequence originated from murine rDNA promoter led to a pattern of repositioned nucleosomes specific for SNF2H and SNF2L (figure 5.11 B lanes 7 - 9). The same DNA sequence was interpreted differently and guided each human ISWI remodeler to position the nucleosomes to distinct end-positions. Promoter sequence of the *Drosophila hsp70* gene showed also a distinct positioning pattern after remodeling with both enzymes (figure 5.11 B lanes 10 - 12). This capability to interpret biologically relevant promoter sequences was already shown to be specific for remodeler from different subfamilies [Rippe et al., 2007]. The results presented here suggest, that remodeling activity of SNF2H is not only sequence specific but highly dependent on length of nucleosomal linker DNA. For the SNF2H containing complex hACF activity as DNA dependent length sensor was already described [Yang et al., 2006]. Activity of the highly similar remodeling enzyme SNF2L is obviously independent of extranucleosomal DNA and binding to nucleosomes is also stronger.
To further elucidate the functional differences of SNF2H and SNF2L, a 200 bp DNA fragment with nucleosomes located at two different sites was used. On the 33-NPS1-20 DNA the nucleosomes were centrally positioned with linker DNA shorter than 40 bp. As already seen in figure 5.11 A, SNF2H was unable to remodel such nucleosomes (compare figure 5.11 A lane 4 and 7 and B lane 1). Using the terminal positioned nucleosomes with one longer DNA linker, dramatically increased SNF2H remodeling activity. The enzyme effectively moved the histone octamers to center of this DNA fragment (figure 5.11 B lane 4). Such directional movement was shown for hACF to be caused by a reduced remodeling rate on nucleosomes with 20 bp of flanking DNA [Yang et al., 2006].

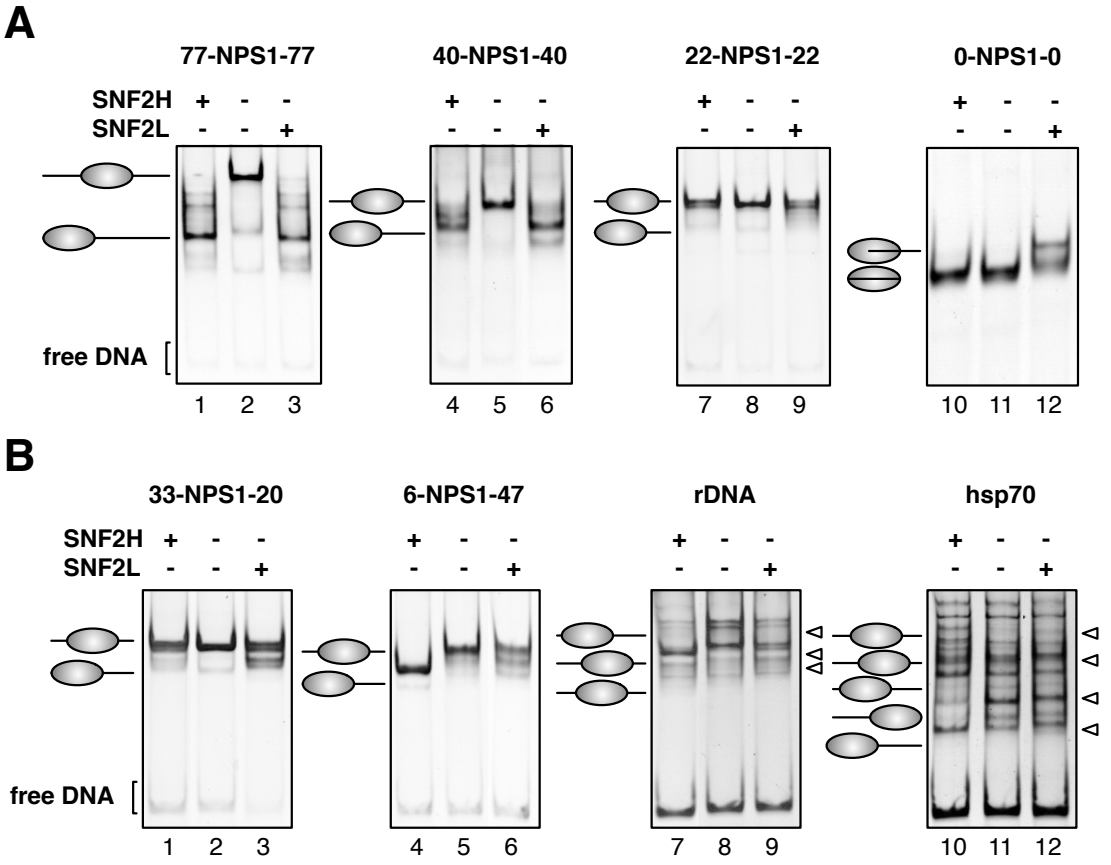

Figure 5.11: **Remodeling activity of human ISWI ATPases**
(A) 200 nM of each centrally NPS1 positioned mono-nucleosome with 77, 40, 22 and 0 bp long linker was incubated with 100 nM remodeler and 2 µM ATP for 90 min. Changed nucleosome positioning could be followed as change in the electrophoretic mobility on a native 4.5 - 6 % PAA gel. With flanking DNA shorter than 40 bp, SNF2H was unable to move the histone octamer towards the end of the sequence (lanes 7 and 10). SNF2L was still re-positioning nucleosomes without DNA overhang (lane 12).
(B) 200 bp nucleosomal DNA with asymmetric (6-NPS1-47) or almost symmetric linker DNA (20-NPS1-33) and natural DNA sequence like murine rDNA promoter (248 bp) or *Drosophila* hsp70 promoter (359 bp) were assembled into chromatin and used as remodeling substrates under the mentioned conditions (A). SNF2H did not move nucleosomes with shorter flanks, like 20 bp and 33 bp (lane 1), but efficiently moved a nucleosome when 47 bp of flanking DNA were present at one side (lane 4). The natural promoter sequences showed that hISWI machines are remodeling not only DNA length dependent, but also sequence dependent. Both machines interpreted the rDNA sequence and hsp70 promoter differently and established specific positioning patterns (lane 8 vs 9 and 11 vs 12). Differences in the nucleosome positioning patterns are highlighted by arrows.

In the experiments presented here, SNF2H moved asymmetric nucleosomes with one 47 bp long DNA overhang efficiently to the center (figure 5.12 A). Once moved to the center of the nucleosomal DNA, the linker became significantly shorter than 47 base pairs. Below the minimal length SNF2H needs for successful remodeling, the reaction rate for nucleosome sliding is highly reduced. Therefore the movement into the reverse direction from the center to a terminal position was limited. Due of this kinetic discrimination the central positioned nucleosomes got highly enriched.
In comparison to SNF2H, the remodeling activity of SNF2L was independent of extranucleosomal DNA length. Starting with an asymmetric 6-NPS1-47 substrate SNF2L moved the nucleosome away from the end (figure 5.12 B). But this motor was also able to catalyze the opposite movement of the histone octamer from the center (33-NPS1-20) to the end (figure 5.11 B lane 6). No discrimination of nucleosomes with shorter linker DNA was detectable. SNF2L would continuously remodel nuclesomes with different linker DNA, forming an equilibrium.

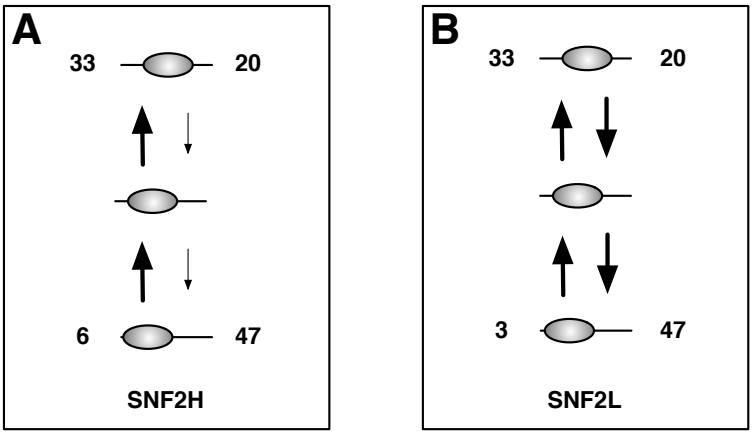

Figure 5.12: **Equilibrium of the remodeling reaction catalyzed by SNF2H and SNF2L**
(A) Asymmetric 6-NPS1-47 nucleosomes were efficiently moved to the center. With a linker length being below the critical minimum, the reaction rate for sliding back from the center to the end-position is reduced.
(B) SNF2L moved the nucleosome away from the end. But it was also able to catalyze movement of the histone octamer from the center (33-NPS1-20) to the end.

5.1.8 Determination of nucleosome positioning by MNase footprinting

Separating the linker-free 0-NPS1-0 nucleosomes after remodeling by SNF2L (figure 5.1.2 A lane 12) and analyzing the observed pattern allowed an indirect characterization of the structural changes. In order to determine nucleosome positions more directly and to address the question whether SNF2L moved the histone octamer over the end of the DNA, MNase foot printing experiments were performed.

As illustrated in figure 5.13 A and B, 0-NPS1-0 nucleosomes were incubated in a remodeling reaction with identical amounts of SNF2H or SNF2L. The reaction was stopped after 90 min by adding an excess of short DNA fragments (35 bp). Under these competitive conditions, the nucleosomes were released from the enzyme. Subsequently MNase was added to the nucleosomes and the reaction was stopped after different time points (30, 60, 240 s) to partially hydrolyse accessible DNA sequences. The histone bound DNA remained inaccessible to the nuclease. Undigested DNA was isolated after degradation of all proteins. Size distribution of the fragments was analyzed in high resolution on a capillary electrophoresis system in our laboratory together with Andreas Fuchs.

This analysis revealed that after remodeling of the linker-less nucleosomes with SNF2L, a small terminal stretch of DNA was accessible for nuclease cleavage (see black arrows in figure 5.13 D). Partial MNase digestion led to degradation of this extranucleosomal NPS1 DNA. In the SNF2L remodeling reaction fragments smaller than the intact NPS1 sequence were detected after 30 s of incubation with MNase. This was not the case when the remodeling reaction was performed with SNF2H (figure 5.13 C). In these samples only two peaks corresponding to full length NPS1 and the 35 bp competitor were detectable.

The presence of 35 bp competitor DNA after 30 and 60 seconds of incubation with MNase indicated that digestion was still limited under these conditions. Thus the highlighted signal peak after 60 s digestion of the 0-NPS1-0 nucleosome remodeled by SNF2L in 5.13 D was rather unlikely formed by a MNase artefact, caused by over-digestion of these nucleosomes. The even distribution of unremodeled and remodeled nucleosomes detected by the EMSA in 5.13 B are in line with the comparable signal intensities of 0-NPS1-0 full-lenth and truncated DNA after 240 s of digestion in 5.13 D. A more detailed quantitative size measurement of the truncated NPS1 sequence failed. The tested low molecular weight DNA ladder showed a good separation on the CE capillary. But comparing the migration time of different NPS1 constructs to marker DNA fragments revealed that these curved nucleosome postitioning DNA sequences moved slower than estimated from their linear sequence length. This retardation of nucleosome postitioning DNA sequences has also been reported for separation on native PAA gels [Lowary and Widom, 1998].

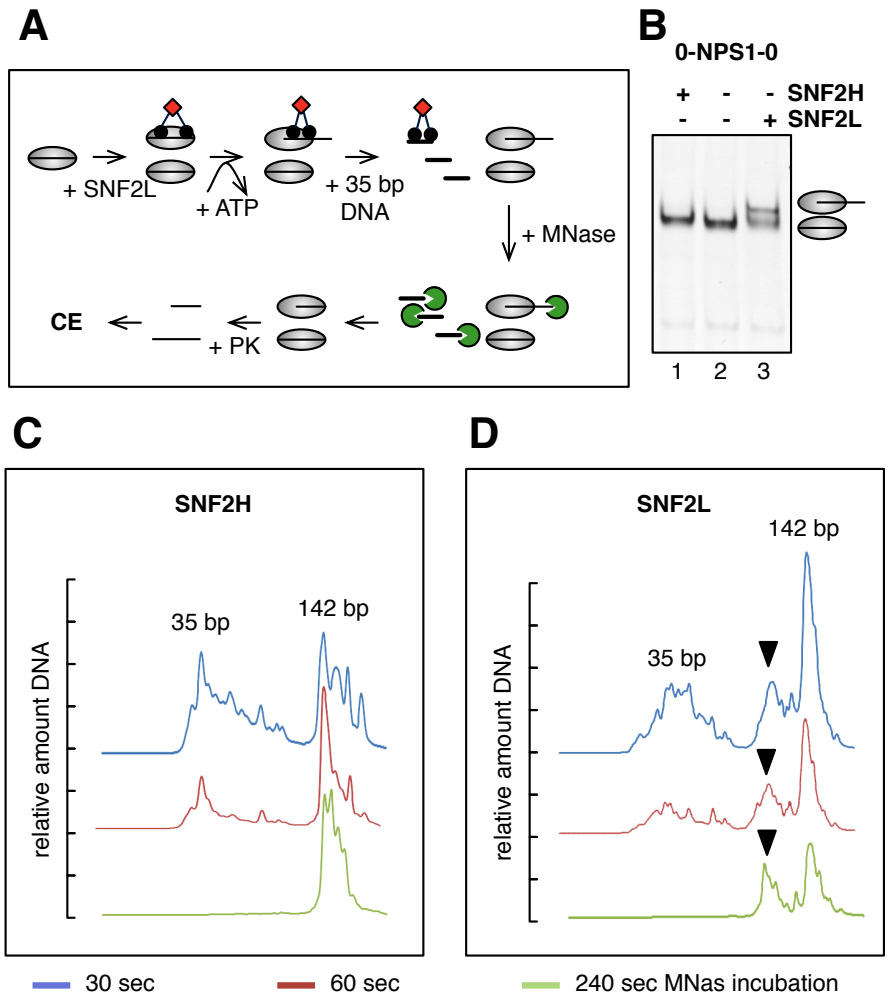

Figure 5.13: **Analyzing MNase accessibility of 0-NPS1-0 nucleosomes after remodeling**

(A) 0-NPS1-0 linker-free nucleosomes were incubated with SNF2L and SNF2H in presence of ATP. Remodeling reaction was stopped by addition of 35 bp long competitor DNA in vast excess and DNA sequences accessible to MNase were digested. After nuclease reaction proteins were digested by proteinase K and remaining DNA was precipitated. High resolution analysis of non digested DNA fragments was done with a capillary electrophoresis (CE).
(B) After nucleosome sliding and addition of competitor DNA part of each sample was analyzed on a native 6 % PAA gel. Rest of each sample was further processed as described.
(C) MNase digestion was stopped after 30, 60 and 240 s and remaining DNA fragments were separated on a CE. The relative UV signal at 260 nM was plotted as a function of the retention time, proportional to the DNA size.
(D) Analysis of SNF2L remodeling end-products. Fragments smaller than 142 bp 0-NPS1-0 DNA and larger than 35 bp competitor were specifically generated by increased MNase accessibility upon SNF2L incubation and are highlighted by arrows.

5.1.9 Kinetic analysis of the remodeling reaction

In the course of a remodeling reaction, binding to the substrate is the initial step. The subsequent nucleosome translocation is an ATP dependent step. In order to gain deeper insight into the remodeling mechanism of SNF2H and SNF2L and to elucidate the influence of the substrate affinity on the remodeling activity, kinetic analyses were performed. Taking advantage of the structural changes induced upon nucleosome remodeling, a highly senstitve FRET-based method was used. The dynamic binding studies were done in collaboration with the group of Prof. Dr. Jens Michaelis at the Department of Chemistry and Biochemistry at the Ludwig-Maximilians-University Munich. FRET burst experiments and raw data analyses were done by Wolfgang Kügel.
A nucleosomal DNA encoding the strong NPS1 positioning signal with a 6 bp and 47 bp linker DNA was labelled with two different fluorescent dyes. These labels were integrated into the DNA by assembling the 200 bp DNA sequence from 10 different overlapping oligonucleotides (see figure 5.14 A). Two of these oligos were designed to contain an atto 532 and an atto 647 fluorophor covalently linked to a deoxythymidine nucleotide at position - 64 and + 14 relative to the dyad axis of the 147 bp NPS1 sequence. After several cycles of annealing and ligation with thermo stable DNA ligase in a ligase chain reaction (LCR) a 200 bp double stranded DNA sequence was generated. This work was done by Barbara Treutlein.
Fluorescence resonance energy transfer (FRET) is a distance dependent transfer of excitation from a donor dye to an acceptor molecule. According to the general equation the transfer efficiency (E) is dependent on the distance of the donor-acceptor-pair (R) and the Förster distance R_0, indicating the distance at which 50 % of the energy is transferred [Forster, 1948; Stryer, 1978].

$$E = \frac{1}{1+(R/R_0)^6}$$

Because FRET is dependent on the inverse sixth power of the distance of donor and acceptor (R), small structural changes have a huge impact on the FRET efficiency (E) [Stryer, 1978].
Assembly of this DNA into nucleosomes led to specific three dimensional positioning of both labels in direct proximity closed to the nucleosomal entry/exit site (see figure 5.14 B). For this distance of 40 - 45 Å, a FRET efficiency from donor to acceptor dye of 90 - 92 % was estimated. As seen in figure 5.14 C after assembly of the free DNA into nucleosomes, a high FRET signal was detected specifically for the nucleosomes (compare lanes 8 and 9).

When directly measuring the fluorescence of the donor dye by excitation at 532 nm wavelength and using the corresponding emission filter almost no atto 532 fluorescence was detectable for the nucleosomes, in contrast to DNA (lanes 4 and 5). The excitation energy was transferred to the acceptor dye, and after excitation of the atto 647 dye emitted at the acceptor specific wavelength, longer than the emission filter window.

Upon incubation of these double-labelled nucleosomes with a remodeling enzyme in presence of ATP the nucleosome was translocated to a central position (see also figure 5.11 B lanes 4 - 6). As a consequence of this translational movement of the nucleosome the DNA at label position - 64 was no longer part of the nucleosomal core particle. The three dimensional distance between donor and acceptor dye increased to more than 110 Å and dramatically reduced the FRET efficiency to 0 %.
Following this decrease of FRET efficiency allowed an exact measurement of the remodeling reaction kinetics. An example of such a kinetic measurement with SNF2H is shown in figure 5.15 A. To allow a comparative analysis of the dynamics of SNF2H and SNF2L, enzyme concentrations were chosen under which both proteins did not form stable complexes with the nucleosomes (see also figure 5.8 in section 5.1.4). Relative FRET efficiency of single substrate molecules were measured in diluted solutions as short fluorescence bursts when diffusing through a small focal volume. The FRET intensity histogram of a nucleosome population (28 nM) upon incubation with SNF2H (17 nM) was plotted as a two dimensional graph. Starting at time point t_0, almost all nucleosomes had a FRET efficiency higher than 0.75 (red). Upon incubation with SNF2H the FRET efficiency decreased and a population of nucleosomes with FRET efficiencies smaller than 0.2 raised (blue). In the upper panel, an integration over the whole time scale for all three FRET efficiency groups is depicted. As expected, the sum of high FRET and low FRET events was comparable, while the low populated mean FRET signals did non change. One reason why the mean FRET intensities did not change could be that these nucleosomes were not properly assembled and thus not recognized by the enzymes as substrates. The signals of each group (high, mean and low) were then plotted as a function of reaction time (figure 5.15 B). Fitting the data with single exponential fits (see method section for details) allowed to determine the reaction time T_l.
Analyzing the reaction time T_l in dependency of SNF2H and SNF2L, concentrations revealed differences in nucleosome affinity in presence of ATP. As illustrated in figure 5.15 C T_l of SNF2H and SNF2L was first determined for an enzyme-substrate-ratio of 2.5:1. To exclude effects caused by differences in the fraction of active enzyme, activity was normalized to these values. Then, the concentration of enzyme was decreased in several steps (1.0, 0.5, 0.33 and 0.25 compared to the amount used intially).

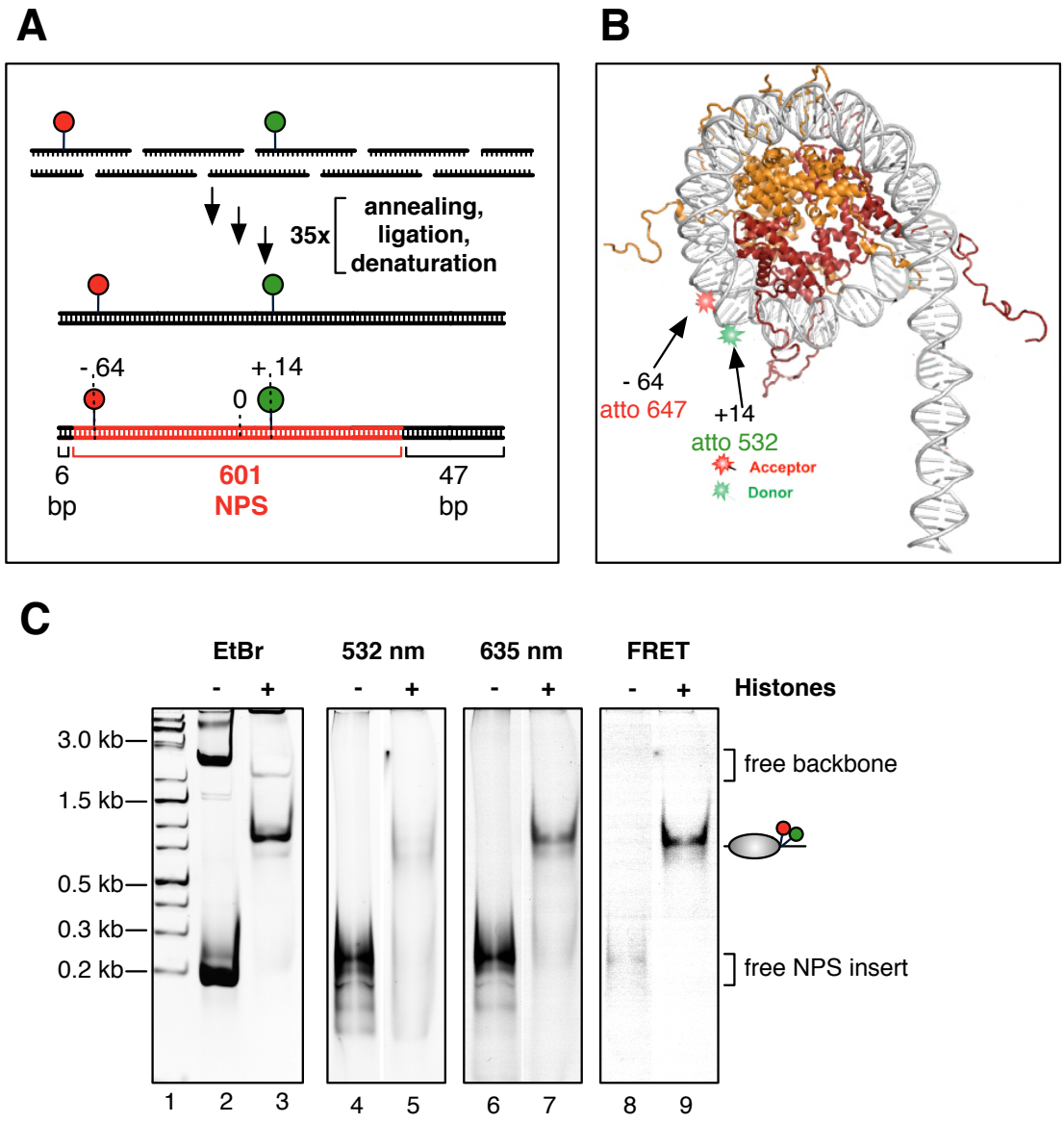

Figure 5.14: **Assembly of atto 532/atto 647 labelled nucleosomes**
(A) Nucleosomal DNA was reconstructed by ligase chain reaction (LCR) using oligonucleotides and thermostable DNA ligase. In two oligonucleotides of the plus strand a specific deoxythymidine nucleotide was covalently linked to fluorescent dyes. 200 bp 6-NPS1-47 DNA with an atto 647 fluorescent label at position - 64 and atto 532 at postion + 14 relative to the dyad axis of the NPS1 sequence (0) was generated.
(B) Wrapping the DNA around a histone octamer forming a nucleosomes would position atto 532 donor and atto 632 acceptor dye in direct proximity close to the nucleosomal enty/exit site.
(C) 0.5 µg double labelled DNA were mixed with 4.5 µg unlabelled 6-NPS1-47 DNA restriction digested plasmid (see section 5.1.7). This mixture was assembled into nucleosomes (total DNA shown in lanes 2 and 3). Fluorescence of the donor dye was shown after excitation with a 532 nm laser (lanes 4 and 5). Acceptor fluorescence of the same gel was demostrated after excitation with a 635 nm laser in lanes 6 and 7. Using the 532 nm laser for excitation of 532 atto dye and the 647 atto acceptor fluorescence filter allowed detection of the FRET from donor to acceptor.

Since not the total enzyme fraction was active, for a complete conversion of the substrate each enzyme molecule had to remodel more than one nucleosome. Thus several rounds of substrate binding, nucleosome movement and dissociation of the enzyme-substrate-complex had to take place (figure 5.15 D). A direct linear correlation of enzyme-substrate-ratio and the overall reaction time T_l could be expected and was plotted in green.
The reduction of the total reaction velocity within the samples remodeled by SNF2L (blue points) correlated well with the enzyme dilution. All data points for SNF2L reflected nicely the expected trend plotted in green. The larger values for $1/T_l$ of SNF2H relative to the expected green line indicated a change in at least one of the binding constants of SNF2H.
The rate constant of the catalytic reaction k_{rem} could be expected not to be influenced by the enzyme concentration. Thus the relatively higher reaction velocity observed upon SNF2H dilution was caused either by an increase in the rate for substrate binding k_{on}, or by an increase in the end-product release rate k_{off}. As it was rather unlikely that upon enzyme dilution the affinity to the substrate would increase, a change in k_{off} was most likely the reason for the deviations observed for SNF2H. Therefore, under the conditions tested k_{off} was rate limiting for the total reaction and different for SNF2H and SNF2L.

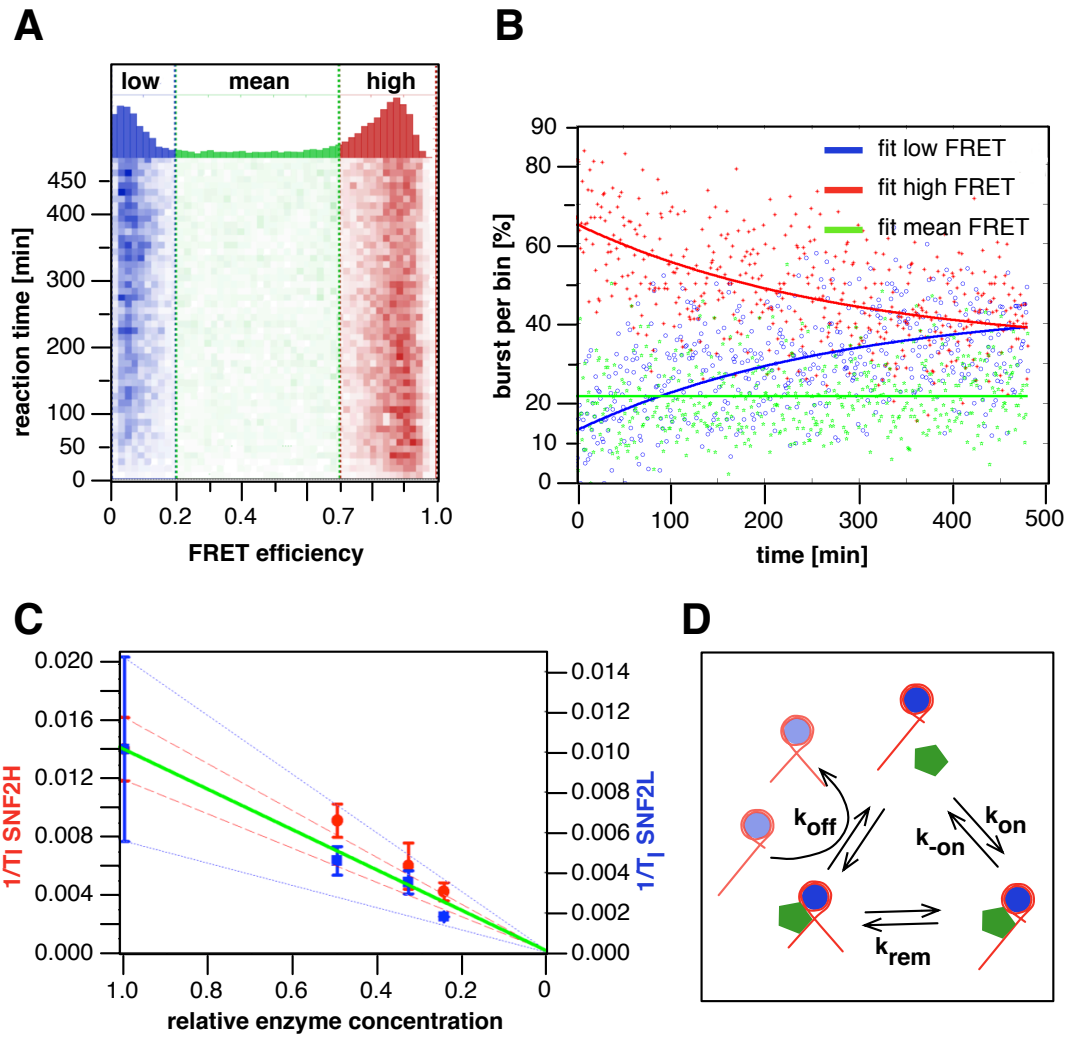

Figure 5.15: **Remodeling kinetics monitored by FRET changes**
(A) 2D histogram of FRET efficiency (color scale) measurement with SNF2H (17 nM) and 6-NPS1-47 nucleosomes (28 nM) showing a decrease of the FRET efficiency during remodeling reaction. The histogram was segmented in three parts, low, medium and high FRET. The integration on top was done for each segment over the complete measurement time.
(B) Fluorescence bursts (%) of high, medium or low FRET analyzed in time bins of 60 sec over the total measurement time. Nucleosomes were moved and relative distance of donor and acceptor dye increased. Intensity of the high FRET fraction (red stars) decreased and simultaneously the low FRET population (blue circles) increased. The medium FRET fraction stayed constant. Using single exponentials fits high FRET and low FRET data were fitted (solid lines).
(C) Remodeling speed ($1/T_l$) for SNF2L (blue) and SNF2H (red) as a function of the relative amount of enzyme in the sample (1, 0.5, 0.33 and 0.25 relative enzyme concentration, compared to first measurement). To monitor dynamics an enzyme concentration was used under which binding was transient only, thus a linear dependence of remodeling speed with remodeler concentration was expected (green line). A deviation corridor based on the standard error of the first data point is shown by red dashed (SNF2H) and blue doted (SNF2L) lines.

5.1.10 Binding and remodeling of SNF2H and SNF2L with poly-nucleosomes

Mono-nucleosomes are the most commonly used substrates for *in vitro* remodeling experiments. To address the question whether the human ISWI remodeler SNF2H and SNF2L also bind to the more physiologic arrays of nucleosomes, experiments with circular and linear chromatin arrays were performed. For binding studies, nucleosomes were assembled by salt dialysis assembly on linearized plasmid DNA (14 kb), resulting in arrays of approximately 85 times repeating nucleosomes (figure 5.4). Binding of SNF2H and SNF2L to the arrays could be easily monitored by the reduced mobility in the agarose gel due to the formation of high molecular weight complexes.
The Hill coefficient of SNF2H was comparable to results from the experiment using mono-nucleosomal fragments 22-NPS1-22 (figure 5.16 B). Strikingly, the at least twofold differences in the Hill coefficient between SNF2H and SNF2L observed when using mono-nuclesomal fragments disappeared (n SNF2H 6.8 ± 2.3 and n SNF2L 6.0 ± 0.8). For highly cooperative binding of SNF2L interacting to more than one nucleosome *in-cis* seemed to be essential, whereas for SNF2H binding to single nucleosomes was sufficient and not dependent on higher-order chromatin structure.
Testing the remodeling activity of SNF2H and SNF2H on regular, 200 bp spaced nucleosomal arrays showed a clear qualtitative shortening of linker DNA length. This effect was ATP dependent and not caused by solely binding to the chromatin (compare lanes 2, 3 and 4, 5, and 10, 11). For both remodeler, a reduced nuclease accessibility was observed, thus more MNase was needed to get a clear nucleosomal pattern (compare lanes 3, 5, 6, 11 and 12). The mono- and di-nucleosomal fragments were significantly shorter than 200 and 400 bp. The chromatin spacing shrank down to 170 bp upon incubation with both enzymes and ATP. Nevertheless, quantitative differences in the reactivity on these poly-nucleosomal substrates could not be excluded, since this analysis only addressed the qualitative differences at the reaction end-point.

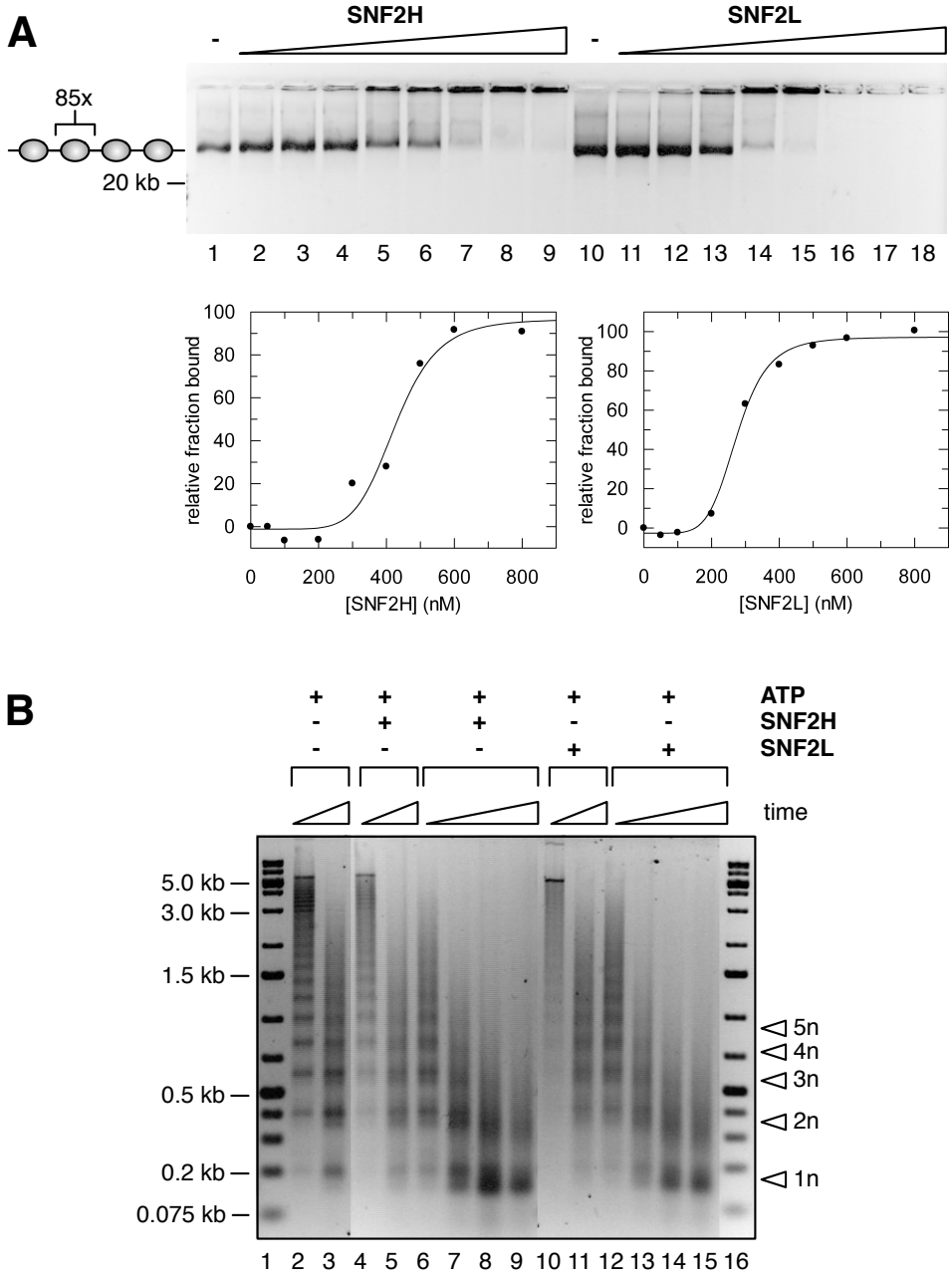

Figure 5.16: **Activity of SNF2H and SNF2L on poly-nucleosomes**
(A) An array consisting of 85 repeats of 170 bp spaced nucleosomes was assembled on linearized 14 kb plasmid DNA. 3.3 nM poly-nucleosomes (= 260 nM mono-nucleosomes) were incubated with 0, 50, 100, 200 up to 800 nM enzyme (lanes 1 - 9 and 10 - 18) and loaded on a TBE-agarose gel. Hill coefficients for SNF2H $n = 6.8 \pm 2.3$ and for SNF2L $n = 6.0 \pm 0.8$ were comparable; half maximal binding was $K_{1/2} = 428 \pm 25$ nM for SNF2H and 275 ± 7 nM for SNF2L. **(B)** 24 nM of circular poly-nucleosomes with 200 bp spacing (= 290 nM mono-nucleosomes) were incubated with 1.5 mM ATP and 550 nM Snf2H or SNF2L. Remodeling reaction was stopped with excess of free DNA, nucleosome spacing was analyzed by MNase with 20 and 60 s digestion time for lanes 2, 3, 4, 5, 10, 11. MNase concentration was increased 3x and reactions were stopped after 30, 80, 160, 200 s for lanes 6 - 9, 12 - 15.

5.1.11 ATPase activity of SNF2H and SNF2L

For the ISWI class remodeler like dISWI and hSNF2H it was known that they are only slightly stimulated by free DNA. Under the conditions tested here, SNF2H and SNF2L hydrolyzed 1 - 4 % of ATP in presence of free DNA (figure 5.17). As shown previously, addition of nucleosomes with symmetric 77 bp DNA overhangs to the enzymes dramatically increased the ATPase activity of both homologs (see figure 5.5 in section 5.1.3). To test whether functional differences like linker DNA dependent remodeling are based on differential ATPase activity, comparative ATP-hydrolysis tests were perfomed. The enzymes were incubated with a set of qualtitative different nucleosomal substrates and amount of hydrolyzed ATP was determined after 0, 45 and 90 minutes (figure 5.17 A). The rate ATP was hydrolyzed by SNF2H did not change significantly in presence of nucleosomes with 77 down to 22 bp linker or poly-nucleosomes (45 - 48 % ATP hydrolyzed). The relative increase of the ATPase rate for 0-NPS-0 nucleosomes could be caused by a systematically higher concentration of this chromatin sample. Because for both enzymes, same amounts of identical nucleosome samples were used, such errors were eliminated by normalization of one remodeler to the other.
Reducing the length of linker DNA dramatically decreased ATPase activity of SNF2L (figure 5.17 B). Normalized to the activity of SNF2H upon incubation of SNF2L, the hydrolysis rate dropped from 0.88 (77-NPS1-77) twofold to 0.41 (0-NPS1-0) (see figure 5.17 C). Activity in presence of poly-nucleosomes with approximately 23 bp of free linker DNA, also used for binding (see figure 5.16 A), showed a rate of 0.56 ± 0.03, which was within the range of 0 and 22 bp long mono-nucleosomal DNA overhangs. Thus, ATPase activity was not stimulated on poly-nucleosomes, but mainly driven by length of the linker DNA. For all chromatin substrates, experiments were repeated as technical duplicates and error bars represent standard deviation.
As shown in figure 5.17 D ATPase activity of SNF2L is dependent on the interaction with N-terminal tails of histone H4. It was known for dISWI and hSNF2H that binding of the remodelers to the histone tails via the SANT domains activate the catalytic helicase domains [Clapier et al., 2002, 2001]. The reduction to basal ATPase activity (below 5 %), when octamers with a truncated version of H4 lacking the N-terminal tail were assembled into nucleosomes proofed that interaction with H4-tails was also for activation of SNF2L essential.

Comparing these results with the remodeling assays (fig 5.11 in section 5.1.7) supported the idea, that remodeling activity was not directly regulated by the ATPase activity of this enzyme.

Although SNF2H was remodeling and binding nucleosomes with longer linker DNA more efficient than those with short or no linker DNA (figures 5.9 and 5.11), there was no correlation of ATP-hydrolysis rate and nucleosomal linker length. Especially in case of the 22-NPS1-22 and even more striking for 0-NPS1-0, where no remodeling was detectable, ATPase activity was uncoupled from effective nucleosome sliding. With this substrate the remodeling machine was wasting energy in a futile reaction, at least under the conditions tested in this *in vitro* assays.

For SNF2L both processes, ATP hydrolysis and nucleosome translocation, were not uncoupled. SNF2L showed a reduced ATP consumption when the remodeling activity was weak, which was the case for the linker-free NPS1 construct. The longer the extranucleosomal DNA was, the better the nucleosomes were remodeled (Fig 5.11 A) and the more ATP was consumed by SNF2L. This correlation between remodeling and ATPase activity dependent of overhanging DNA revealed that the ATPase rate of SNF2L is regulated in dependency of nucleosomal linker DNA length. But for this proteins, binding to nucleosomes was independent of linker length (figure 5.9).

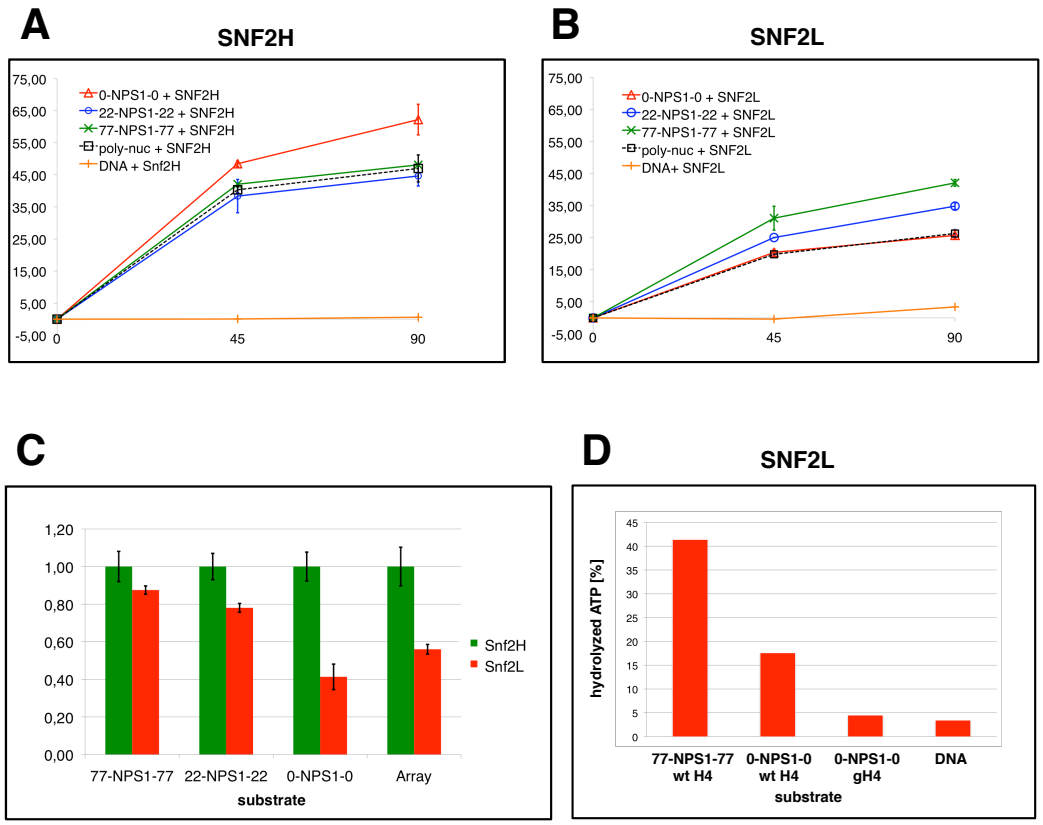

Figure 5.17: **ATP hydrolysis of both hISWI isoforms stimulated by different co-substrates**

(A) SNF2H (120 nM) was mixed with ATP (5 µM) and 250 nM of free DNA or different mononucleosomes with 0, 22 and 77 bp flanking DNA or comparable amounts of nucleosomes assembled in an array with 170 bp spacing. Mg^{2+} dependent reaction was stopped after 0, 45 and 90 min by addition of EDTA and radioactive phosphate was separated from unhydrolyzed ATP and quantified. Relative ATPase activity was calculated by substracting the P_i signal at t_0 from each data point of a time course series.

(B) Corresponding experiment with the same substrate samples and SNF2L (120 nM).

(C) ATPase activity of SNF2L in presence of each tested substrate was normalized to activity of SNF2H. Error bars represent s. d. The rate ATP is hydrolyzed by SNF2L decreases when flanking DNA is shortened; 0.88 ± 0.02 (77-NPS1-77), 0.78 ± 0.02 (22-NPS1-22) to 0.41 ± 0.07 (0-NPS1-0). Activity on a nucleosomal array with approximately 23 bp of free linker DNA showed a rate of 0.56 ± 0.03, which in between the values received from 0 and 22 bp long mono-nucleosomal DNA overhangs.

(D) Activity of SNF2L is dependent on the presence of N-terminal H4-tails. Incubation of SNF2L with 0-NPS1-0 nucleosomes assembled with octamers with a H4 deletion mutant lacking N-terminal and instead of wildtype chicken histone octamers significantly reduced ATP-hydrolysis rate.

5.1.12 Localization of paralogous remodeler in mouse 3T3 nuclei

The observed differences in binding and remodeling only gave indirect hint on cellular function *in vivo*. Therefore both remodeler were expressed in mammalian cells to analyze sub-cellular distribution. Co-expression of SNF2H and SNF2L tagged with green fluorescent protein (GFP) and the red variant (RFP) allowed a comparative analysis of the distribution within the same cell. These microscopic studies were done in collaboration with Fabian Erdel from the laboratory of Dr. Karsten Rippe at the Research Group *Genome Organization & Function* at the DKFZ and the BioQuant in Heidelberg.

To exclude a specific impact of the fluorescent protein, SNF2H was first expressed as a GFP- and a RFP-tagged form in one cell and checked for the nuclear distribution in mouse 3T3 cells. Figure 5.18 clearly shows no differences in the localization of GFP- or RFP-tagged SNF2H (A - C). For the comparison of both paralogs GFP-tagged SNF2H and RFP-tagged SNF2L were co-expressed. The concentration of SNF2H increased with the DNA and displayed distinct pattern at pericentric heterochromatin foci (figure 5.18 F). This SNF2H enrichment was more pronounced compared to SNF2L, which was more evenly distributed throughout the nucleus (D). Especially at the nucleolar boundary an enrichment of SNF2H was detectable. If this observed differences were a direct consequence of binding to nucleosomes at specific chromatin regions, or association to regulatory subunits, like Acf1 of Tip5, or epigenetic marks, e.g. histone modifications, influenced the distribution observed, remained unclear at this point. But theses results obtained *in vivo* provided further evidence for differences between both highly similar human ISWI remodeler. This underlined the relevance of the differences observed *in vitro*.

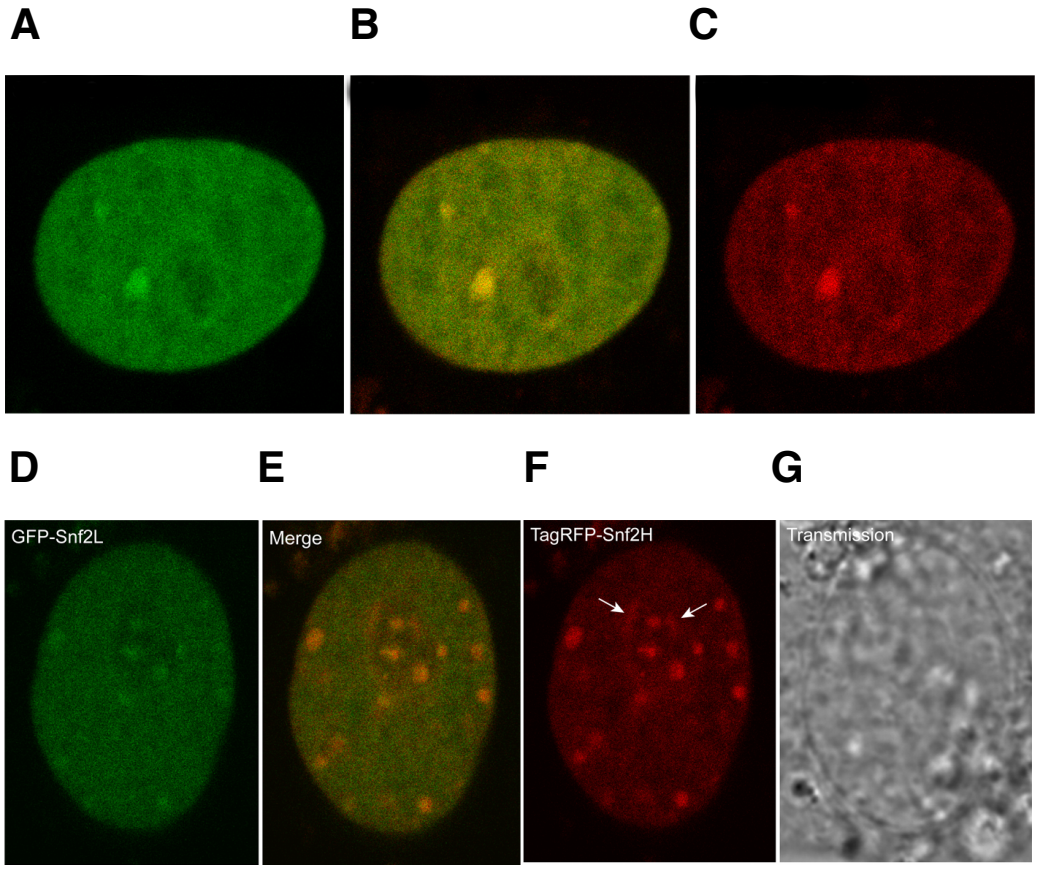

Figure 5.18: **Subcellular localization of co-expressed GFP-tagged SNF2H and SNF2L-RFP in mouse 3T3 cells**

(A + C) Confocal images of 3T3 cells expressing SNF2H-GFP (A) and SNF2H-RFP (C).
(B) Merge of A and C both pictures is shown.
(D) Localization of SNF2L-GFP after co-expression with SNF2H-RFP.
(F) Distribution of SNF2H-RFP within the same cell shown in D.
(E) Merge of D and F depicted here.
(G) Light transmission picture of the cell shown in D - F.

5.2 Structural and functional analysis of human chromatin

Epithelia carcinoma cells from the HeLa line were used to analyze the chromatin structure of human cells. The functional activity of genomic regions is regulated by the structural organization within the nucleus. Therefore this analysis addressed the question of chromatin accessibility linked to gene activity.
In previous studies dealing with the question of global nucleosome positioning and chromatin structure [Segal et al., 2006; Miele et al., 2008; Valouev et al., 2008] non-nucleosomal linker DNA was completely degraded by micrococcal nuclease (MNase) and the remaining 147 bp long mono-nucleosomal DNA fragments were isolated and subsequently analyzed. Other groups interested in the chromatin architecture extracted nuclei, added limited amounts of MNase and subsequently characterized relative large chromatin fragments [Gilbert et al., 2004].
The experimental approach presented here took advantage of the limited fragmentation of chromatin by MNase *in vivo*. From these partially digested chromatin samples, mono-nucleosomal, but also di- and tri-nucleosomal DNA fragments were purified. By using different amounts of nuclease under limiting conditions, a more detailed view on the functional nature of the released chromatin fragments should be possible (see also figure 5.19).

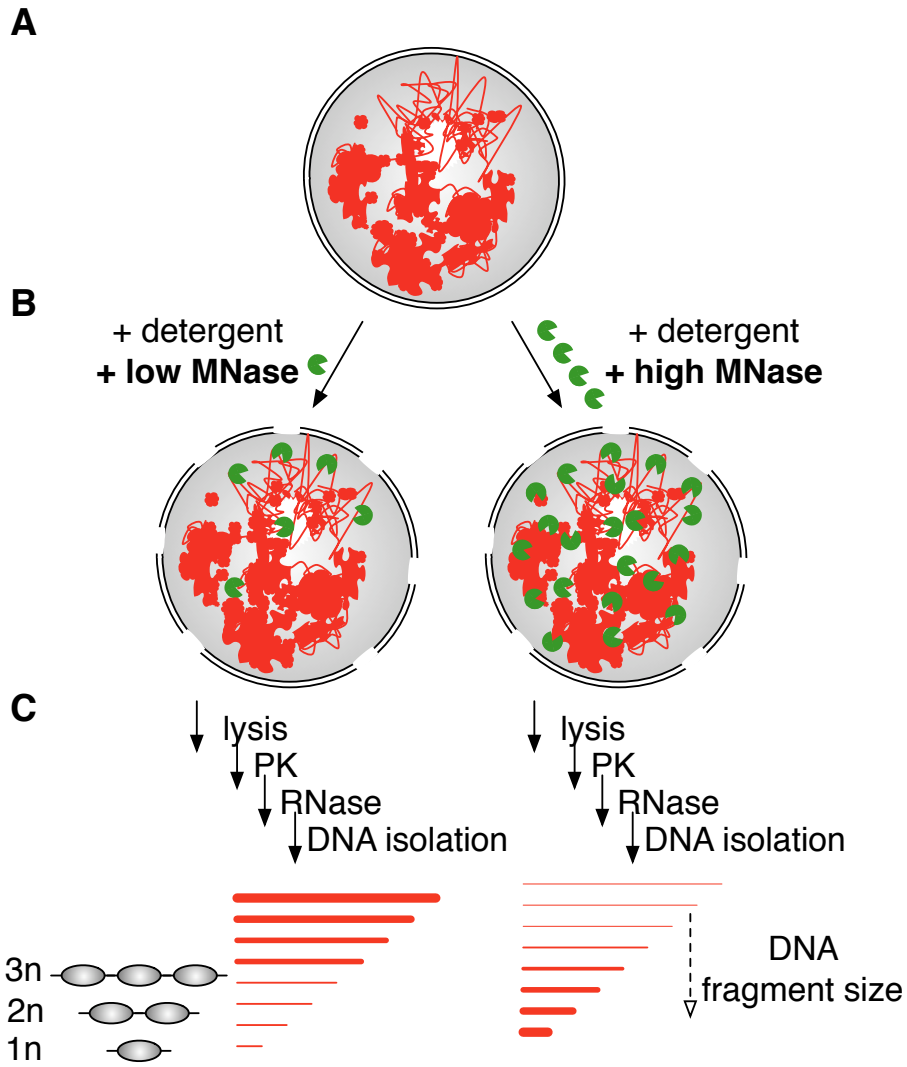

Figure 5.19: **Schematic illustration of chromatin accessibility analyzed by differential MNase digest**

(A) Within a nucleus, DNA (red) is compacted to different levels. This compaction is dependent on the activity of the chromatin domains.

(B) By adding detergent to the cells, cytoplasmic and nuclear membranes are permeabilized. At very low MNase concentrations, only very open structures are cleaved (left panel). If higher MNase amounts are used, the enzyme can also enter more dense chromatin regions and digest these domains as well.

(C) MNase digestion is stopped and Proteinase K (PK) and RNase degrade all cellular proteins and RNA. After isolation of genomic DNA different pools of DNA fragments are expected. At low nuclease concentrations only a subpopulation is fragmented to small sizes (e. g. 1n, 2n and 3n nucleosomes). With high MNase amounts, most DNA is degraded to smaller fragments while only few larger fragments are left (thickness of each line corresponds to relative proportion of these fragment sizes).

5.2.1 Isolation of chromatin fragments after differential MNase digestion

In order to study nuclear architecture and chromatin compaction mono-, di- and tri-nucleosomal DNA sequences were released from human chromatin *in vivo* and subsequently purified to high homogenity. Based on the protocols described in the methods section mono-, di- and tri-nucleosomal DNA was purified from HeLa cells.

5.2.1.1 Fragmentation of human chromatin by MNase *in vivo*

Amounts of MNase were titrated to optimize chromatin fragmentation within HeLa cells. After adding increasing amounts of nuclease, ranging from 50 to 1000 units, to a fixed number of cells, an increased fragmentation of chromatin was detected. Partial cleavage of linker DNA led to formation of a nucleosomal ladder, in which MNase protected nucleosomal fragments formed distinct DNA bands after deproteinization.

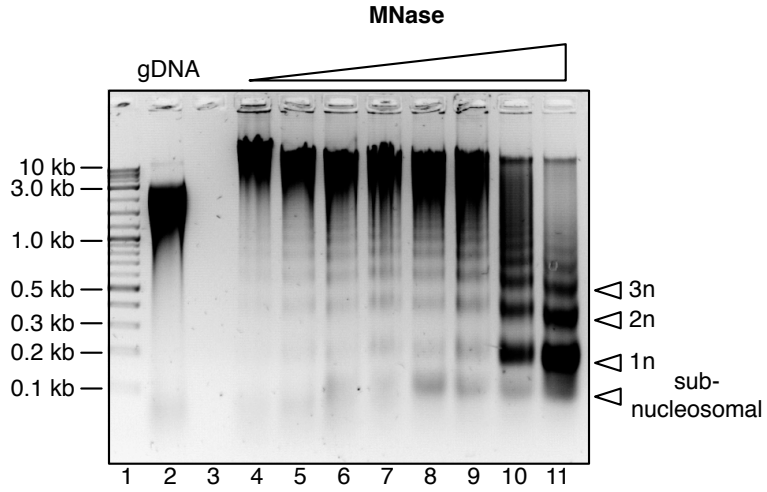

Figure 5.20: **Differential digestion of HeLa chromatin with increasing amounts of MNase**
For each condition, 2x 10^7 cells were permeabilized with detergent and 25, 50, 100, 150, 200, 250, 500, and 1000 units of MNase were added (lane 4 -11). Samples were deproteinized and DNA was purified. Not MNase treated genomic DNA (gDNA) was also isolated and served as negative control. Because intact gDNA hardly enters agarose gels, the sample was sonicated to shear gDNA prior loading (lane 2). For each lane 1 µg of DNA sample was loaded on a 1.3 % agarose gel.

With 1000 units of MNase the mono-nucleosomal (1n) band was predominant, but also di- and tri-nucleosomal fragments (2n and 3n) were still present (see figure 5.20 lane 11). Reducing the amount of MNase to less than 250 units resulted in formation of mainly

higher molecular weight fragments, larger than 1 kb (see figure 5.20 lane 4 - 8). Thus 250 units of nuclease were used as minimal amount of enzyme needed to release 1n, 2n and 3n nucleosomal DNA fragments (see figure 5.20 lane 9). Within all four lanes from 8 - 11 (figure 5.20), DNA fragments shorter than 100 bp were detectable. Since these fragments were shorter than the 147 bp long mono-nucleosomal fragments, they were referred to sub-nucleosomal fragments. The release of these small DNA fragments from the chromatin did not correlate with the amount of MNase used for DNA hydrolysis. While the signal of the 1n band increased with raising amounts of nuclease, the sub-nucleosomal signal remained constant.

5.2.1.2 Purification of nucleosomal DNA from HeLa cells

As shown in figure 5.20, addition of 250 and 1000 units MNase to 2x 10^7 human HeLa cells led to optimal differential chromatin fragmentation. For further experiments 250 units MNase were used to release chromatin fragments under "low" MNase conditions and 1000 units for the corresponding "high" MNase setup. DNA fragments were purified by gel elution after electrophoretic separation on agarose gels (figure 5.21). For the high MNase samples 1n, 2n and 3n DNA could be purified after separation from a preparative gel without further treatment.
Because of the very limited digestion under low MNase conditions 1n, 2n and 3n nucleosomal DNA resembled only a small subfraction of total DNA. To avoid overloading of the preparative agarose gel, smaller nucleosomal DNA fragments were enriched prior separation. Incubation of the DNA with polyethylene glycol allowed a size selective DNA precipitation. Adding PEG 8000 to a final concentration of 7 % (w/v) to the DNA samples induced precipitation of all DNA fragments larger than 500 bp. After precipitation 3n, 2n, 1n and sub-nucleosomal DNA was specifically enriched in the supernatant (see figure 5.21 B lane 2 and 3). Loading this pre-separated DNA samples to preparative agarose gels allowed good separation and subsequent isolation of each DNA fragment (see figure 5.21 C). Under these more stringent conditions sub-nucleosomal DNA separated into two distinct fragment populations. One fragment pool was smaller than 100 bp and the other fragments had an average size below 75 bp (figure 5.21 C lane 1 - 3). The size of 1n nucleosomal DNA was estimated to be approximately 150 bp, whereas 2n and 3n DNA was 350 bp and 550 bp long. These isolated nucleosomal DNA samples were used for further structural and functional analyses.

5.2.2 Localization of purified chromatin fragments within human genome analyzed by fluorescence *in situ* hybridization

The first structural analysis using nucleosomal DNA fragments released by different amounts of MNase was done by fluorescent *in situ* hybridization (FISH). These experiments were done by Dr. Attila Németh in collaboration with Prof. Dr. Thomas Cremer at the Department Biology II, Ludwig-Maximilians University Munich.
With a length of approximately 550 bp, 3n nucleosomal DNA could be directly used as hybridization probes. 3n DNA was specifically fluorescently labelled, 3n low MNase with FITC and 3n high MNase with Cy3 (see figure 5.22 B) and without further amplification hybridized to diploid human metaphase chromosomes (2D) as well as fixed nuclei (3D).

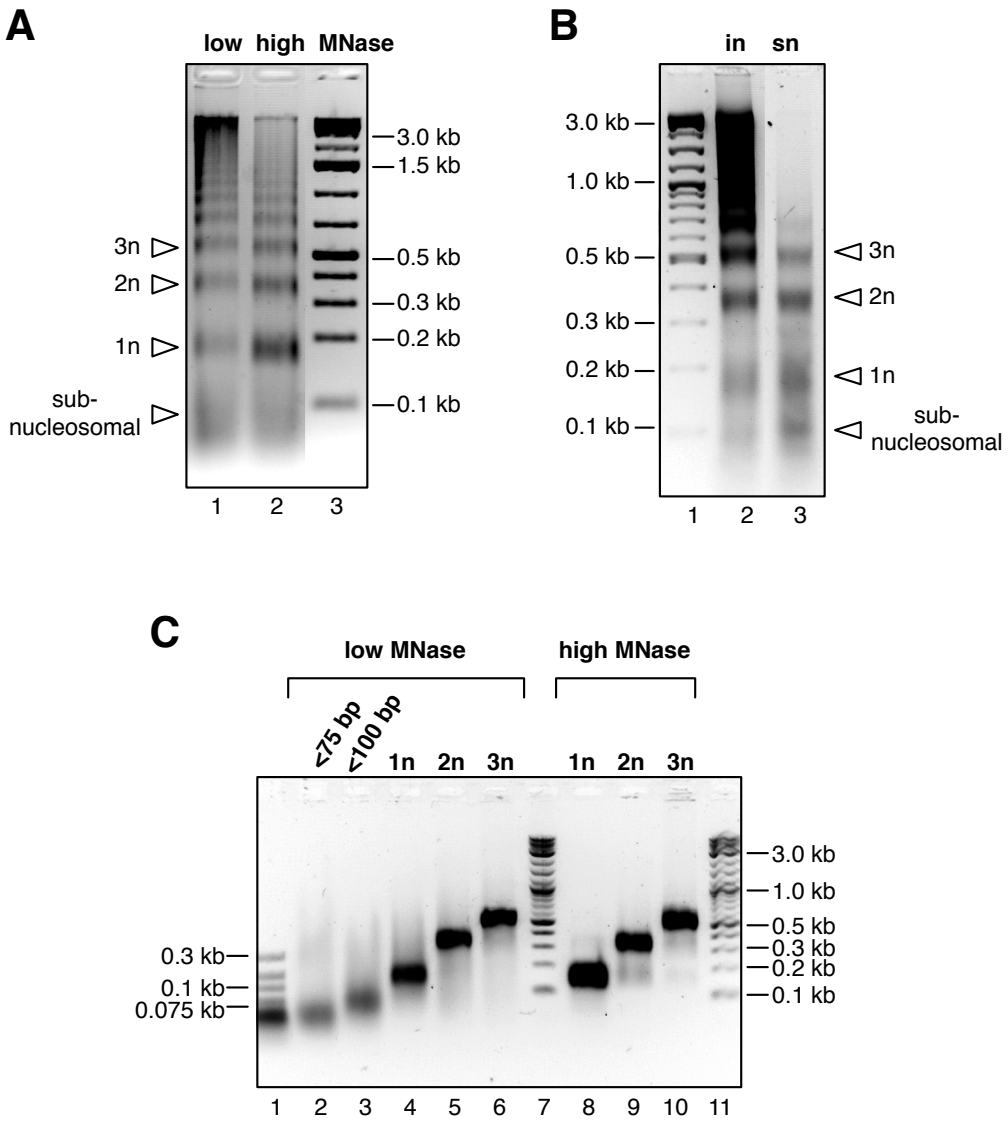

Figure 5.21: **Isolation of mono-, di- and tri-nucleosomal DNA**
(A) HeLa cells were treated with low and high doses of MNase (250 and 1000 units). Chromatin was deproteinized and purified DNA was separated on a 1.3 % agarose gel, stained with 0.01 % SybrSafe. Bands corresponding to mono-, di- and tri-nucleosomal DNA fragments are indicated by arrows (1n , 2n, and 3n). The sub-nucleosomal DNA is a population of fragments shorter than 100 bp.
(B) Before quantitative separation of 1n, 2n and 3n nucleosomal DNA under low MNase conditions (lane 2, input) DNA fragments larger than tri-nucleosomes were separated by precipitation with 7 % PEG while shorter DNA remained in the supernatant (lane 3, sn).
(C) Purified nucleosomal DNA after gel elution. Under low MNase condition the sub-nucleosomal DNA was gel purified and consisted of two distinct fractions. All electrophoretic separations were done using 1.3 % agarose gels stained with 0.01 % SybrSafe.

5.2.2.1 Local distribution of 3n nucleosomal DNA on metaphase chromosomes

The local hybridization of 3n chromatin fragments released under low and high MNase conditions was investigated by 2D FISH to metaphase chromosomes of human diploid lymphocytes. FITC labelled 3n low MNase DNA was hybridized together with Cy3 labelled 3n high MNase DNA to metaphase spreads of these cells. The total DNA distribution was visualized by staining with DAPI.
As shown in figure 5.22 C and D, for each signal channel a picture was taken, and a merge of all three signals allowed a direct comparison. Hybridization of FITC and Cy3 labelled 3n DNA revealed no difference (figure 5.22 C). The low MNase, high MNase and merge picture displayed a predominant hybridization to centromeres and the juxtacentromeric heterochromatin for different chromosomes. Also some telomeric regions were highlighted, but less intense. Both, telomeres and cetromeres are rich in repetitve DNA elements. Even if only a small fraction of the 3n nucleosomal DNA was digested out of telomeric or centromeric regions, strong signals would be expected due to the repetitive structure of these chromosome domains.
As displayed in figure 5.22, some 3n DNA was released from these parts of the chromosome. Repetitive DNA signals were suppressed by repetitive competitor DNA (Cot1). In presence of Cot1 competitor, specific signals for each 3n probe were detected (figure 5.22 D). Both DNA probes hybridized to different chromosomes and specific regions of these chromosomes. Even under these competitive conditions, 3n high MNase probes hybridized to centromeres.

A more detailed analysis is shown in figure 5.23. Centromeres were generally free of 3n low MNase signals but rich in 3n high MNase staining. Some chromosomes were weakly stained by FITC labelled probes, but certain acrocentric chromosomes displayed a specific enrichment for the 3n low MNase signals at the p-arms. In general, both probes showed a specific hybridization pattern to human chromosomes when repetitive signals were suppressed. At a higher resolution, the distinct differences became obvious. Strikingly, no hybridization of 3n low MNase probes to the centromeres was detectable, when comparing the signal in picture E - G. However, they were specifically stained by 3n high MNase probes.

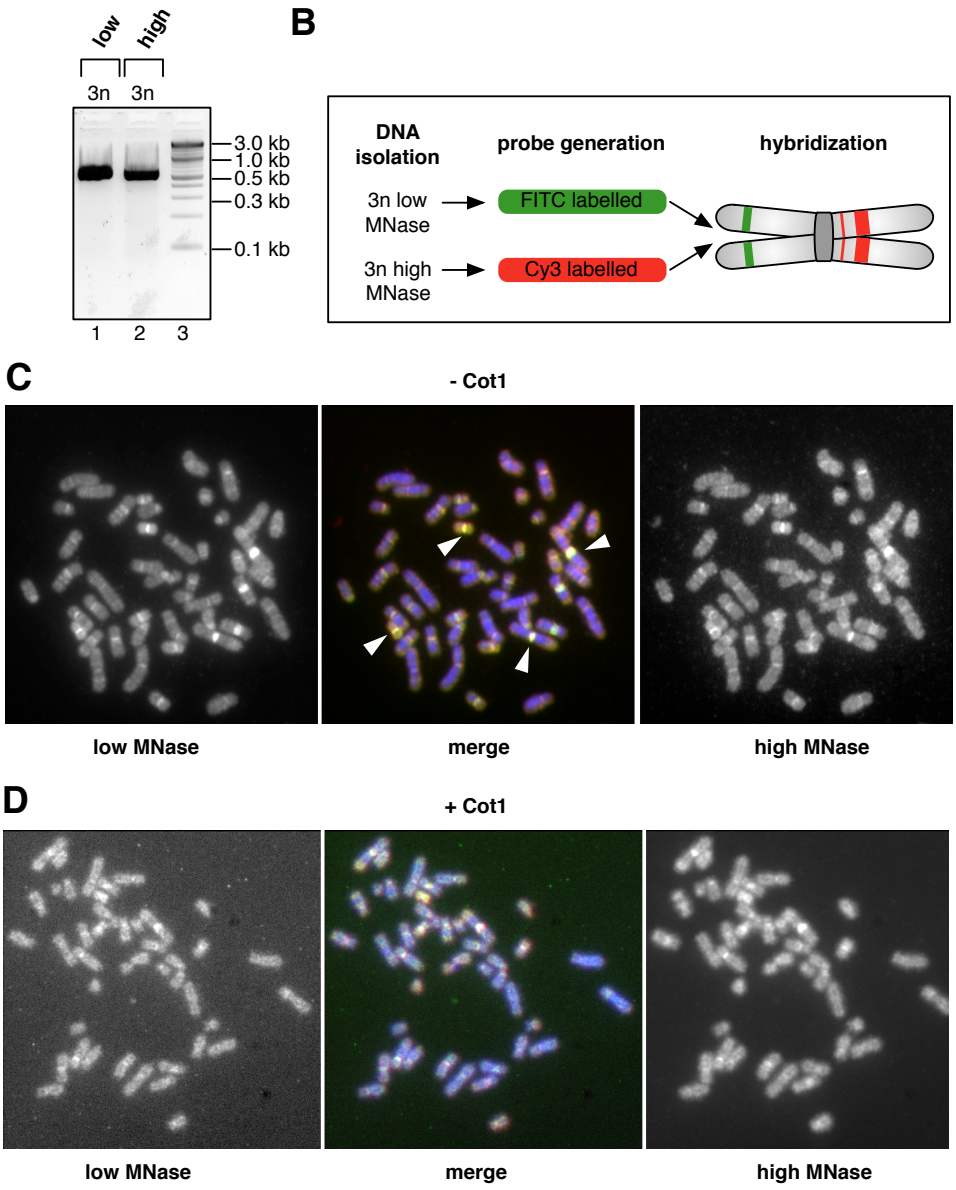

Figure 5.22: **Preparation of 3n probes and 2D FISH on metaphase spread chromosomes**

(A) 3n nucleosomal DNA was purified after treating the cells with low and high doses of MNase. Purity of each sample was checked on 1.3 % agarose gels.

(B) Purified DNA fragments were fluorescently labelled to generate FISH probes. 3n DNA from low MNase treated cells was FITC labelled, 3n high MNase was Cy3 labelled. These fluorescent probes were hybridized to metaphase chromosomes.

(C) Hybridization of 3n probes to human metaphase chromosomes from diploid lymphocytes. Without Cot1 signals from repetitive DNA elements were not suppressed. Left panel displays hybridization of 3n low MNase probes and right panel shows hybridization of 3n high MNase probes. The central picture was generated by overlaying all three channels. DAPI staining is shown in blue, 3n low in green and 3n high in red.

(D) In presence of Cot1 DNA, repetitive signals were suppressed and 3n low and high specific signals can be distinguished.

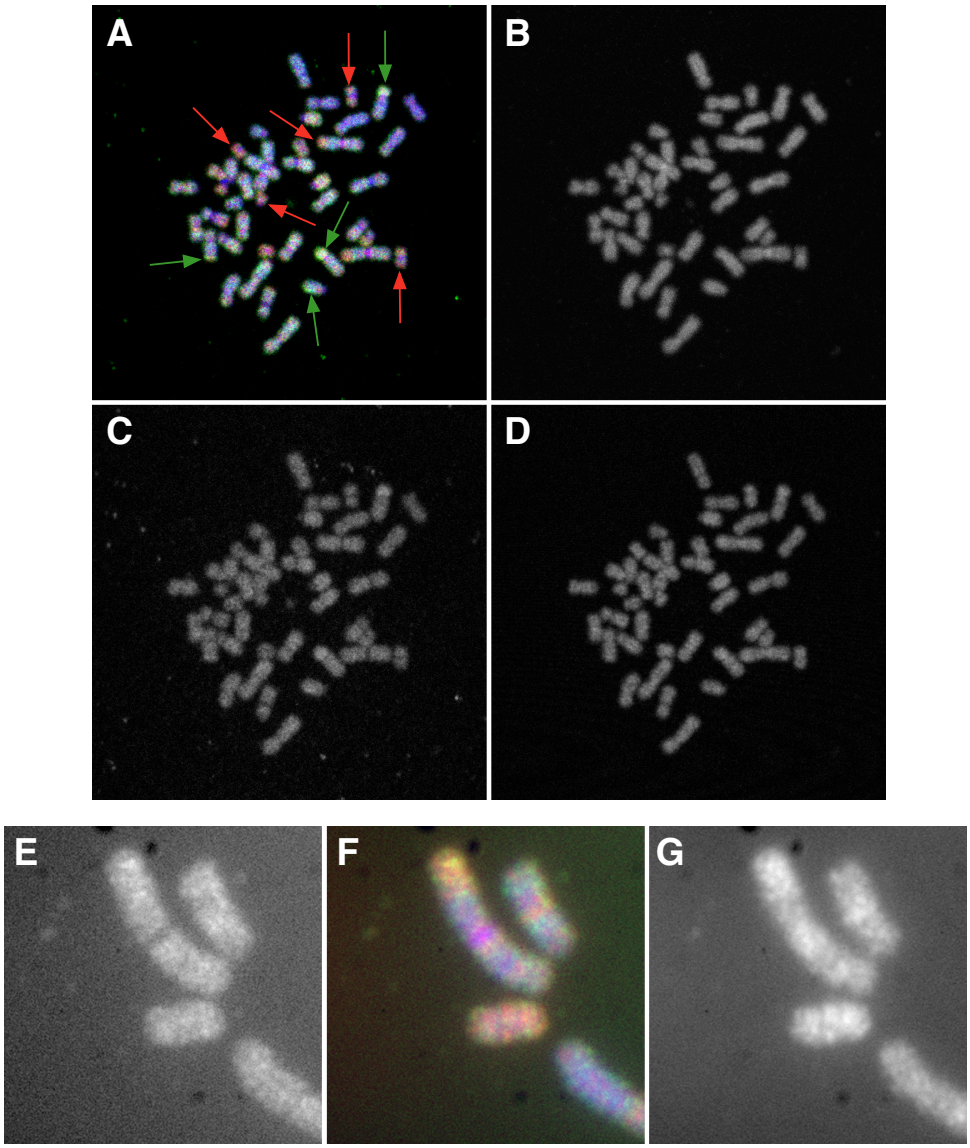

Figure 5.23: **Identification of 3n low and high specific signals in 2D FISH**
(A) Overlay of all three signals shown in B - D. Arrows highlight regions of chromosomes showing an increased signal for 3n low (green) or 3n high (red). DAPI staining is shown in blue.
(B) DNA staining of diploid human lymphocyte chromosomes with DAPI.
(C) Signal of 3n low MNase probes (green) after hybridization to chromosomes.
(D) 3n high MNase probes (red) hybridized to chromosomes.
(E) Picture of 3n low MNase hybridized to metaphase chromosomes in higher resolution.
(F) Merge of E and G with 3n low signals in green, 3n high in red and DAPI in blue.
(G) 3n high MNase probes as described in E.

5.2.2.2 Global localization of 3n nucleosomal DNA within human nuclei (3D FISH)

The initial analysis of the two-dimensional distribution of 3n DNA along metaphase chromosomes displayed clear differences. Therefore in a next step the three-dimensional localization of these sequences was investigated. The same FITC and Cy3 labelled probes (section 5.2.2.1) were used for 3D hybridization to fixed human IMR-90 fibroblast-like cell nuclei. These diploid cells were formaldehyde fixed and stacks of pictures in z-axis were taken in FITC, Cy3, and DAPI channel (figure 5.24).
Hybridization to intact nuclei underlined the observed differences in the distribution of the released 3n low and 3n high DNA sequences. The Cy3 high MNase signal was correlating in most regions with the blue DAPI signals. But some areas with a reduced DNA density also showed a clear high MNase DNA staining, indicating that the probe was not hybridizing unspecifically or genome wide. The 3n low signal in the FITC channel displayed an even more specific pattern. Especially figure 5.24 C demonstrates that only small defined regions of the nucleus were stained by this probe. These signals did not correlate to DNA density and were hardly co-localizing with 3n high signals in the Cy3 channel. Under these very limited digestion conditions small, open and therefore non-heterochromatic domains were released. How far these very early digested accessible chromatin foci were part of active euchromatin domains remained unclear at this point of the analysis.

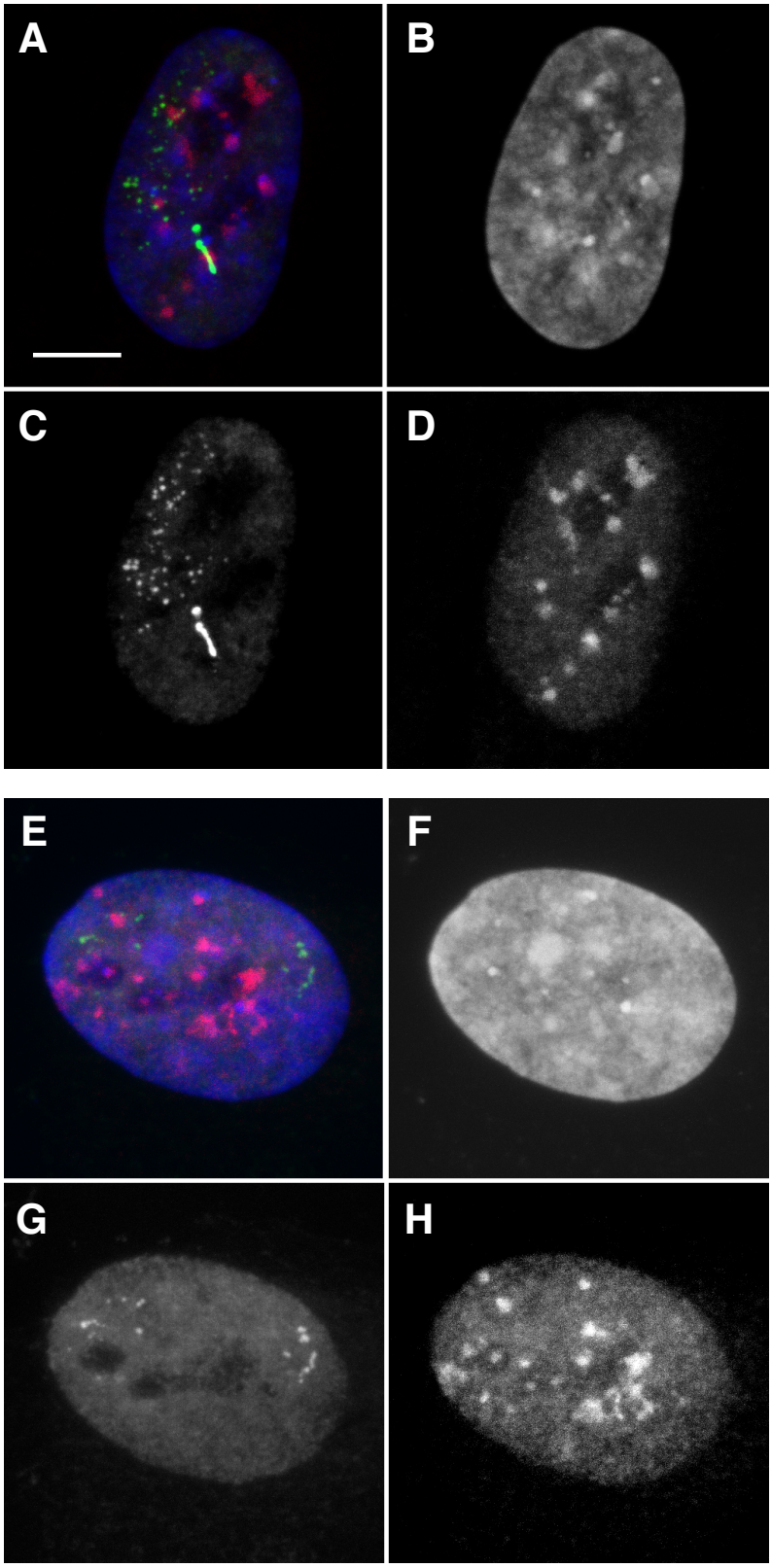

Figure 5.24: **Z-stack projection of 3D FISH with human IMR90 nuclei** **(A, E)** Overlay of B - D or F - H respectively. **(B, F)** DNA staining of human IMR90 nuclei with DAPI. **(C, G)** Signal of 3n low MNase probes (green) after hybridization. **(D, H)** 3n high MNase probes (red) hybridized to nuclei.

5.2.3 Global accessibility of 3n fragments to chromatin analyzed by southern blotting

The microscopic results in section 5.2.2 already displayed differences in the genome wide distribution of 3n DNA fragments. To address the interdependency between chromatin structure and MNase accessibility more generally, the distribution of these DNA samples within differentially fragmented genomic DNA was analyzed by southern blotting. Chromatin from HeLa cells was treated with different amounts of MNase (62.5, 250, 1000 and 2000 U), gel separated and transferred to a membrane. 3n nucleosmal DNA samples were radioactively labelled with ^{32}P and hybridized to these fragments (figure 5.25).

Untreated genomic DNA was isolated and digested with different restriction endonucleases after purification. These samples were used as controls for specificity of the hybridization. *EcoRI* with a 6 bp long and *MspI* with a 4 bp recognition sequence generated specific fragment patterns (figure 5.25 B lane 2 and 3). As indicated in figure 5.25, nucleosomal bands ranging from 1n up to 7n were detectable in SybrSafe staining after digestion with 500 (lane 5) and 1000 units MNase (lane 6). The distinct pattern seen in the *EcoRI* control after hybridization of the 3n low MNase probe, especially between 500 and 1500 bp, indicated that the signal was probe specific. The general hybridization pattern was similar to the SybrSafe staining. Slight differences in the intensities of 1n and 2n nucleosomal DNA in figure 5.25 panel A lane 6 and 7 compared to the signal of the probe in panel B lane 6 and 7 were detectable. On DNA level, the signal for the 1n fragments was the same or even larger than the one for 2n nucleosomes. In contrast, the southern blot signal for 2n nucleosomes was more intense than for 1n. This could indicate that the domains, from which 3n low MNases probes were initially isolated, are less susceptible to complete hydrolysis down to mono-nucleosomal levels.

Also the 3n high MNase probe hybridized specifically (figure 5.26 lane 1) to the blot. Again the 1n signal was decreased while the 2n signal was comparable to the DNA staining. Especially for the larger DNA fragments, no significant differences were detectable. Inefficient transfer of DNA at the edge of the gel could be one reason why specifically the most bottom signals were decreased. As already shown in section 5.2.2, differences between 3n high and 3n low MNase DNA were only detectable, if repetitive signals were suppressed (see figure 5.22 C and D). In the southern blot experiments shown here, repetitive DNA signals were not suppressed. These results gave further hints for the presence of repetitive genetic elements within the purified chromatin fractions.

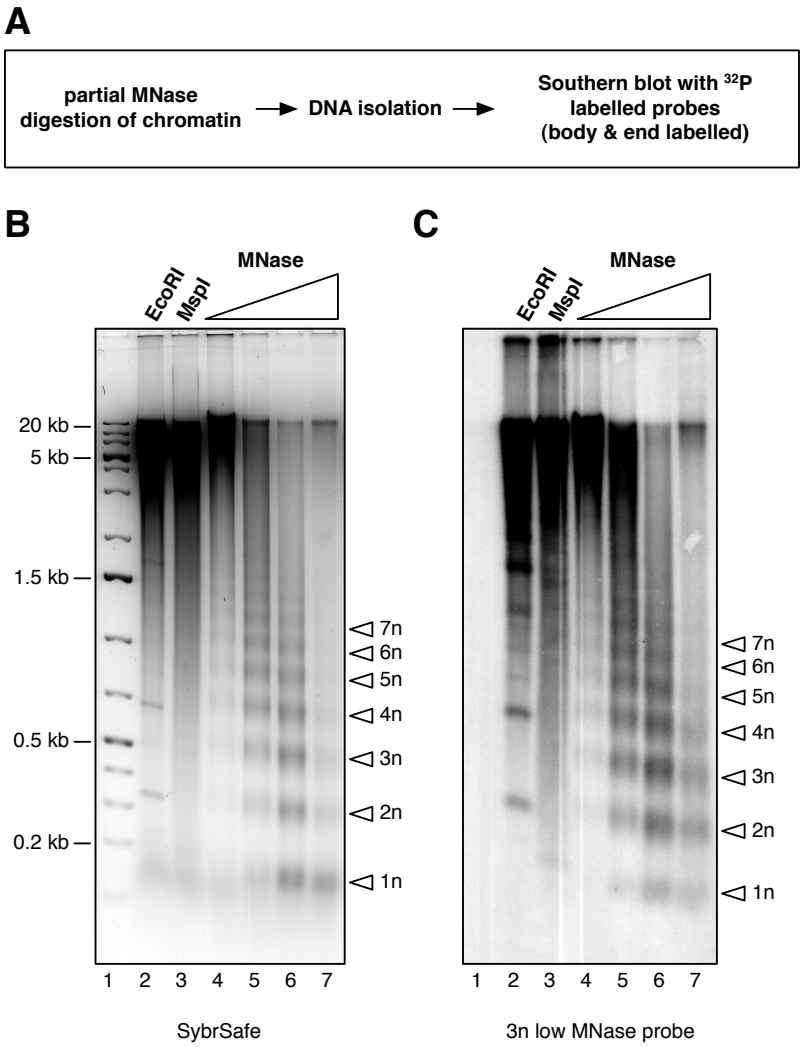

Figure 5.25: **Southern blotting of 3n low MNase DNA to partially digested HeLa DNA**

(A) Schematic illustration of the experimental approach. HeLa chromatin is partially digested with different amounts of MNase *in vivo*, after deproteinization, DNA is isolated and separated on agarose gels. Different specific, radioactive DNA probes are hybridized to separated chromatin fragments.

(B) HeLa cells were permeabilized and chromatin was partially digested with 62.5, 250, 1000 and 2000 U MNase (lane 4 - 7). DNA was isolated and for each condition 5µg were separated on a 1.3 % agarose gel and subsequently stained with SybrSafe. 1n to 7n nucleosomal bands are indicated by arrows. Not MNase treated genomic DNA was also isolated and digested with *EcoRI* and *MspI* after extraction. 5µg of these specifically fragmented DNA samples were used as positive controls for hybridization (lane 2 and 3).

(C) Autoradiogram of transferred DNA shown in **A** after hybridization of ^{32}P body-labelled 3n low MNase probes.

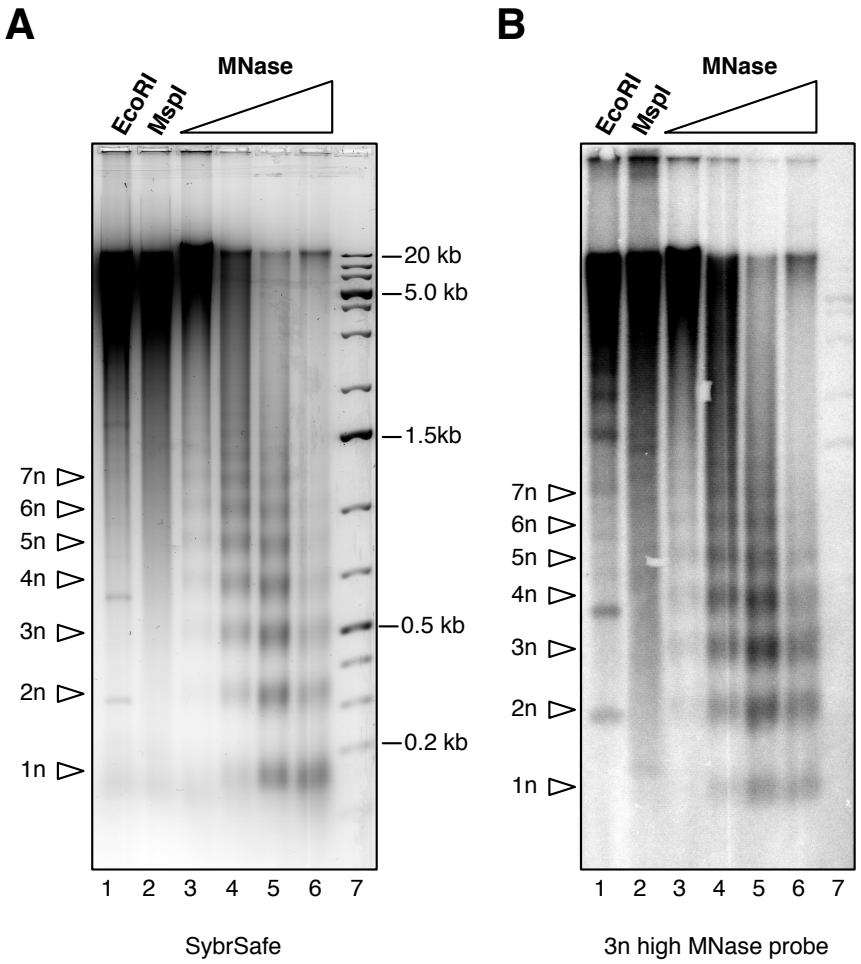

Figure 5.26: **Southern blotting of 3n high MNase DNA to partially digested HeLa DNA**

(A) HeLa cells were permeabilized and chromatin was partially digested with 62.5, 250, 1000 and 2000 U MNase (lane 3 - 6). DNA was isolated and for each condition 5 µg were separated on a 1.3 % agarose gel and subsequently stained with SybrSafe. 1n to 7n nucleosomal bands are indicated by arrows. Not MNase treated genomic DNA was also isolated and digested with *EcoRI* and *MspI* after extraction. 5 µg of these specifically fragmented DNA samples were used as hybridization controls in lane 1 and 2.

(B) Autoradiogram of transferred DNA shown in **A** after hybridization of ^{32}P body-labelled 3n high MNase probes.

5.2.4 Distribution of repetitive DNA elements within fragmented HeLa chromatin

The distribution of repetitive DNA sequences within partially digested chromatin was analyzed also by southern blotting. As already shown in section 5.2.3, differentially digested chromatin was separated and transferred to a membrane. Genomic HeLa DNA was digested by sequence specific restriction endonucleases and used as positive control. Since the 2D FISH experiments without repression of repetitive signals showed a clear centromeric localization, a 30 bp short centromere specific oligonucleotide was chosen as first probe. This centromere specific probe was directed against the CENP-B box alphoid DNA sequence [Matera and Ward, 1992].

Figure 5.27 B lane 2 proved a specific hybridization of the probe to the *EcoRI* digested HeLa DNA. When comparing 3n DNA signals after 250 and 1000 units MNase treatment (figure 5.27 A lane 4 and 5) to the southern blot signal at that size (figure 5.27 B lane 4 and 5), no differences were detectable. Therefore under both digestion conditions, the same portion of total DNA fragments was released from centromeric regions. Using even more (lane 6) or less (lane 2) MNase did not lead to a significant enrichment or depletion of centromeric sequences in the released fragment pool.

Telomeres are also an important heterochromatic domain formed by repetitive sequence elements. Therefore the same experimental approach was performed with a 42 bp telomere specifc oligonucleotide. The sequence of this probe encoded seven repeats of the 6 bp long telomere sequence motif [Blasco, 2007; Canela et al., 2007]. The *MspI* digested genomic DNA showed a specific hybridzation pattern (figure 5.28 B lane 9). When comparing the spacing of bulk chromatin to the pattern observed for centromeric chromatin, qualitative differences were observable. Nucleosomal bands in the DNA staining in figure 5.28 A showed a clear pattern with sharp bands. The southern blot bands in figure 5.28 B were less defined, and smearing down, compared to blotting of the centromeric probe in 5.27 B. These broader bands indicated that a fraction of telomeric chromatin had a closer spacing than the canonical spacing of bulk chromatin, as also seen in earlier studies [Tommerup et al., 1994].

With respect to the chromatin accessibility, telomeres were not preferentially digested by low or high doses of MNase, as was also shown before for centromeres. For the differentially digested chromatin samples in lane 3 - 8, no difference in the global distribution of DNA staining (figure 5.28 A) and the telomere specific hybridization signal (figure 5.28 B) was detectable.

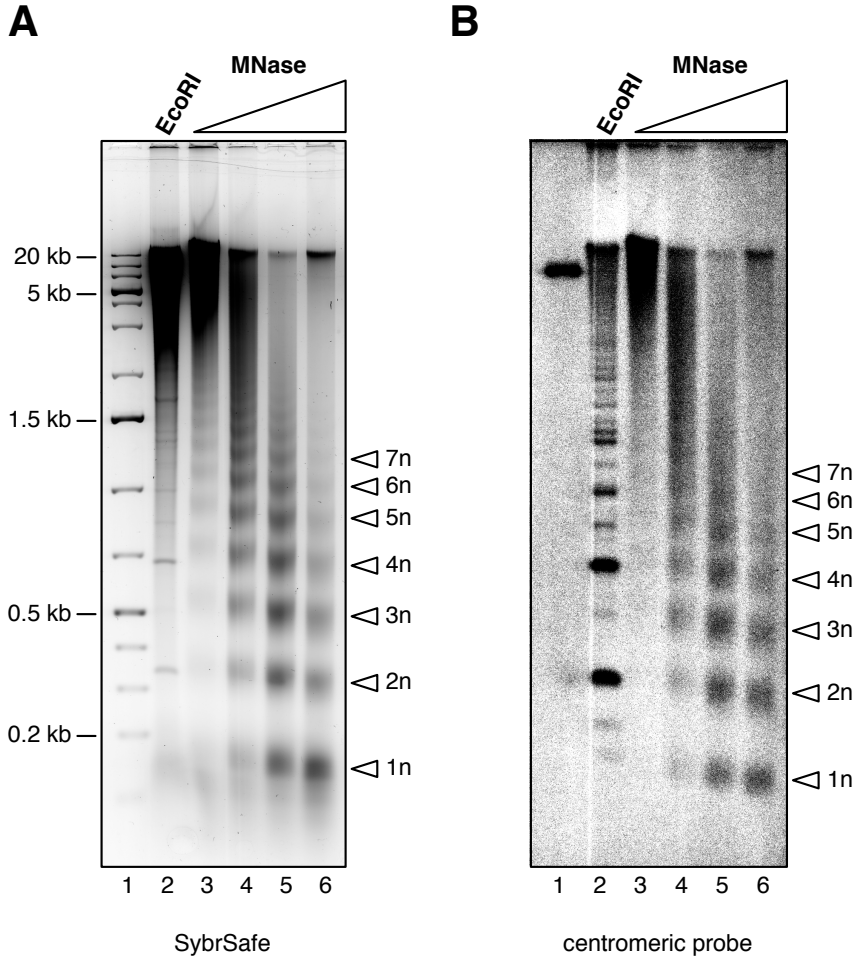

Figure 5.27: **Southern blot hybridization of a centromere specific probe to partially digested HeLa DNA**

(A) 5 µg of HeLa DNA isolated after partial digestion with 62.5, 250 1000 and 2000 U MNase (lane 3 - 6) were separated on a 1.3 % agarose gel and stained with SybrSafe. Lane 2 shows genomic DNA fragmented specifically with *EcoRI* used as positive control for hybridization. 1n to 7n nucleosomal bands are indicated by arrows.

(B) Autoradiogram of transferred DNA shown in **A** after hybridization of ^{32}P end-labelled centromere specific oligonucleotide probe.

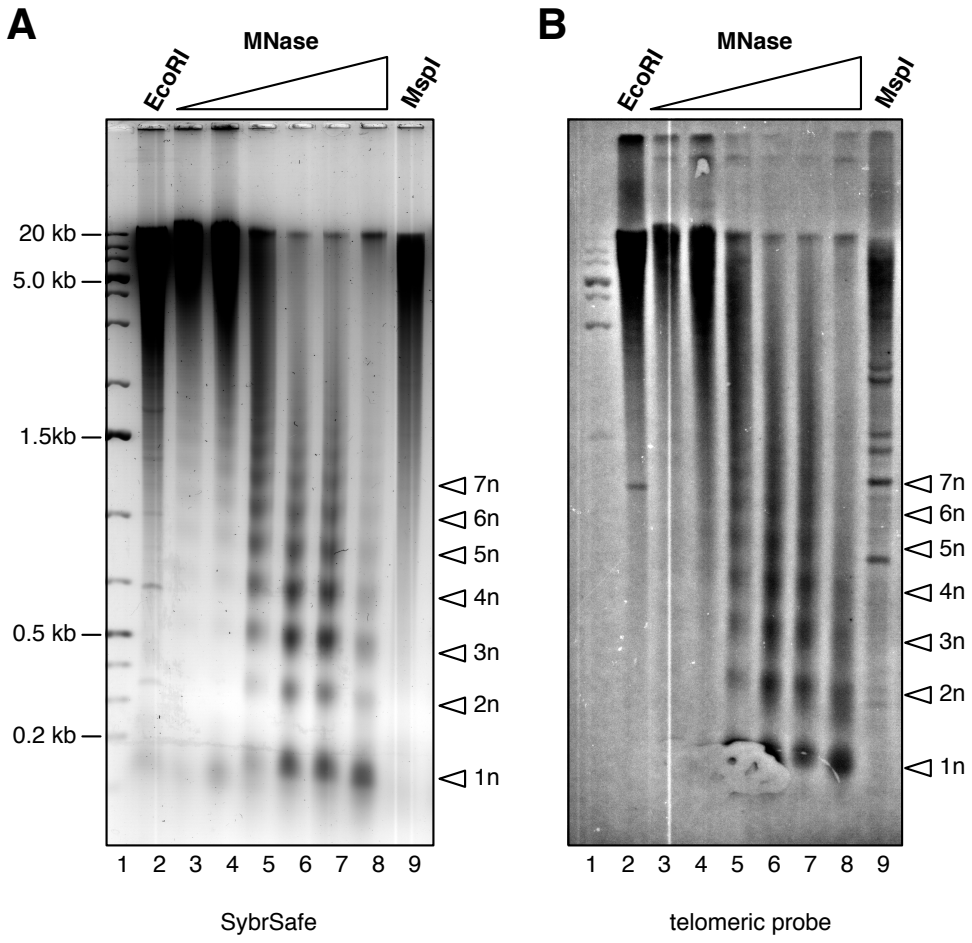

Figure 5.28: **Distribution of telomere specific DNA fragments within partially digested HeLa chromatin**

(A) 5 µg of HeLa DNA isolated after partial digestion with 62.5, 250 1000, 1000 and 2000 U MNase (lane 4 - 8) were separated on a 1.3 % agarose gel and stained with SybrSafe. As controls 5 µg genomic DNA fragmented specifically with *EcoRI* and *MspI* were loaded in parallel (lane 2 and 9). 1n to 7n nucleosomal bands are indicated by arrows.

(B) Autoradiogram of transferred DNA shown in **A** after hybridization of ^{32}P end-labelled telomere specific oligonucleotide probe.

Another class of repetitive elements are the Alu sequences. They make up to 10 % of the human genome [Lander et al., 2001], and their distribution within the fragmented DNA was analyzed. With a length of 300 base pairs they belong to the short interspersed elements (SINEs) and are distributed throughout the whole human genome [Batzer and Deininger, 2002]. Since they were first described as *AluI* restriction endonuclease sensitive elements, this enzyme was used to specifically digest the genomic DNA for the positive control. Based on the Alu-subfamily consensus sequence [Batzer and Deininger, 2002], a 46 bp oligonucleotide probe was synthesized and radioactively labelled. The hybridization of this probe was specific as the control in lane 2 (figure 5.29) underlined. DNA staining displayed a major portion of genomic DNA with a median length of 500 bp, while the southern blot gave a signal peak between 200 and 400 bp length, reflecting the Alu-repeat length (panel A vs. B). The genome wide distribution of these repetitive elements was also observed when partially digesting the chromatin. A slight increase of the 1n signal with respect to the 2n signal could be observed when comparing the blot signal to the DNA staining. For 3n fragments released under high and low MNase conditions (figure 5.29 lane 5 and 6) the signals for the Alu-repeats reflected the total DNA distribution. For these highly abundant genomic elements no specific enrichment within one of the chromatin fractions was detectable.

Because the highly repetitive elements were evenly distributed throughout the fragment populations, a more specifically localized and less abundant repetitive sequence was tested for its distribution. The ribosomal DNA of a human cell is arranged in clusters of 43 kb long tandemly repeated *rRNA* genes, encoding the 18S, 5.8S and 28S rRNA transcripts. These clusters are found on the five acrocentric chromosomes 13, 14, 15, 21 and 22. The reverse complement of a 50 bp long stretch of sequence upstream of the 5'-external transcribed spacer (5'-ETS) was used to generate an end-labelled radioactive probe. Figure 5.30 B demonstrates that signal intensities obtained from hybridization of end-labeled probes are too low, if the target sequence is not a highly repetitive DNA element. To obtain better signal intensities, a longer body-labelled probe containing more than one radioactive ^{32}P atom per probe-molecule would be necessary.

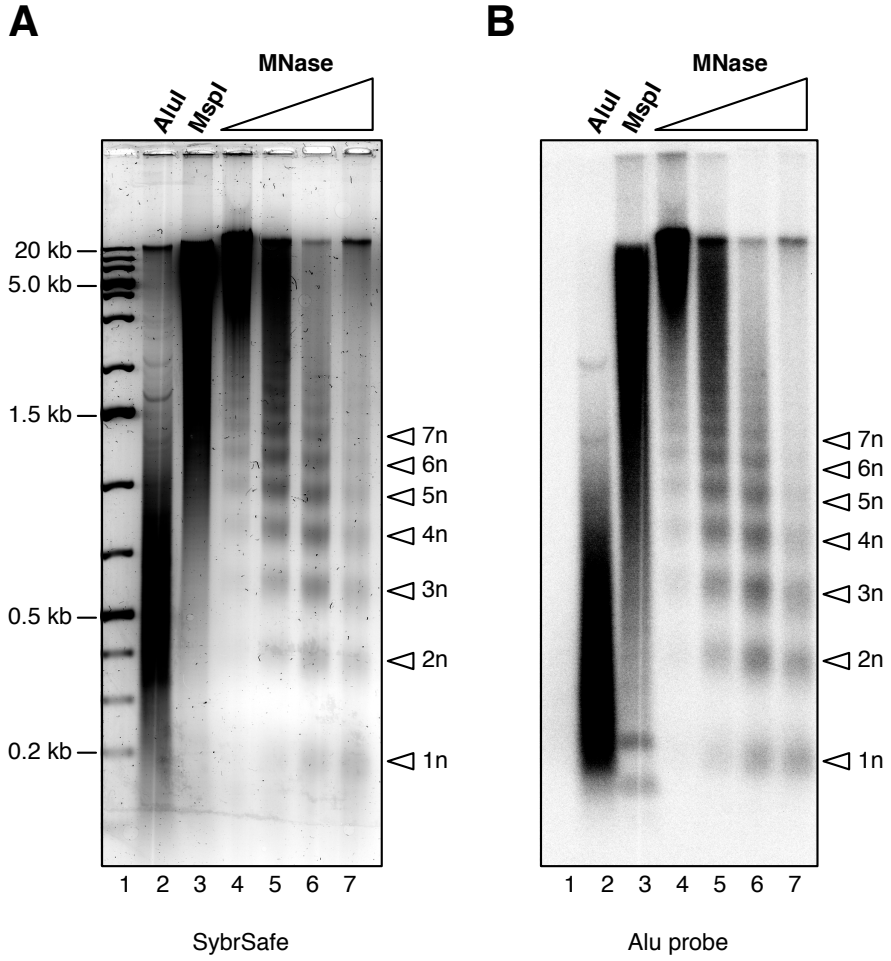

Figure 5.29: **Distribution of Alu repeats within partially digested HeLa chromatin**

(A) 5 µg of HeLa DNA isolated after partial digestion with 62.5, 250, 1000 and 2000 U MNase (lane 4 - 7) were separated on a 1.3 % agarose gel and stained with SybrSafe. Lane 1 and 2 show 5 µg genomic DNA digested with *AluI* and *MspI* used as positive controls. 1n to 7n nucleosomal bands are indicated by arrows.

(B) Autoradiogram of transferred DNA shown in **A** after hybridization of ^{32}P end-labelled oligonucleotide specific for Alu repeats.

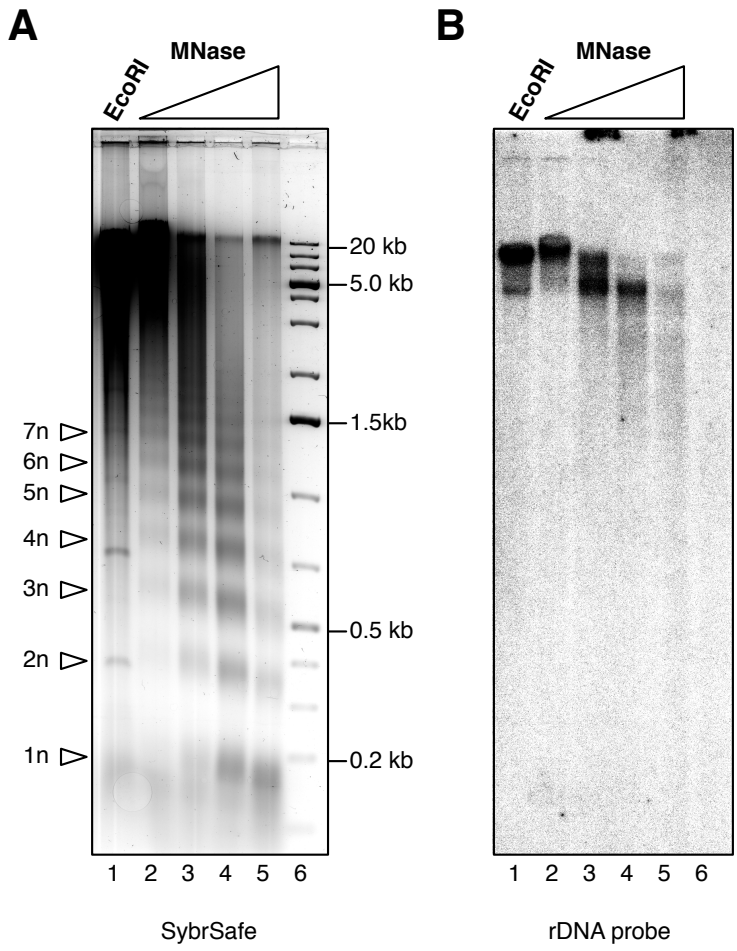

Figure 5.30: **Southern blot hybridization of a rDNA specific probe to partially digested HeLa DNA**

(A) 5 µg of HeLa DNA isolated after partial digestion with 62.5, 250, 1000 and 2000 U MNase (lane 2 - 5) were separated on a 1.3 % agarose gel and stained with SybrSafe. Lane 1 shows 5 µg genomic DNA digested with *EcoRI* used as positive control. 1n to 7n nucleosomal bands are indicated by arrows.

(B) Autoradiogram of transferred DNA shown in **A** after hybridization of end-labelled oligonucleotide specific for rDNA 5'ETS leader sequence.

5.2.5 Methylation of nucleosomal DNA *in vivo*

DNA methylation is a functional epigentic mark associated with heterochromatin formation. Methylation of CpG dinucleotides regulates gene expression in mammalian genomes and in general 60 - 90 % of all CpG sites are methylated [Jeltsch, 2002]. Especially CpG dinucleotides in repetitive DNA elements of constitutive heterochromatin are highly methylated [Smit, 1999; Yoder et al., 1997a]. In order to initially test for the association of differentially digested nucleosomal DNA with heterochromatin, the relative methylation states were detected using specific antibodies in an ELISA assay. These experiments were performed in collaboration with Dr. Max Felle at our institute.

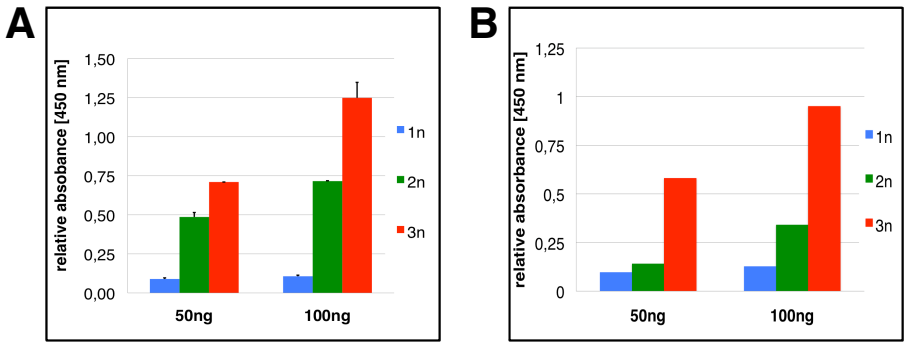

Figure 5.31: **Relative DNA methylation of 1n, 2n and 3n nucleosomal DNA** **(A)** Methylation of 50 and 100 ng of 1n, 2n, 3n nucleosomal DNA, purified after high MNase treatment, detected by a methylation specific antibody and calorimetrically measured by ELISA as technical duplicate. **(B)** Corresponding analysis with low MNase treated 1n, 2n, 3n DNA.

The used methylation specific antibodies allowed a fast and accurate measurement of the relative DNA methylation. Partial digestion of chromatin allowed an indirect analysis of the DNA methylation in the linker region. The results in 5.31 demonstrate that methylation of genomic DNA in HeLa cells is mainly restricted to this nucleosomal linker DNA. Mono-nucleosmal DNA showed no significant DNA methylation compared to di- and tri-nucleosomal DNA. The relative methylation signal correlated with the relative DNA length. Since identical amounts of DNA were used, this increase reflected the larger amount of linker DNA present in the sample. The effect was seen for 1n, 2n and 3n after high MNase (A) and low MNases treatment (B). Thus the used approach was suitable for analyzing DNA methylation in chromatin indirectly. Methylation of high and low MNase digested DNA sample groups did not differ significantly. For the low MNase digested samples the signal intensities were slightly smaller, but this reflected rather the variation between different experiments than a biologically relevant effect.

5.2.6 Transcriptional activity of 3n nucleosomal DNA

As shown by microscopic studies, 3n low MNase DNA resembled a specific fragment population digested from highly accessible chromatin regions. To gain further insight into the functional status at these regions, comparative hybridization to ENCODE DNA microarray was performed. The bioinformatic analysis of the microarray data was done by our collaboration partner Javier Santoyo-Lopez, PhD, from the laboratory of Joaquin Dopazo, PhD, at Bioinformatics & Genomics Department Prince Felipe Research Centre (CIPF) in Valencia, Spain.

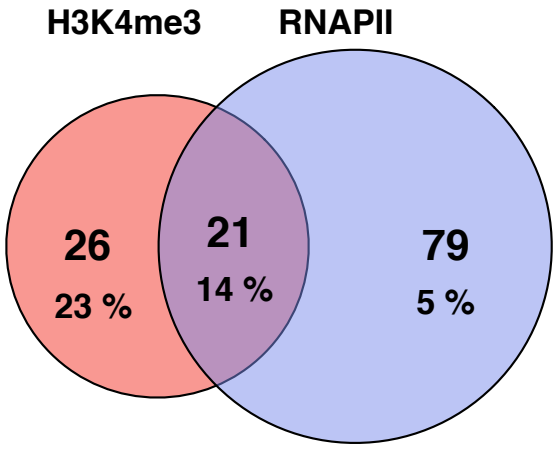

Figure 5.32: **Association of 3n low DNA with marks for active euchromatin** Graphical representation of the functional data from the ENCODE microarray. The total numbers indicate the quantity of ENCODE regions known to be associated with the H3K4me3 and **RNA P**olymerase **II** (RNAPII) that were overrepresented within the 3n low DNA compared to 3n high MNase DNA. 21 regions were found to be double positive for both active marks. The percentages indicate the fraction of those regions from which transcripts were detected.

The hybridization pattern was analyzed and significantly overpresented signal peaks were compared to other functional data from HeLa S3 cells available for the ENCODE data set. None of 3n low DNA signals peaks (6492 in total) showed a correlation with the repressive modifications H3K27me3. 47 ENCODE regions that are known to interact with the activating H3K4me3 mark and 101 associated with **RNA P**olymerase **II** (RNAPII) were over-represented within the 3n low MNase DNA sample. Almost half of H3K4me3 positive regions (21) was double positive for both active marks [Consortium et al., 2007]. Transcripts were found from 5 % of the RNAPII associated regions. Compared to this, H3K4me3 positive chromatin domains displayed a higher transcriptional activity, with 26 % for H3K4me3 solely or 21% with RNAPII in addition.

This correlation was also observed for the technical duplicate, but the total numbers were smaller. 15 regions were H3K4me3 positive, 70 RNAPII associated and 12 double positive for both marks.
Therefore a fraction of the 3n DNA fragments isolated after low MNase treatment was released out of actively transcribed regions.

6 Discussion

6.1 Comparative analysis of human ISWI homologs SNF2H and SNF2L

6.1.1 Cooperative nucleosome binding of SNF2H and SNF2L

The results presented in chapter 5 section 5.1.4 demonstrated that human ISWI remodeler are cooperative chromatin binder. This cooperativity was observed for SNF2H and SNF2L, but differences in the mechanism of binding were detectable. For all tested mononucleosomal substrates SNF2H acted as a highly cooperative binder, with Hill coefficients 2 to 3 times higher than for SNF2L (7.1 - 9.5 compared to 2.4 - 3.6). The cooperativity was independent of extranucleosomal DNA length or symmetry of the substrate. These data indicated that binding of the first remodeler molecule was relatively weak, but increased the affinity for the next molecule, thus triggering the binding of further enzyme. Cooperativity of SNF2L significantly increased and Hill coefficients became similar to those of SNF2H (6.0 ± 0.8 or 6.8 ± 2.3) when poly-nucleosomes were used as binding partner. Obviously if interacting with mono-nucleosomes, SNF2L was binding less cooperative. The interaction to more than one single nucleosome in *cis* seemed to be crucial for cooperative binding.

If these changes in the affinity were mediated by direct protein-protein contacts between two ISWI remodeler, or a consequence of conformational changes in the nucleosome, induced upon binding of the first enzyme molecule remained unclear. Analysis of the protein-protein-interaction of SNF2H or SNF2L respectively revealed, that under native conditions, in absence of DNA or nucleosomes, both homologs intrinsically form di- and tetramers. Based on the results in chapter 5 section 5.1.6, almost all SNF2H and SNF2L molecules are present as oligomers, since no monomeric protein was detectable. For ISWI class remodeler it had been proposed, that the enzymatically active units are formed by protein dimers [Strohner et al., 2005; Racki and Narlikar, 2008], but conclusive experimental evidence for this idea was missing yet.

This strong tendency for protein-protein interaction could indicate, that binding to a nucleosome is further impairing these protein-protein-interactions.

But still, conformational changes at the nucleosome can not be ruled out as the driving force of cooperativity.
In contrast to these findings, binding to DNA was only weakly cooperative and both enzymes showed a Hill coefficient of n = 1.72. DNA binding was known to be mediated by the positively charged SLIDE domain [Grüne et al., 2003]. Obviously these interactions alone were not sufficient to allow binding of multiple active remodeler units. For recruitment of further enzyme molecules, facilitating cooperative binding, the interaction to core histones obviously is crucial.
Recently also another group found evidence for cooperative nucleosome binding by hSNF2H [Racki et al., 2009]. The apparent binding constant reported there, using Cy3 labelled mono-nucleosomes with one asymmetric 40 bp linker DNA, was $K_{1/2} = 633 \pm 48$ nM. This result is comparable to $K_{1/2} = 306 \pm 6$ nM for the corresponding experiment shown here in section 5.1.4 figure 5.8 with 6-NPS1-47 nucleosomes. Strikingly, the cooperativity observed was relatively weak with $n = 1.8 \pm 0.12$ compared to $n = 7.3 \pm 1.2$ in the experiment presented here. This deviation could be caused by differences in the experimental approaches. Those published data were based on the increase of fluorescence upon binding of SNF2H to the labelled nucleosome. Thus binding of SNF2H was only detected, if the fluorophor was also interacting. Since only the short linker of the nucleosmal DNA was Cy3 labelled, possibly the binding data based on this approach showed a selectivity for binding events at certain sites of the nucleosome. The band shift experiments in section 5.1.4 detect nucleosome binding in general, limited only by the substrate-enzyme-complex stability. As a consequence no discrimination or overrepresentation of binding events at specific sites occurred. The low values for the cooperativity could implicate that with the used system, only certain cooperative binding steps are detected, which are not reflecting the complete process leading to full nucleosome binding seen in band shift experiments.

6.1.2 Affinity of human ISWI remodeler to chromatin

SNF2H and SNF2L differed qualitatively in the way they bound to nucleosomes and quantitatively in the affinity to these substrates. For all tested substrates, mono-nucleosomes and poly-nucleosomes, SNF2L showed a higher affinity to chromatin, as reflected by the relatively smaller values for $K_{1/2}$ compared to SNF2H.
The competitive binding experiments further revealed that the affinity of SNF2H to nucleosomes is enhanced with increasing linker DNA. In comparison SNF2L was binding independent of DNA linker length. When analyzing binding of SNF2H and SNF2L to mono-nucleosomes in competition with free DNA, the DNA was preferentially bound. For the yeast ISWI family member ISW2 it was published, that a 20 bp long extranucleosomal DNA is essential for stable binding [Kagalwala, 2004]. The data shown here indicate that this was also the case for human ISWI remodeler. Binding of these remodeler to nucleosomes is mainly stabilized by interaction to the free linker DNA, since nucleosomal core particle, lacking any linker DNA, hardly form stable complexes [He et al., 2008].
These differences in the nucleosome affinity were also observed in presence of ATP. As shown in chapter 5 section 5.1.9, under non binding conditions both enzymes exhibited differences in the dissociation rate k_{off} for the enzyme-substrate-complex. Upon dilution k_{off} rate for SNF2H was higher than for SNF2L, indicating less stable interaction with the remodeled nucleosome, facilitating a faster remodeling of the substrate molecules.
For those mono-nucleosomes with symmetric DNA linker, SNF2L also showed a qualitatively different binding. Opposite to its paralog, SNF2L formed well defined stable substrate-enzyme complexes, detectable as sharp bands in the band shift assays (chapter 5 section 5.1.5). SNF2H formed complexes with the nucleosomes that were inaccessible to native gels. The specific binding was independent of linker length, but the effect was lost, if asymmetric nucleosomes were used. Interaction with both linker DNA at the nucleosomal entry/exit site is probably a prerequisite for coordinated binding. In general binding to nucleosomes with one linker was still possible, but further recruited remodeler molecules were not properly aligning to the first one, thus binding not orientated (see figure 6.1). These observed qualitative differences were independent of the exact protein concentration, thus unbiased by potential variations in the exact protein amounts used.

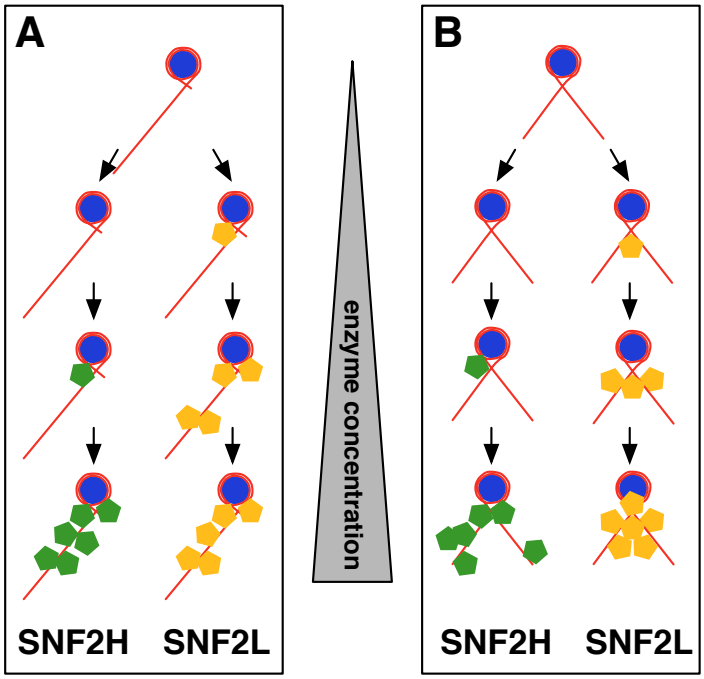

Figure 6.1: **Binding model of SNF2H and SNF2L to symmetric and asymmetric mono-nucleosomes**

(A) Binding to asymmetric mono-nucleosomes with only one long DNA linker led to formation of the same complexes of nucleosomes (blue and red) and SNF2H (green) or SNF2L (orange). The affinity of SNF2H to nucleosomes was weaker.

(B) In Presence of two symmetric linker DNA at the nucleosomal entry and exit site allowed defined alignment of SNF2L to the nucleosomes. Binding of the first SNF2L complex to linker DNA at the entry/exit site facilitated further steps of coordinated binding of other SNF2L molecules.

6.1.3 Nucleosome remodeling catalyzed by SNF2H and SNF2L

Further functional differences of both remodeling enzymes were observed, when comparing catalytic activity. Remodeling assays performed with nucleosomes assembled on promoter sequences from the rDNA and the *hsp70* gene displays nucleosome-positioning patterns specific for SNF2H and SNF2L (section 5.1.7). For hSNF2H and its ortholog from *Drosophila*, ISWI, it was known, that both remodeler interpret sequence/structure information specifically and establish different nucleosome-positioning patterns on the *hsp70* gene fragment [Rippe et al., 2007]. This functional specialization observed for orthologous remodeler was also seen for the two human ISWI paralogs.
The interpretation of the artificial nucleosome positioning sequences was comparable. Both enzymes identified the same signals targeting the nucleosomes to similar regions of these artificial DNA sequences.
But they clearly differed in the minimal linker length sufficient for nucleosome sliding. SNF2H required linker DNA longer than 20 bp [He et al., 2006b], like ISWI remodeler from yeast [Zofall et al., 2004]. Below this minimal linker length SNF2H kinetically discriminates remodeling of those nucleosomes. It is proposed that by this mechanism SNF2H acts as a length sensor in chromatin remodeling [Yang et al., 2006]. Here this length dependent activity was not observed for SNF2L, which was able to translocate even nucleosomes with no linker DNA. The histone octamer was pushed over the end of the NPS1 sequence, generating a short stretch of extranucleosomal DNA accessible for nuclease digestion (see section 5.1.8).
These differences in the minimal linker DNA length also influenced the directionality of the remodeling reaction. Higher remodeling rates at longer nucleosomal linker guide the movement of the histone octamer into direction of the longer linker, leading to a more central positioned nucleosome (see also figure 5.12). If after repositioning, the linker was shorter than the minimal length, a sliding back in the reverse direction was kinetically disfavoured. On DNA fragments with a linker DNA much longer than the needed minimum, different translational positions at the centre could be established, since only movement directly to the edge of the sequence was discriminated. For some artificial 601 based constructs these distinct remodeling intermediates were detected [Yang et al., 2006] (figure 6.2 A).

Performing a remodeling reaction with the NPS1 based chromatin (section 5.1.7) resulted in a terminal positioning of the nucleosomes. In this case, the sequence specific positioning was even more dominant than the activity as spacing factor. Usage of NPS1 DNA flanked by natural promoter sequences could explain the different observations (figure

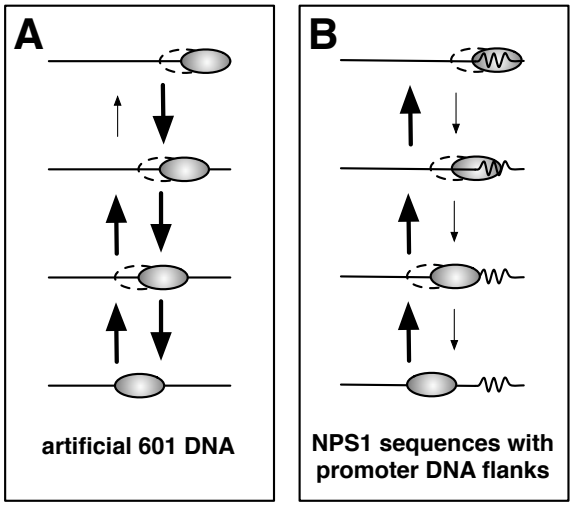

Figure 6.2: **Sequence dependent remodeling activity of SNF2H and SNF2L**
(A) Remodeling activity of SNF2H on artificial 601 nucleosomes with long linker DNA as described [Yang et al., 2006]. DNA ruler activity leads to several remodeling intermediates, if linker length is longer than the critical minimum. Thus direct terminal positioning is disfavoured by reduced remodeling rates for this reaction (arrow size indicates activity rate).
(B) In presence of natural DNA motives with specific sequence/structure information in the linker region (curved line), like the promoter sequences in the NPS1 linker, nucleosome positioning by the ISWI remodeling gets specifically directed, also to terminal positions.

6.2). While also sequence specific interpretation of the promoter DNA in the linker was possible for the NPS1 constructs, this was not the case for the 601 DNA. Experiments performed with 601 DNA focus on sequence independent activity driven by spatial constraints. In combination with natural positioning sequences the DNA specific positioning proved that beside spatial constraints regarding the linker length also sequence/structure information were interpreted by the remodeler anchoring the nucleosomes at specific positions.

6.1.4 ATPase activity of SNF2H and SNF2L

Strikingly the ATPase activity was not correlating with the observed remodeling activity. Although for SNF2H no remodeling of the linker-less nucleosomes was detectable the enzyme was hydrolyzing ATP at relative high rates (section 5.1.11). For all tested nucleosomal substrates SNF2H showed comparable ATPase rates, independent of linker length, also for poly-nucleosomes. Thus the catalytic activity of the helicase domains was stimulated in presence of any nucleosomal co-substrate and not regulated in feed-

back with effective nucleosome sliding. The opposite was the case for SNF2L, where the ATPase activity level nicely reflected the nucleosomal linker length. Core nucleosomes lacking any linker stimulated ATPase activity only to half of the level compared to long linker DNA. This corresponded well to the remodeling activity, since core nucleosomes were less efficient remodeled than those with long extranucleosomal DNA (section 5.1.7). In combination with the binding data, which showed that SNF2L does not discriminate between substrates of different linker DNA length in terms of binding and remodeling, both isoforms are able to act differentially on substrates of variant structures. As shown schematically in figure 6.3 both enzymes form regularly spaced chromatin, but their specificity is regulated at different levels. While for SNF2H affinity to nucleosomes is dependent on linker length, preferring more open structures, it is impossible for SNF2L to distinguish the nucleosomal substrate at this step. For SNF2L the nucleosome translocation in the subsequent catalytic step is controlled by regulating the ATPase activity dependent on the linker DNA. Since SNF2L is more active in presence of longer linker DNA, the nucleosome movement is directed into the same direction like in the case for SNF2H. In summary, both enzymes lead to formation of regularly spaced nucleosomal arrays, at least *in vitro*. This complementary regulation allows integration of further regulatory input at specific reaction steps possibly relevant for the more complex situation *in vivo*.

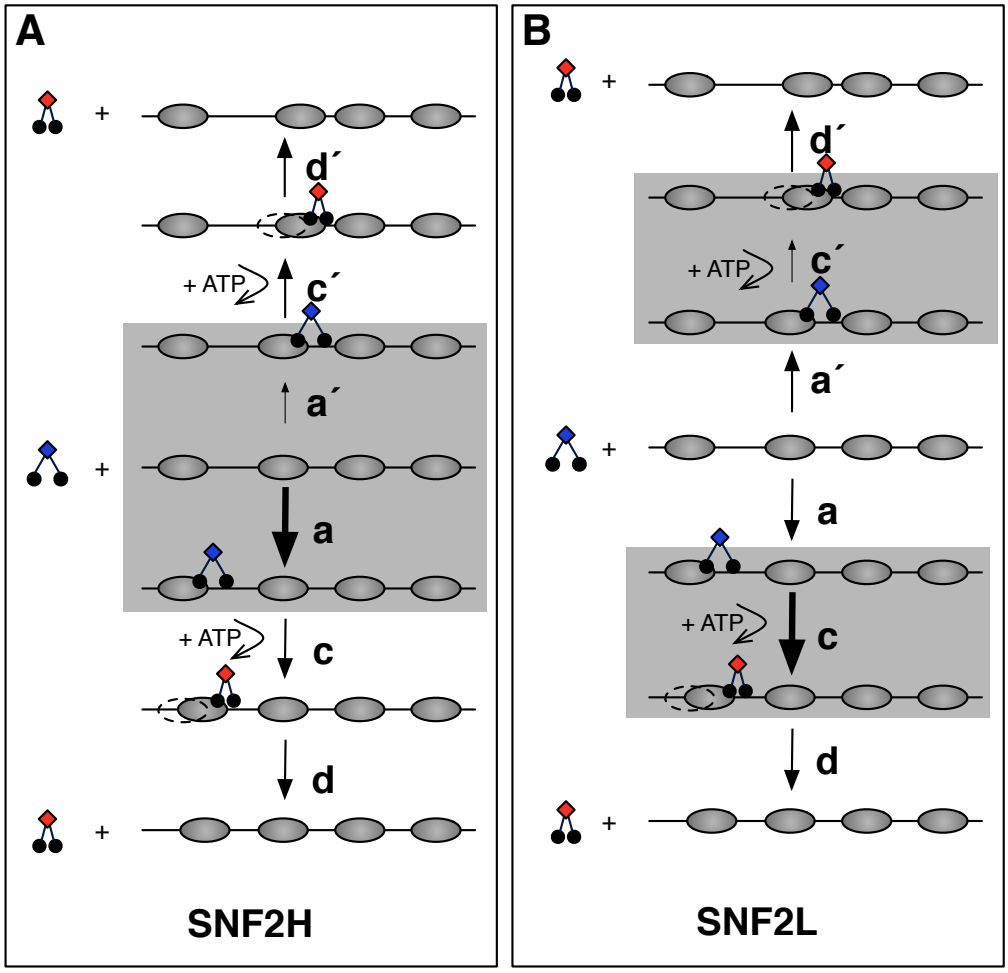

Figure 6.3: **Activity regulation model for SNF2H and SNF2L**
(A) On irregular spaced chromatin, nucleosomes with different linker length compete for remodeler binding. SNF2H (blue) binds to nucleosomes with longer linker DNA with a higher affinity, association rate a $\gg$ a'. In an ATP-dependent reaction, the remodeler catalyzes a conformational change (red) leading to a movement of the nucleosome along the DNA. This ATP consuming reaction is independent of extranucleosomal DNA c = c'. In a last step the enzyme dissociates from the reaction end product d = d'. The association step driving the equilibrium towards the specific regular spaced product is highlighted in grey.
(B) Binding of SNF2L (blue) is independent of the length of the linker DNA. Association rates are the same for short and long linker DNA a = a'. The ATP-dependent catalysis step kinetically controls the position of the reaction equilibrium (highlighted in grey). The longer the extranucleosomal DNA is, the more efficient the nucleosome is remodeled c $\gg$ c'. In a last step the reaction end product is released by the enzyme d = d' according to the release model [Rippe et al., 2007].

6.1.5 Biological relevance and further perspectives

In mouse 3T3 cells GFP- and RFP-tagged SNF2H displayed a clear nuclear localization. At pericentric heterochromatin foci increased remodeler density was detecable (see section 5.1.12). Such localization at heterochromatic regions was also known for the SNF2H containing remodeling complex WSTF [Bozhenok et al., 2002]. In contrast to this, SNF2L did not display such distinct nuclear pattern. This could be a consequence of recruitment into different remodeling complexes, like the SNF2H specific WSTF complex, or specific binding to distinct chromatin domains.
Nevertheless the observed differences in nuclear distribution further support the biological relevance of the elucidated functional differences presented in this work. The conditions used for the molecular *in vitro* experiments reflected physiologic conditions regarding concentration of ATP [Beis and Newsholme, 1975], ionic strength, temperature and also amount of remodeling enzyme. Recent studies in human U2OS cells revealed cellular concentrations in the higher nano molar range for SNF2H and the catalytically inactive splice variant SNF2L+13 [Erdel et al., 2010 in submission].
Cooperative binding to DNA is known for transcription factors (e. g. ETS1 and RUNX1) and suggested to be an important mechanism for transcriptional synergy and the specific occupancy of these DNA interacting factors [Goetz et al., 2000; Hollenhorst et al., 2009; He et al., 2009]. The cooperative binding of ISWI remodeler to nucleosomes presented here indicates, that at least certain remodeling enzymes use comparable regulative mechanisms. Due to the function as chromatin dependent enzymes, this effect is predominantly seen for the interaction with nucleosomes and hardly with free DNA. In combination with further activation signals, such cooperative binding could facilitate the rapid structural change at specific sites within a genome in response to external stimuli.
Comparison of the human ISWI remodeler further revealed that both differ on several functional levels. Since the catalytic and the substrate binding domains are highly conserved, the very divergent N-terminal domain could play a role in these processes. An unknown function as protein-protein-interaction domain or as a substrate binding motif could be suggested. To elucidate the detailed molecular basis of the revealed functional differences, experiments with deletion mutants and chimeric proteins with a swapped domain structure would be of interest. Whether the observed functional differences reflect a selective binding to distinct nucleosomal substrates could be further addressed *in vivo*. As a first test SNF2H and SNF2L could be tagged and over-expressed in human cells. A chromatin immunoprecipitation using the protein tag and subsequent hybridization of the crosslinked DNA to microarrays (ChIP-Chip), or sequencing of the DNA fragments (Chip-Seq) should gain deeper insights into the substrate specificity of both paralogs.

6.2 Structural and functional analysis of human chromatin

6.2.1 Isolation of chromatin fragments by differential MNase digestion

Based on the differential digestion of chromatin and subsequent gel purification of the specific fragments, quantitative amounts of highly pure DNA could be isolated. As demonstrated in section 5.2.1 (figure 5.20), using optimized amounts of nuclease of mono-, di- and tri-nucleosomal DNA fragments could be isolated. The size of the DNA fragments reflected the average length of 47 bp for nucleosomal linker DNA in HeLa cell chromatin [Lohr et al., 1977].
Under low MNase conditions, also sub-nucleosomal DNA was quantitatively isolated. Due to the limited size of the fragments, labelling of the samples failed. However, an efficient method for isolation of these fragments is established now. Therefore, further efforts should answer the question of the detailed structure of the DNA and whether it corresponds to non-canonical nucleosomes. The observed fragment size of 100 bp and 75 bp corresponds to the length of DNA that is wrapped around hexamers, that bind 50 bp less DNA than canonical nucleosomes [Hutcheon et al., 1980; Zlatanova et al., 2009]. Tetrasomes are even smaller, DNA is wrapped in only one helical turn around the tetramer core [Levchenko et al., 2005; Zlatanova et al., 2009]. Thus non-canonical nuclesomes could be one reason for the reduced size of DNA fragments compared to the 147 bp mono-nucleosome. A method of choice to analyze the sequence information of those fragments would be next generation sequencing. The Illumina/Solexa platform would allow parallel sequencing of millions of DNA molecules. Since in general DNA fragments shorter than 800 bp are used, for this application the limited length of the sub-nucleosomal DNA could complicate the analysis here, too.

6.2.2 Local and global distribution of purified chromatin fragments within the human genome

The specific hybridization of 3n low MNase digested fragments to human chromatin in 2D and 3D proved the feasibility of this analytical approach. Despite the presence of repetitive DNA elements in both tri-nucleosomal fractions, a specific localization of signals was detectable for both groups upon suppression of those repeating sequences. The 2D FISH experiments with metaphase chromosomes revealed that the highly digested 3n samples displayed clear centromeric signals associated with constitutive heterochromatin, whereas those regions hardly showed 3n low MNase staining. However, in the three-dimensional distribution the low MNase samples hybridized to regions of weak DNA density, thus to

non-heterochromatic regions, whereas 3n high MNase co-localized with DAPI staining in most areas. These data indicate that limited amounts of MNase preferentially digest very open chromatin regions, as was already shown for larger chromatin fragments with MNase and DNaseI [Gilbert et al., 2004; Consortium et al., 2007].

6.2.3 Distribution of 3n nucleosomal DNA and repetitive elements within fragmented HeLa chromatin

If repetitive signals were not suppressed, FISH and southern blotting experiments with 3n DNA proved that a fraction of both DNA samples was released from repetitive genomic regions. Approximately 40% of the human genome are composed of repetitive transposable DNA elements [Lander et al., 2001; Biémont and Vieira, 2006]. The southern blot experiments with probes specific for centromeres and telomeres displayed no enrichment of DNA from those regions in differentially digested chromatin samples. With respect to the resolution obtained by the applied method, no differences in the accessibility of these heterochromatic domains were observed. The digestion rate of Alu repeats was also comparable to the fragmentation rate of total DNA. As they are highly abundant and distributed throughout the genome, their distribution reflected overall chromatin fragmentation. Furthermore the relative methylation level of the nucleosomal fragments showed comparable CpG dinucleotide modifications for both conditions. This result fits to observations made for repetitive DNA sequences, since high methylation levels are known for constitutive heterochromatin formed by those abundant DNA elements, e. g., at centromeres and telomeres [Smit, 1999; Yoder et al., 1997a]. This overall methylation level does not exclude subtle differences in the CpG methylation at functionally important DNA motives, like promoters, that would have a great impact on the activity of specific genes. In summary, the low resolution analysis of the overall distribution of repetitive DNA elements and the relative methylation level indicated that DNA fragments from heterochromatic regions were not enriched in the high MNase treated samples.
Differences in the methylation levels of nucleosmal DNA correlated with the linker length. It was shown that methylation of DNA by *de novo* and maintenance DNA methyltransferases (DNMT1 and DNMT3a) significantly decreases when DNA is bound by a histone octamer [Robertson et al., 2004]. Therefore DNMTs are also restricted in their access to DNA by nucleosomes. The results presented here indicate that also *in vivo* methylation of non-nucleosomal linker DNA shows much higher methylation levels, whereas core nucleosmal DNA stretches are much less modified. As an initial result, the isolation of nucleosomal sequences with different linker DNA sizes resembles a promising approach to further study the methylation level and regulation of these accessible regions *in vivo*.

6.2.4 Transcriptional activity of the open chromatin fraction

The comparative hybridization to the ENCODE microarray gave further evidence for the enrichment of open and active euchromatin regions within low MNase treated chromatin fragments.
Because the ENCODE DNA is complementary to 1 % of the human genome, only a fraction of all 25,000 genes active within a human cell can be detected. Therefore those active regions detected by this approach resembled only a small representative population of all active genomic elements. ENCODE regions over-represented in the 3n low MNase samples were associated with marks of active chromatin, H3K4me3 and RNAPII in this case. Almost 50 % of all active marks were found at the same regions. Furthermore comparison to expression arrays showed that a significant fraction of these genomic segments is not only in a conformation facilitating transcription, but for 14.3 % of those elements active transcription is shown.
In combination with the 3D-localization of these DNA fragments, these results underline that open chromatin regions can be released specifically by limiting amounts of MNase. This nuclease sensitivity does not only reflect structural arrangements of chromatin within the nucleus, but also the transcriptional activity can be displayed by this approach.

6.2.5 Further perspectives

The initial analysis presented here shows that differential digestion of chromatin *in vivo* is a feasible approach to investigate chromatin structure and the functional status of the released genomic regions.
Based on the established protocol, a more detailed characterization of the chromatin structure can be done. To overcome the limitation of the DNA microarray, next generation sequencing would be an interesting approach to further push the project. Based on the Solexa technology all sequences present in the 3n low MNase sample will be revealed within a few sequencing reactions, instead of being limited to 1 % of the total genome.
Furthermore besides characterization of the HeLa chromatin structure in general, also questions regarding structural dynamics can be addressed. Therefore manipulation of nuclear chromatin remodeling machinery and the structural consequences of this can be analysed. Depletion of endogenous SNF2H by RNAi or overexpression of ectopic remodeling enzyme are possible initial experimental steps. Subsequent isolation of open chromatin regions and hybridization to DNA microarrays or Solexa sequencing should elucidate the structural and functional consequences of those manipulations.

7 Appendix

7.1 *Curriculum Vitae*

Name:	Exler
First name:	Josef H.
Nationality:	German
Date of birth:	03.03.1981
Place of birth:	Ibbenbüren, Germany

Education:

01/01/2007 – present	PhD student at the Institute of Biochemistry III, University of Regensburg; Prof. Dr. H. Tschochner, Supervisor Prof. Dr. G. Längst "Nuclear architecture and structural dynamics -molecular basis of chromatin remodeling induced by human ISWI machines-"
since 04/2009	PhD student representative of the Regensburg International Graduate School of Life Science for the Cellular Biochemistry and Biophysics section
11/2007 – 10/2009	PhD fellowship of the Elitenetzwerk Bayern
01/2007 – 07/2010	PhD fellowship of e-fellows.net
03/2006 – 08/2006	Master‘s Thesis at the Institute of Biotechnology, Technical University of Munich; Prof. Dr. J. Buchner, Supervisor Prof. Dr. T. Scheibel "Analysis of the polymeric character of recombinant spider silk proteins and their phase separation behavior during the spinning process"
10/2004 – 08/2006	Graduate student in Biochemistry, Technical University of Munich
04/2004 – 06/2004	Bachelor‘s Thesis at Institute for Genetics, Technical University of Munich; Prof. Dr. A. Gierl, Supervisor Dr. Ulrich Genschel "Biosynthesis of phospho pantothate acid in *Escherichia coli* and *Methanosarcina mazei*"
10/2004 – 08/2006	Undergraduate student in Biochemistry, Technical University of Munich
06/2000	High-school diploma (Abitur), Gymnasium Bad Nenndorf

Internships:

04/2005 – 06/2005	Harvard University Boston, Harvard Medical School, Laboratory of Markus Frank, MD, ABCB5 as a multidrug resistance transporter
08/2004 – 09/2004	Hannover Medical School (Medizinische Hochschule Hannover), Institute for Clinical Biochemistry, Laboratory of Prof. Dr. S. Lenzen

7.2 List of publications

Exler, J. H., Kügel, W., Erdel, F., Fuchs, A., Rippe, K., Michaelis, J. and Längst, G. (2010). SNF2H and SNF2L are highly cooperative nucleosome binders with distinct molecular properties. in preparation.

Felle, M., Fuchs, A., Exler, J. H. and Längst, G. (2010) Nucleosomes protect DNA from DNA methylation in vivo and in vitro. in preparation.

Felle, M.*, Exler, J. H.*, Merkl, R., Dachauer, K., Brehm, A., Grummt, I. and Längst, G. (2010). DNA sequence encoded repression of rRNA gene transcription in chromatin. Nucleic Acids Res., published online and in press.

Exler, J. H., Hümmerich, D. and Scheibel, T. (2007). 46(19):3559-62. Spider silk‘s amphiphilic properties are important for spinning. Angew. Chem. Int.

(*) these authors contributed equally to this work

7.3 Conferences

April 1st - 5th 2009 Poster presentation at the 3rd Marie Curie - Genome Architecture in Relation to Disease (MC-GARD) conference on higher order of genome architecture in Edinburgh, Scotland
Exler, J. H, Felle, M., Merkl R., Dachauer K., Brehm A., Grummt and Längst, G.
A nucleosomal switch regulates the activity of rRNA genes.

September 22th - 23th 2008 Talk at the 4th Symposium of the Regensburger Zentrum für Biochemie und Biophysik (RZBB) in Kostenz, Germany
Chromatin Remodeling: Molecular basis of chromatin fluidity catalyzed by remodeling complexes

7.4 Supplementary Methods

7.4.1 Purification of histone octamers form chicken red blood erythrocytes

Core histone octamers were purified from chicken red blood erythrocytes following the protocol described here. This work was done in the laboratory by our technical assistance Regina Gröbner-Ferreira.
50 ml blood from adult chicken was centrifuged for 4 min at 3000 rpm in benchtop centrifuge in 50 ml corning tubes. After centrifugation the layer of lipids and the supernatant was removed and red blood cells were resuspended in wash buffer (140 mM NaCl, 15 mM sodium citrate, 10 mM Tris pH 7.5 and 0.25 mM PMSF). Washing steps were repeated twice and erythrocytes were resuspended in 10 ml ice cold Buffer A + 0.5 % NP40 (340 mM sucrose, 60 mM KCl, 15 mM NaCl, 15 mM Tris 7.5, 15 mM BME, 0.5 mM spermidine, 0.15 mM spermine, 0.25 mM PMSF). Solution was immediately filtered through 8 layers of Miracloth into a 50 ml conical tube and nuclei were centrifuged for 5 min, at $4°C$ at 3200 rpm in benchtop centrifuge. Supernatant was removed and nuclei pellet was washed in Buffer A (without NP-40). Washing was repeated until nuclei were white. The four core histones were purified from nuclei by binding chromatin fragments to hydroxyl apatite resin, washing away histone H1 with 0.6 M NaCl, and eluting the histones from the resin-bound DNA at 2.5 M NaCl [Workman et al., 1991]. Nuclear pellet containing 6 mg DNA was resuspended in 25 ml HAP buffer (50 mM sodium phosphate pH 6.8, 0.48 M NaCl, 1 mM 2-mercaptoethanol and 0.5 mM PMSF, 1µM pepstatin A, 1µM leupeptin) and gently stirred for 10 min at $4°C$. DNA was sonified using Brandson Sonifier (Output Control 5, Cycle 40 %) until solution was completely soluable. While stirring 10 g hydroxyl apatite and 50 ml HAP buffer were added and suspension was centrifuged for 5 min at 4500 rpm and $4°C$. Resin was washed 3x with 80 ml HAP, 5x with 80 ml HAP 0.7 M NaCl and 5x eluted with 15 ml HAP 2.5 M NaCl. Protein concentration of fractions was determined by measuring the absorbance at 230 nm. The extinction coefficient was calculated to be 4.3 A_{230} units/mg histones/ml. Histones were concentrated to 2 to 10 mg/ml by dialysis in a 6 - 8 kD MWCO membrane tube against solid PEG 8000; protease inhibitors were added freshly. Glycerol was added to a final concentration of 50 %. The salt concentration was about 1 M and long term storage was done at - $80°C$ (up to several years). Finally the purity of the core histones was analyzed by SDS-PAGE (17 %).

7.4.2 Analysis of remodeling kinetics by measurement of FRET burst

The dynamic binding studies based on FRET were done in collaboration with the group of Prof. Dr. Jens Michaelis at the Department of Chemistry and Biochemistry at the Ludwig-Maximilians-University Munich.

7.4.2.1 Synthesis of atto532 and atto647 double fluorescently labelled nucleosomal DNA by ligase chain reaction

Design and synthesis of atto532/647 fluorescently labelled NPS1 nucleosomal DNA was done by Barbara Treutlein from the group of Prof. Dr. Jens Michaelis. Labelled and unlabelled oligos for DNA syntheses were purchased via IBA BioTAGnology (Göttingen). The synthesis of 200 bp DNA from 10 oligonucleotides was based on the Ligase Chain Reaction (LCR) [Barany, 1991] using Taq DNA Ligase (New England Biolabs). 200 nM of each oligonucleotide were mixed with 20 µl enzymes in a total volume of 500 µl of 1x Taq ligase buffer. The LCR was carried out in a MJ Research PTC-100 thermal cycler. Detailed description of the protocol established by Barbara Treutlein depicted below.

Table 7.2: **LCR protocol for ligation of 6-NPS1-47 FRET construct**

Step	**Time**	**Temperature**	
initial denaturation	2 min	94°C	
ligation	6 min	65°C	35x
denaturation	30 s	94°C	
final denaturation	10 min	94°C	
final annealing	cooling 1°C / 5 min		

In a final step, the raw DNA product was denatured at 94°C for 10 minutes and then allowed to reconstitute during a slow annealing process of a decrease by 1°C every 5 minutes. The crude DNA product was purified by Anion Exchange Chromatography using a MonoQ 5/50 GL column (Amersham Bioscience, Freiburg) (0.5 ml/min; Buffer A: 20 mM Tris/HCl pH 8.0, Buffer B: 1 M NaCl, 20 mM Tris/HCl pH 8.0; gradient: 40 % - 100 % Buffer B in 15 CV) followed by Size Exclusion Chromatography using a Superose 6 PC 3.2/30 column (GE Healthcare, Freiburg,) (SEC Buffer: 100 mM NaCl, 20 mM Tris/HCl, 1 mM EDTA, pH 8.0). Peak fractions containing target DNA were pooled and concentrated to approximately 50 µl using MICROCON centrifugal filter devices YM-30 (Millipore, Billerica, USA).

7.4.2.2 FRET burst analysis

FRET burst experiments and raw data analysis were done by Wolfgang Kügel from the group of Prof. Dr. Jens Michaelis. In order to gain real-time kinetic information of nucleosome remodeling by SNF2H and SNF2L we performed single-molecule measurements. Nucleosomes assembled on DNA labelled with an atto532 dye molecule at position + 14 and with an atto647N dye at position - 64 were used. Experiments were performed in absence of ATP at enzyme concentrations under which most SNF2H/L was not binding stably to the nucleosomes, to gain information about the influence of binding and unbinding on the remodeling speed. Due to the high sensitivity of this fluorescent bases approach and a 1:20 mixture of double labelled and unlabelled 0-NPS1-54 nucleosomes were used. The total concentration of nucleosomes was 28 nM and remodeler concentrations of 17, 23, 34 and 69 nM were used in a buffer containing KCl (4.55 mM), Tris (20 mM), EGTA (0.5 mM), $MgCl_2$ (1.5 mM) and 10 % glycerol. Under these conditions nucleosomes were stable for several hours (data not shown). The confocal measurements were performed using pulsed interleaved excitation (PIE) [Müller et al., 2005] of 532 nm (Pico-TA- Picoquant, power before objective 100 µW) and 640 nm (LDH-D-C-640, Picoquant, power before objective 100 µW) at a repetition rate of 26.66 MHz. Fluorescence was separated for polarization and color, detected on four avalanche-photo-diodes (green channel AQRH-14, red channel AQR-16, Perkin Elmer). Photon arrival times were recorded using four single-photon-counting-modules (Becker&Hickl SPC-150) and data were processed using custom software written in MATLAB (MathWorks). Data collection was started 30 s after the addition of 430 µM ATP and the collected photons were sorted into three different channels according to arrival time and detector. An all photons burst search (APBS) is performed on the photon streams [Nir et al., 2006]. The Stoichiometry **(S)** and FRET Efficiency **(E)** are calculated including predetermined correction factors according to:

$$\mathrm{E} = \frac{GR - de*RR - cr*GG}{GR - de*RR - cr*GG + \gamma*GG} \text{ and } \mathrm{S} = \frac{GR - de*RR - cr*GG + \gamma*GG}{GR - de*RR - cr*GG + \gamma*GG + RR}$$

Where **GR** are the red photons after green excitation, **RR** are the red photons after red excitation, **GG** are the green photons after green excitation, **de** is the percentage of direct excitation, **cr** is the percentage of crosstalk and γ is a factor correcting for the different efficiencies of the red and green detection channels [Lee et al., 2005]. Multi molecular events were removed from the data as described (see next section) using TDS < 0.45 and TDSr < 0.5. Remaining donor and acceptor only bursts were removed by a stoichiometry threshold. The two dimensional histogram of FRET efficiency versus time was calculated for each measurement and segmented into three parts. Low FRET (0 -

20 % FRET = LF), medium FRET (20 - 70 % FRET = MF) and high FRET (70 - 100 % FRET = HF). The time trace was binned into 60 second intervals and the percentage of bursts in each of the three FRET areas was calculated for each bin. A global single exponential fit with

$$\begin{gathered} \text{MF} = \text{constant}, \\ \text{LF (t)} = \text{LF}(\infty) - \text{C} * e^{-\frac{\tau}{Tl}} \\ \text{and HF (t)} = 1 - \text{MF} - \text{LF (t)} \end{gathered}$$

was performed on the resulting data using a maximum likelihood estimation algorithm. The extracted remodeling velocity v= $1/\text{T}_l$ was plotted versus the relative amount of remodeler compared to the samples with the highest remodeler concentration.

7.4.2.3 Quality control of the received FRET burst raw data

The following quality criteria and equation were developed by Wolfgang Kügel. In order to monitor nucleosome remodeling kinetics by measuring the FRET efficiency of nucleosomes diffusing through the focus of a confocal microscope, it was important to achieve a sufficient time resolution. Therefore, the number of complexes diffusing through the confocal volume had to be high and with that, the possibility that a multi molecule event occurs in the measurements was not negligible. For a homogeneous population with only a single FRET species this was not a problem, however if several FRET states exist, multi-molecule events of different species would result in false FRET values. In addition there was also the possibility that impurities such as donor and acceptor only labelled complexes could be observed at the same time as double labelled complexes thus falsifying the calculated FRET efficiencies. However, it was very unlikely that two independently diffusing complexes entered and exited the excitation volume exactly at the same time. Therefore it was possible to differentiate these multi molecular events from single molecule events and to exclude them from further analysis. This was done by calculation of the characteristic **T**ime-**D**eviation-**S**ignal (TDS):

$\text{TDS} = ((\text{D}_{total}\text{-D}_{green}) + |\text{T}_{total} - \text{T}_{green}|) * (1 - \text{P}) + ((\text{D}_{total} - \text{D}_{fret}) + |\text{T}_{total} - \text{T}_{fret}|) * \text{P} * \gamma$ (**eq. 1**)

$\mathbf{D}_x$ was the burst duration, $\mathbf{T}_x$ was the mean-macrotime (the time where 50 % of the respective photons has arrived), γ was a factor correcting for the different efficiencies of the red and green detection channels and **P** was the proximity ratio given by the number of photons in the burst as

$$P = \frac{N_{fret}}{N_{fret}+N_{green}} \textbf{ (eq. 2)}.$$

Independently diffusing molecules involved in a multi molecule event would cause a deviation of the mean-macro-time calculated for all photons of a burst and the mean-macro-time for the individual photons of one color. These burst properties were used to calculate the TDS for each burst by analyzing the differences between the values calculated from all photons and the ones calculated for individual channels to exclude an influence of the respective FRET efficiency. E . g. for a high FRET burst where only very few green photons are detected a simple green TDS calculated according to

$$TDS_g = ((D_{total}\text{-}D_{green}) + |T_{total} - T_{green}|)$$

would be very noisy due to the poor statistics and did not contain much useful information. Accordingly, for low FRET complexes a TDS calculated by

$$TDS_f = ((D_{total} - D_{fret}) + |T_{total} - T_{fret}|)$$

would be noisy due to the fact that in this case only few photons were detected in the red channel after green excitation. Therefore we computed the TDS of these two channels simultaneously and adjusted the relative value of the green versus the red TDS according to the percentage of photons detected.
Equitation (1) is generally applicable to burst analysis data and allowed detection of almost all cases of bursts containing more than one molecule at a time except multi molecule events containing low (0 %) FRET double labelled and donor only molecule mixtures. The latter species was identified using an experimental setup that employed **P**ulsed **I**nterleaved **E**xcitation (PIE) [Müller et al., 2005; Lee et al., 2005; Kapanidis et al., 2005]. With a PIE setup a second criterion using the additional information of red photons after red excitation could be defined.

$$TDS_{red} = ((D_{total} - D_{red}) + |T_{total} - T_{red}|)$$

Here, the number of photons detected in the red channel after red excitation would be independent of the FRET efficiency. To demonstrate the capabilities of this method, a sample containing 23-NPS1-67 nucleosomes as well as impurities of donor only and acceptor only complexes was measured. In order to stress the discussed effects for these test experiments the concentration of molecules was chosen to be high enough that most bursts detected showed multi-molecule characteristics (150 pM double labelled nucleosomes). Up to now data cleanup was done generally done by selecting bursts through a stoichiometry criterion [Kapanidis et al., 2004; Lee et al., 2005]. For example in the

described experiments histograms would have been calculated from bursts with stoichiometry values between 0.45 and 0.77 (figure 7.1 A) leading to a washed-out FRET efficiency histogram especially in the medium FRET area and an unnaturally sharp cut off in the stoichiometry distribution. In comparison using stringent thresholds of TDS $<$ 0.1 and $\text{TDS}_{red-PIE} < 0.1$ in the TDS parameter space we receive a clean stoichiometry distribution showing peaks of distinct FRET efficiencies (figure 7.1 B). In addition the resulting FRET histogram is almost identical with data measured at far higher dilutions. While these tests were performed at concentrations higher than normal, such that almost 95 % of all bursts are multi molecule events, they nicely visualize the capabilities of this method. Under regular conditions where only a few percent of all events are multimolecular the appropriate TDS thresholds are determined by iterative optimization of Stoichiometry/TDSx and Efficiency/TDSx plots.

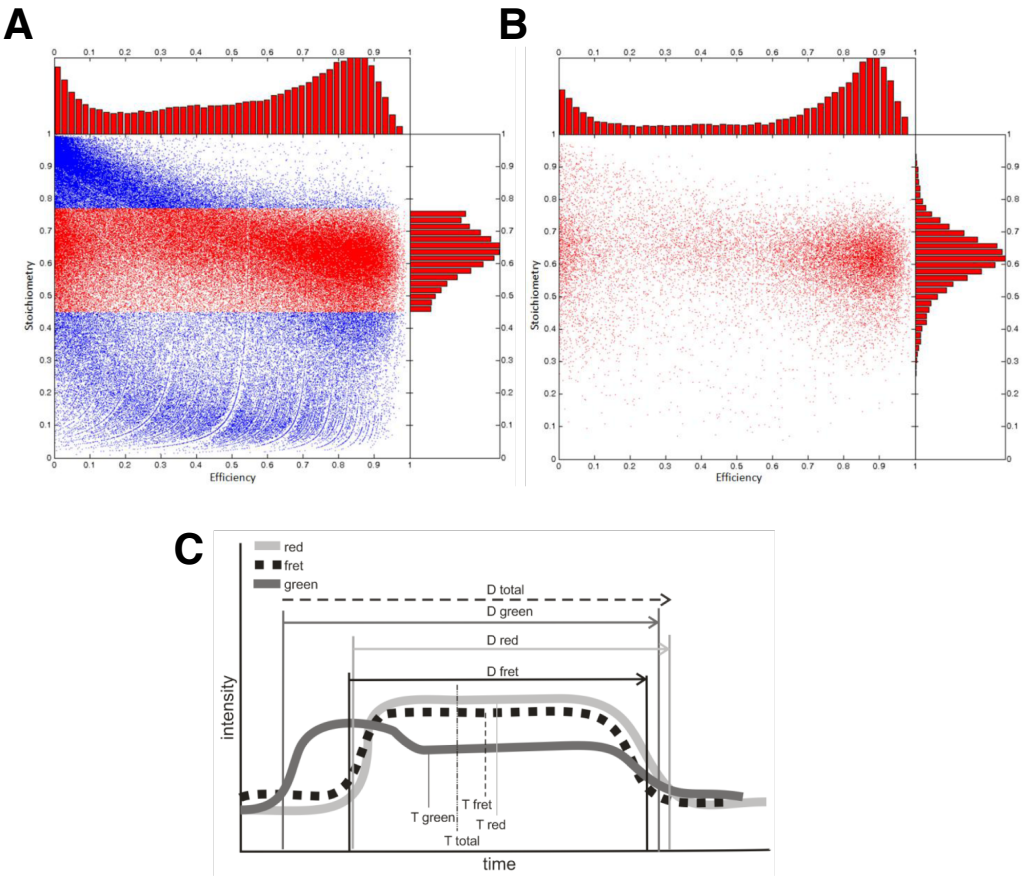

Figure 7.1: **Quality criteria for FRET burst analyses**
(A) Two dimensional plot of stoichiometry versus efficiency showing all bursts (blue) of 23-NPS1-67 nucleosomes containing donor and acceptor only impurities. Labels were positioned at the same sites used for the 0-NPS1-54 construct. Bursts within a limited stoichiometry area (S = 0.45 - 0.77) that would have previously been selected for data analysis were used for one dimensional projections of FRET efficiency (top) and stoichiometry (right) are highlighted in red.
(B) Two dimensional stoichiometry versus efficiency plot of the same dataset showing only bursts with TDS and $TDS_{red-PIE}$ smaller than 0.1.
(C) Schematic representation of the definition of duration and mean-macro-time in case of a theoretical multi molecule event containing a donor only and a double labelled high FRET species.

7.5 Sequences

7.5.1 NPS1 DNA sequence

gatcttttgaggtccggttcttttcgttatggggtcatatgtttgggccacctccccatggtatgacttccaggtatggatccagaatcctggtg
ctgaggctgctcaattggttgtagcaagctctagcactgcttaaatgcatgtacgcgcggtcccctgtgttttaactgccaaggggattactcc
ctagtctccaggcatgtgtcagatatatacagctagctagcaaagaaaactcgagaaatttctcttaaggccgttattctctagattcgttttgt
gactctccctctctgtactaa

7.5.2 N-His$_6$-SNF2H amino acid sequence

N-terminal tag and linker is printed in bold:
msyyhhhhhhdydipttenlyfqgitslykkagslkepiqstgsssaaepppppppesapskpaasiasggsnssnkggpegv
aaqavasavsagpadaemeeifddaspgkqkeiqepdptyeekmqtdranrfeyllkqtelfahfiqpaaqktptsplkmkpgrprikkde
kqnllsvgdyrhrrteqeedeelltesskatnvctrfedspsyvkwgklrdyqvrglnwlislyengingilademglgktlqtisllgymkhyr
nipgphmvlvpkstllhnwmsefkrwvptlrsvcligdkeqraafvrdvllpgewdvcvtsyemlikeksvfkkfnwrylvideahriknek
sklseivrefkttnrllltgtplqnnlhelwsllnfllpdvfnsaddfdswfdtnnclgdqklverlhmvlrpfllrrikadvekslppkkevkiyv
glskmqrewytrilmkdidilnsagkmdkmrllnilmqlrkccnhpylfdgaepgppyttdmhlvtnsgkmvvldkllpklkeqgsrvli
fsqmtrvldiledycmwrnyeycrldgqtphderqdsinaynepnstkfvfmlstragglginlatadvvilydsdwnpqvdlqamdrah
rigqtktvrvfrfitdntveeriveraemklrldsiviqqgrlvdqnlnkigkdemlqmirhgathvfaskeseitdedidgilergakktaemn
eklskmgesslrnftmdtessvynfegedyrekqkiaftewieppkrerkanyavdayfrealrvsepkapkaprppkqpnvqdfqffpprl
fellekeilfyrktigykvprnpelpnaaqaqkeeqlkideaeslndeeleekekklltqgftnwnkrdfnqfikanekwgrddieniarevegkt
peevieysavfwercnelqdiekimaqiergeariqrrisikkaldtkigrykapfhqlrisygtnkgknyteeedrflicmlhklgfdkenvyd
elrqcirnspqfrfdwflksrtamelqrrcntlitlierenmeleekekaekkkrgpkpstqkrkmdgapdgrgrkkklkl

7.5.3 N-His$_6$-SNF2L amino acid sequences

N-terminal tag and linker is printed in bold:
msyyhhhhhhdydipttenlyfqgitslykkagslkepiqstgseqdtaavaatvaaadatativviedeqpgpstsqeeg
aaaaateataatekgekkkeknvssfqlklaakapksekemdpeyeekmkadrakrfefllkqtelfahfiqpsaqksptsplnmklg
rprikkdekqslisagdyrhrrteqeedeellsesrktsnvcirfevspsyvkggplrdyqirglnwlislyengvngilademglgktlqt
iallgylkhyrnipgphmvlvpkstllhnwmnefkrwvpslrvicfvgdkdaraafirdemmpgewdvcvtsyemvikeksvfkkf
hwrylvideahriknekskslseivrefkstnrllltgtplqnnlhelwallnfllpdvfnsaddfdswfdtknclgdqklverlhavlkpfll
rriktdvekslppkkeikiylglskmqrewytkilmkdidvlnssgkmdkmrllnilmqlrkccnhpylfdgaepgppyttdehivsn
sgkmvvldkllaklkeqgsrvlifsqmtrlldiledycmwrgyeycrldgqtpheereeaieafnapnsskfifmlstragglginlasad
vvilydsdwnpqvdlqamdrahrigqkkpvrvfrlitdntveeriveraeiklrldsiviqqgrlidqqsnklakeemlqmirhgathv
faskeseltdedittilergekktaemnerlqkmgesslrnfrmdieqslykfegedyrekqklgmvewieppkrerkanyavdayfr
ealrvsepkipkaprppkqpnvqdfqffpprlfellekeilyyrktigykvprnpdipnpalaqreeqkkidgaepltpeeteekekllt
qgftnwtkrdfnqfikanekygrddidniarevegkspeevmeysavfwercnelqdiekimaqiergeariqrrisikkaldakiary

kapfhqlriqygtskgknyteeedrflicmlhkmgfdrenvyeelrqcvrnapqfrfdwfiksrtamefqrrcntlisliekenmeieer
eraekkkratktpmvkfsafs

Eidesstattliche Erklärung

Hiermit erkläre ich, Josef H. Exler, an Eides statt, dass die hier vorliegende Promotionsarbeit selbstständig verfasst und unter alleiniger Verwendung der angegebenen Hilfsmittel angefertig wurde.
Die Arbeit wurde bisher weder im In- noch im Ausland in gleicher oder ähnlicher Form einer anderen Prüfungsbehörde vorgelegt.

Regensburg, 19.05.2010

Josef H. Exler

Bibliography

Aalfs, J. D., Narlikar, G. J., and Kingston, R. E. (2001). Functional differences between the human ATP-dependent nucleosome remodeling proteins BRG1 and SNF2H. *J. Biol. Chem.*, 276(36):34270–8.

Alilat, M., Sivolob, A., Révet, B., and Prunell, A. (1999). Nucleosome dynamics. Protein and DNA contributions in the chiral transition of the tetrasome, the histone (H3-H4)2 tetramer-DNA particle. *J Mol Biol*, 291(4):815–41.

Badenhorst, P., Voas, M., Rebay, I., and Wu, C. (2002). Biological functions of the iswi chromatin remodeling complex nurf. *Genes Dev*, 16(24):3186–98.

Bannister, A. J., Schneider, R., Myers, F. A., Thorne, A. W., Crane-Robinson, C., and Kouzarides, T. (2005). Spatial distribution of di- and tri-methyl lysine 36 of histone H3 at active genes. *J Biol Chem*, 280(18):17732–6.

Banting, G. S., Barak, O., Ames, T. M., Burnham, A. C., Kardel, M. D., Cooch, N. S., Davidson, C. E., Godbout, R., McDermid, H. E., and Shiekhattar, R. (2005). CECR2, a protein involved in neurulation, forms a novel chromatin remodeling complex with SNF2L. *Hum. Mol. Genet.*, 14(4):513–24.

Bao, Y. and Shen, X. (2007). Ino80 subfamily of chromatin remodeling complexes. *Mutat Res*, 618(1-2):18–29.

Barak, O., Lazzaro, M. A., Cooch, N. S., Picketts, D. J., and Shiekhattar, R. (2004). A tissue-specific, naturally occurring human SNF2L variant inactivates chromatin remodeling. *J. Biol. Chem.*, 279(43):45130–8.

Barak, O., Lazzaro, M. A., Lane, W. S., Speicher, D. W., Picketts, D. J., and Shiekhattar, R. (2003). Isolation of human NURF: a regulator of Engrailed gene expression. *EMBO J.*, 22(22):6089–100.

Barany, F. (1991). The ligase chain reaction in a PCR world. *PCR Methods Appl*, 1(1):5–16.

Batzer, M. A. and Deininger, P. L. (2002). Alu repeats and human genomic diversity. *Nat. Rev. Genet.*, 3(5):370–9.

Beis, I. and Newsholme, E. A. (1975). The contents of adenine nucleotides, phosphagens and some glycolytic intermediates in resting muscles from vertebrates and invertebrates. *Biochem J*, 152(1):23–32.

Belz, T., Pham, A.-D., Beisel, C., Anders, N., Bogin, J., Kwozynski, S., and Sauer, F. (2002). In vitro assays to study protein ubiquitination in transcription. *Methods*, 26(3):233–44.

Berger, I., Fitzgerald, D. J., and Richmond, T. J. (2004). Baculovirus expression system for heterologous multiprotein complexes. *Nat Biotechnol*, 22(12):1583–7.

Bernstein, B. E., Kamal, M., Lindblad-Toh, K., Bekiranov, S., Bailey, D. K., Huebert, D. J., McMahon, S., Karlsson, E. K., Kulbokas, 3rd, E. J., Gingeras, T. R., Schreiber, S. L., and Lander, E. S. (2005). Genomic maps and comparative analysis of histone modifications in human and mouse. *Cell*, 120(2):169–81.

Bertani, G. (1951). Studies on lysogenesis. I. The mode of phage liberation by lysogenic Escherichia coli. *J Bacteriol*, 62(3):293–300.

Biémont, C. and Vieira, C. (2006). Genetics: junk DNA as an evolutionary force. *Nature*, 443(7111):521–4.

Black, B. E., Jansen, L. E. T., Maddox, P. S., Foltz, D. R., Desai, A. B., Shah, J. V., and Cleveland, D. W. (2007). Centromere identity maintained by nucleosomes assembled with histone H3 containing the CENP-A targeting domain. *Mol Cell*, 25(2):309–22.

Blasco, M. A. (2007). The epigenetic regulation of mammalian telomeres. *Nat Rev Genet*, 8(4):299–309.

Blum, H., Beier, H., and Gross, H. J. (1987). Improved silver staining of plant proteins, rna and dna in polyacrylamide gels. *ELECTROPHORESIS*, 8(2):93 – 99.

Boveri, T. (1909). Die Blastomerenkerne von Ascaris megalocephala und die Theorie der Chromosomenindividualität. *Arch Zellforsch*, 3:181–268.

Boyer, L. A., Langer, M. R., Crowley, K. A., Tan, S., Denu, J. M., and Peterson, C. L. (2002). Essential role for the sant domain in the functioning of multiple chromatin remodeling enzymes. *Mol Cell*, 10(4):935–42.

Boyer, L. A., Latek, R. R., and Peterson, C. L. (2004). The sant domain: a unique histone-tail-binding module? *Nat Rev Mol Cell Biol*, 5(2):158–63.

Bozhenok, L., Wade, P. A., and Varga-Weisz, P. (2002). WSTF-ISWI chromatin remodeling complex targets heterochromatic replication foci. *EMBO J.*, 21(9):2231–41.

Bradford, M. M. (1976). A rapid and sensitive method for the quantitation of microgram quantities of protein utilizing the principle of protein-dye binding. *Anal Biochem*, 72:248–54.

Brand, P., Lenser, T., and Hemmerich, P. (2010). Assembly dynamics of PML nuclear bodies in living cells. *PMC Biophys*, 3(1):3.

Brehm, A., Tufteland, K. R., Aasland, R., and Becker, P. B. (2004). The many colours of chromodomains. *Bioessays*, 26(2):133–40.

Brouwer, A. K., Schimmel, J., Wiegant, J. C. A. G., Vertegaal, A. C. O., Tanke, H. J., and Dirks, R. W. (2009). Telomeric DNA mediates de novo PML body formation. *Mol Biol Cell*, 20(22):4804–15.

Cairns, B. R. (2007). Chromatin remodeling: insights and intrigue from single-molecule studies. *Nat Struct Mol Biol*, 14(11):989–96.

Campos, E. I. and Reinberg, D. (2009). Histones: annotating chromatin. *Annu Rev Genet*, 43:559–99.

Canela, A., Vera, E., Klatt, P., and Blasco, M. A. (2007). High-throughput telomere length quantification by FISH and its application to human population studies. *Proc. Natl. Acad. Sci. U.S.A.*, 104(13):5300–5.

Cao, R., Wang, L., Wang, H., Xia, L., Erdjument-Bromage, H., Tempst, P., Jones, R. S., and Zhang, Y. (2002). Role of histone H3 lysine 27 methylation in Polycomb-group silencing. *Science*, 298(5595):1039–43.

Carninci, P., Yasuda, J., and Hayashizaki, Y. (2008). Multifaceted mammalian transcriptome. *Curr Opin Cell Biol*, 20(3):274–80.

Chakravarthy, S., Gundimella, S. K. Y., Caron, C., Perche, P.-Y., Pehrson, J. R., Khochbin, S., and Luger, K. (2005). Structural characterization of the histone variant macroH2A. *Mol Cell Biol*, 25(17):7616–24.

Chen, J., Morosan-Puopolo, G., Dai, F., Wang, J., and Brand-Saberi, B. (2010). Molecular cloning of chicken cecr2 and its expression during chicken embryo development. *Int J Dev Biol*, 54(5):925–9.

Chin, J., Längst, G., Becker, P. B., and Widom, J. (2004). Fluorescence anisotropy assays for analysis of ISWI-DNA and ISWI-nucleosome interactions. *Meth Enzymol*, 376:3–16.

Clapier, C. and Cairns, B. (2009). The Biology of Chromatin Remodeling Complexes. *Annu. Rev. Biochem.*

Clapier, C. R., Längst, G., Corona, D. F., Becker, P. B., and Nightingale, K. P. (2001). Critical role for the histone H4 N terminus in nucleosome remodeling by ISWI. *Mol. Cell. Biol.*, 21(3):875–83.

Clapier, C. R., Nightingale, K. P., and Becker, P. B. (2002). A critical epitope for substrate recognition by the nucleosome remodeling ATPase ISWI. *Nucleic Acids Res.*, 30(3):649–55.

Collins, N., Poot, R. A., Kukimoto, I., García-Jiménez, C., Dellaire, G., and Varga-Weisz, P. D. (2002). An ACF1-ISWI chromatin-remodeling complex is required for DNA replication through heterochromatin. *Nat. Genet.*, 32(4):627–32.

Conaway, R. C., Brower, C. S., and Conaway, J. W. (2002). Emerging roles of ubiquitin in transcription regulation. *Science*, 296(5571):1254–8.

Consortium, E. P., Birney, E., Stamatoyannopoulos, J. A., Dutta, A., Guigó, R., Cuff, J., Gnerre, S., Jaffe, D. B., Chang, J. L., Lindblad-Toh, K., Lander, E. S., Koriabine, M., Nefedov, M., Osoegawa, K., Yoshinaga, Y., Zhu, B., and de Jong, P. J. (2007). Identification and analysis of functional elements in 1human genome by the ENCODE pilot project. *Nature*, 447(7146):799–816.

Corona, D. F. V. and Tamkun, J. W. (2004). Multiple roles for iswi in transcription, chromosome organization and dna replication. *Biochim Biophys Acta*, 1677(1-3):113–9.

Cremer, M., Grasser, F., Lanctôt, C., Müller, S., Neusser, M., Zinner, R., Solovei, I., and Cremer, T. (2008). Multicolor 3D Fluorescence In Situ Hybridization for Imaging Interphase Chromosomes. *Methods Mol Biol*, 463:205–39.

Cremer, M., Küpper, K., Wagler, B., Wizelman, L., von Hase, J., Weiland, Y., Kreja, L., Diebold, J., Speicher, M. R., and Cremer, T. (2003). Inheritance of gene density-

related higher order chromatin arrangements in normal and tumor cell nuclei. *J Cell Biol*, 162(5):809–20.

Cremer, M., von Hase, J., Volm, T., Brero, A., Kreth, G., Walter, J., Fischer, C., Solovei, I., Cremer, C., and Cremer, T. (2001). Non-random radial higher-order chromatin arrangements in nuclei of diploid human cells. *Chromosome Res*, 9(7):541–67.

Cremer, T., Küpper, K., Dietzel, S., and Fakan, S. (2004). Higher order chromatin architecture in the cell nucleus: on the way from structure to function. *Biol Cell*, 96(8):555–67.

Croft, J. A., Bridger, J. M., Boyle, S., Perry, P., Teague, P., and Bickmore, W. A. (1999). Differences in the localization and morphology of chromosomes in the human nucleus. *J Cell Biol*, 145(6):1119–31.

Dang, W. and Bartholomew, B. (2007). Domain architecture of the catalytic subunit in the isw2-nucleosome complex. *Mol Cell Biol*, 27(23):8306–17.

Dang, W., Kagalwala, M. N., and Bartholomew, B. (2007). The Dpb4 Subunit of ISW2 Is Anchored to Extranucleosomal DNA. *Journal of Biological Chemistry*, 282(27):19418–19425.

de la Escalera, S., Nieto, M. A., and Palacián, E. (1988). Preparation and structural characterization of nucleosomal core particles lacking one H2A.H2B dimer. *Biochem Biophys Res Commun*, 157(2):541–7.

Deuring, R., Fanti, L., Armstrong, J. A., Sarte, M., Papoulas, O., Prestel, M., Daubresse, G., Verardo, M., Moseley, S. L., Berloco, M., Tsukiyama, T., Wu, C., Pimpinelli, S., and Tamkun, J. W. (2000). The iswi chromatin-remodeling protein is required for gene expression and the maintenance of higher order chromatin structure in vivo. *Mol Cell*, 5(2):355–65.

Di Croce, L., Koop, R., Venditti, P., Westphal, H. M., Nightingale, K. P., Corona, D. F., Becker, P. B., and Beato, M. (1999). Two-step synergism between the progesterone receptor and the dna-binding domain of nuclear factor 1 on mmtv minichromosomes. *Mol Cell*, 4(1):45–54.

Dovey, O. M., Foster, C. T., and Cowley, S. M. (2010). Histone deacetylase 1 (HDAC1), but not HDAC2, controls embryonic stem cell differentiation. *Proc Natl Acad Sci U S A*, 107(18):8242–7.

Ebbert, R., Birkmann, A., and Schüller, H. J. (1999). The product of the snf2/swi2 paralogue ino80 of saccharomyces cerevisiae required for efficient expression of various yeast structural genes is part of a high-molecular-weight protein complex. *Mol Microbiol*, 32(4):741–51.

Eberharter, A. and Becker, P. B. (2004). Atp-dependent nucleosome remodelling: factors and functions. *J Cell Sci*, 117(Pt 17):3707–11.

Eberharter, A., Ferrari, S., Längst, G., Straub, T., Imhof, A., Varga-Weisz, P., Wilm, M., and Becker, P. B. (2001). Acf1, the largest subunit of CHRAC, regulates ISWI-induced nucleosome remodelling. *EMBO J.*, 20(14):3781–8.

Ehrlich, M., Gama-Sosa, M. A., Huang, L. H., Midgett, R. M., Kuo, K. C., McCune, R. A., and Gehrke, C. (1982). Amount and distribution of 5-methylcytosine in human dna from different types of tissues of cells. *Nucleic Acids Res*, 10(8):2709–21.

Eitoku, M., Sato, L., Senda, T., and Horikoshi, M. (2008). Histone chaperones: 30 years from isolation to elucidation of the mechanisms of nucleosome assembly and disassembly. *Cell Mol Life Sci*, 65(3):414–44.

Elfring, L. K., Deuring, R., McCallum, C. M., Peterson, C. L., and Tamkun, J. W. (1994). Identification and characterization of drosophila relatives of the yeast transcriptional activator snf2/swi2. *Mol Cell Biol*, 14(4):2225–34.

English, C. M., Adkins, M. W., Carson, J. J., Churchill, M. E. A., and Tyler, J. K. (2006). Structural basis for the histone chaperone activity of asf1. *Cell*, 127(3):495–508.

Erdel, F., Schubert, T., Marth, C., Längst, G., and Rippe, C. (2010). Human ISWI chromatin remodelling complexes identify their nucleosome substrate via a continous sampling mechanism. *submitted*.

Fazzio, T. G., Huff, J. T., and Panning, B. (2008). An rnai screen of chromatin proteins identifies tip60-p400 as a regulator of embryonic stem cell identity. *Cell*, 134(1):162–74.

Felle, M., Exler, J. H., Merkl, R., Dachauer, K., Brehm, A., Grummt, I., and Längst, G. (2010). DNA sequence encoded repression of rRNA gene transcription in chromatin. *Nucleic Acids Res*.

Felsenfeld, G. (1978). Chromatin. *Nature*, 271(5641):115–22.

Felsenfeld, G. and Groudine, M. (2003). Controlling the double helix. *Nature*, 421(6921):448–53.

Finlan, L. E., Sproul, D., Thomson, I., Boyle, S., Kerr, E., Perry, P., Ylstra, B., Chubb, J. R., and Bickmore, W. A. (2008). Recruitment to the nuclear periphery can alter expression of genes in human cells. *PLoS Genet*, 4(3):e1000039.

Fischle, W., Wang, Y., and Allis, C. D. (2003). Binary switches and modification cassettes in histone biology and beyond. *Nature*, 425(6957):475–9.

Fitzgerald, D. J., Berger, P., Schaffitzel, C., Yamada, K., Richmond, T. J., and Berger, I. (2006). Protein complex expression by using multigene baculoviral vectors. *Nat Methods*, 3(12):1021–32.

Flanagan, J. F., Mi, L.-Z., Chruszcz, M., Cymborowski, M., Clines, K. L., Kim, Y., Minor, W., Rastinejad, F., and Khorasanizadeh, S. (2005). Double chromodomains cooperate to recognize the methylated histone h3 tail. *Nature*, 438(7071):1181–5.

Flaus, A., Martin, D. M. A., Barton, G. J., and Owen-Hughes, T. (2006). Identification of multiple distinct snf2 subfamilies with conserved structural motifs. *Nucleic Acids Res*, 34(10):2887–905.

Forster, T. (1948). Zwischenmolekulare energiewanderung und fluoreszenz. *Annalen der Physik*, 6(2).

Gao, X., Tate, P., Hu, P., Tjian, R., Skarnes, W. C., and Wang, Z. (2008). Es cell pluripotency and germ-layer formation require the swi/snf chromatin remodeling component baf250a. *Proc Natl Acad Sci U S A*, 105(18):6656–61.

Gaspar-Maia, A., Alajem, A., Polesso, F., Sridharan, R., Mason, M. J., Heidersbach, A., Ramalho-Santos, J., McManus, M. T., Plath, K., Meshorer, E., and Ramalho-Santos, M. (2009). Chd1 regulates open chromatin and pluripotency of embryonic stem cells. *Nature*, 460(7257):863–8.

Gilbert, N., Boyle, S., Fiegler, H., Woodfine, K., Carter, N. P., and Bickmore, W. A. (2004). Chromatin architecture of the human genome: gene-rich domains are enriched in open chromatin fibers. *Cell*, 118(5):555–66.

Goetz, T. L., Gu, T. L., Speck, N. A., and Graves, B. J. (2000). Auto-inhibition of Ets-1 is counteracted by DNA binding cooperativity with core-binding factor alpha2. *Mol Cell Biol*, 20(1):81–90.

Golderer, G. and Gröbner, P. (1991). ADP-ribosylation of core histones and their acetylated subspecies. *Biochem J*, 277 (Pt 3):607–10.

Greaves, I. K., Rangasamy, D., Devoy, M., Marshall Graves, J. A., and Tremethick, D. J. (2006). The X and Y chromosomes assemble into H2A.Z-containing [corrected] facultative heterochromatin [corrected] following meiosis. *Mol Cell Biol*, 26(14):5394–405.

Grüne, T., Brzeski, J., Eberharter, A., Clapier, C. R., Corona, D. F. V., Becker, P. B., and Müller, C. W. (2003). Crystal structure and functional analysis of a nucleosome recognition module of the remodeling factor ISWI. *Mol Cell*, 12(2):449–60.

Guillemette, B. and Gaudreau, L. (2006). Reuniting the contrasting functions of H2A.Z. *Biochem Cell Biol*, 84(4):528–35.

Guo, X. W., Th'ng, J. P., Swank, R. A., Anderson, H. J., Tudan, C., Bradbury, E. M., and Roberge, M. (1995). Chromosome condensation induced by fostriecin does not require p34cdc2 kinase activity and histone H1 hyperphosphorylation, but is associated with enhanced histone H2A and H3 phosphorylation. *EMBO J*, 14(5):976–85.

Hamiche, A., Sandaltzopoulos, R., Gdula, D. A., and Wu, C. (1999). ATP-dependent histone octamer sliding mediated by the chromatin remodeling complex NURF. *Cell*, 97(7):833–42.

Hanai, K., Furuhashi, H., Yamamoto, T., Akasaka, K., and Hirose, S. (2008). Rsf governs silent chromatin formation via histone h2av replacement. *PLoS Genet*, 4(2):e1000011.

Hancock, R. (2000). A new look at the nuclear matrix. *Chromosoma*, 109(4):219–25.

Hartlepp, K. F., Fernández-Tornero, C., Eberharter, A., Grüne, T., Müller, C. W., and Becker, P. B. (2005). The histone fold subunits of drosophila chrac facilitate nucleosome sliding through dynamic dna interactions. *Mol Cell Biol*, 25(22):9886–96.

Hassan, Y. I. and Zempleni, J. (2006). Epigenetic regulation of chromatin structure and gene function by biotin. *J Nutr*, 136(7):1763–5.

Haushalter, K. A. and Kadonaga, J. T. (2003). Chromatin assembly by DNA-translocating motors. *Nat Rev Mol Cell Biol*, 4(8):613–20.

He, X., Chen, C.-C., Hong, F., Fang, F., Sinha, S., Ng, H.-H., and Zhong, S. (2009). A biophysical model for analysis of transcription factor interaction and binding site arrangement from genome-wide binding data. *PLoS One*, 4(12):e8155.

He, X., Fan, H.-Y., Garlick, J. D., and Kingston, R. E. (2008). Diverse regulation of SNF2h chromatin remodeling by noncatalytic subunits. *Biochemistry*, 47(27):7025–33. 0-601-0 binding.

He, X., Fan, H.-Y., Narlikar, G. J., and Kingston, R. E. (2006a). Human ACF1 alters the remodeling strategy of SNF2h. *J. Biol. Chem.*, 281(39):28636–47.

He, X., Fan, H.-Y., Narlikar, G. J., and Kingston, R. E. (2006b). Human ACF1 alters the remodeling strategy of SNF2h. *J. Biol. Chem.*, 281(39):28636–47.

Hendzel, M. J., Wei, Y., Mancini, M. A., Van Hooser, A., Ranalli, T., Brinkley, B. R., Bazett-Jones, D. P., and Allis, C. D. (1997). Mitosis-specific phosphorylation of histone H3 initiates primarily within pericentromeric heterochromatin during G2 and spreads in an ordered fashion coincident with mitotic chromosome condensation. *Chromosoma*, 106(6):348–60.

Hermann, A., Gowher, H., and Jeltsch, A. (2004). Biochemistry and biology of mammalian dna methyltransferases. *Cell Mol Life Sci*, 61(19-20):2571–87.

Ho, L. and Crabtree, G. R. (2010). Chromatin remodelling during development. *Nature*, 463(7280):474–84.

Ho, L., Jothi, R., Ronan, J. L., Cui, K., Zhao, K., and Crabtree, G. R. (2009). An embryonic stem cell chromatin remodeling complex, esbaf, is an essential component of the core pluripotency transcriptional network. *Proc Natl Acad Sci U S A*, 106(13):5187–91.

Hollenhorst, P. C., Chandler, K. J., Poulsen, R. L., Johnson, W. E., Speck, N. A., and Graves, B. J. (2009). DNA specificity determinants associate with distinct transcription factor functions. *PLoS Genet*, 5(12):e1000778.

Hong, L., Schroth, G. P., Matthews, H. R., Yau, P., and Bradbury, E. M. (1993). Studies of the DNA binding properties of histone H4 amino terminus. Thermal denaturation studies reveal that acetylation markedly reduces the binding constant of the H4 "tail" to DNA. *J Biol Chem*, 268(1):305–14.

Horn, P. J. and Peterson, C. L. (2002). Molecular biology. Chromatin higher order folding–wrapping up transcription. *Science*, 297(5588):1824–7.

Huang, H., Kahana, A., Gottschling, D. E., Prakash, L., and Liebman, S. W. (1997). The ubiquitin-conjugating enzyme Rad6 (Ubc2) is required for silencing in Saccharomyces cerevisiae. *Mol Cell Biol*, 17(11):6693–9.

Hutcheon, T., Dixon, G. H., and Levy-Wilson, B. (1980). Transcriptionally active mononucleosomes from trout testis are heterogeneous in composition. *J Biol Chem*, 255(2):681–5.

International Human Genome Sequencing Consortium (2004). Finishing the euchromatic sequence of the human genome. *Nature*, 431(7011):931–45.

Ito, T., Levenstein, M. E., Fyodorov, D. V., Kutach, A. K., Kobayashi, R., and Kadonaga, J. T. (1999). Acf consists of two subunits, acf1 and iswi, that function cooperatively in the atp-dependent catalysis of chromatin assembly. *Genes Dev*, 13(12):1529–39.

Jacobson, M. K. and Jacobson, E. L. (1999). Discovering new ADP-ribose polymer cycles: protecting the genome and more. *Trends Biochem Sci*, 24(11):415–7.

Jacobson, R. H., Ladurner, A. G., King, D. S., and Tjian, R. (2000). Structure and function of a human TAFII250 double bromodomain module. *Science*, 288(5470):1422–5.

Jeltsch, A. (2002). Beyond Watson and Crick: DNA methylation and molecular enzymology of DNA methyltransferases. *Chembiochem*, 3(4):274–93.

Jones, P. A. and Liang, G. (2009). Rethinking how dna methylation patterns are maintained. *Nat Rev Genet*, 10(11):805–11.

Kagalwala, M. N. (2004). Topography of the ISW2-nucleosome complex: insights into nucleosome spacing and chromatin remodeling. *EMBO J.*, 23(10):2092–104.

Kapanidis, A. N., Laurence, T. A., Lee, N. K., Margeat, E., Kong, X., and Weiss, S. (2005). Alternating-laser excitation of single molecules. *Acc Chem Res*, 38(7):523–33.

Kapanidis, A. N., Lee, N. K., Laurence, T. A., Doose, S., Margeat, E., and Weiss, S. (2004). Fluorescence-aided molecule sorting: analysis of structure and interactions by alternating-laser excitation of single molecules. *Proc Natl Acad Sci U S A*, 101(24):8936–41.

Kasten, M., Szerlong, H., Erdjument-Bromage, H., Tempst, P., Werner, M., and Cairns, B. R. (2004). Tandem bromodomains in the chromatin remodeler rsc recognize acetylated histone h3 lys14. *EMBO J*, 23(6):1348–59.

Kepert, J. F., Mazurkiewicz, J., Heuvelman, G. L., Tóth, K. F., and Rippe, K. (2005). Nap1 modulates binding of linker histone h1 to chromatin and induces an extended chromatin fiber conformation. *J Biol Chem*, 280(40):34063–72.

Khorasanizadeh, S. (2004). The nucleosome: from genomic organization to genomic regulation. *Cell*, 116(2):259–72.

Kim, J. K., Huh, S. O., Choi, H., Lee, K. S., Shin, D., Lee, C., Nam, J. S., Kim, H., Chung, H., Lee, H. W., Park, S. D., and Seong, R. H. (2001). Srg3, a mouse homolog of yeast swi3, is essential for early embryogenesis and involved in brain development. *Mol Cell Biol*, 21(22):7787–95.

Kim, J. K., Samaranayake, M., and Pradhan, S. (2009). Epigenetic mechanisms in mammals. *Cell Mol Life Sci*, 66(4):596–612.

Kissing, A. C. (1976). That what all is made for - key function of a fundamental factor -. *Mol End Neph Desc EN*, 1.

Klochendler-Yeivin, A., Fiette, L., Barra, J., Muchardt, C., Babinet, C., and Yaniv, M. (2000). The murine snf5/ini1 chromatin remodeling factor is essential for embryonic development and tumor suppression. *EMBO Rep*, 1(6):500–6.

Kornberg, R. D. (1974). Chromatin structure: a repeating unit of histones and DNA. *Science*, 184(139):868–71.

LabFAQS (2010). Roche lab faqs. *Roche Applied Science Lab FAQS*, 3.

Lachner, M., O'Carroll, D., Rea, S., Mechtler, K., and Jenuwein, T. (2001). Methylation of histone H3 lysine 9 creates a binding site for HP1 proteins. *Nature*, 410(6824):116–20.

Lanctôt, C., Cheutin, T., Cremer, M., Cavalli, G., and Cremer, T. (2007). Dynamic genome architecture in the nuclear space: regulation of gene expression in three dimensions. *Nat Rev Genet*, 8(2):104–15.

Lander, E. S., Linton, L. M., Birren, B., Felsenfeld, A., Wetterstrand, K. A., Patrinos, A., Morgan, M. J., de Jong, P., Catanese, J. J., Osoegawa, K., Shizuya, H., Choi, S., Chen, Y. J., Szustakowki, J., and Consortium, I. H. G. S. (2001). Initial sequencing and analysis of the human genome. *Nature*, 409(6822):860–921.

Längst, G., Bonte, E. J., Corona, D. F., and Becker, P. B. (1999). Nucleosome movement by CHRAC and ISWI without disruption or trans-displacement of the histone octamer. *Cell*, 97(7):843–52.

Larsen, F., Gundersen, G., Lopez, R., and Prydz, H. (1992). Cpg islands as gene markers in the human genome. *Genomics*, 13(4):1095–107.

Laurent, B. C., Treich, I., and Carlson, M. (1993). The yeast snf2/swi2 protein has dna-stimulated atpase activity required for transcriptional activation. *Genes Dev*, 7(4):583–91.

Lazzaro, M. A. and Picketts, D. J. (2001). Cloning and characterization of the murine Imitation Switch (ISWI) genes: differential expression patterns suggest distinct developmental roles for Snf2h and Snf2l. *J Neurochem*, 77(4):1145–56.

Lee, N. K., Kapanidis, A. N., Wang, Y., Michalet, X., Mukhopadhyay, J., Ebright, R. H., and Weiss, S. (2005). Accurate FRET measurements within single diffusing biomolecules using alternating-laser excitation. *Biophys J*, 88(4):2939–53.

LeRoy, G., Orphanides, G., Lane, W. S., and Reinberg, D. (1998). Requirement of rsf and fact for transcription of chromatin templates in vitro. *Science*, 282(5395):1900–4.

Levchenko, V., Jackson, B., and Jackson, V. (2005). Histone release during transcription: displacement of the two H2A-H2B dimers in the nucleosome is dependent on different levels of transcription-induced positive stress. *Biochemistry*, 44(14):5357–72.

Levy, S., Sutton, G., Ng, P. C., Feuk, L., Halpern, A. L., Walenz, B. P., Axelrod, N., Huang, J., Kirkness, E. F., Denisov, G., Lin, Y., MacDonald, J. R., Pang, A. W. C., Shago, M., Stockwell, T. B., Tsiamouri, A., Bafna, V., Bansal, V., Kravitz, S. A., Busam, D. A., Beeson, K. Y., McIntosh, T. C., Remington, K. A., Abril, J. F., Gill, J., Borman, J., Rogers, Y.-H., Frazier, M. E., Scherer, S. W., Strausberg, R. L., and Venter, J. C. (2007). The diploid genome sequence of an individual human. *PLoS Biol*, 5(10):e254.

Li, J., Längst, G., and Grummt, I. (2006). Norc-dependent nucleosome positioning silences rrna genes. *EMBO J*, 25(24):5735–41.

Li, W., Nagaraja, S., Delcuve, G. P., Hendzel, M. J., and Davie, J. R. (1993). Effects of histone acetylation, ubiquitination and variants on nucleosome stability. *Biochem J*, 296 (Pt 3):737–44.

Lohr, D., Corden, J., Tatchell, K., Kovacic, R. T., and Van Holde, K. E. (1977). Comparative subunit structure of HeLa, yeast, and chicken erythrocyte chromatin. *Proc Natl Acad Sci U S A*, 74(1):79–83.

Lowary, P. T. and Widom, J. (1998). New DNA sequence rules for high affinity binding to histone octamer and sequence-directed nucleosome positioning. *J. Mol. Biol.*, 276(1):19–42.

Loyola, A., Huang, J.-Y., LeRoy, G., Hu, S., Wang, Y.-H., Donnelly, R. J., Lane, W. S., Lee, S.-C., and Reinberg, D. (2003). Functional analysis of the subunits of the chromatin assembly factor rsf. *Mol Cell Biol*, 23(19):6759–68.

Luger, K. (2003). Structure and dynamic behavior of nucleosomes. *Curr Opin Genet Dev*, 13(2):127–35.

Luger, K., Mäder, A. W., Richmond, R. K., Sargent, D. F., and Richmond, T. J. (1997). Crystal structure of the nucleosome core particle at 2.8 A resolution. *Nature*, 389(6648):251–60.

Luger, K. and Richmond, T. J. (1998). The histone tails of the nucleosome. *Curr Opin Genet Dev*, 8(2):140–6.

Lusser, A. and Kadonaga, J. T. (2003). Chromatin remodeling by atp-dependent molecular machines. *Bioessays*, 25(12):1192–200.

Lusser, A., Urwin, D. L., and Kadonaga, J. T. (2005). Distinct activities of chd1 and acf in atp-dependent chromatin assembly. *Nat Struct Mol Biol*, 12(2):160–6.

Margueron, R. and Reinberg, D. (2010). Chromatin structure and the inheritance of epigenetic information. *Nat Rev Genet*, 11(4):285–96.

Martens, J. H. A., O'Sullivan, R. J., Braunschweig, U., Opravil, S., Radolf, M., Steinlein, P., and Jenuwein, T. (2005). The profile of repeat-associated histone lysine methylation states in the mouse epigenome. *EMBO J*, 24(4):800–12.

Martínez-Balbás, M. A., Tsukiyama, T., Gdula, D., and Wu, C. (1998). Drosophila nurf-55, a wd repeat protein involved in histone metabolism. *Proc Natl Acad Sci U S A*, 95(1):132–7.

Matera, A. G. and Ward, D. C. (1992). Oligonucleotide probes for the analysis of specific repetitive DNA sequences by fluorescence in situ hybridization. *Hum. Mol. Genet.*, 1(7):535–9.

Mayer, C., Neubert, M., and Grummt, I. (2008). The structure of norc-associated rna is crucial for targeting the chromatin remodelling complex norc to the nucleolus. *EMBO Rep*, 9(8):774–80.

Mayer, C., Schmitz, K.-M., Li, J., Grummt, I., and Santoro, R. (2006). Intergenic transcripts regulate the epigenetic state of rrna genes. *Mol Cell*, 22(3):351–61.

McGhee, J. D. and Felsenfeld, G. (1980). Nucleosome structure. *Annu Rev Biochem*, 49:1115–56.

Medina, I., Carbonell, J., Pulido, L., Madeira, S. C., Goetz, S., Conesa, A., Tárraga, J., Pascual-Montano, A., Nogales-Cadenas, R., Santoyo, J., García, F., Marbà, M., Montaner, D., and Dopazo, J. (2010). Babelomics: an integrative platform for the analysis of transcriptomics, proteomics and genomic data with advanced functional profiling. *Nucleic Acids Res.*

Metzker, M. L. (2010). Sequencing technologies - the next generation. *Nat Rev Genet*, 11(1):31–46.

Miele, V., Vaillant, C., d'Aubenton Carafa, Y., Thermes, C., and Grange, T. (2008). DNA physical properties determine nucleosome occupancy from yeast to fly. *Nucleic Acids Res*, 36(11):3746–56.

Mito, Y., Henikoff, J. G., and Henikoff, S. (2005). Genome-scale profiling of histone H3.3 replacement patterns. *Nat Genet*, 37(10):1090–7.

Mondal, T., Rasmussen, M., Pandey, G. K., Isaksson, A., and Kanduri, C. (2010). Characterization of the RNA content of chromatin. *Genome Res.*

Müller, B. K., Zaychikov, E., Bräuchle, C., and Lamb, D. C. (2005). Pulsed interleaved excitation. *Biophys J*, 89(5):3508–22.

Natsume, R., Eitoku, M., Akai, Y., Sano, N., Horikoshi, M., and Senda, T. (2007). Structure and function of the histone chaperone cia/asf1 complexed with histones h3 and h4. *Nature*, 446(7133):338–41.

Neigeborn, L. and Carlson, M. (1984). Genes affecting the regulation of suc2 gene expression by glucose repression in saccharomyces cerevisiae. *Genetics*, 108(4):845–58.

Németh, A., Conesa, A., Santoyo-Lopez, J., Medina, I., Montaner, D., Péterfia, B., Solovei, I., Cremer, T., Dopazo, J., and Längst, G. (2010). Initial genomics of the human nucleolus. *PLoS Genet*, 6(3):e1000889.

Németh, A., Strohner, R., Grummt, I., and Längst, G. (2004). The chromatin remodeling complex NoRC and TTF-I cooperate in the regulation of the mammalian rRNA genes in vivo. *Nucleic Acids Res.*, 32(14):4091–9.

Nir, E., Michalet, X., Hamadani, K. M., Laurence, T. A., Neuhauser, D., Kovchegov, Y., and Weiss, S. (2006). Shot-noise limited single-molecule FRET histograms: comparison between theory and experiments. *J Phys Chem B*, 110(44):22103–24.

Olins, D. E. and Olins, A. L. (2003). Chromatin history: our view from the bridge. *Nat Rev Mol Cell Biol*, 4(10):809–14.

Paithankar, K. R. and Prasad, K. S. (1991). Precipitation of DNA by polyethylene glycol and ethanol. *Nucleic Acids Res*, 19(6):1346.

Panchenko, T. and Black, B. E. (2009). The epigenetic basis for centromere identity. *Prog Mol Subcell Biol*, 48:1–32.

Pederson, T. and Bhorjee, J. S. (1979). Evidence for a role of RNA in eukaryotic chromosome structure. Metabolically stable, small nuclear RNA species are covalently linked to chromosomal DNA in HeLa cells. *J Mol Biol*, 128(4):451–80.

Peters, A. H. F. M., Kubicek, S., Mechtler, K., O'Sullivan, R. J., Derijck, A. A. H. A., Perez-Burgos, L., Kohlmaier, A., Opravil, S., Tachibana, M., Shinkai, Y., Martens, J. H. A., and Jenuwein, T. (2003). Partitioning and plasticity of repressive histone methylation states in mammalian chromatin. *Mol Cell*, 12(6):1577–89.

Pham, A. D. and Sauer, F. (2000). Ubiquitin-activating/conjugating activity of TAFII250, a mediator of activation of gene expression in Drosophila. *Science*, 289(5488):2357–60.

Pickart, C. M. (2001). Mechanisms underlying ubiquitination. *Annu Rev Biochem*, 70:503–33.

Poirier, M. G., Bussiek, M., Langowski, J., and Widom, J. (2008). Spontaneous access to DNA target sites in folded chromatin fibers. *J. Mol. Biol.*, 379(4):772–86.

Poot, R. A., Dellaire, G., Hülsmann, B. B., Grimaldi, M. A., Corona, D. F., Becker, P. B., Bickmore, W. A., and Varga-Weisz, P. D. (2000). HuCHRAC, a human ISWI chromatin remodelling complex contains hACF1 and two novel histone-fold proteins. *EMBO J.*, 19(13):3377–87.

Rabel, C. (1885). Über Zellteilung. *Morph JB*, 10.

Racki, L. R. and Narlikar, G. J. (2008). ATP-dependent chromatin remodeling enzymes: two heads are not better, just different. *Curr. Opin. Genet. Dev.*, 18(2):137–44.

Racki, L. R., Yang, J. G., Naber, N., Partensky, P. D., Acevedo, A., Purcell, T. J., Cooke, R., Cheng, Y., and Narlikar, G. J. (2009). The chromatin remodeller ACF acts as a dimeric motor to space nucleosomes. *Nature*, 462(7276):1016–21.

Ransom, M., Dennehey, B. K., and Tyler, J. K. (2010). Chaperoning histones during dna replication and repair. *Cell*, 140(2):183–95.

Rea, S., Eisenhaber, F., O'Carroll, D., Strahl, B. D., Sun, Z. W., Schmid, M., Opravil, S., Mechtler, K., Ponting, C. P., Allis, C. D., and Jenuwein, T. (2000). Regulation of chromatin structure by site-specific histone H3 methyltransferases. *Nature*, 406(6796):593–9.

Rhodes, D. and Laskey, R. A. (1989). Assembly of nucleosomes and chromatin in vitro. *Methods Enzymol*, 170:575–85.

Richmond, T. J. and Davey, C. A. (2003). The structure of DNA in the nucleosome core. *Nature*, 423(6936):145–50.

Rippe, K., Schrader, A., Riede, P., Strohner, R., Lehmann, E., and Längst, G. (2007). DNA sequence- and conformation-directed positioning of nucleosomes by chromatin-remodeling complexes. *Proc. Natl. Acad. Sci. U.S.A.*, 104(40):15635–40.

Robertson, A. K., Geiman, T. M., Sankpal, U. T., Hager, G. L., and Robertson, K. D. (2004). Effects of chromatin structure on the enzymatic and DNA binding functions of DNA methyltransferases DNMT1 and Dnmt3a in vitro. *Biochem Biophys Res Commun*, 322(1):110–8.

Robinson, P. J. J., An, W., Routh, A., Martino, F., Chapman, L., Roeder, R. G., and Rhodes, D. (2008). 30 nm chromatin fibre decompaction requires both H4-K16 acetylation and linker histone eviction. *J Mol Biol*, 381(4):816–25.

Robinson, P. J. J. and Rhodes, D. (2006). Structure of the '30 nm' chromatin fibre: a key role for the linker histone. *Curr Opin Struct Biol*, 16(3):336–43.

Rodríguez-Campos, A. and Azorín, F. (2007). RNA is an integral component of chromatin that contributes to its structural organization. *PLoS One*, 2(11):e1182.

Roth, S. Y., Denu, J. M., and Allis, C. D. (2001). Histone acetyltransferases. *Annu Rev Biochem*, 70:81–120.

Sambrook, J. and Russell, D. W. (2000). *Molecular cloning: a laboratory manual*, volume 03. Cold Spring Harbor Laboratory.

Santoro, R. and Grummt, I. (2005). Epigenetic mechanism of rrna gene silencing: temporal order of norc-mediated histone modification, chromatin remodeling, and dna methylation. *Mol Cell Biol*, 25(7):2539–46.

Santoro, R., Li, J., and Grummt, I. (2002). The nucleolar remodeling complex norc mediates heterochromatin formation and silencing of ribosomal gene transcription. *Nat Genet*, 32(3):393–6.

Santos-Rosa, H., Schneider, R., Bannister, A. J., Sherriff, J., Bernstein, B. E., Emre, N. C. T., Schreiber, S. L., Mellor, J., and Kouzarides, T. (2002). Active genes are tri-methylated at K4 of histone H3. *Nature*, 419(6905):407–11.

Schägger, H. and von Jagow, G. (1991). Blue native electrophoresis for isolation of membrane protein complexes in enzymatically active form. *Anal Biochem*, 199(2):223–31.

Schalch, T., Duda, S., Sargent, D. F., and Richmond, T. J. (2005). X-ray structure of a tetranucleosome and its implications for the chromatin fibre. *Nature*, 436(7047):138–41.

Segal, E., Fondufe-Mittendorf, Y., Chen, L., Thåström, A., Field, Y., Moore, I. K., Wang, J.-P. Z., and Widom, J. (2006). A genomic code for nucleosome positioning. *Nature*, 442(7104):772–8.

Shen, X., Mizuguchi, G., Hamiche, A., and Wu, C. (2000). A chromatin remodelling complex involved in transcription and dna processing. *Nature*, 406(6795):541–4.

Shi, Y., Lan, F., Matson, C., Mulligan, P., Whetstine, J. R., Cole, P. A., Casero, R. A., and Shi, Y. (2004). Histone demethylation mediated by the nuclear amine oxidase homolog LSD1. *Cell*, 119(7):941–53.

Sims, 3rd, R. J., Chen, C.-F., Santos-Rosa, H., Kouzarides, T., Patel, S. S., and Reinberg, D. (2005). Human but not yeast chd1 binds directly and selectively to histone h3 methylated at lysine 4 via its tandem chromodomains. *J Biol Chem*, 280(51):41789–92.

Smit, A. F. (1999). Interspersed repeats and other mementos of transposable elements in mammalian genomes. *Curr Opin Genet Dev*, 9(6):657–63.

Smith, B. C. and Denu, J. M. (2009). Chemical mechanisms of histone lysine and arginine modifications. *Biochim Biophys Acta*, 1789(1):45–57.

Sobel, R. E., Cook, R. G., Perry, C. A., Annunziato, A. T., and Allis, C. D. (1995). Conservation of deposition-related acetylation sites in newly synthesized histones h3 and h4. *Proc Natl Acad Sci U S A*, 92(4):1237–41.

Stanek, D. and Neugebauer, K. M. (2006). The Cajal body: a meeting place for spliceosomal snRNPs in the nuclear maze. *Chromosoma*, 115(5):343–54.

Sterner, D. E. and Berger, S. L. (2000). Acetylation of histones and transcription-related factors. *Microbiol Mol Biol Rev*, 64(2):435–59.

Stokes, D. G., Tartof, K. D., and Perry, R. P. (1996). Chd1 is concentrated in interbands and puffed regions of drosophila polytene chromosomes. *Proc Natl Acad Sci U S A*, 93(14):7137–42.

Stopka, T. and Skoultchi, A. I. (2003). The iswi atpase snf2h is required for early mouse development. *Proc Natl Acad Sci U S A*, 100(24):14097–102.

Strahl, B. D. and Allis, C. D. (2000). The language of covalent histone modifications. *Nature*, 403(6765):41–5.

Strickfaden, H., Zunhammer, A., van Koningsbruggen, S., Köhler, D., and Cremer, T. (2010). 4d chromatin dynamics in cycling cells, theodor boveri's hypotheses revisited. *Nucleus*, 1:3(1-15).

Strohner, R., Nemeth, A., Jansa, P., Hofmann-Rohrer, U., Santoro, R., Längst, G., and Grummt, I. (2001). Norc–a novel member of mammalian iswi-containing chromatin remodeling machines. *EMBO J*, 20(17):4892–900.

Strohner, R., Németh, A., Nightingale, K. P., Grummt, I., Becker, P. B., and Längst, G. (2004). Recruitment of the nucleolar remodeling complex NoRC establishes ribosomal DNA silencing in chromatin. *Mol. Cell. Biol.*, 24(4):1791–8.

Strohner, R., Wachsmuth, M., Dachauer, K., Mazurkiewicz, J., Hochstatter, J., Rippe, K., and Längst, G. (2005). A 'loop recapture' mechanism for ACF-dependent nucleosome remodeling. *Nat. Struct. Mol. Biol.*, 12(8):683–90.

Stryer, L. (1978). Fluorescence energy transfer as a spectroscopic ruler. *Annu Rev Biochem*, 47:819–46.

Sun, Z.-W. and Allis, C. D. (2002). Ubiquitination of histone H2B regulates H3 methylation and gene silencing in yeast. *Nature*, 418(6893):104–8.

Tagami, H., Ray-Gallet, D., Almouzni, G., and Nakatani, Y. (2004). Histone h3.1 and h3.3 complexes mediate nucleosome assembly pathways dependent or independent of dna synthesis. *Cell*, 116(1):51–61.

Talbert, P. B. and Henikoff, S. (2010). Histone variants–ancient wrap artists of the epigenome. *Nat Rev Mol Cell Biol*, 11(4):264–75.

Tanabe, H., Müller, S., Neusser, M., von Hase, J., Calcagno, E., Cremer, M., Solovei, I., Cremer, C., and Cremer, T. (2002). Evolutionary conservation of chromosome territory arrangements in cell nuclei from higher primates. *Proc Natl Acad Sci U S A*, 99(7):4424–9.

Tommerup, H., Dousmanis, A., and de Lange, T. (1994). Unusual chromatin in human telomeres. *Mol. Cell. Biol.*, 14(9):5777–85.

Tremethick, D. J. (2007). Higher-order structures of chromatin: the elusive 30 nm fiber. *Cell*, 128(4):651–4.

Tsukiyama, T. and Wu, C. (1995). Purification and properties of an atp-dependent nucleosome remodeling factor. *Cell*, 83(6):1011–20.

Vakoc, C. R., Sachdeva, M. M., Wang, H., and Blobel, G. A. (2006). Profile of histone lysine methylation across transcribed mammalian chromatin. *Mol Cell Biol*, 26(24):9185–95.

Valouev, A., Ichikawa, J., Tonthat, T., Stuart, J., Ranade, S., Peckham, H., Zeng, K., Malek, J. A., Costa, G., McKernan, K., Sidow, A., Fire, A., and Johnson, S. M. (2008). A high-resolution, nucleosome position map of C. elegans reveals a lack of universal sequence-dictated positioning. *Genome Res*, 18(7):1051–63.

van Holde, K. E. (1989). Chromatin. *Springer series in molecular biology*, pages XII,497 p.

Vaquero, A., Loyola, A., and Reinberg, D. (2003). The constantly changing face of chromatin. *Sci Aging Knowledge Environ*, 2003(14):RE4.

Varga-Weisz, P. D., Wilm, M., Bonte, E., Dumas, K., Mann, M., and Becker, P. B. (1997). Chromatin-remodelling factor chrac contains the atpases iswi and topoisomerase ii. *Nature*, 388(6642):598–602.

Venter, J. C., Adams, M. D., Myers, E. W., Li, P. W., Mural, R. J., Sutton, G. G., ..., Turner, R., Venter, E., Wang, M., Wen, M., Wu, D., Wu, M., Xia, A., Zandieh, A., and Zhu, X. (2001). The sequence of the human genome. *Science*, 291(5507):1304–51.

von Hippel, P. H. and Felsenfeld, G. (1964). Micrococcal nuclease as a probe of dna conformation. *Biochemistry*, 3:27–39.

Whitehouse, I., Stockdale, C., Flaus, A., Szczelkun, M. D., and Owen-Hughes, T. (2003). Evidence for dna translocation by the iswi chromatin-remodeling enzyme. *Mol Cell Biol*, 23(6):1935–45.

Widom, J. (2001). Role of DNA sequence in nucleosome stability and dynamics. *Q. Rev. Biophys.*, 34(3):269–324.

Wolffe, A. P. (1997). Histone H1. *Int J Biochem Cell Biol*, 29(12):1463–6.

Wolffe, A. P. and Kurumizaka, H. (1998). The nucleosome: a powerful regulator of transcription. *Prog Nucleic Acid Res Mol Biol*, 61:379–422.

Workman, J. L. and Kingston, R. E. (1998). Alteration of nucleosome structure as a mechanism of transcriptional regulation. *Annu. Rev. Biochem.*, 67:545–79.

Workman, J. L., Taylor, I. C., Kingston, R. E., and Roeder, R. G. (1991). Control of class II gene transcription during in vitro nucleosome assembly. *Methods Cell Biol*, 35:419–47.

Wu, R. S. and Bonner, W. M. (1981). Separation of basal histone synthesis from S-phase histone synthesis in dividing cells. *Cell*, 27(2 Pt 1):321–30.

Wysocka, J., Swigut, T., Xiao, H., Milne, T. A., Kwon, S. Y., Landry, J., Kauer, M., Tackett, A. J., Chait, B. T., Badenhorst, P., Wu, C., and Allis, C. D. (2006). A PHD finger of NURF couples histone H3 lysine 4 trimethylation with chromatin remodelling. *Nature*, 442(7098):86–90.

Xiao, H., Sandaltzopoulos, R., Wang, H. M., Hamiche, A., Ranallo, R., Lee, K. M., Fu, D., and Wu, C. (2001). Dual functions of largest nurf subunit nurf301 in nucleosome sliding and transcription factor interactions. *Mol Cell*, 8(3):531–43.

Yan, Z., Wang, Z., Sharova, L., Sharov, A. A., Ling, C., Piao, Y., Aiba, K., Matoba, R., Wang, W., and Ko, M. S. H. (2008). Baf250b-associated swi/snf chromatin-remodeling complex is required to maintain undifferentiated mouse embryonic stem cells. *Stem Cells*, 26(5):1155–65.

Yang, J. G., Madrid, T. S., Sevastopoulos, E., and Narlikar, G. J. (2006). The chromatin-remodeling enzyme ACF is an ATP-dependent DNA length sensor that regulates nucleosome spacing. *Nat. Struct. Mol. Biol.*, 13(12):1078–83.

Ye, J., Osborne, A. R., Groll, M., and Rapoport, T. A. (2004). Reca-like motor atpases–lessons from structures. *Biochim Biophys Acta*, 1659(1):1–18.

Ye, Y., Xiao, Y., Wang, W., Wang, Q., Yearsley, K., Wani, A. A., Yan, Q., Gao, J.-X., Shetuni, B. S., and Barsky, S. H. (2009). Inhibition of expression of the chromatin remodeling gene, SNF2L, selectively leads to DNA damage, growth inhibition, and cancer cell death. *Mol Cancer Res*, 7(12):1984–99.

Yoder, J. A., Soman, N. S., Verdine, G. L., and Bestor, T. H. (1997a). DNA (cytosine-5)-methyltransferases in mouse cells and tissues. Studies with a mechanism-based probe. *J Mol Biol*, 270(3):385–95.

Yoder, J. A., Walsh, C. P., and Bestor, T. H. (1997b). Cytosine methylation and the ecology of intragenomic parasites. *Trends Genet*, 13(8):335–40.

Yoo, A. S. and Crabtree, G. R. (2009). Atp-dependent chromatin remodeling in neural development. *Curr Opin Neurobiol*, 19(2):120–6.

Zhang, Y. and Reinberg, D. (2001). Transcription regulation by histone methylation: interplay between different covalent modifications of the core histone tails. *Genes Dev*, 15(18):2343–60.

Zink, D., Cremer, T., Saffrich, R., Fischer, R., Trendelenburg, M. F., Ansorge, W., and Stelzer, E. H. (1998). Structure and dynamics of human interphase chromosome territories in vivo. *Hum Genet*, 102(2):241–51.

Zlatanova, J., Bishop, T. C., Victor, J.-M., Jackson, V., and van Holde, K. (2009). The nucleosome family: dynamic and growing. *Structure*, 17(2):160–71.

Zofall, M., Persinger, J., and Bartholomew, B. (2004). Functional role of extranucleosomal DNA and the entry site of the nucleosome in chromatin remodeling by ISW2. *Mol. Cell. Biol.*, 24(22):10047–57.

Zofall, M., Persinger, J., Kassabov, S. R., and Bartholomew, B. (2006). Chromatin remodeling by ISW2 and SWI/SNF requires DNA translocation inside the nucleosome. *Nat. Struct. Mol. Biol.*, 13(4):339–46.